Identification and characterization of antigen-specific T cells in infectious disease and cancer using the example of SARS-CoV-2 and bladder carcinoma

Inaugural Dissertation

zur

Erlangung des Doktorgrades

Dr. nat. med.

der Medizinischen Fakultät

und

der Mathematisch-Naturwissenschaftlichen Fakultät

der Universität zu Köln

vorgelegt von

Charlyn Dörnte

aus Duisburg

Miltenyi Biotec, Bergisch Gladbach

2025

Identification and characterization of antigen-specific T cells in infectious disease and cancer using the example of SARS-CoV-2 and bladder carcinoma

Inaugural Dissertation

zur

Erlangung des Doktorgrades

Dr. nat. med.

der Medizinischen Fakultät

und

der Mathematisch-Naturwissenschaftlichen Fakultät

der Universität zu Köln

vorgelegt von

Charlyn Dörnte

aus Duisburg

Miltenyi Biotec, Bergisch Gladbach

2025

Betreuer:	Prof. Dr. Holger Winkels
Referenten:	Prof. Dr. Florian Klein
	Prof. Dr. Kay Hofmann
Datum der mündlichen Prüfung:	12.11.2024

Table of Content

Introduction 1
The role of antigen-specific T cells in disease 1
Innate immune cell activation is a prerequisite for antigen-specific T cell responses 2
T-cell development in the thymus 5
T cell activation is induced by three signals 8
T cell effector functions 9
Pathways of peptide-MHC Class I and II assembly and peptide loading 11
The role of HLA polymorphisms in T-cell epitope identification 14
Immune responses in SARS-CoV-2 infections 17
Aim of this project 21
Methods 23
Peptide design for *in vitro* stimulation approaches 23
PMBC isolation from whole blood 23
Expansion of antigen-specific T cells 24
Sequential Walk – an *in vitro* stimulation assay 24
In silico peptide-binding prediction analysis 26
Assessment of neutralizing-antibody titers 26
T cell stimulation with SARS-CoV-2 PepTivators® 27
MHC-monomer synthesis 27
Coupling of biotinylated PMMA beads to MHC-monomers 28
Multiplex HLA-binding assay 28
Dissociation and immunological phenotyping of bladder carcinoma samples 29
Isolation of neutrophil granulocytes 29
DNA Extraction for whole exome sequencing 30
Data analysis and statistics 30
Results 31

First-generation vaccines provide immunological memory against SARS-CoV-2 B.1.1.529 variant 31

Sequential *in vitro* T-cell stimulation and *in silico* NetMHC(II)pan approaches enable the identification of SARS-CoV-2-specific T-cell epitopes 41

T cell epitope mapping in SARS-CoV-2 structural proteins 46

Unfavorable HLA molecules cause prolonged disease and decreased frequencies of virus-specific $CD8^+$ T cells 48

Concept and establishment of a multiplex HLA binding assay 56

Human bladder carcinomas: a potential model system to identify neoantigens via MHC multiplex analyses 63

Discussion 67

SARS-CoV-2 T-cell epitopes and role of low affinity binders 67

Immunogenic protein regions differ between vaccinated and convalescent individuals 69

Low frequencies of virus-specific $CD8^+$ T cell responses accompanied by high bystander activation is observed in more severe COVID-19 71

T-cell immunity is preserved against SARS-CoV-2 B.1.1.529 in individuals vaccinated with 1^{st} generation COVID-19 vaccines 72

Introducing a new tool for the efficient identification of MHC-binding peptides and recognition by cognate T cells 74

Bladder carcinoma presents with a potential high mutational burden and varying numbers of immune cell infiltrates 75

Conclusions 76

References 79

Appendix 85

Supplementary Information 85

List of Abbreviations 145

List of Reagents 148

List of Devices 150

List of Consumables 151

List of Software 152

Acknowledgements 153

List of Publications 154

Declaration / eidesstattliche Erklärung 155

Introduction

The role of antigen-specific T cells in disease

The human immune system evolved to protect the organism against invading pathogens and harmful processes associated with cellular changes like cancer. It is divided into two main arms: the innate and the adaptive immune system. Innate immunity is the first line of defense and is essential for the recognition of the invading pathogen as foreign. Innate immune cells react fast through non-specific pathways, thereby initiating a first immune response. Depending on the immune cell subtype, innate immune cells directly kill severely damaged cells or extracellular pathogens through different mechanisms. However, the action of those cells alone is insufficient to effectively protect the organism from the magnitude of different and constantly mutating pathogens.

In contrast, *adaptivity* is defined as the ability to change in order to suit changing conditions.[1] This marks the most crucial characteristic of the adaptive immune system. Its response is raised highly specified for distinct pathogens and thereby able to respond target-specific. It is built up from cellular and humoral components. T lymphocytes and B lymphocytes (from now on referred to as *T cells* and *B cells*) belong to the cellular compartment of the adaptive immune system. They can act target-specific by recognizing specific antigens to protect the organism against damage induced by cancer or invading pathogens like viruses through non-redundant effector functions. Additionally, the development of longed-lived memory cells enables fast immune responses by T- and B-cells upon reinfection with the same pathogen, which is the underlying mechanism allowing vaccination.

Antigen-specific T cell responses play a key role in the successful clearance of viral infections and cancer cells. Upon infection of a host cell with a viral entity, e.g., with the severe respiratory syndrome coronavirus 2 (SARS-CoV-2), the host cellular replication machinery is forced to produce new virions that finally become assembled and lead to the death of the host cell upon their release into the extracellular matrix. However, the presentation of virus-derived peptides on cell-surface major histocompatibility complex (MHC) molecules by innate, antigen-presenting cells (APCs) and presentation to T cells ensures the recognition, activation, and subsequent killing of infected cells by virus-specific cytotoxic cluster of differentiation- (CD) 8^+ T lymphocytes (CTLs). In addition, the secretion of virus-neutralizing antibodies by B cells, which represent the humoral compartment of adaptive immunity, depends on the help of activated virus-specific $CD4^+$ T helper cells.

In contrast to viral infections, cancer is a diverse set of pathologies initially defined by six functional hallmarks, including a sustained proliferative signal, resistance to cell death, evasion from growth suppressors, induction of angiogenesis, activation of invasion and metastasis, and enabling of replicative immortality.[2] One characteristic that enables the acquisition of multiple of these cancer hallmarks is the genomic instability and accumulation of mutations in cancer cells.[3] Antigens arising from mutated proteins exclusively expressed by the cancer cell, so-called neoantigens, are promising targets for immunotherapies. Neoantigen-specific T cells, in turn, directly kill cancer cells upon recognition and orchestrate anti-tumor immune responses.

Given the importance of antigen-specific T cells, e.g., for cancer- and virus-related pathologies, the identification of the specific epitopes, i.e., the peptide structures recognized by the T cells, is fundamental for the basic understanding of immunopathological processes within a specific disease and, in particular, for the development of therapeutic approaches.

In the following sections, first, mechanisms for activation of the innate immune system, regarding the initiation of an immune response will be shortly introduced. Afterward, T cells' maturation and differentiation process, as cellular players of the adaptive immune system and focus within this project, will be explained. Therein, special attention is given to the molecules and receptors contributing to T cell activation. Second, the kinetics within a perfect generic immune reaction are explained before; third, recapitulating the immune response and kinetics in SARS-CoV-2 infections. Finally, the specific aims of this Ph.D. project are introduced.

Innate immune cell activation is a prerequisite for antigen-specific T cell responses

Innate immunity is the first line of defense, which reacts non-specifically and early after infection to prevent (further) damage to the organism, thereby providing an initial danger signal and mounting an adaptive immune response. Differentiating from the hematopoietic stem cells, different cell types mature into cellular players of the innate immune system: macrophages, dendritic cells (DCs), natural killer (NK) cells, as well as neutrophil-, eosinophil-, and basophil granulocytes. These largely tissue-resident cells all have different effector functions, including direct killing capacities, phagocytosis, and signaling, which will be partially discussed later in this thesis. A central function of DCs and macrophages (and B cells) is the pathogen recognition, uptake, processing into small peptides, and final presentation of those peptides to mature naïve lymphocytes. Therefore those cells are called APCs. This presentation of virus-derived peptides aims for the activation of adaptive immune cells. However, the first step in initiating pathogen

uptake and processing into peptides is the recognition of an invading microbe as foreign. This process requires the detection of pathogen-associated molecular patterns (PAMPs) or damage-associated molecular patterns (DMAPs) by pathogen recognition receptors (PRRs) that are expressed on the outer cell membrane, for the recognition of extracellular microbes, or intracellularly, for the recognition of intracellular microbes. There are four main classes of PRRs: (1) Toll-like receptors (TLRs), (2) NOD-like receptors (NLRs), (3) C-type lectin receptors (CLRs), and (4) retinoic acid-inducible gene I (RIG-I)-like receptors (RLRs). Upon recognition of a foreign species or cellular damage, a receptor-specific intracellular signaling cascade is initiated, leading to the expression of pro-inflammatory genes. For example, receptors involved explicitly in anti-SARS-CoV-2 immune responses are members of the RLR family, RIG-I, and melanoma differentiation-associated protein 5 (MDA5), which both recognize viral RNA and DNA within the cytosol of infected cells.[4,5] The specific recognition of viral RNA is mediated via the interaction of the RIG-I receptors' carboxy-terminal domain (CTD) with di- or triple phosphorylated 5' ends and non-methylated 2'O-groups of the first nucleotide of viral RNA molecules. These molecular structures are specific to viral RNA (**Figure 1**).[6,7] The specific working mechanism of MDA5 remains to be elucidated. The induced expression of pro-inflammatory genes leads to the recruitment and activation of additional innate immune cells, including phagocytes, like macrophages and dendritic cells. To date, numerous innate immune receptors have been described as recognizing distinct molecular structures.[8] However, this repertoire is insufficient to target the variety of pathogens the human organism can potentially encounter, and neither does the action of innate immune cells alone resolve severe infections. Upon death of the infected host cell, cellular and viral proteins are exposed into the extracellular matrix by induced apoptosis or viral budding. As mentioned before, for an effective viral clearance from the host organism, APCs take up and process those cellular and viral components to single peptides for the subsequent presentation to and hence activation of cells of the adaptive immunity. In turn, the activated adaptive immune cells are equipped with the potential to act pathogen-specific and build an immunological memory, which is essential for an effective clearance of the microbe from the organism and a fast response upon re-infection, respectively. To successfully present pathogen-derived peptides to T cells, those peptides are loaded onto MHC Class I and Class II molecules expressed on the APC. These complexes are therefore termed peptide-MHC (pMHC) complexes. The molecular processes involved in the peptide loading onto MHCs and presentation to T cells will be explained in detail in the following chapters.

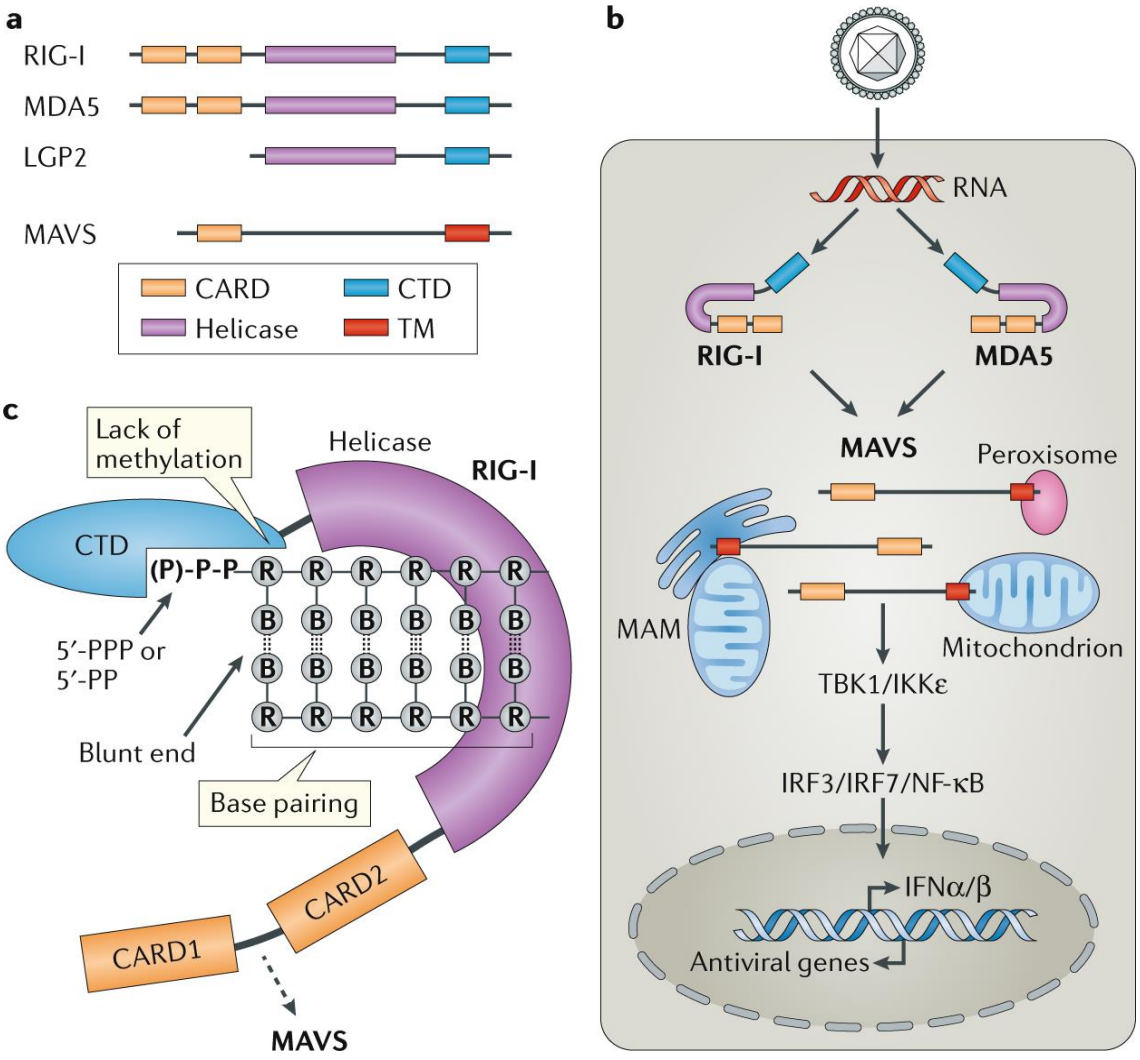

Reprinted from "RIG-I-like receptors: their regulation and roles in RNA sensing"
Rehwinkel, J., & Gack, M. U. ; *Nature reviews. Immunology* (2020)
Retrieved from: https://doi.org/10.1038/s41577-020-0288-3

Figure 1. RLR structure and activation process. (A) Illustrative structure of mitochondrial antiviral-signaling protein (MAVS) and retinoid acid-inducible gene I (RIG-I)-like receptors (RLRs): RIG-I, melanoma differentiation-associated protein 5 (MDA5) and laboratory of genetics and physiology 2 (LGP2). RLRs consist of a carboxy-terminal domain (CTD) and a Helicase domain. RIG-I and MDA5 additionally include two caspase activation and recruitment domains (CARDs) that are important for signaling. **(B)** Signaling pathway of RIG-I and MDA5. Upon binding of viral RNA, the receptors undergo a conformational change that allows CARD domains to multimerize with CARD domains expressed by MAVS proteins expressed on peroxisomes, mitochondria, and mitochondrial-associated membranes (MAM). This triggers the signaling via a TANK-binding kinase 1 (TBK1) and IκB kinase-ε (IKKε). These kinases transduce the signal to transcription factors interferon regulatory factor 3 (IRF3) and IRF7 as well as to nuclear-factor-κB (NF-κB), which induce expression of type I interferons and other antiviral genes. **(C)** Recognition and binding of viral RNA to RIG-I. Viral RNA is recognized by its di- or triple phosphorylation at the 5'-end, which interacts with the CTD domain, and the lack of methylation of 2'-O group of the first nucleotide, while the residual RNA molecule binds to the Helicase domain. Here, base-pairing takes place. This induces a conformational change to an active state, enabling the multimerization of CARD domains.

T-cell development in the thymus

Target-specificity, as adaptive immune cells' major characteristic, enables tailored and timely limited immune responses against invading pathogens. In T cells and B cells, target-specificity is reached by the T cell receptor (TCR) or B cell receptor (BCR) in B cells, which specifically recognize and, therefore, solely react against cognate antigens presented by the APCs. Fully differentiated and mature T cells express a functional TCR and a CD4 or CD8 co-receptor molecule. The latter defines the cellular sub-lineages of T cells, which bear different effector functions. The development of mature naïve T cells, i.e., a T cell expressing a yet pathogen-unexperienced functional TCR, starts within the thymus (**Figure 2**). Lymphoid progenitor cells enter the thymus via high endothelial venules at the cortico-medullary junction. During the first developmental steps, these progenitor cells pass through four double negative (DN) stages (DN 1 to DN4), as they do not express any CD4 or CD8 co-receptor molecules. During these stages, cells proliferate before they initiate the expression of a pre-TCR, consisting of a mature TCR β-chain and an invariant pre-Tα-chain. After successfully expressing the TCR β-chain, genes for the TCR α-chain are rearranged, forming a complete TCR. At this stage, the developing T cell expresses both CD8 and CD4 co-receptor molecules and is therefore said to be double-positive (DP). Here, the selection process starts, as cortical thymic epithelial cells present a specific set of self-peptides to the DP cell. The lack of affinity to bind to self-MHC class I and II molecules and downstream signaling leads to cell death due to insufficient survival signals. In contrast, cells with a particular affinity are positively selected. DP-lymphocytes recognizing MHC Class I molecules become single-positive for the expression of CD8, while those cells recognizing MHC Class II molecules maintain to express CD4 co-receptor molecules solely. Both single-positive cellular subsets cells start to express the chemokine receptor CCR7 and migrate to the thymic medulla. There, cells interact with $CCL19^+$ and $CCL21^+$ APCs, such as medullary thymic epithelial cells or dendric cells that present self-peptides. A strong recognition of these self-peptide MHCs leads to the depletion of those lymphocytes via apoptosis to prevent autoimmunity. This process is called negative selection.[9] However, for the sake of completeness, it is important to mention that a small proportion of developing lymphocytes that recognize self-peptide with an intermediate strength survive and differentiate into natural killer T cells (NKT cells) and T-regulatory cells (Tregs). These cells play an essential role in preventing autoimmunity.

To react against a broad variety of pathogens, the total pool of T cells need to recognize as many pathogen-derived peptides as possible. This is ensured by the genomic recombination of

gene segments, which encode for the variable, antigen-binding regions of the α- and β-chain of the TCR. A process which is called VDJ-recombination. Herein, the Variable- (V), Diversity- (D), and Joining (J) gene segments encoding for a complete TCR β-chain and Variable and Joining-gene segments encoding for the partnering TCR α-chain are genetically recombined. Together, these genes encode for a complete TCR and, therefore, its target protein-interaction site (**Figure 3**). Within this process, recombination activation gene (RAG) recombinases specifically cut DNA segments, which are rejoined at the produced boundaries to ensure the generation of functional receptor chains. Each individual bears approximately 50 functional V-gene segments, 27 functional D-gene segments, and six functional J segments.[10] The expression of a functional TCR after successful recombination of the genes mentioned above leads to allelic exclusion, which prevents the induction of additional recombination from the second alleles provided by the double, maternally and parenterally inherited chromosome set. Thereby, it is ensured that T cells with only a single specificity develop.[11,12] However, failed TCR gene recombination leading to a non-functional TCR can be rescued through recombination of the second allele set, generally increasing the chance for the expression of a functional TCR. At the same time, this second set of alleles within the human genome contributes to an even greater diversity of potential TCR specificities. Another factor contributing to the increased diversity of TCRs and their specificities represents the junctional diversity arising from imprecise joining recombined gene segments. Together, these processes lead to an exceptional diversity of, in total, 10^{18} different possible TCR specificities.[9] As a result, every individual expresses a unique set of different TCR specificities, which makes investigations of antigen-specific T cell responses and those that apply to a general public very complex. A similar process for the BCR ensures polyclonality of the B cell compartment.

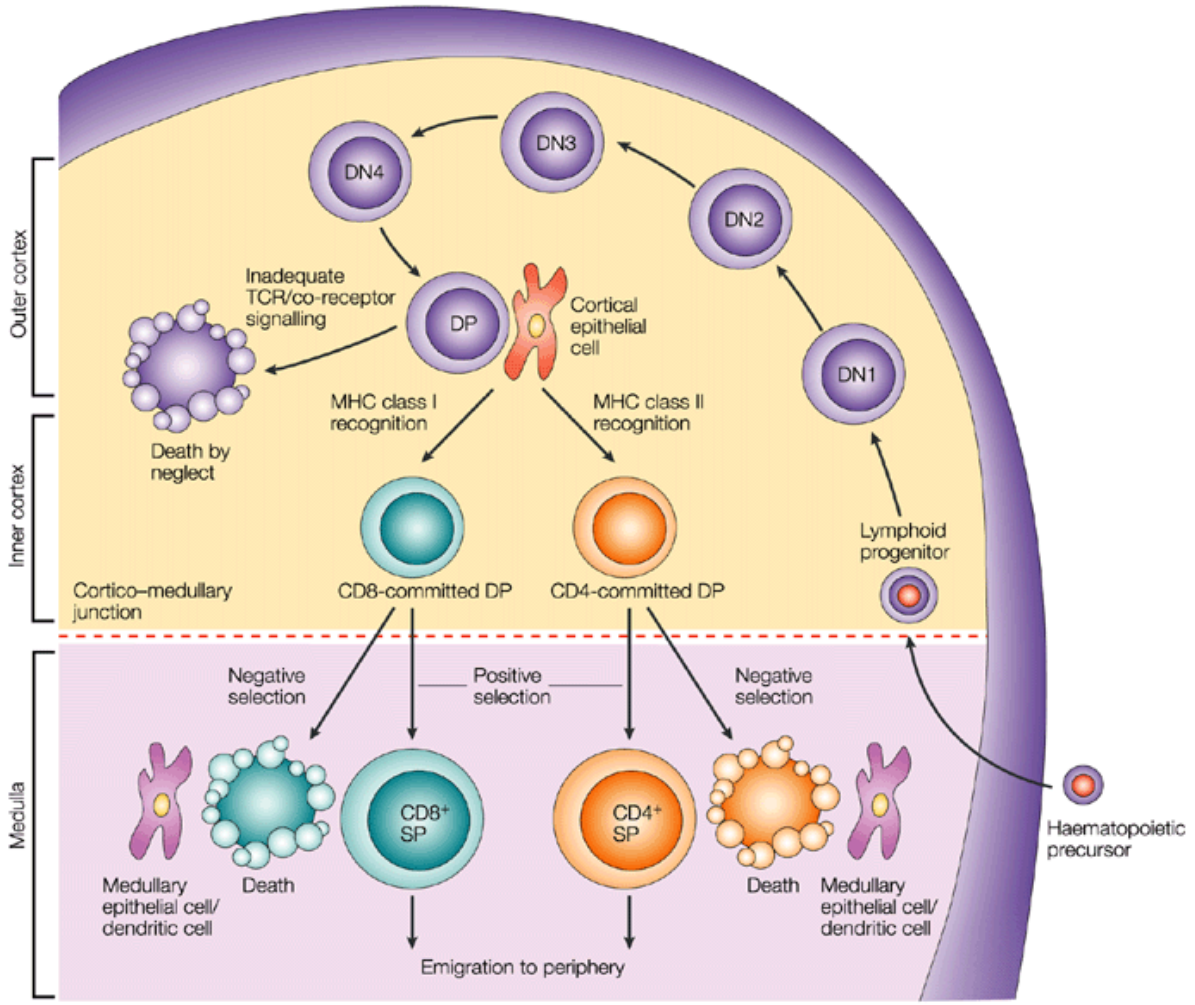

Reprinted from "T cell development and the CD4-CD8 lineage decision" by Ronald N. Germain (2002)
Retrieved from: https://www.nature.com/articles/nri798

Figure 2. Development of T lymphocytes in the thymus. The development of T cells is initiated by the entry of lymphoid progenitor cells into the thymus at the cortico-medullary junction. Here, maturation of the progenitor cells starts as double negative (DN) cells, i.e. the absence of CD4 or CD8 co-receptor molecules, and the initial proliferation. During further development cells start to express a pre-T cell receptor (preTCR), consisting of a fully rearranged TCR β-chain and a pre Tα-chain, which leads to further proliferation of cells, followed by the double positive (DP) expression of CD4 and CD8 co-receptor and the initiation of TCR α-chain gene rearrangement. At this DP-stage cells undergo a first selection process, by the interaction of the fully arranged αβTCR with self-peptide Major histocompatibility complex (MHC) Class I and Class II molecules expressed on cortical epithelial cells. Too weak interactions thereby lead to death by neglect, while too strong interaction causes apoptosis (negative selection) to prevent auto-immune reactions. Finally, cells that interact with intermediate strength are positive selected and mature into single positive CD4+ or CD8+ T cells, recognizing pMHC Class II and pMHC Class I, respectively. These cells finally migrate into the periphery.

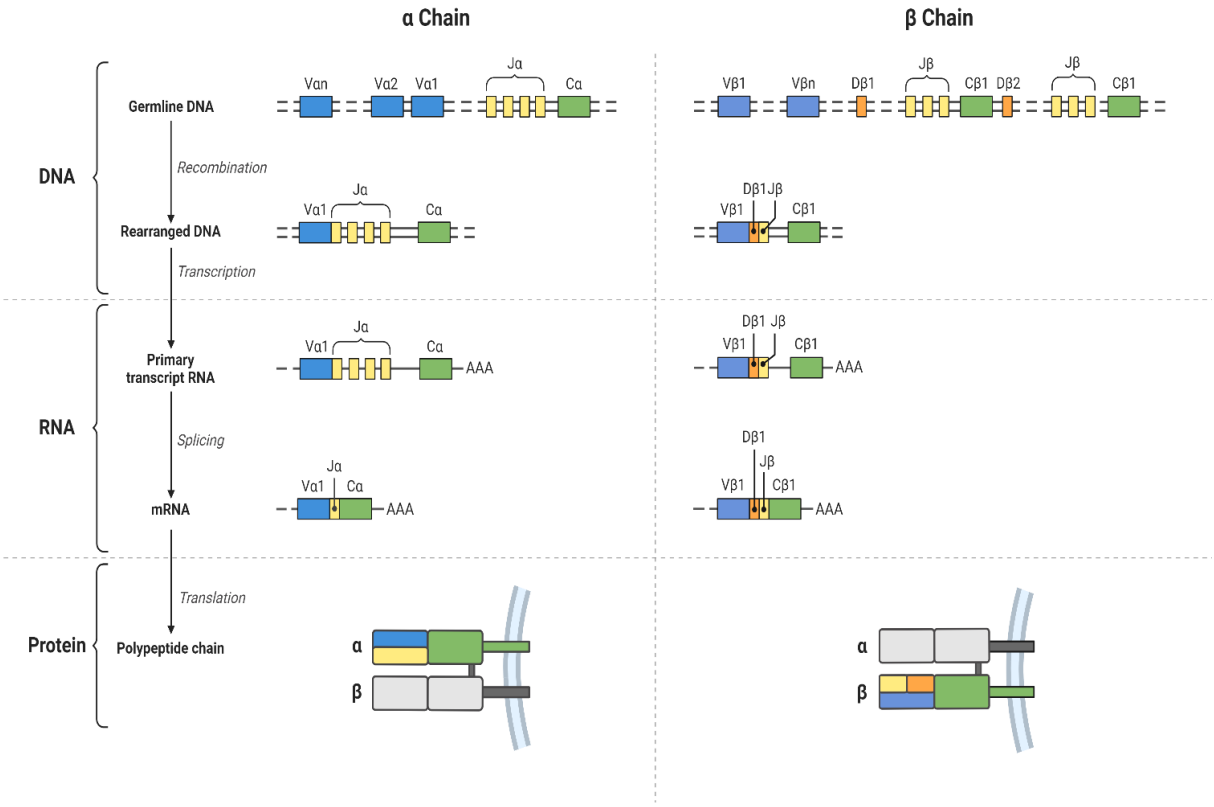

reprinted from "T cell receptors (Alpha and Beta Chain)" by Akiko Iwasaki (2020)
Retrieved from https://app.biorender.com/biorender-templates/figures/all/t-5f4445e74e6d2f00ac0ec2cb-t-cell-receptors-alpha-and-beta-chains

Figure 3. Rearrangement of the V(D)J gene segments for the formation of a functional T cell receptor. For the assembly of a functional T cell receptor (TCR), first, the V(D)J gene segments are rearranged, before being transcribed, spliced and translated into a functional β- and α-chain. This procedure starts with the recombination of D- and J-gene segments of the β-chain. Afterwards, also the V-gene segments are rearranged. The fully rearranged DNA is transcribed and spliced into a functional RNA chain that is translated into a functional β-chain. This procedure is repeated for the α-chain, which lacks the D-gene segments. The numerous gene segments, and their rearrangement allows the expression of a variety of different TCR molecules that are able to recognize multiple different pMHC combinations.

T cell activation is induced by three signals

After successful expression of a functional TCR and passage through the selection processes in the thymus, the mature naïve $CD4^+$ or $CD8^+$ T cell migrates into the periphery to home into the paracortical area of a lymph node via high endothelial venules (HEVs).[13,14] Next to T cells, professional APCs, like DCs and B cells, infiltrate these secondary lymphoid organs. Activated DCs expressing pMHC complexes on their surface interact with T cells expressing a cognate TCR binding to both a portion of the MHC as well as a pathogen or cancer peptide presented via the MHC. Through this interaction, pathogen-derived or damage-associated peptides are activating the T cell. Those peptides that are recognized by the T cell are termed *T cell epitopes*, while the ancestor protein is called *T cell antigen*. Next to this TCR-pMHC interaction (Signal

1), two additional signals are needed that initiate a complete activation of the antigen-specific T cell: (Signal 2) signaling via CD28 and CD80 / CD86 and other co-stimulatory molecules and (Signal 3) signaling via cytokines secreted by the DC that are interacting with cytokine receptors present on the T cell (**Figure 4**; left box: "Co-stimulation"). After this activation, a process also called *T cell priming*, the T cell starts to proliferate, accompanied by the autocrine secretion of IL-2.[15] Other cytokines secreted by the DC, which will be introduced in a later section, in turn, lead to the differentiation of activated T cells into effector $CD8^+$ and $CD4^+$ T cells. To terminate this interaction, the CD28 interaction is replaced by the competitive CD80/CD86-binder CTLA-4. This termination procedure allows for tight regulation of the inflammatory response and prevents explicitly over-activation (**Figure 4**; right box: "Co-inhibition").[9]

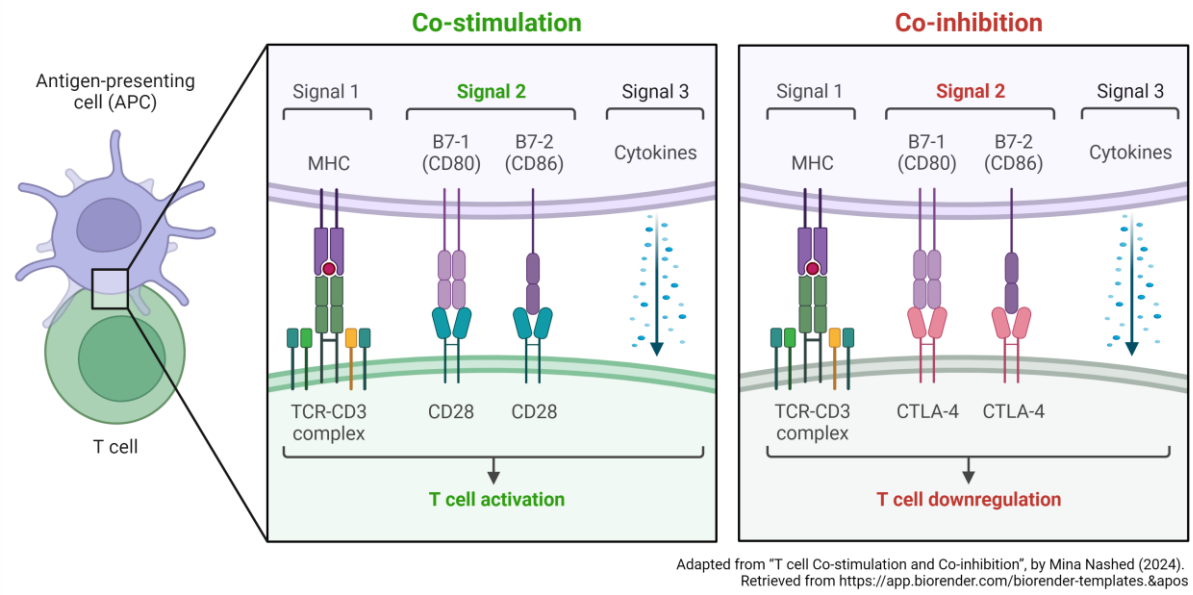

Figure 4. Stimulatory and inhibitory signals contributing to T cell activation and downregulation. Upon activation of naïve T lymphocytes, the cell first receives three stimulatory signals (left box; "Co-stimulation): (1) Interaction of MHC class I or class II molecules, which are expressed on any somatic cell or antigen-presenting cells, respectively, with a cognate TCR, (2) the interaction of B7-1/-2 with CD28; and (3) the secretion of pro-inflammatory cytokines. To terminate the T cell activation process (right box; "Co-inhibition"), i.e., to prevent overstimulation, the B7-1/-2 interaction is replaced with binding to the antagonistic cytotoxic T-lymphocyte-associated protein 4 (CTLA-4).

T cell effector functions

As described, cytokines secreted by the APC upon activation induce the proliferation and differentiation of T cells. Specifically, the activation of naïve $CD8^+$ T cells leads to their

differentiation into cytotoxic T cells (CTLs), which involves the signaling through various cytokines, including type-I interferons and IL-12.[16,17] Once migrated into the periphery, these cells can directly recognize, e.g., virus-infected cells in a pMHC Class I-dependent manner. After recognition of the cognate antigen, the CTL kills the target cell via different mechanisms: (1) extrinsically via the induction of FasL-mediated apoptosis, or (2) intrinsically via the release of cytotoxic granules containing Perforin, Granzyme, and Granulysin that together initiate the release of cytochrome c from target-cell mitochondria, which in turn induce the activation of DNA-cutting caspase enzymes.[9]

In comparison to CTLs, a direct killing capacity of $CD4^+$ T cells has also been described[18]. However, details of a killing mechanism remain to be investigated. In contrast, $CD4^+$ T cells mainly differentiate into various lineages of T helper cells, depending on the peptide-origin and cytokine signal they receive upon interaction with the APC: T_H1, T_H2, or T_H17 effector $CD4^+$ T cells (**Figure 5**). These cellular sub-lineages support the activation of CTLs and/or innate immune cells by releasing different pro-inflammatory cytokines, thereby orchestrating the cellular immune response. Antigens derived from intracellular pathogens, like bacteria or viruses, induce the release of IL-12 and INF-γ by the APC, activating intracellular STAT1 / STAT4 signaling. As a response, the T–bet–expressing T_H1 differentiated cell releases INF-γ, a proinflammatory cytokine which, upon other functions, supports macrophage activation and $CD8^+$ T cell-driven responses. Instead, extracellular parasites induce the release of IL-4 by the APC, activating intracellular STAT6 signaling. In response, $CD4^+$ T cells differentiate toward GATA3-expressing TH2 cells, releasing mainly IL-4, IL-5, and IL-13, which support the activation of mast cells, eosinophils, and basophil granulocytes. Lastly, extracellular bacteria and fungi induce the release of IL-6, IL-23, IL-1β, and TGF-β from the APC, which in turn induces intracellular STAT3 signaling in the activated T cell. The resulting RORγt-expressing T_H17 T cells release IL-17, which recruits neutrophil granulocytes to the site of inflammation. Additionally, as a response to all pathological and infectious entities presented as peptides to naïve $CD4^+$ T cells, the lymphocyte differentiates into T follicular helper cells (T_{FH} cells). These specialized cells play an essential role in supporting the affinity maturation and class switching of B cells and their BCR within the germinal center reaction of lymph nodes, as they provide survival signals to those B cells that successfully present peptides on MHC Class II molecules with high affinity. This ensures the production of high-affinity antibodies and long-lived antibody-producing plasma cells.

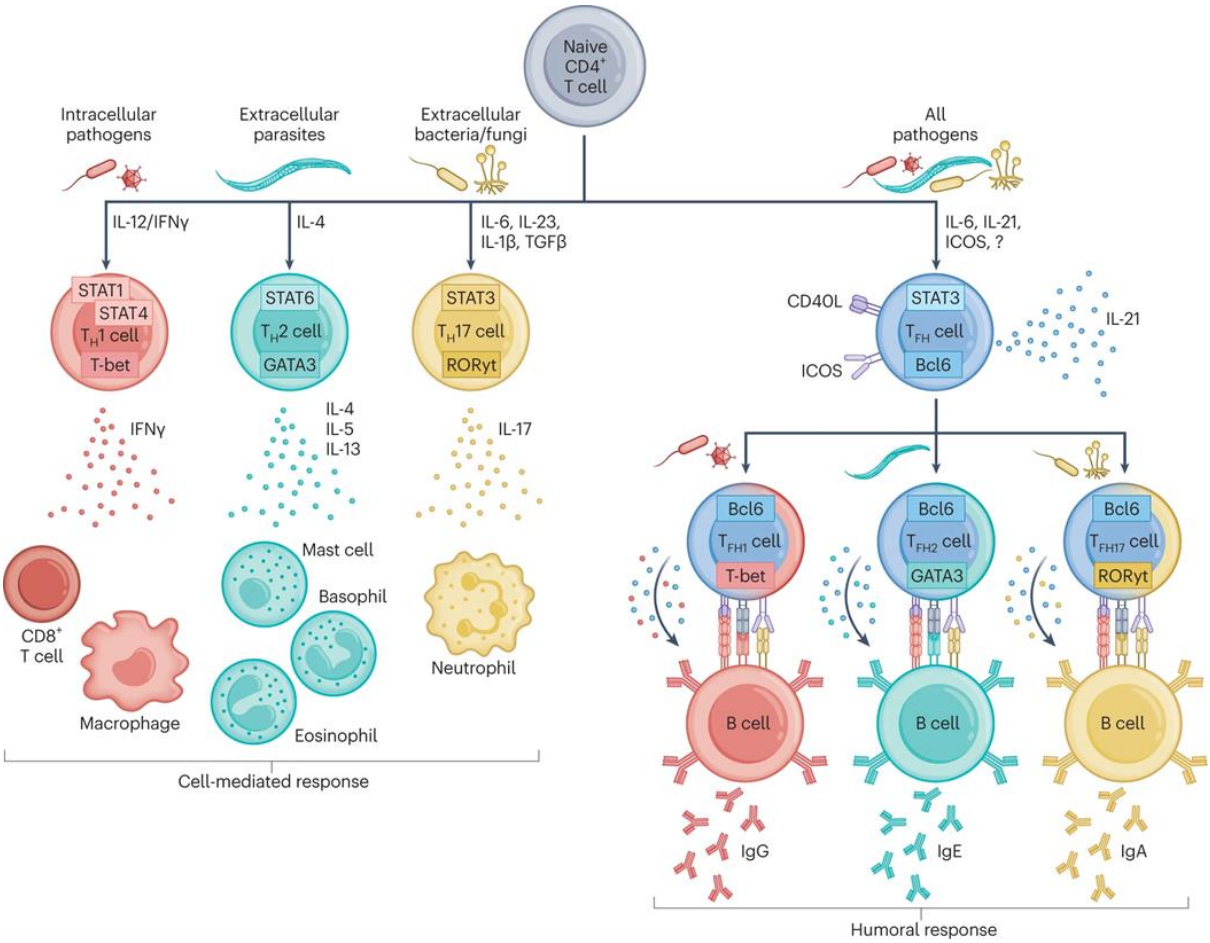

Reprinted from "CD4+ T cell memory" by Künzli & Masopust (2023)
Retrieved from (DOI:) 10.1038/s41590-023-01510-4

Figure 5. Differentiation of CD4$^+$ T cells into activated effector cells. Depending on the various sources and types of pathogens, the cytokine signals secreted upon CD4$^+$ T cell activation differ and initiate differentiation and maturation into various effector cells. Intracellular pathogens, triggering the secretion of IL-12 and IFN-γ and intracellular STAT1 and STAT4 signaling, lead to differentiation towards T_H1 cells that support cytotoxic CD8$^+$ T cell and macrophage responses. Extracellular parasites, initiating secretion of IL-4 and intracellular STAT6 signaling, lead to differentiation towards T_H2 cells. They amplify the responses by the innate immune cells, i.e., mast cells, basophils, and eosinophils. Lastly, extracellular bacteria or fungi initiate the secretion of IL-6, IL-23, IL-1β, as well as TGF-β and subsequent intracellular STAT3 signaling, leading to differentiation into T_H17 cells. This leads to support of the immune response by neutrophil granulocytes. Additionally, all pathogens induce the differentiation into follicular T helper cells (T_{FH} cells) by signaling via, e.g., IL-6, IL-21, and ICOS and subsequent intracellular STAT3 signaling. Those cells play a key role in supporting the B cell affinity maturation and class switching through the expression of the transcription factor Bcl6, leading to the secretion of high-affinity antibodies by long-lived plasma cells.

Pathways of peptide-MHC Class I and II assembly and peptide loading

As described, the adaptive immune system is activated by the presentation of pathogen-derived peptides to antigen-unexperienced lymphocytes that subsequently proliferate and differentiate into effector and memory cells. Hence, professional APCs, like dendritic cells, fulfill an

interconnecting function of innate to adaptive immunity. In this process of peptide presentation, peptides are generated and loaded onto MHC Class I and MHC Class II molecules, which interact with TCRs on $CD8^+$ and $CD4^+$ T cells, respectively. The cellular pathways through which peptides are generated and loaded onto MHC Class I and II molecules differ (**Figure 6**). Intracellular proteins are processed by the proteasome into small peptide fragments. These peptides are subsequently transported via the transporter associated with antigen processing (TAP) into the endoplasmic reticulum (ER). There, peptides are loaded onto MHC Class I molecules to form a stable pMHC complex. From the ER-membrane transport vesicles carrying the assembled pMHC complexes are formed, aimed for the transport to and finally the expression on the outer cell membrane of the APC but also nearly every somatic cell (**Figure 6**; A "MHC Class I Pathway).[19] Contrastingly, peptides presented on MHC Class II molecules are mainly originating from extracellular proteins and, unlike to MHC class I molecules, MHC class II-expression is restricted to APCs. Those proteins are taken up by phagocytosis, macropinocytosis, or endocytosis. The produced phagosome, macropinosome, or endosome fuse with protease-containing lysosomes to process antigens into small peptide fragments. Simultaneously, MHC Class II molecules are assembled within the ER and stabilized by an invariant chain (Ii) that binds with the MHC class II-associated invariant chain peptide (CLIP) protein to the peptide binding cleft of the MHC molecule. The MHC molecule is transported by lysosomes into the cytosol and melts with the peptide-containing endosome. Here, the Ii is replaced by cognate peptides that bind stably to the MHC peptide binding cleft. The fully assembled pMHC class II complex is transported to and expressed on the outer cell membrane of antigen-presenting cells as DCs, B cells, and macrophages (**Figure 6**; B "MHC Class II Pathway).[20]

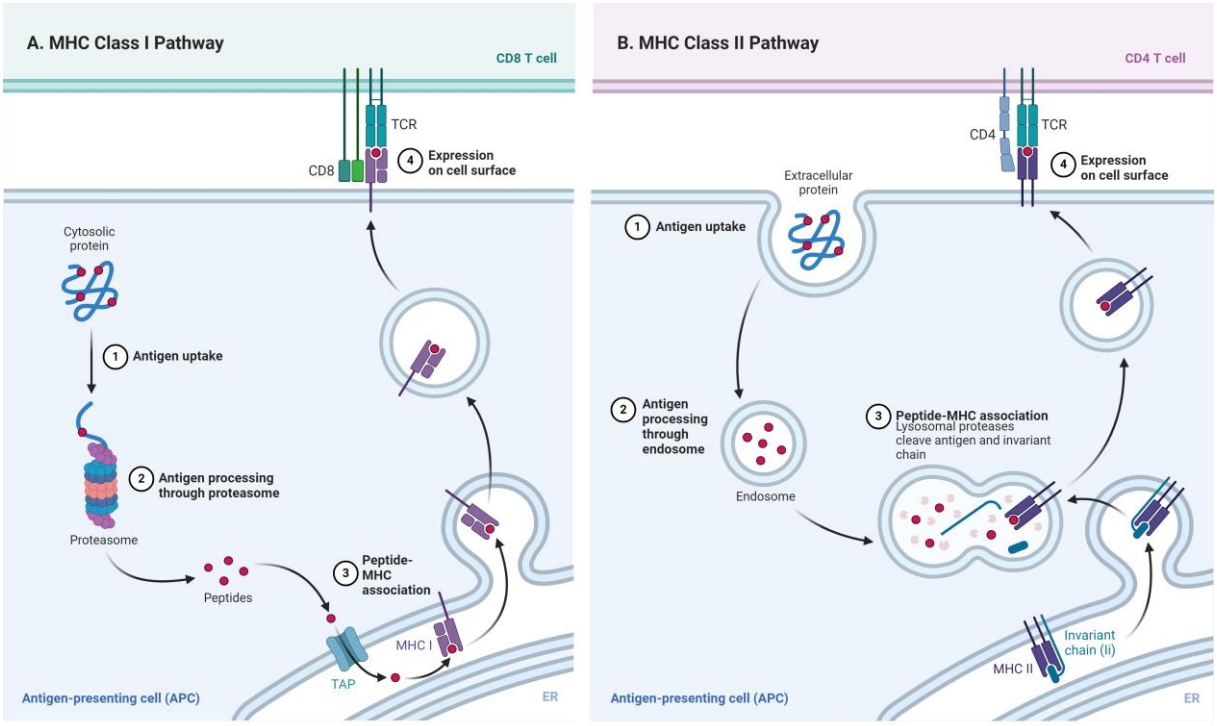

Figure 6. Cellular expression pathways of MHC Class I and MHC Class II molecules. (A) Cytosolic proteins are degraded by the proteasome into peptides that subsequently migrate via the transporter associated with antigen processing (TAP) into the endoplasmic reticulum (ER). There, peptides anchor to the MHC class I molecule to form a stable complex (pMHC). Finally, the protein complex is transported via vesicles to the cell membrane. pMHC class I molecules successfully expressed on the cell surface are recognized by cognate TCRs of $CD8^+$ T cells. **(B)** Extracellular proteins are taken up by an antigen-presenting cell (APC) via endocytosis. Within the formed endosomes, proteins are degraded into peptides. Simultaneously, non-mature MHC class II molecules assembled within the ER and stabilized by an invariant chain (Ii) that binds to the peptide-binding groove are transported in lysosomes to fuse with the peptide-containing endosomes. Within these endolysosomes, the Ii is replaced by an antigen peptide. Finally, the pMHC class II molecule is transported to the membrane for expression on the outer cell surface, where it interacts with cognate TCRs of $CD4^+$ T cells.

A cellular process that allows the presentation of extracellular pathogens on MHC class I molecules is called *cross presentation*. This process is of central importance for the priming of $CD8^+$ T cells with specificity for viral- or tumor-antigens that did not infect APCs but any other somatic cell that itself does not have the capability of antigen presentation.[21] Even though the exact mechanism of peptide cross-presentation is not yet fully resolved, several theories exist on how extracellular antigens are released into the cytosol and loaded onto MHC class I molecules. The most likely pathway involves the release of exogenous proteins from the endosome, followed by subsequent degradation by the proteasome into peptides and the translocation of those peptides via TAP into the ER for assembly to MHC Class I molecules.[22]

The role of HLA polymorphisms in T-cell epitope identification

As described, MHC Class I and II molecules fulfill a central role in initiating an adaptive immune response by $CD8^+$ and $CD4^+$ T cells, respectively. Nonetheless, the nature of the immune response is not only influenced by the cellular restriction of the MHC molecules but also by the peptides that are loaded onto the MHC and able to interact with the cognate TCR. Despite its small size compared to the MHC, the peptide contributes to an average of 29% to the complete pMHC-TCR interaction.[23] The molecular structures of the MHC Class I and Class II molecules allow interaction with peptides of different lengths: MHC Class I molecules have an enclosed peptide binding cleft, which is formed by the α1 and α2 sub-domain of the α-chain, binding eight to eleven amino acid-long peptides. Therein, peptides are anchored with their second amino acid within the B-pocket and their last amino-acid residue within the F-pocket (**Figure 7**; A "MHC Class I"). In contrast, the peptide binding cleft of MHC Class II molecules is formed by the β1- and α1-subdomain, which are formed by the two not covalently bound β- and α-chains, respectively. The flexible conformation without fixed anchoring points allows peptides with a median length of 12 to 24 amino acids to bind to the MHC (**Figure 7**; B "MHC Class II").[24] To evaluate the ability of a specific peptide to bind to an MHC, which is defined by the affinity of the peptide to bind to the sequence of the allele, additional aspects need to be considered: The genomic region of the human MHC (from now on also referred to as human leukocyte antigen (HLA)) locus is polygenic and highly polymorphic, with the result that every individual expresses six different genes encoding for HLA Class I (HLA-A, -B and -C) and at least six different genes encoding for HLA class II (HLA-DR, -DQ and -DP).[25] For each of those genes, and especially for HLA Class I genes, numerous alleles exist (**Figure 8**) bearing highly variable regions mainly within the peptide binding interaction site, except for the α1 sub-domain of the HLA Class II molecule (**Figure 9**). Each HLA allele can bind multiple different peptides. Consequently, each individual expresses a nearly unique set of HLA alleles. Together with the heterogeneity within the peptide specificities of TCRs, each individual can react against various pathogens. This bears advantages for protecting humans against pathogens on a population level. However, as a direct consequence of this high diversity, identifying and analyzing pathogen-specific, public T cell epitopes, i.e., T cell epitopes that a large group of individuals shares, is complex and laborious. Specifically, to identify as many T cell epitopes as possible via *in vitro* T cell stimulation approaches, large cohorts of study subjects that cover a diverse background of HLA alleles and TCR specificities are needed. Likewise, the development of cellular T cell-based therapeutics and vaccines requires it to work effectively for a broad public. Hence, both specificities targeted by a cellular therapy, as well as epitopes

included within vaccine formulations, ideally represent highly immunogenic regions that are recognized by as many HLA alleles as possible.

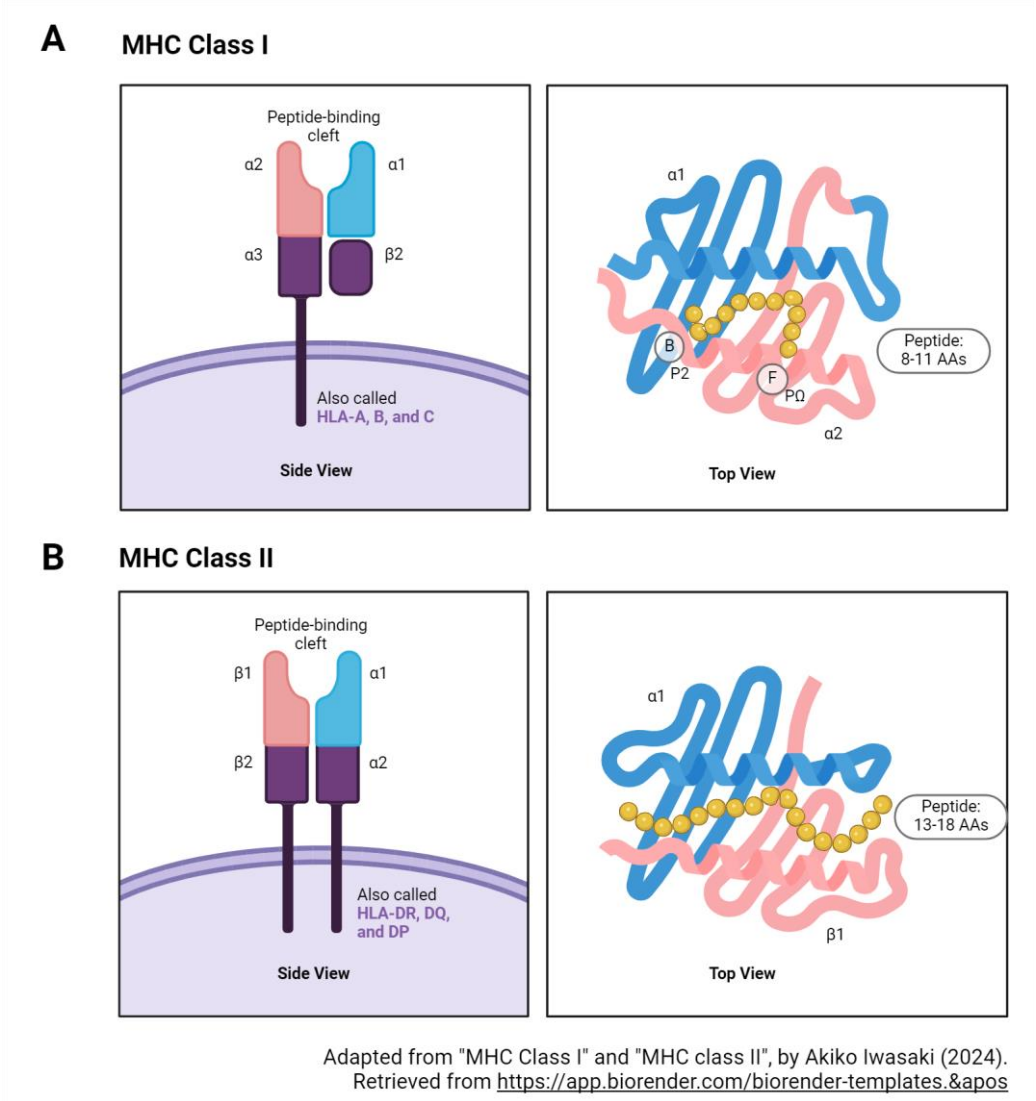

Figure 7. Molecular structure of major histocompatibility complex (MHC) class I and MHC class II molecules. (A) Side view of an MHC class I molecule (left image). The α-chain consists of three subunits (α1, α2, and α3), with α1 and α2 forming the peptide-binding cleft. A top view of the peptide binding cleft (right image) shows the enclosed structure, allowing peptides of a median length of 8-11 amino acids (AAs) to anchor. The B-pocket represents the anchor point for the second peptide residue (P2), while the F-pocket represents the anchor point for the last peptide residue (PΩ). **(B)** Side view of an MHC class II molecule (left image). The peptide-binding cleft is formed by the α1 and β1 subunits of the α- and β-chain, respectively. The top view of the peptide-binding cleft (right image) shows the open conformation, allowing peptides of a median length of 13-18 AAs to anchor.

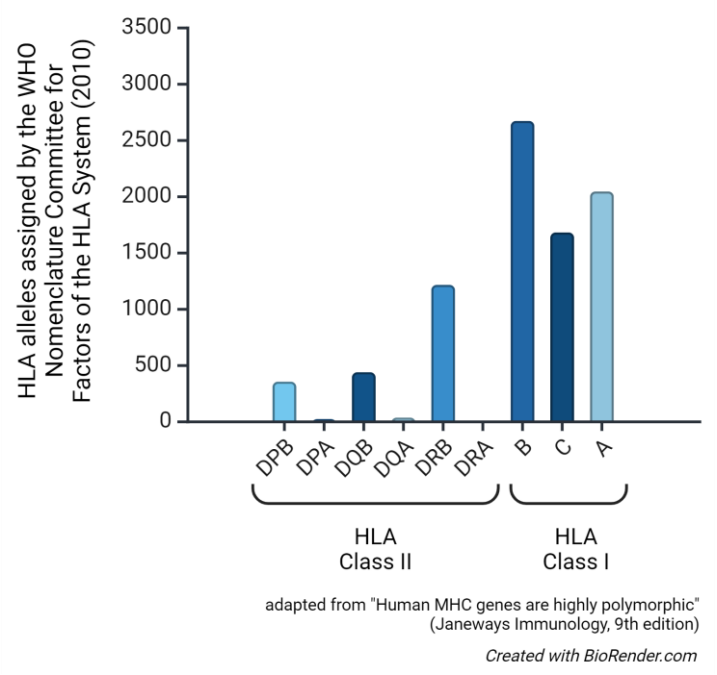

Figure 8. Numbers of HLA molecules assigned by the WHO Nomenclature Committee in 2010. Number of HLA alleles assigned by the WHO Nomenclature Committee for Factors of the HLA System in 2010 for HLA class II (DPB, DPA, DQB, DQA, DRB, and DRA) and HLA class I (B, C, and A) molecules.

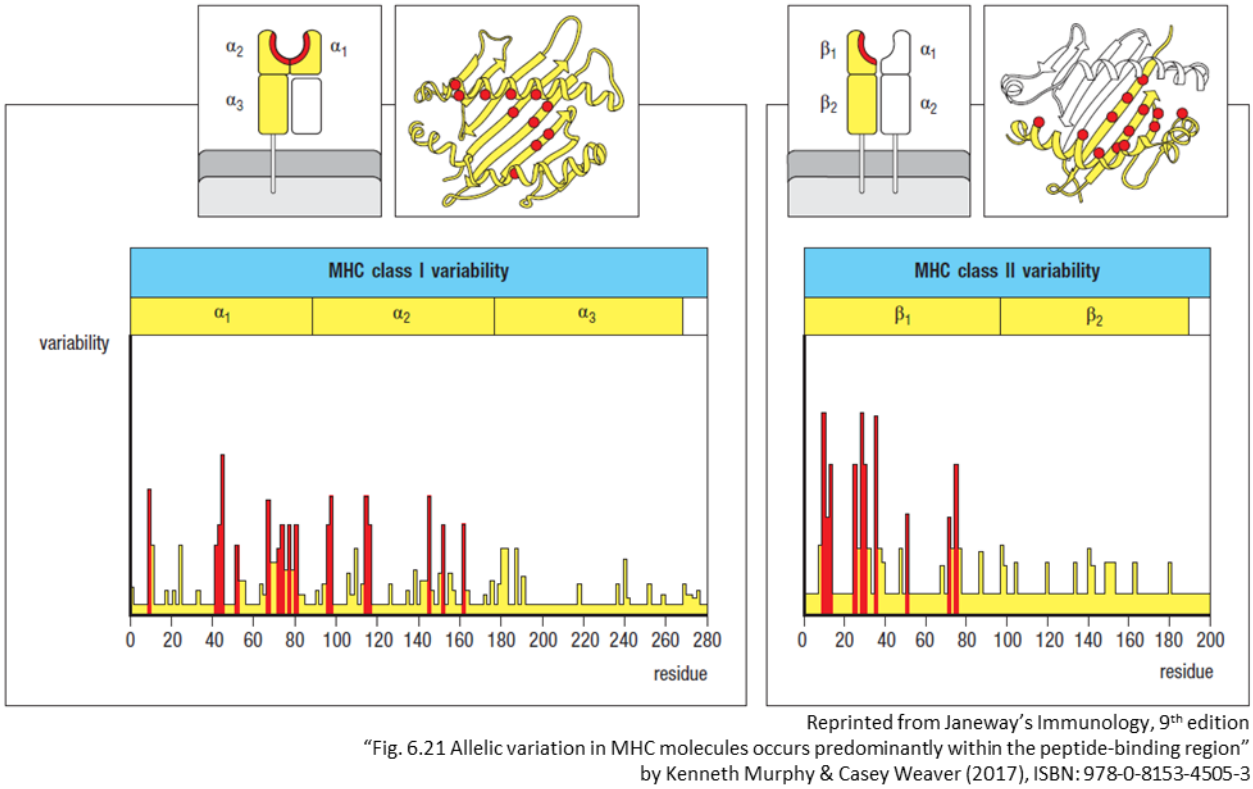

Figure 9. High genetic variability within the peptide-binding regions induces polymorphism among MHC Class I and Class II alleles. The high diversity of peptides presented by either MHC

Class I or MHC Class II molecules results from high genetic variability predominantly found within the peptide binding residues of the molecules. More precisely, the highest variability for MHC Class I alleles is found within peptide-binding residues of the α1- and α2-subdomain, while the α3-domain remains relatively conserved among alleles (left box). MHC Class II molecules, in contrast, show the highest degrees of diversity within the β1-peptide binding subdomain, while the α1-region remains to be conserved. But here, also the non-interacting protein-domains show comparatively slight variation (right box).

Immune responses in SARS-CoV-2 infections

Coronavirus disease 2019 (COVID-19) is a respiratory disease caused by a viral infection with SARS-CoV-2 that requires the development of an effective virus-specific immune response to eliminate the virus from the host. The emergence of SARS-CoV-2 created a nearly unique momentum as the virus, as a novel member of the beta-coronavirus family, spread very fast without any treatment options available at the date of its appearance. Therefore, the World Health Organization (WHO) declared a public health emergency of international concern over the global outbreak of this novel coronavirus in January 2020.[26] Hence, deciphering the immunopathological mechanisms in SARS-CoV-2 infections has been and still is fundamental for the development of effective therapeutics.

Upon entry of SARS-CoV-2 to the host organism, the virion attaches with its Spike protein to the angiotensin-converting enzyme 2 (ACE2) receptor, which is expressed on the outer cell surface of the target cell. Subsequently, a conformational change of the Spike protein allows the target-cell's TMPRSS2 protease to enzymatically cut the protein at the border of the S1- and S2-subunit. Afterward, the activated S2-subunit binds to the target cell membrane, which induces the fusion of the viral and cellular membrane, finally resulting in the release of viral positive-sensed single-stranded RNA into the cytosol (**Figure 10**).[27] This infection of the host cell is sensed by cells of the innate immune system, as explained in the previous chapter. Ideally, the innate immune response initiation is mediated early after infection, as observed in perfect examples of generic infections (**Figure 11**; A).[28] However, SARS-CoV-2 infections are characterized by a variety of possible symptoms and disease courses ranging from asymptomatic diseases to severe disease courses marked by the development of life-threatening acute respiratory disease syndrome. Depending on the disease course, the kinetics of virus-specific immune responses alter. In general, in SARS-CoV-2 infections, the innate immune response is slightly delayed and reaches approximately half of the magnitude compared to perfect examples of a generic infection. Subsequently, the virus-specific T- and B-cell responses are also delayed. However, it still reaches comparable response strengths. Consequently, the viral load can be limited to a medium magnitude, leading to average COVID-

19 disease courses. (**Figure 11**; B). In contrast, severe SARS-CoV-2 infections are characterized by an even more delayed innate immune response that continually increases in strength, accompanied by a high viral load. The latter reaches a plateau as soon as an appropriate B cell, and thereby, antibody responses develop. Of note, a virus-specific T cell response does not develop at all or with very low magnitude, pointing towards a key role of T cell responses for effective viral clearance (**Figure 11**; C).[28,29] This was additionally supported by a mouse study, demonstrating a significant reduction of antibodies' ability to clear virally infected cells in $CD8^+$ T cell-depleted mice.[30]

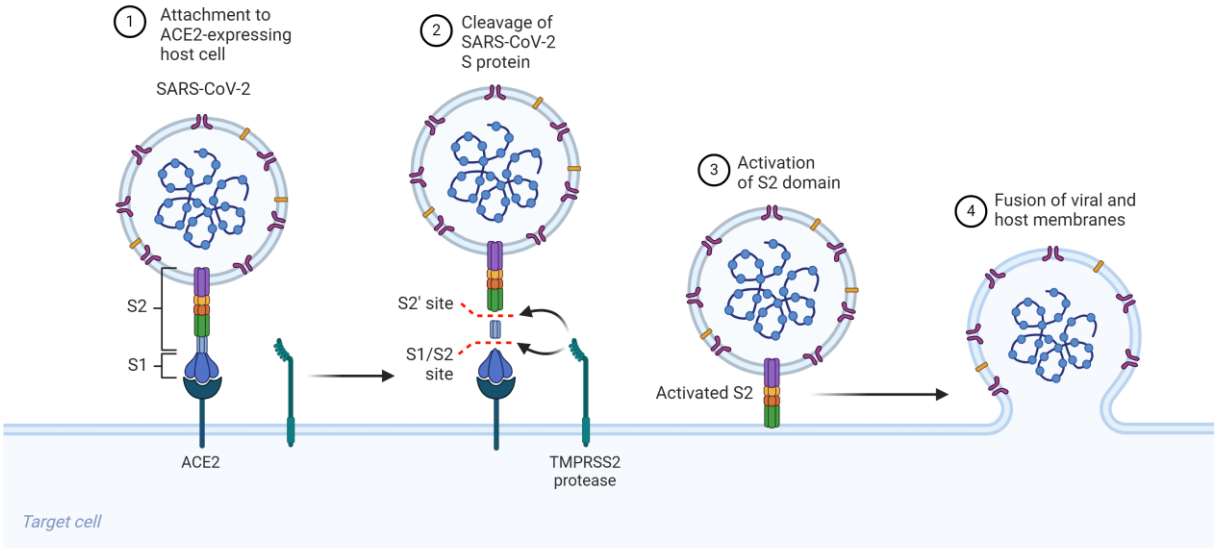

Figure 10. Mechanism of SARS-CoV-2 viral entry into the host cell. Host cells are infected by a SARS-CoV-2 virus via (1) attachment to angiotensin-converting enzyme 2 (ACE2) - positive host cells, e.g., expressed in the lung, (2) the cleavage of SARS-CoV-2 Spike (S) protein by the host cells' TMPRSS2-protease that is followed by a conformational change and therewith (3) activation of the S2-subunit. Lastly, (4) the viral body fuses with the host cell's membrane to release viral RNA into the cellular cytoplasm.

Next to the aforementioned alterations within the response timing and strengths, the T cells' epitope-specificities within the infection's resolution phase also vary depending on the disease course (**Figure 12**).[31] Mild disease courses are characterized by dominating $CD8^+$ T cell responses, showing a slight preference for recognizing SARS-CoV-2 structural proteins. In contrast, severe SARS-CoV-2 infections are dominated by $CD4^+$ T cell responses that identify various epitopes, with most T cells recognizing SARS-CoV-2 structural proteins. However, information on the epitope repertoire among SARS-CoV-2 – specific memory T cells is pending. The latter is essential to estimate the individuals' vulnerability to mutated virus-variants upon

re-infection who gained immunity via infection with a former virus variant or first-generation vaccines, which are based on the sequence of the ancestral virus strain (also called Wuhan strain). Mutations, especially within the Spike protein, potentially lead to viral immune evasion if located within epitopes of neutralizing antibodies (nABs). Since the outbreak of SARS-CoV-2, several variants of concern (VOCs) have evolved, bearing one or multiple mutations, with Omicron being the dominant variant when this thesis was written (April 2024). (**Figure 13**).

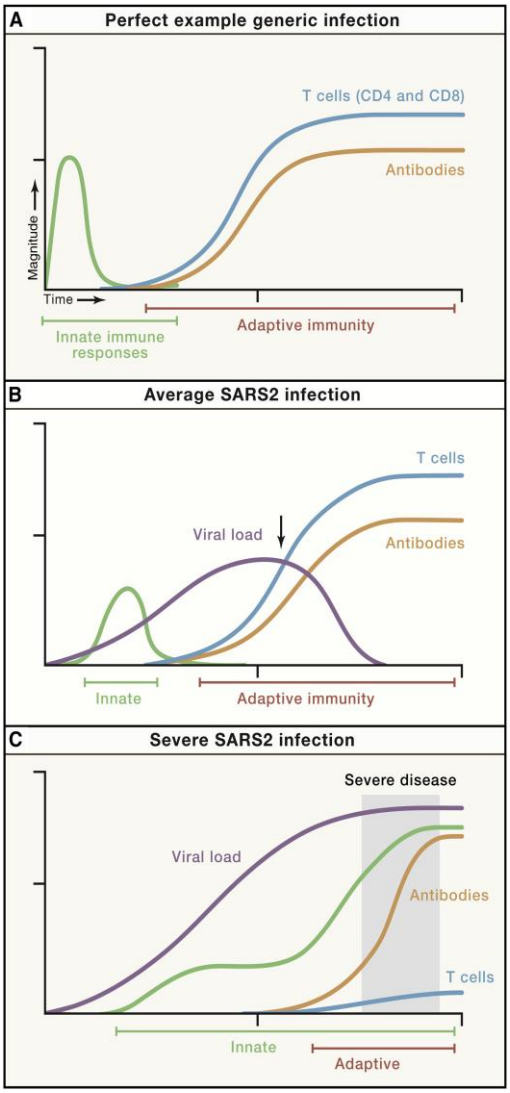

reprinted from "Adaptive immunity to SARS-CoV-2 and COVID-19"
by Alessandro Sette and Shane Crotty (2021);
Retrieved from: 10.1016/j.cell.2021.01.007

Figure 11. Immune response models to mild, average, and severe SARS-CoV-2 infections. (A) Kinetics in a perfect example of a generic infection. **(B)** Kinetics of an average SARS-CoV-2 infection. Innate and adaptive immune responses slow but fully develop. The viral load can be controlled to raise maximal to medium magnitudes before declining. **(C)** Kinetics of a severe SARS-CoV-2 infection. The latter is characterized by a major increase in the viral load, which failed to be controlled by the belayed innate and adaptive immune response. However, antibody responses still develop, while T-cell responses are nearly absent.

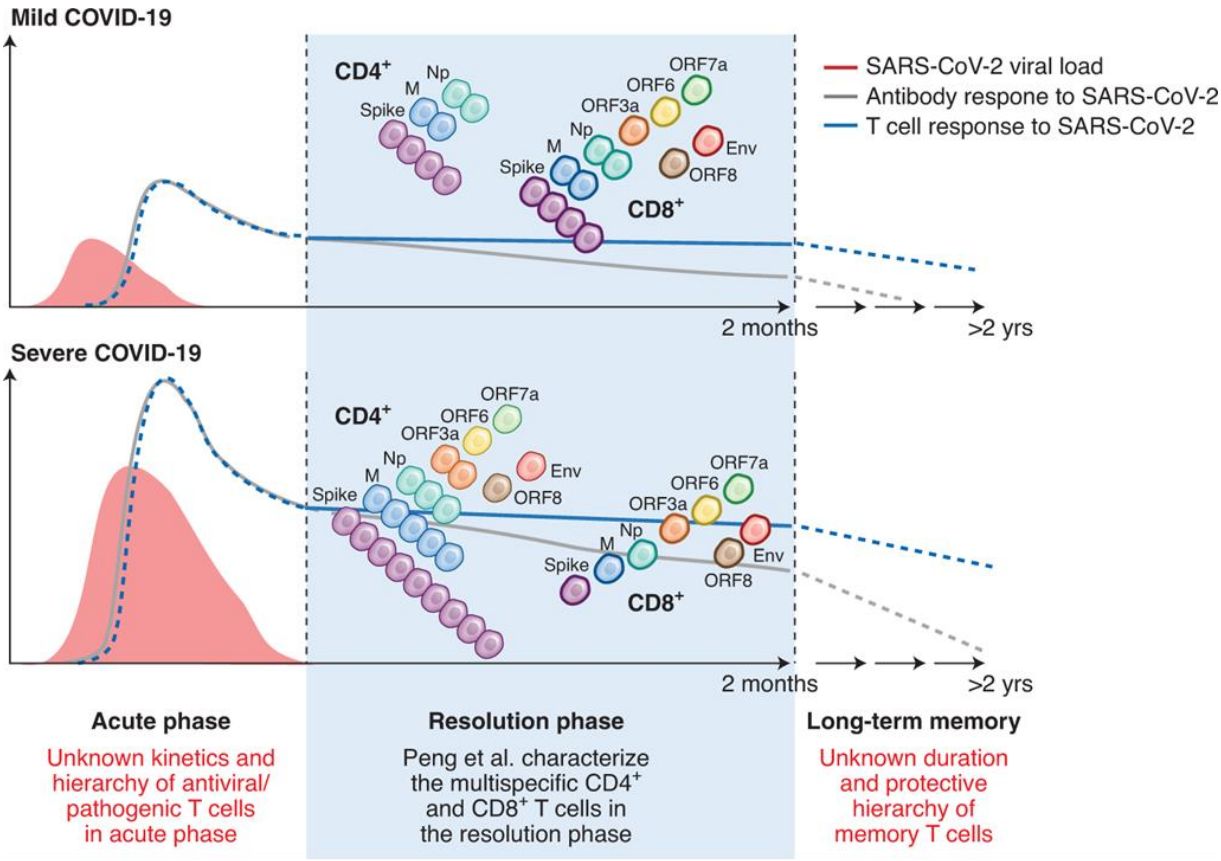

Reprinted from Swadling L, Maini MK. "T cells in COVID-19 - united in diversity" Nat Immunol. 2020 Nov;21(11):1307-1308. doi: 10.1038/s41590-020-0798-y. PMID: 32895541.

Figure 12. T cell repertoire in mild and severe COVID-19 infections. Viral load (red curve) and two-month kinetics of SARS-CoV-2 – specific antibody response (grey line) and T cell responses (blue line) in mild (upper graph) and severe COVID-19 infections (lower graph). The T cell epitope repertoire within the resolution phase of COVID-19 disease, described by Peng et al., is illustrated for $CD4^+$ and $CD8^+$ T cells. Dotted lines indicate speculative predictions, while solid lines represent validated relative magnitudes of B- and T-cell responses. Origin-proteins for epitopes are abbreviated with: M: Membrane; Np: Nucleoprotein; ORF3a/6/7a/8: Open-reading frame; Env: Envelope.

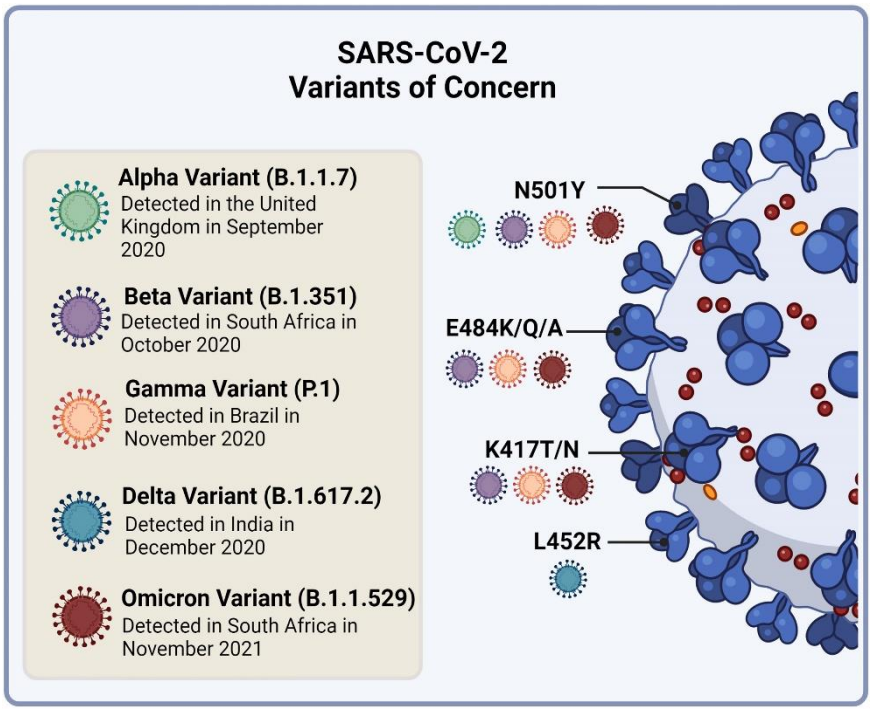

reprinted from " SARS-CoV-2 Variants, Vaccines, and Host Immunity" by Mistry et. Al (2022)
retrieved from: https://doi.org/10.3389/fimmu.2021.809244

Figure 13. SARS-CoV-2 Variants of Concern (VOCs). SARS-CoV-2 variants of concern (left box) and their mutations within the Spike receptor-binding domain sequence with relevance to immune evasion. Substitution of L452R is unique to Delta Variant. K417T/N, E484K/Q/A, and N501Y substitutions are detected for Omicron, Gamma, and Beta variants. Lastly, a single N501Y substitution was detected for the Alpha variant.

Aim of this project

As explained, severe SARS-CoV-2 infections are associated with the absence of virus-specific T-cell responses, which underlines the importance of T cells for effective viral clearance. Furthermore, due to high evolutionary pressure, especially new virus clades' SARS-CoV-2 Spike protein, the main target of nABs, is rapidly changing. This results in a more infectious virus and eventually reduced efficacy of developed vaccines[32] and protection from former natural infection.[33]

Therefore, with the identification of virus-specific T-cell epitopes, this project aimed to investigate and estimate the stability of the T-cell response against novel strains of SARS-CoV-2. To fulfill this aim, several project work packages were defined in the course of the project:

1. As a first use case, T-cell responses against the SARS-CoV-2 Omicron variant were determined in twice- and triple-vaccinated individuals who received first-generation vaccines. Such analyses allowed us to make initial assumptions about the stability of the T-cell response.

2. To estimate whether potential upcoming virus strains could pose a threat to the stability of the T cell response, it was determined whether T cell epitopes are located within regions of the viral proteins that preferentially show high mutational burden or remain unaltered. This information allows assumptions about the expected persistence of antigen-specific T cells and continuous protection during SARS-CoV-2 viral evolution.
3. Changing T-cell epitope landscapes were observed for mild to severe COVID-19 disease courses. Therefore, we ascertained potential underlying causes for severe infections by looking into T-cell epitope landscapes and T-cell response strength in individuals categorized based on their expression of predisposing HLA haplotypes.
4. Since the conventional approach for T cell epitope characterization bears several disadvantages, the major ones being the high number of needed study subjects and the time-consuming approach, an additional goal of this project was the development of a novel experimental procedure enabling a faster and more efficient identification of T cell epitopes: a multiplex HLA binding assay, which allows a time efficient and reliable identification of T cell epitopes.

Methods

Peptide design for *in vitro* stimulation approaches

Peptides originating from SARS-CoV-2 structural S, M, and N proteins were synthesized. Those peptides are mainly 15-amino acids long, consecutive peptides, bearing an 11-amino acid long overlap to the following peptide. Thereby, the complete sequences of the proteins (NIH GenBank ID for the Spike protein: QHD43416.1; the Membrane protein: QHD43419.1; the Nucleocapsid protein: QHD43423.2) are covered, resulting in 362 single peptides originating from the S-, 110 single peptides originating from the N-, and 62 peptides originating from the M-protein. Those peptides were additionally pooled into 36 S-, 11 N-, and 6 M-protein peptide pools.

To evaluate the T cell reactivity against protein regions that are mutated within the B.1.1.529 Omicron-strain of the SARS-CoV-2 Spike protein, a peptide pool including peptides that cover all mutated regions within the B.1.1.529 Spike protein (PepTivator® SARS-CoV-2 Prot_S B.1.1.529/BA.1 Mutation Pool, Cat. No. 130-129-928), as well as a reference pool including the very same peptides in their wildtype variant (PepTivator® SARS-CoV-2 Prot_S B.1.1.529/BA.1 WT Reference Pool, Cat. No. 130-129-927) were designed and synthesized.

PMBC isolation from whole blood

Whole blood was collected from each study subject after informed consent and following the declaration of Helsinki.[34] From those samples, peripheral blood mononuclear cells (PMBCs) were isolated via density gradient centrifugation using Pancoll® (Pan Biotech, Aidenbach, Germany, Cat. No. P04-60500), following the manufacturer's instructions. After collecting the isolated PBMCs in a new 50 mL Falcon tube, cells were resuspended in CliniMACS PBS/EDTA buffer (Miltenyi Biotec, Cat. No. 200-070-025) and centrifuged at 300 g for 10 min. Afterward, the supernatant was discarded, and cells were washed twice using CliniMACS buffer and centrifugation at 200 g for 10 min to remove residual thrombocytes. Finally, PBMCs were resuspended in RPMI-1640 medium (BioWest, Nuaillé, France, Cat. No. L0501-500) supplemented with 5% human AB-serum (Capricorn, Ebsdorfergrund, Germany, Cat. No. HUM-3B, Lot. CP20-3472), 1x Anti/Anti (Thermo Fisher Scientific, Waltham, USA, Cat. No. 11580486) and 2 mM L-Glutamine (Lonza, Basel, Switzerland, Cat. No. BE17-605E) (from now on referred to as *supplemented* RPMI medium). Cell numbers were estimated using a Sysmex XP-300 device (Sysmex, Norderstedt, Germany). Cells are subsequently plated out (A)

on a 96-well plate at a concentration of 1E6 cells / 0.1 mL supplemented RPMI medium / well for stimulation after 24 h incubation, or (B) on 6 well plate at a concentration of 5E6 cells / 5 mL supplemented RPMI medium together with 100 iU / mL IL-2 and 1µg / mL SARS-CoV-2 PepTivator® Prot_S Complete, -Prot_M or -Prot_N. PBMCs plated out under both conditions were incubated at 37°C, 5% CO_2.

Expansion of antigen-specific T cells

PBMCs plated out on a 6 well plate after isolation, as explained above, were utilized for 14-day expansion towards SARS-CoV-2 S, -M, or -N specific T cells depending on the PepTivator peptides that were added to the cell suspension. The medium was refreshed every two to three days by gentle removal of 2.5 mL medium and subsequent re-addition of freshly prepared supplemented RPMI medium and 250 iU / 2.5 mL IL-2 (Miltenyi Biotec, Cat. No. 130-097-745). After 14 days, cells were harvested in a 15 mL Falcon and filled with fresh, pre-warmed medium. Afterward, cell numbers were estimated using the Sysmex XP-300 device and plated out on a 96-well flat bottom plate to proceed with re-stimulation.

Sequential Walk – an *in vitro* stimulation assay

To identify immunogenic protein regions, i.e. genomic regions with a capacity to induce a T-cell response, peptides were synthesized as described above. To increase efficacy, peptides were first pooled, covering a total sequence length of 50 amino acids. Each pool consists of ten consecutive, overlapping peptides with a median length of 15 amino acids. After a peptide pool has been identified as immunogenic, all single peptides out of those pools were tested in a single-peptide, donor-specific manner to identify single immunogenic 15-mer peptides. All experimental verifications were performed by *in vitro* stimulation approaches. Therein, PBMCs were plated out in a 96-well flat-bottom plate (Falcon, New York, USA, Cat. No. 353072) at a concentration of 1E6 cells / 0.1 mL supplemented RPMI medium / well freshly after isolation or after 14-day expansion and 24 h prior to the stimulation. To induce stimulation, SARS–CoV–2–derived peptide pools or single peptides at a concentration of 1 µg/mL/peptide were added to the cells and incubated for 6 h at 37 °C with 5% CO_2. For each stimulation experiment, a negative, unstimulated control and two positive controls stimulated with CytoStim™ (Miltenyi Biotec, Cat. No. 130-092-173) and SARS-CoV-2 PepTivators® covering the Spike, Nucleocapsid and Membrane protein (Miltenyi Biotec, Cat. No. 130-129-712, 130-126-699, 130-126-703) were prepared. After 2 h incubation, 2 µg/mL Brefeldin-A (Sigma-Aldrich, St. Louis, USA, Cat. No. B7651) was added to each well to prevent cytokine secretion

by the activated T cells. Subsequently, cells were stained intracellularly for cytokines associated with activation and cell surface markers. All incubation steps were done at room temperature if not explicitly indicated differently. After stimulation and the addition of 100 µL PBS/EDTA buffer (2 mM) to each well, cells were transferred into a 96-well V-bottom plate (Sigma-Aldrich, St. Louis, USA, Cat. No. Z667234). Next, additional 100 µL PBS/EDTA-buffer was added to each well before the plate was centrifuged at 300 g for 5 min. Afterward, the supernatant was discarded, and cells were resuspended in 99 µL PBS and 1 µL VioBility 405/452 fixable dye (Miltenyi Biotec, Cat. No. 130-130-420). After gentle mixing, cells were incubated for 10 min in the dark. Subsequently, cells were washed by adding 200 µL PBS/EDTA/BSA buffer and centrifugation at 300 g for 10 min. For the following fixation, cells were resuspended in 100 µL PBS/EDTA/BSA buffer and 100 µL Inside Fix solution (Inside Stain Kit, Miltenyi Biotec, Cat. No. 130-090-477) and finally incubated for 20 min in the dark. To wash the cells, 100 µL PBS/EDTA/BSA buffer was added, and cells were centrifuged at 300 g for 5 min. The supernatant was discarded before adding 250 µL Inside Perm Solution (Inside Stain Kit, Miltenyi Biotec, Cat. No. 130-090-477) and subsequent centrifugation at 300 g for 5 min. Supernatants were completely and gently aspirated. Then, cells were stained (intracellularly) by the addition of the following antibody cocktail: anti-human CD14 – VioBlue (Clone: REA599; Miltenyi Biotec; Cat. No. 130-110-525), anti-human CD20 – VioBlue (Clone: REA780; Miltenyi Biotec, Cat. No. 130-111-531), anti-human CD3 – APC (Clone: REA613; Miltenyi Biotec, Cat. No. 130-113-135), anti-human CD4 – VioBright515 (Clone: REA623; Miltenyi Biotec, Cat. No. 130-114-535), anti-human CD8 – VioGreen (Clone: REA734; Miltenyi Biotec, Cat. No. 130-110-684), anti-human TNF-α – PE-Vio770 (Clone: cA2; Miltenyi Biotec, Cat. No. 130-120-492), anti-human INF-γ – PE (Clone: REA600; Miltenyi Biotec, Cat. No.: 130-113-496), anti-human IL-2 – PEVio615 (Clone: REA689; Miltenyi Biotec, Cat. No. 130-111-307) and anti-human CD154 – APCvio770 (Clone: 5C8; Miltenyi Biotec, Cat. No. 130-114-130). All antibody-conjugates were added at a final concentration of 1:50 in 100 µL Inside Perm. Cells were incubated for 10 min in the dark before adding 200 µL Inside Perm and subsequent centrifugation at 300 g for 5 min. The supernatant was discarded entirely, and cells were resolved in PBS/EDTA/BSA buffer for final flow cytometric analysis. Data was acquired using the MACS Quant 16- flow cytometer (Miltenyi Biotec, Cat. No. 130-109-803).

To evaluate T cell responses to peptides derived from mutated regions within the B.1.1.529 / Omicron subregion, both *in vitro* stimulation and intracellular staining were performed similarly.

In silico peptide-binding prediction analysis

NetMHCpan 4.0 (https://services.healthtech.dtu.dk/services/NetMHCpan-4.0/) and NetMHCIIpan 4.0 (https://services.healthtech.dtu.dk/services/NetMHCIIpan-4.0/) were used for the *in silico* prediction of peptide binding affinities to HLA molecules. Therefore, HLA alleles representing 95% of alleles expressed in the European area (**Table 1**). Evaluation of potential weak and strong binding peptides was based on the EL-Rank thresholds of 0.5 and 2 for the binding to HLA Class I and 2 and 5 for the binding to HLA Class II molecules, respectively. Based on the estimated binding affinities and prediction of strong, weak, or absent interactions of peptides with HLA alleles of interest, the effect of mutations that were observed within the novel SARS-CoV-2 B.1.1.529 / Omicron variant was evaluated using Microsoft Excel.

Table 1. HLA Class I and II alleles included within NetMHC(II)pan-based *in silico* peptide binding prediction analyses. Listed HLA Class I and Class II alleles included within the *in silico* peptide binding prediction to cover 95% of alleles expressed among the European-Caucasian population.

HLA Class I alleles			**HLA Class II alleles**
HLA-A alleles	**HLA-B alleles**	**HLA-C alleles**	**HLA-DRB1 alleles**
HLA-A*0101	HLA-B*0702	HLA-C*0102	HLA-DRB1*0101
HLA-A*0201	HLA-B*0801	HLA-C*0202	HLA-DRB1*0301
HLA-A*0301	HLA-B*1402	HLA-C*0303	HLA-DRB1*0401
HLA-A*1101	HLA-B*1501	HLA-C*0304	HLA-DRB1*0701
HLA-A*2402	HLA-B*1502	HLA-C*0401	HLA-DRB1*0901
HLA-A*2601	HLA-B*1801	HLA-C*0501	HLA-DRB1*1501
HLA-A*2902	HLA-B*2705	HLA-C*0602	HLA-DRB1*1101
HLA-A*3303	HLA-B*3501	HLA-C*0701	HLA-DRB1*1301
HLA-A*6801	HLA-B*4001	HLA-C*0702	HLA-DRB1*1401
	HLA-B*4002	HLA-C*0801	HLA-DRB1*0404
	HLA-B*4402		HLA-DRB1*0405
	HLA-B*4403		HLA-DRB1*0407
	HLA-B*4501		HLA-DRB1*0411
			HLA-DRB1*0803
			HLA-DRB1*1302

Assessment of neutralizing-antibody titers

The following procedures were performed with the help of Dr. Angeliki Datsi from the Institute for Transplantation Diagnostics and Cell Therapeutics at the University Clinic Düsseldorf.

Two serological assays were used for the determination of levels of SARS-CoV-2 Spike S1-specific IgA and IgG antibodies (EuroImmun, Germany) and SARS-CoV-2 Nucleocapsid-

specific IgG antibodies (Elecsys®, Roche Diagnostic Test). Neutralizing antibodies were assessed by microscopic evaluation of the virus-induced cytopathic effect (CPE). These nAB titers were defined as the highest dilution at which CPE was absent. Specifically, an nAB titer of 1:160 was defined as threshold for the binary representation of virus neutralization capacity. For the validation of this procedure, serum from non-infected individuals served as a negative control, while sera from two SARS-CoV-2 infected individuals served as a positive control.

T cell stimulation with SARS-CoV-2 PepTivators®

The following procedures were performed with the help of Dr. Angeliki Datsi from the Institute for Transplantation Diagnostics and Cell Therapeutics at the University Clinic Düsseldorf.

For the stimulation of T cells of study subjects of cohort D, PBMCs were collected from whole blood donations via density gradient centrifugation three weeks post first positive SARS-CoV-2 PCR tests. Afterward, the cells were dissolved in X-Vivo 15 medium (Lonza; Cat. No. 11695120) plated out on a 96-well plate at a concentration of 1E6 cells / 100 µL / well. Stimulation was performed by adding 1 µg / mL PepTivators followed by 6 h incubation. A positive control stimulated with PMA/Ionomycin and a negative, unstimulated control was prepared for every donor. After 30 min stimulation, 5 ng/mL Brefeldin A (BioLegend; Cat. No. 420601) was added to prevent the release of cytokines from the cell. Subsequently cells were stained using the following antibodies: anti-CD3-PE-Dazzle (BioLegend, Cat. No. 300446), anti-CD4 BV650 (BioLegend, Cat. No. 317436), anti-CD8 VioGreen (Miltenyi Biotec, Cat. No. 130-113-164), anti-CD45RO-BV570 (BioLegend, Cat. No. 304226), anti-CD154-PE-Cy7 (BioLegend, Cat. No. 310832) and anti-IFN-γ-BV421 (BioLegend, Cat. No. 502532). All antibodies were used in a 1:100 dilution. Staining was done according to the manufacturer's instructions. Data assessment was performed by flow cytometry using the CytoFlex S– flow cytometer (Beckmann Coulter). Each sample was normalized to the negative control for appropriate data evaluation to exclude unspecific responses and background signals.

MHC-monomer synthesis

The synthesis of the biotinylated-HLA monomers with a loaded FITC-labeled placeholder peptide (A) *A*0101-His-Cys/ pp50 (245-253)_V3 FITC-bio* and (B) *A*0201-His.Cys / pp65 (495-503)_V4 FITC-bio* was performed internally by the group of Dr. Marek Wieczorek at Miltenyi Biotec.

Coupling of biotinylated PMMA beads to MHC-monomers

Please note that the following sections are part of a patent application (EP23216590.2) at the European Patent Office, submitted on the 14th of December, 2023.

Per reaction, 20,000 PolyAn Red4 0.2 or 5.5 Streptavidin-polymethylmethacrylate (PMMA) beads (PolyAn, Berlin, Cat. No. 7667842) were dissolved in 1 mL PBS/EDTA/BSA buffer and centrifuged at 3000 g for 1 min. The supernatant was discarded, and beads were washed by adding 1 mL PBS/EDTA/BSA buffer and centrifugation at 3000 g for 1 min. Next, the supernatant was discarded, and beads were resolved in the following conjugated peptide-FITC / HLA monomer-solutions at a final concentration of 100 nM: (A) A*0101-His-Cys/ pp50 (245-253)_V3 FITC-bio, or (B) A*0201-His.Cys / pp65 (495-503)_V4 FITC-bio. Coupling was done for 15 min at room temperature and constant rotation at 550 rpm using the ThermoMixer™ C (Eppendorf, Hamburg Cat. No. 5382000015), allowing for uniform binding of biotinylated HLA monomers to streptavidin-beads. Lastly, conjugates were washed twice using 1 mL PBS/EDTA/BSA buffer and centrifugation at 3000 g for 1 min. Finally, the conjugates were resolved in 1 mL PBS/EDTA buffer.

Multiplex HLA-binding assay

Please note that the following sections are part of a patent application (EP23216590.2) at the European Patent Office, submitted on the 14th of December, 2023.

After the successful coupling of the aforementioned biotinylated-pFITC/HLA monomers to streptavidin-PMMA beads, the exchange of the MHC-binding peptide by an HLA-specific examination peptide was catalyzed. To reach this aim, coupled beads were plated out at a concentration of 20,000 beads / 50 µL into a 96-well round bottom plate. Next, the peptide-exchange reaction mix was added consisting of: (I) examination peptide (ExPep) pp50 (245-253), or pp65 (495-503) at a final concentration of 400 µM, (II) exchange catalyst DIP72 (Met-Ala-Ser), or DIP82 (Z-Val-Met) at a final concentration of 5 mM and (III) PBS/EDTA buffer for the exchange on HLA*0101 and HLA*0201, respectively. The reaction mix was incubated for 16 h, at room temperature, under constant shaking at 450 rpm and protected from light. After that, all samples were transferred into a 0.2 µm FiltrEX™ 96-well filter plate (Corning®, Corning, USA, Cat. No. 3504) and centrifuged at 500 g for 2 min. Next, the beads were washed using 250 µL PBS/EDTA/BSA buffer and centrifuged at 500 g for 2 min. Lastly, the beads were suspended in 120 µL PBS/EDTA/BSA buffer and flow cytometrically analyzed at a MACS Quant 16-flow cytometer.

Dissociation and immunological phenotyping of bladder carcinoma samples

Biopsies of bladder carcinoma cells were collected after informed consent and following the declaration of Helsinki[34]. Samples were collected by Dr. Dimitri Barski, senior physician at the Lukas Hospital in Neuss (Germany), in MACS Tissue Storage Solution (Miltenyi Biotec, Cat. No. 130-100-008), stored at 4°C and transferred to Miltenyi Biotec in Bergisch Gladbach (Germany). Samples were dissociated using the human tissue dissociation kit (Miltenyi Biotec, Cat. No. 130-095-929) following the manufacturer's instructions. In short, samples were cut into small tissue fragments before getting enzymatically dissociated using the human tumor dissociation kit (Miltenyi Biotec, Cat. 130-095-929) and the gentleMACS™ Octo Dissociator with Heaters (Miltenyi Biotec, Cat. No. 130-096-427), following the manufacturer's instructions. Afterward, the number of viable tumor cells was determined by staining of viable cells using Propidium Iodide (PI). For this, 1E6 cells were dissolved in 100 µL RPMI-1640 medium and stained with 1 µL PI. Flow cytometric analysis was performed using the MACS Quant 16-flow cytometer.

Furthermore, if sufficient cell material was available, 0.5-1E7 dissociated cells were used to assess the immunological phenotype of the individual tumor samples using the 8-color immunophenotyping kit (Miltenyi Biotec, Cat. No. 130-120-640) and applying the manufacturer's instructions. In short, cells were dissolved in 100 µL PBS/EDTA/BSA buffer and stained for 10 min, at 4°C and in the dark using the 8-color immunophenotyping reaction mix at a final concentration of 1:11 and 7-AAD (Miltenyi Biotec, Cat. No. 130-111-568) as life/dead-marker at a final concentration of 1:110. Afterward, cells were washed using 1 mL PBS/EDTA/BSA buffer and centrifuged at 300 g for 10 min. Finally, the supernatant was discarded, and cells were resuspended in 200 µL PBS/EDTA/BSA buffer for flow cytometric analysis at the MACS Quant 16-flow cytometer.

Isolation of neutrophil granulocytes

Neutrophil granulocytes were negatively isolated as healthy reference material for WES using the MACSxpress® whole blood neutrophil isolation kit, human (Miltenyi Biotec, Cat. No. 130-104-434), following the manufacturer's instructions. In short, 2 mL whole blood was mixed with 0.5 mL reconstituted buffer A and 0.5 mL buffer B in a 15 mL Falcon tube. After 15 min incubation in the MACSmix™ Tube rotator, the reaction mix was put into the MACSxpress® separator for 10 min. Afterward, neutrophil granulocytes were magnetically separated from

residual cell material and were, therefore, pipetted into a new 15 mL Falcon tube. After twice washing with 10 mL PBS/EDTA and centrifugation at 300 g for 5 min, cells were resuspended in 2 mL RPMI-1640 medium.

DNA Extraction for whole exome sequencing

Tumor samples and neutrophil granulocytes, which were used as healthy reference material, were isolated as described above for the analysis via whole exome sequencing and subsequent candidate neoantigen identification. The DNA from both cell sources was isolated using the Dneasy® Blood & Tissue kit (Qiagen, Hilden, Cat. No. 69504), following the manufacturer's instructions. First, cells were lysed using proteinase K and loaded onto the Dneasy® mini spin column. Second, DNA released from lysed cells was bound to the Dneasy® membrane during centrifugation while other cellular material passed through. Finally, after twice washing to remove residual contamination, the DNA was eluted in water and stored at -70°C. The internal NGS core facility of Miltenyi Biotec has performed the DNA isolation and storage.

Data analysis and statistics

For the analysis of acquired flow-cytometric data FlowJo™ version 10.8.1 and MACS Quantify™ Versions 2.13 and 3.0 were used. Raw data were analyzed and plotted using Microsoft Excel, GraphPad Prism 9, and BioRender. Statistical tests that have been performed on data from individual samples and experiments are indicated within respective figure legends.

Results

First-generation vaccines provide immunological memory against SARS-CoV-2 B.1.1.529 variant

Data presented in the following section has been published in the international peer-reviewed journal Communications Medicine in November 2022. DOI: 10.1038/s43856-022-00203-7

The Omicron strain, which showed multiple mutations, especially within the Spike protein and a rapid spreading in November 2021, raised first concerns regarding the sustained protection via first-generation vaccines based on the viral sequence of the wildtype / Wuhan-strain. Simultaneously, booster vaccinations were recommended by the WHO[35] and the German vaccination advisory board *Ständige Impfkommission (STIKO)*[36], which should protect from severe disease due to waning vaccine effectiveness, especially in immunocompromised individuals. Until now, a complete COVID-19 vaccination consists of two vaccine doses administered on average two to four weeks apart to build proper immunity.[37–42] To test whether a third booster vaccination supports the anti-viral immune response against the novel Omicron-strain, we determined the T cell response strength within twice and triple-vaccinated individuals upon stimulation with peptide pools covering the mutated regions of the B.1.1.529 variant (**Figure 14**). To achieve this, first, 83 15-mer peptides covering the mutated regions of the B.1.1.529 Spike protein were synthesized and pooled (Prot_S B.1.1.529 Mutation Pool). Thereby, mutated positions were incorporated at every possible position within the peptides to represent each potential epitope (**Figure 14**, A). As a reference, the same peptides were synthesized in their wildtype (WT), non-mutated variant, to evaluate the changes induced within the Omicron-variant (Prot_S WT Reference Pool). Along with a peptide pool covering the complete sequence of the wildtype Spike protein (Prot_S Complete), which is used to evaluate the proportion of the T cell response induced by mutated parts of the Spike protein, those peptide pools were used for *in vitro* stimulation of PBMCs of study subjects from two different cohorts: (A) twice vaccinated (n=8) and (B) triple vaccinated (n=10) individuals (**Figure 14**; B). In more detail, PBMCs isolated from whole blood of every study subject were stimulated with the aforementioned peptide pools. For each donor, a negative, unstimulated control was prepared as a reference (w/o peptides). A detailed overview of individuals' background information on age, sex as well as on type and date of vaccine administration is provided (**Supplementary Table 1**). The response of the T cells was assessed by flow cytometric analysis of T cells stained for intracellular cytokines and cell surface markers

associated with T cell activation (**Figure 15**). Here, pre-gating was performed via a selection of lymphocytes, the exclusion of doublet cells, the selection of $CD3^+$ cells, and subsequent division into single $CD4^+$ and $CD8^+$ T cells. Among $CD4^+$ T cells, frequency changes were evaluated based on INF-γ^+CD154$^+$-double positive cells. Among $CD8^+$ T cells, frequency changes were assessed based on TNF-α^+INF-γ^+-double positive cells.

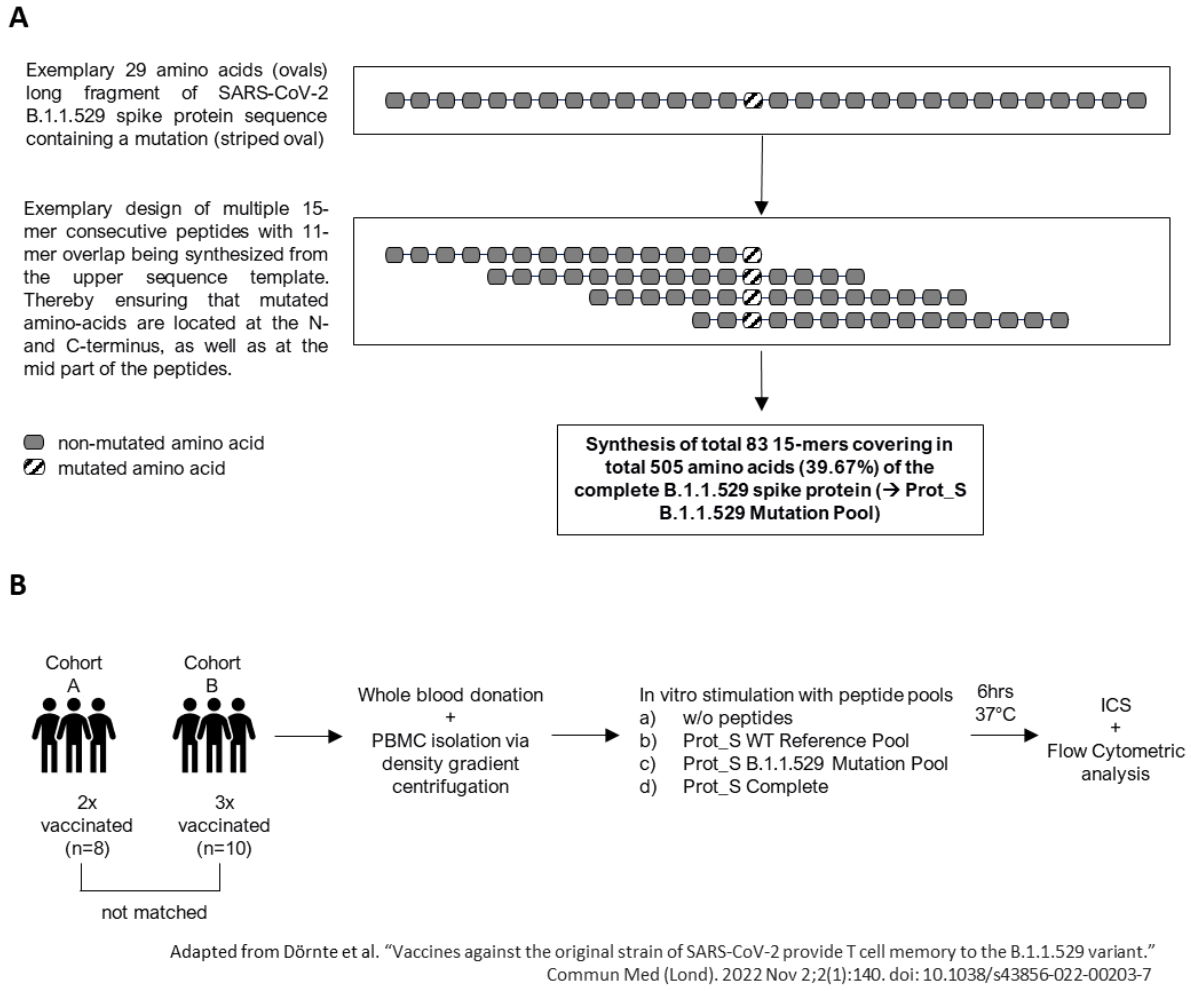

Adapted from Dörnte et al. "Vaccines against the original strain of SARS-CoV-2 provide T cell memory to the B.1.1.529 variant." Commun Med (Lond). 2022 Nov 2;2(1):140. doi: 10.1038/s43856-022-00203-7

Figure 14. Peptide (pool) design concept and in vitro experimental workflow. (A) Exemplary peptide design for consecutive 15-mer peptides with 11-mer overlap originating from SARS-CoV-2 B.1.1.529 strain. Mutated amino acids compared to the wildtype SARS-CoV-2 (Wuhan) strain are indicated as striped ovals. Wildtype amino acids are shown as solid ovals. In total, 83 15-mer peptides covering the complete sequence of the B.1.1.529 Spike protein are synthesized and pooled to the Prot_S B.1.1629 Mutation Pool for in vitro testing. **(B)** In vitro testing strategy on two cohorts comprising of (A) twice vaccinated (n=8) and (B) triple vaccinated (n=10) individuals using the following peptide pools: Prot_S WT Reference Pool, Prot_S B.1.1.529 Mutation Pool, and Prot_Complete. The T-cell responses are evaluated by intracellular cytokine staining (ICS) and flow cytometric analysis.

Table 2. Detailed background information on study subjects' age, sex, type, and administration date of vaccines, as well as the date of sample collection. Date of vaccinations refers to the days (d) since the last vaccine has been administered. The date of sample collection refers to the days (d) after receiving the 1st vaccine dose for both groups.

Group	Age	Sex	Vaccine received as 1st dose or Natural Infection	Days after 1st vaccination when receiving the 2nd dose	Vaccine received as 2nd dose	Days after 2nd vaccination when receiving the 3rd dose	Vaccine received as 3rd dose	Day of sample collection after 1st vaccination
2x vaccinated	52	female	Comirnaty	d41	Comirnaty	-	-	d285
	54	male	Comirnaty	d28	Comirnaty	-	-	d237
	49	female	Comirnaty	d22	Comirnaty	-	-	d126
	27	male	Comirnaty	d40	Comirnaty	-	-	d207
	50	female	Comirnaty	d43	Comirnaty	-	-	d216
	30	female	Comirnaty	d42	Comirnaty	-	-	d221
	23	female	Comirnaty	d45	Comirnaty	-	-	d200
	35	female	Comirnaty	d21	Comirnaty	-	-	d52
3x vaccinated	50	male	Comirnaty	d28	Comirnaty	d198	Spikevax	d264
	45	male	Comirnaty	d29	Comirnaty	d196	Comirnaty	d271
	28	male	Comirnaty	d42	Comirnaty	d166	Comirnaty	d241
	53	female	Natural Infection	d185	Comirnaty	d123	Spikevax	d360
	48	female	Comirnaty	d32	Comirnaty	d183	Comirnaty	d250
	46	female	Comirnaty	d28	Comirnaty	d131	Spikevax	d170
	35	female	Vaxzevria	d48	Comirnaty	d159	Spikevax	d241
	41	female	Vaxzevria	d46	Comirnaty	d155	Spikevax	d235
	52	male	Vaxzevria	d77	Comirnaty	d186	Spikevax	d301
	49	female	Vaxzevria	d52	Comirnaty	d102	Spikevax	d249

Comparison of activated $CD4^+$ T cell frequencies in twice- and triple-vaccinated individuals reveals a significant decrease in reactivity against peptides including B.1.1.529-associated mutations (B.1.1.529 Mutation Pool) compared to the non-mutated reference peptides (WT Reference Pool) in twice-vaccinated individuals. The same trend can be observed in triple-vaccinated individuals. However, this difference is not significant (**Figure 16**, A). In contrast, $CD8^+$ T cells show nearly similar frequencies of activated cells upon stimulation with mutated and reference, wildtype peptides, with a slight trend towards increased frequencies of activated $CD8^+$ T cells against the mutated peptide pool (**Figure 16**, B). Looking at the general reactivity of T cells against the complete Spike protein (Prot_S Complete), $CD4^+$ T cells show a significant increase in triple-vaccinated individuals. In contrast, $CD8^+$ T cells again show comparable frequencies for twice- and triple-vaccinated study subjects. Note that for both T cell subsets, increased background activation is observed within the triple-vaccinated group (w/o antigen).

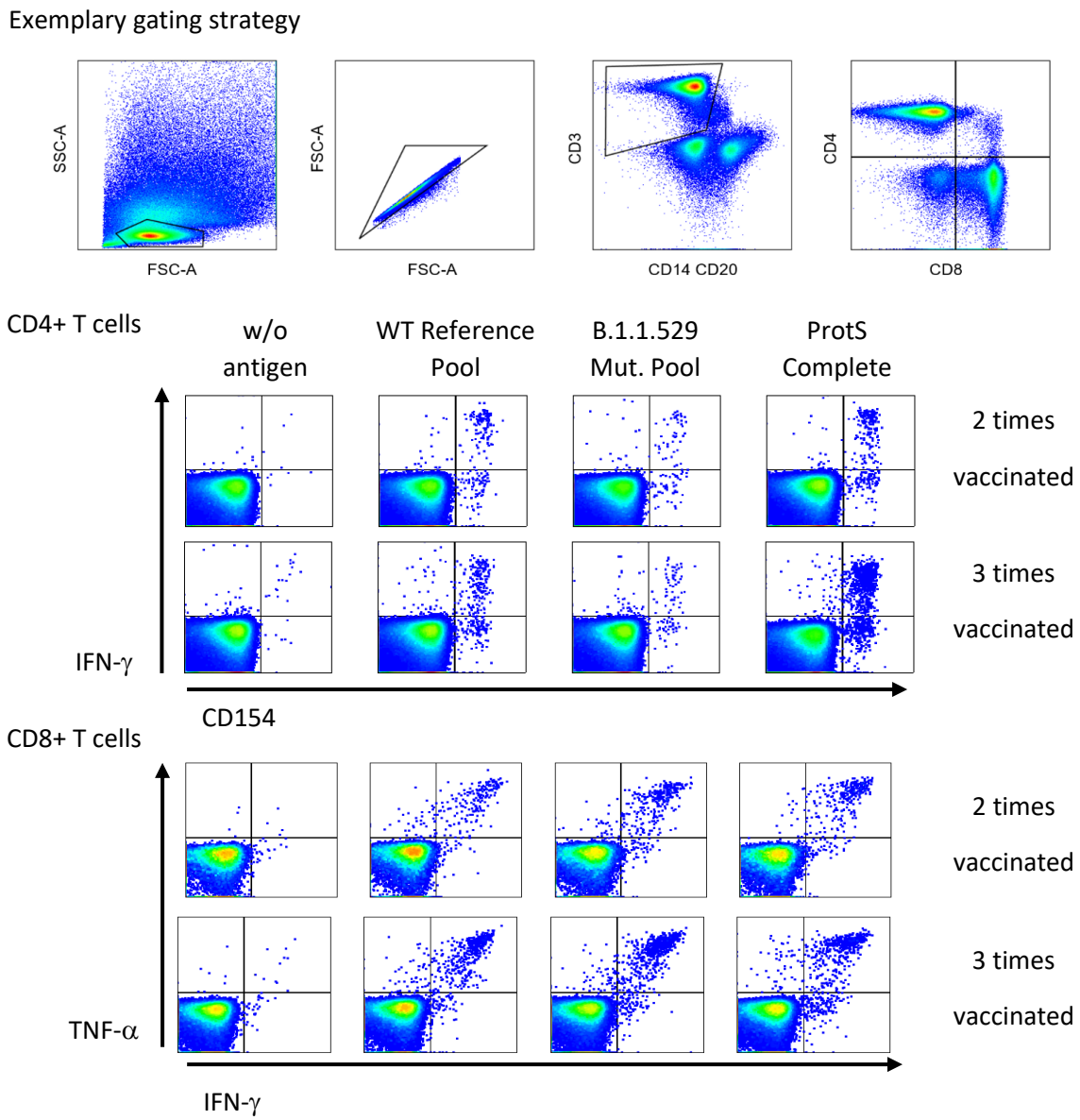

adapted from Dörnte et al.
"Vaccines against the original strain of SARS-CoV-2 provide T cell memory to the B.1.1.529 variant."
Commun Med (Lond). 2022 Nov 2;2(1):140. doi: 10.1038/s43856-022-00203-7

Figure 15. Flow cytometric analysis of T cell responses upon stimulation with Omicron and reference peptide pools. Exemplary gating strategy and dot plots to assess the frequency of activated $CD4^+$ $INF\text{-}\gamma^+CD154^+$ T cells (top) and $CD8^+TNF\text{-}\alpha^+IFN\text{-}\gamma^+$ T cells (bottom) in twice- and triple-vaccinated individuals. A negative, unstimulated control was assessed for each sample (first row), followed by stimulation with the WT Reference Pool, the B.1.1.529 Pool and the Prot_S Complete peptide pool. The labeling of the axes represents the analyzed parameters.

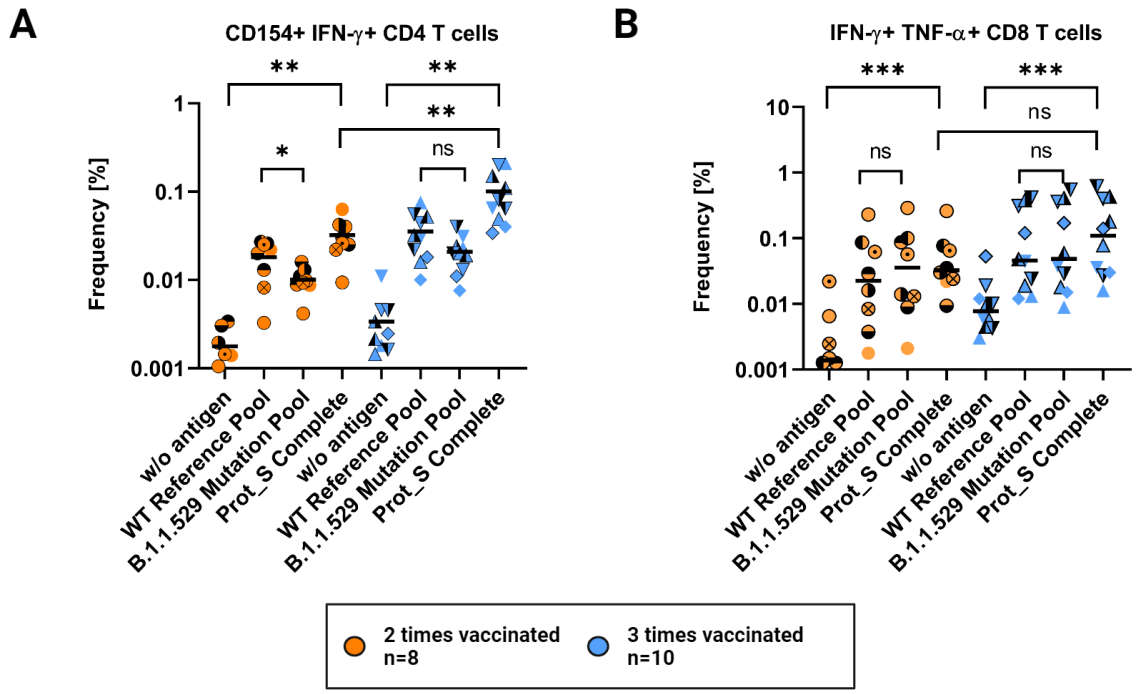

Adapted from Dörnte et al. "Vaccines against the original strain of SARS-CoV-2 provide T cell memory to the B.1.1.529 variant." Commun Med (Lond). 2022 Nov 2;2(1):140. doi: 10.1038/s43856-022-00203-7

Figure 16. Frequency of reactive CD154$^+$INF-γ$^+$CD4$^+$ and INF-γ$^+$TNF-α$^+$CD8$^+$ T cells upon stimulation with distinct SARS-CoV-2 peptide pools in twice and triple-vaccinated individuals. Frequency [%] of **(A)** CD154$^+$INF-γ$^+$CD4$^+$ T cells (y-axes) and **(B)** INF-γ$^+$TNF-α$^+$CD8$^+$ T cells after 6 h stimulation of freshly isolated PBMCs from twice (orange; n=8) and triple vaccinated (blue; n=10) individuals (1) without the addition of stimulatory antigen (w/o antigen), and upon addition of (2) a wildtype reference peptide pool (WT Reference Pool) to (3) a B.1.1.529 Mutation Pool, and a peptide pool covering the complete Spike protein (Prot_C Complete) (x-axes). As CD4 T cells are normally distributed, students´ T-tests with Welch correction were used for the calculation of significance. As CD8 T cells are not normally distributed, Mann–Whitney U-tests were performed. N.s. not significant, *p < 0.05, **p < 0.01, ***p < 0.001.

To evaluate whether a third vaccination with first-generation vaccines supports an anti-SARS-CoV-2 B.1.1.529 immune response, the relative proportions of T cell responses directed against the wildtype and the mutated variant were calculated. Therefore, the relative response upon stimulation with the wildtype-reference pool was subtracted from the relative response upon stimulation with the complete spike protein. This analysis revealed waning immune responses by CD4$^+$ and CD8$^+$ T cells directed against regions of the Spike protein that were mutated within the B.1.1.529 lineage (**Figure 17**). This effect has been shown to be more pronounced in CD4$^+$ T cells than in CD8$^+$ T cells.

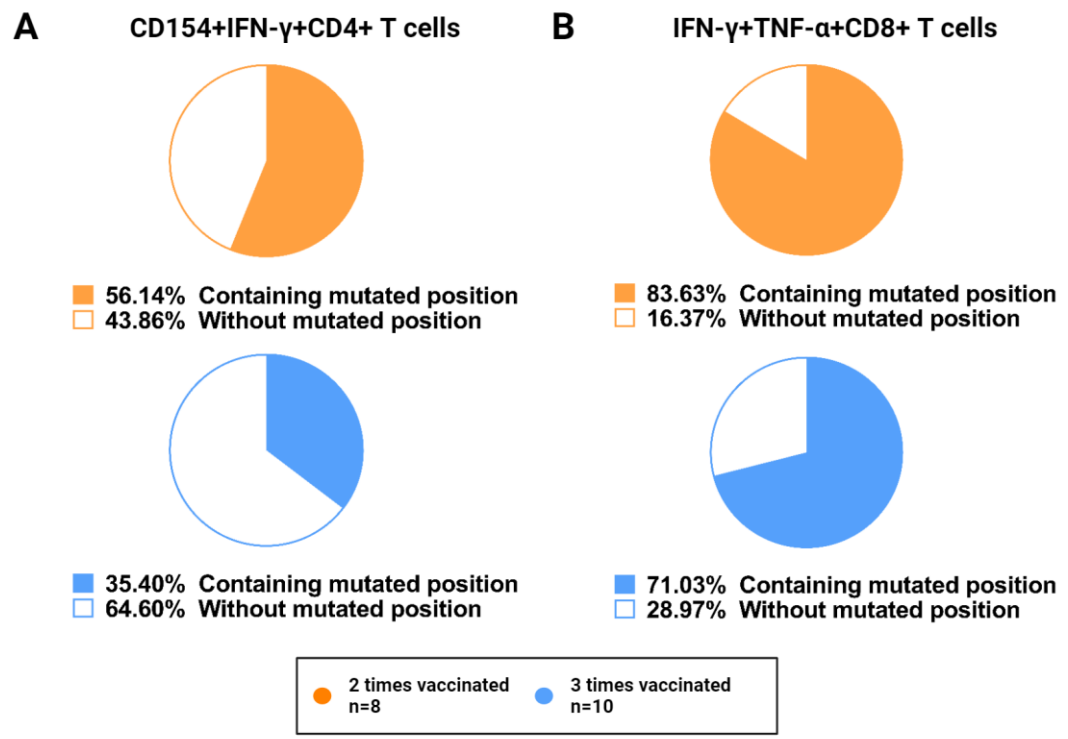

Adapted from Dörnte et al. "Vaccines against the original strain of SARS-CoV-2 provide T cell memory to the B.1.1.529 variant." Commun Med (Lond). 2022 Nov 2;2(1):140. doi: 10.1038/s43856-022-00203-7

Figure 17 . Proportions of T cell responses directed against mutated parts of the SARS-CoV-2 B.1.1.529 in twice and triple-vaccinated individuals. Pie charts representing the ratio of (A) $CD154^{+}INF\text{-}\gamma^{+}CD4^{+}$ T cell – responses and (B) $INF\text{-}\gamma^{+}TNF\text{-}\alpha^{+}CD8^{+}$ T cell – responses induced trough interaction with Spike protein regions containing a mutation associated to the B.1.1529 strain (colored) to responses to non-mutated protein regions, in twice (orange; n=8) and triple (blue; n=10) vaccinated individuals.

To overcome limitations within the availability of study participants and within the number of HLA allotypes that can be represented in this study, *in silico* analyses, including the most commonly expressed HLA allotypes within the European-Caucasian populations, were performed. Herein, prediction of the binding affinities of all 222 9-mer peptides and 83 15-mer peptides, including a mutation associated with the SARS-CoV-2 B.1.1.529 variant, as well as of reference peptides to HLA Class I and HLA Class II molecules were performed using NetMHCpan 4.0 and NetMHCIIpan 4.0, respectively. Finally, the binding affinities of analogous peptides are compared to map the degree of potential immune escape of the B.1.1.529 strain (**Figure 18**). As a measure of the binding affinity, the NetMHC(II)pan-4.0s' eluted ligand percentile ranks (EL-Ranks) are used. Therewith, peptides are categorized into non-binders (NB) (EL > 2 (MHC Class I) / >5 (MHC Class II)), weak binders (WB) (EL 0.5 – 2 (MHC Class I) / 2 – 5 (MHC Class II)) or strong binders (SB) (EL < 0.5 (MHC Class I) / <2 (MHC Class II)).

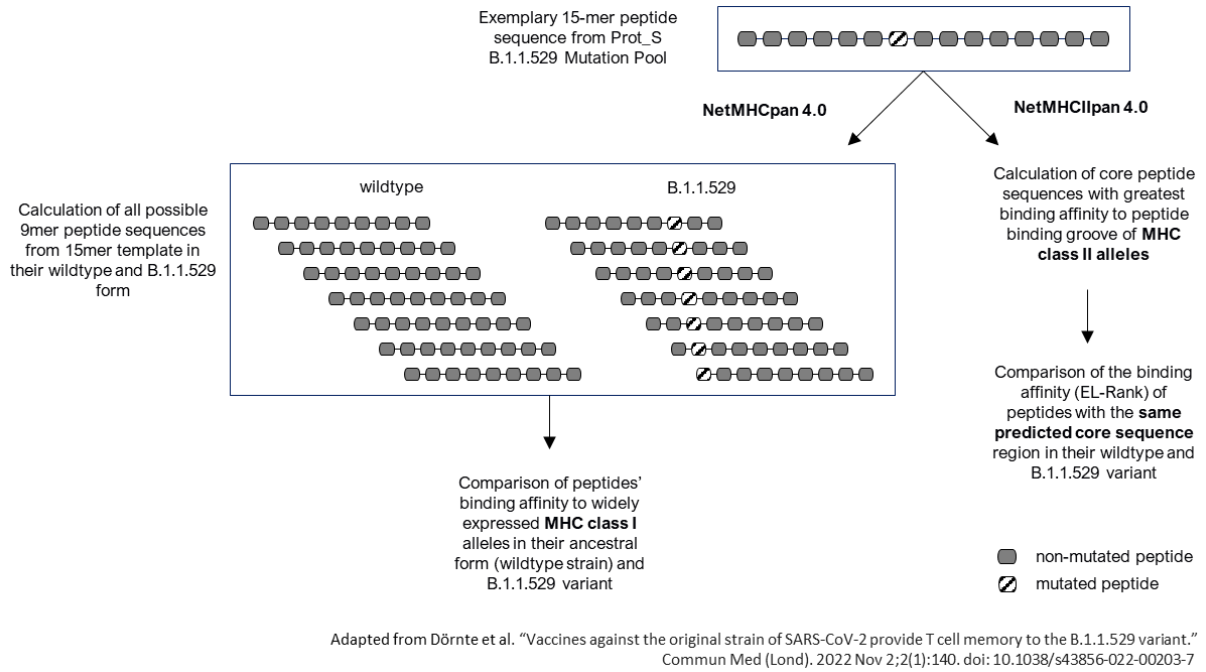

Figure 18. *In silico* binding prediction analysis strategy of SARS-CoV-2 wildtype versus the B.1.1.529 strain–derived peptides. Explanatory illustration for the comparative binding prediction analysis of complementary peptides derived from the SARS-CoV-2 wildtype (Wuhan) and the B.1.1.529 strain, using NetMHCpan 4.0 and NetMHCIIpan 4.0. Mutated peptides are depicted as striped ovals, non-mutated peptides are illustrated as solid ovals.

Changes in the EL-Rank, i.e., the theoretical binding affinity of a peptide to an HLA molecule, caused by the mutations presented by the SARS-CoV-2 B.1.1.529 variant, can result in three different scenarios: (option 1) increasing binding affinities result in (improved) binding to the HLA, (option 2) slightly decreased binding affinities result in worsened binding or (option 3) no binding at all. (**Figure 19**). The total number of conversions among these options, starting from the wildtype to the B.1.1.529 variant, were determined for binding to HLA Class I (**Figure 20**) and HLA Class II (**Figure 21**) allotypes. This analysis allows the identification of HLA allotypes with improved or worsened capacity for interaction with peptides originating from the SARS-CoV-2 B.1.1.529. Likewise, general trends for HLA Class I- and HLA Class II-dependent recognition can be determined. Among HLA Class I allotypes, most positive conversion occurs from non-binding to weak binding peptides. However, similar patterns can be observed for negative conversions. Overall, there is a general trend pointing towards antigen escape, as more antigens present with a worsened than an improved binding affinity. The same applies to HLA Class II allotypes. Overall, the T cell response was only mildly affected by the mutations, which were introduced with the Omicron variant, which suggested a relatively solid T cell response even towards strongly mutated viruses at the time.

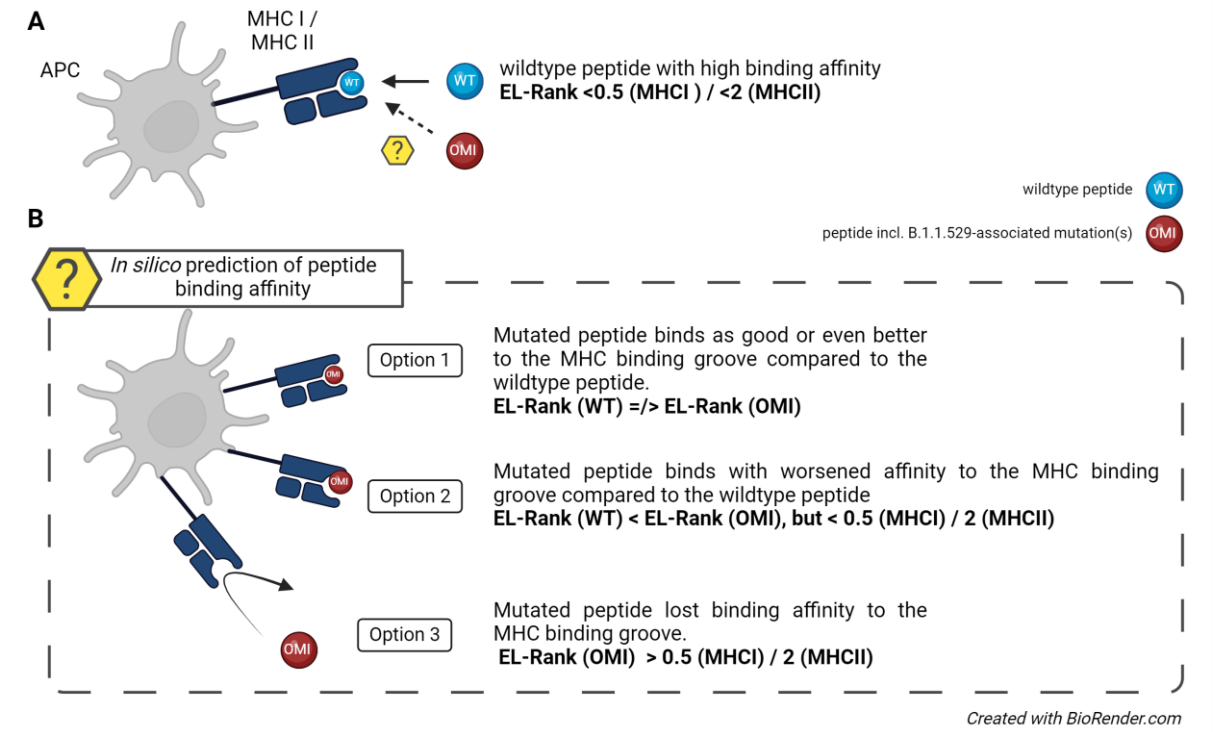

Figure 19. Potential changes in binding of peptides, including B.1.1.529-associated mutations to MHC Class I and Class II molecules. Illustration of (A) the specific research question in the focus of the comparative peptide binding prediction analysis and (B) potential outcomes of such analysis. The NetMHC(II)pan-4.0 eluted ligand percentile ranks (EL-Ranks) that were applied to the analysis are indicated for each scenario for binding to MHC Class I (MHCI) and MHC Class II (MHCII) alleles. WT = wildtype (ancestral Wuhan strain), OMI = peptides including B.1.1.529-associated mutations.

	NB--> SB	NB --> WB	WB --> SB	WB --> NB	SB --> WB	SB --> NB
HLA-A01:01	0	2	1	5	0	5
HLA-A02:01	1	4	0	5	0	5
HLA-A03:01	2	1	1	2	0	2
HLA-A11:01	3	1	0	2	0	2
HLA-A24:02	2	4	1	3	0	3
HLA-A26:01	0	7	0	4	2	4
HLA-A29:02	3	6	2	6	2	6
HLA-A33:03	0	4	1	0	0	0
HLA-A68:01	0	5	0	1	1	1
HLA-B07:02	0	3	0	3	0	3
HLA-B08:01	2	3	0	4	0	4
HLA-B14:02	2	5	2	9	1	9
HLA-B15:01	2	4	2	2	0	2
HLA-B15:02	1	5	1	0	2	0
HLA-B18:01	0	5	0	3	0	3
HLA-B27:05	0	4	0	2	0	2
HLA-B35:01	1	3	1	6	2	6
HLA-B40:01	0	1	0	1	1	1
HLA-B40:02	1	1	0	2	0	2
HLA-B44:02	1	2	0	0	0	0
HLA-B44:03	2	1	0	1	0	1
HLA-B45:01	0	4	0	3	0	3
HLA-C01:02	2	1	2	7	0	7
HLA-C02:02	5	3	1	3	2	3
HLA-C03:03	0	7	0	4	3	4
HLA-C03:04	0	7	0	4	3	4
HLA-C04:01	0	7	0	6	0	6
HLA-C05:01	0	6	0	5	0	5
HLA-C06:02	2	3	2	9	1	9
HLA-C07:01	2	7	1	7	3	7
HLA-C07:02	4	4	0	4	0	4
HLA-C08:01	0	4	1	4	1	4

Re-printed from Dörnte et al.
"Vaccines against the original strain of SARS-CoV-2 provide T cell memory to the B.1.1.529 variant."
Commun Med (Lond). 2022 Nov 2;2(1):140. doi: 10.1038/s43856-022-00203-7

Figure 20. Conversions of complementary peptides derived from the ancestral and B.1.1.529 strains between categories of peptide binding affinity to MHC Class I alleles. Heat map representing the total numbers of conversions between categories of non-binding (NB), weak binding (WB), and strong binding (SB) peptides (y-axis) for indicated MHC Class I alleles (x-axis).

	NB-->SB	NB-->WB	WB-->SB	WB-->NB	SB-->WB	SB-->NB
DRB1_0101	1	1	1	2	0	0
DRB1_0301	0	1	0	1	0	0
DRB1_0401	0	0	0	2	0	1
DRB1_0701	0	2	0	1	1	0
DRB1_0901	0	2	0	4	1	0
DRB1_1501	0	2	1	3	0	0
DRB1_1101	0	1	1	1	0	0
DRB1_1301	0	2	0	0	0	0
DRB1_1401	0	0	1	2	0	0
DRB1_0404	0	1	0	3	0	2
DRB1_0405	0	0	0	4	0	0
DRB1_0407	0	0	0	4	0	0
DRB1_0411	0	0	0	2	0	0
DRB1_0803	1	1	0	1	0	1
DRB1_1302	1	1	0	2	0	0

Re-printed from Dörnte et al.
"Vaccines against the original strain of SARS-CoV-2 provide T cell memory to the B.1.1.529 variant."
Commun Med (Lond). 2022 Nov 2;2(1):140. doi: 10.1038/s43856-022-00203-7

Figure 21. Conversions of complementary peptides derived from the ancestral and B.1.1.529 strains between categories of peptide binding affinity to MHC Class II alleles. Heat map representing the total number of switches between categories of non-binding (NB), weak binding (WB), and strong binding (SB) peptides (y-axis) for indicated MHC Class II alleles (x-axis).

Sequential *in vitro* T-cell stimulation and *in silico* NetMHC(II)pan approaches enable the identification of SARS-CoV-2-specific T-cell epitopes

Data presented in the following section has been published in the international peer-reviewed journal European Journal of Immunology in April 2025. DOI: 10.1002/eji.202451497

The initial analyses of the Omicron variant showed a relatively stable T cell memory induced via first-generation vaccines. To correlate T-cell immunogenic regions to areas of increased mutation rates observed within novel virus strains, could allow however to estimate potential viral immune escape from T cellular adaptive immunity as a potential or likely event in the future. Furthermore, this information indicates protein regions that are of potential interest for incorporation into next-generation vaccines, which aim to elicit a strong T-cell response. Therefore, three research objectives were defined: First, to identify single T-cell epitopes. Second, to unravel differences among immune responses mounted by vaccination and/or infection by mapping immunogenic protein regions. Third, to correlate T-cell immunogenic regions to mutation rates observed within novel virus strains, which allows us to estimate the degree of potential viral immune escape from cellular adaptive immunity

To address those objectives, three cohorts comprising (A) vaccinated (n=27), (B) convalescent (n=33), and (C) vaccinated and convalescent (n=12) individuals were recruited (**Figure 22**, **Supplementary Figure 1**) and tested within *in vitro* peptide stimulation approaches using consecutive peptide (pools) (from now on referred to as sequential walk). Cohorts A and B comprise a comparable number of participants with a comparable median age. Cohort A includes relatively more female study subjects than male study subjects. Due to the nature of the HLA system, similar HLA expression among individuals, which would be ideal for comparative analysis, is not possible. However, as shown for HLA-A (**Figure 22; B**) and all other relevant HLA-alleles (**Supplementary Figure 1**), HLA distribution is comparable for cohorts A and B. For the defined purposes, consecutive 15-mer peptides covering the genomic sequences of the SARS-CoV-2 structural S-, N-, and M-proteins were synthesized and pooled to cover 50 amino acid-long regions (**Figure 23; A**). The subsequent identification of immunogenic protein regions and single peptides was done in three consecutive analysis steps: (1) ascertain the T cell response induced by the aforementioned 50-amino acid long protein regions *in vitro*, (2) identify single 15-mer peptides originating from those protein regions that induce a T-cell response by independent *in vitro* and *in silico* analyses, and (3) verify the 9-mer

core epitope, which originates from immunogenic 15-mer peptides, and its HLA-restriction *in vitro* (**Figure 23; B**). T-cell reactivity, induced as a response to the stimulation with aforementioned 9-mer or 15-mer single peptides or peptide pools, was visualized by staining of activation-associated intracellular cytokines and cell surface marker CD154 and subsequent flow-cytometric analysis (**Figure 24**). As a result of the stimulation with cognate antigen, T-cell activation was positively confirmed if a distinct population of cells, which is double-positive for the expression of activation markers and showed a frequency increase of at least 10% compared to the negative unstimulated control, was found. The results are listed in **supplementary tables 2 to 5.**

A

Cohort	SARS-CoV-2 history	n	sex (female:male)	mean age	Mean interim between vaccination / infection and blood donation (days)	Vaccine Distribution						
						BNT162b2	mRNA-1273	ADZ21222	ADZ21222/ BNT162b2	Ad26.COV2.S	no specified mRNA vaccine	no specified vaccine
A	vaccinated	27	3,5	37	57	17 (63%)	2 (7%)	2 (7%)	1 (4%)	/	2 (7%)	3 (11%)
B	convalescent	33	1,1	41	59	n.A.						
C	vaccinated + convalescent	12	1,4	48	41	3 (25%)	3 (25%)	2 (17%)	/	1 (8%)	/	3 (25%)

B

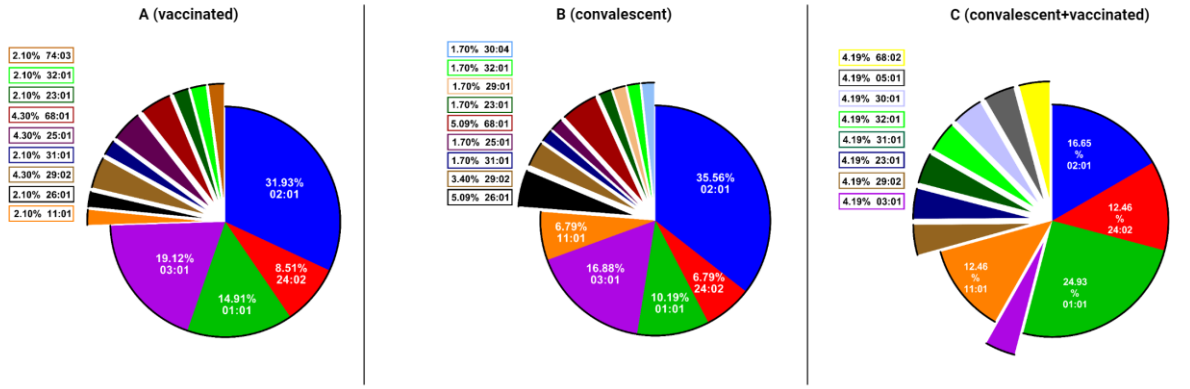

Adapted from " ***Distinct HLA Haplotypes Are Associated With an Altered Strength of SARS-CoV-2-Specific T-Cell Responses and Unfavorable Disease Courses"***, European Journal of Immunology, 2025; DOI: 10.1002/eji.202451497

Figure 22. Demographic information for cohorts A to C. (A) Tabular overview on cohorts' SARS-CoV-2 history, sex ratio, mean age, mean interim days between vaccination/infection and analysis date, and vaccines administered to the study subjects. (B) Exemplary distribution of HLA-A allotypes among cohort A (vac; vaccinated), B (con; convalescent), and C (vac+con; vaccinated and convalescent) (from left to right). The percentage of donors present within the respective cohort is given for each allotype.

Results - Sequential in vitro T-cell stimulation and in silico NetMHC(II)pan approaches enable the identification of SARS-CoV-2-specific T-cell epitopes

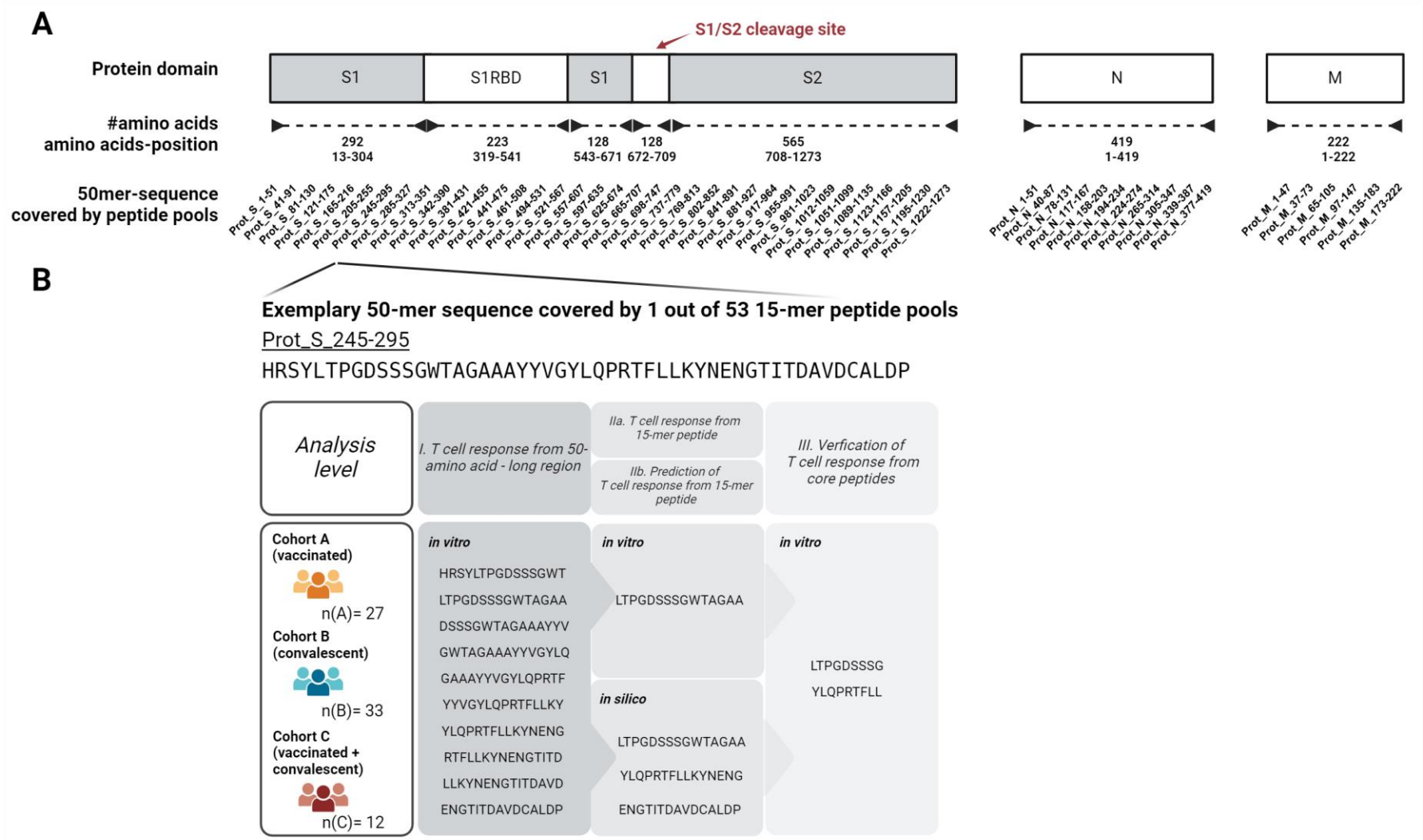

Adapted from " ***Distinct HLA Haplotypes Are Associated With an Altered Strength of SARS-CoV-2-Specific T-Cell Responses and Unfavorable Disease Courses"***, European Journal of Immunology, 2025; DOI: 10.1002/eji.202451497

Figure 23. Peptide design and validation strategy for the identification of SARS-CoV-2 – specific T cell epitopes. (A) Domains of the SARS-CoV-2 Spike (S), Nucleocapsid (N), and Membrane (M) protein, the corresponding number of amino acids and their respective positions, and the sequence coverage of 53, 50 amino acid-long peptide regions from which peptide pools are synthesized. **(B)** Exemplary analysis strategy for the identification of immunogenic 15-mer and 9-mer peptides, i.e., peptides that can induce a T cell response out of protein sequence Prot_S_245-295 in three cohorts of (A) vaccinated (n=27), (B) convalescent (n=33), and (C) vaccinated and convalescent (n=12) individuals. Peptides' capability to induce a T cell response is evaluated on three analysis levels: (I) by in vitro testing of a peptide pool consisting of 10 15-mer peptides, (II) by in vitro testing of single 15-mer peptides derived from immunogenic peptide pools and in silico prediction of theoretical binding affinities of 15-mer peptides, and (III) by in vitro testing of 9-mer core peptides

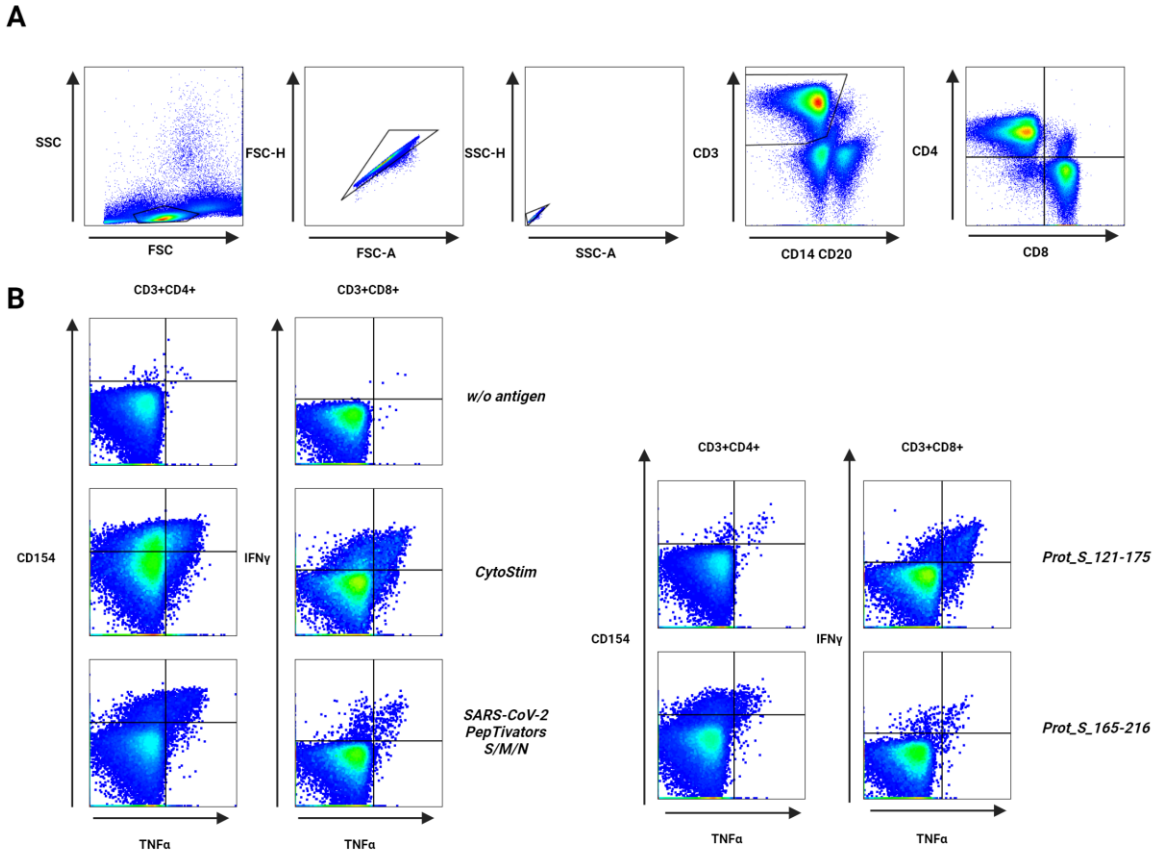

Adapted from " ***Distinct HLA Haplotypes Are Associated With an Altered Strength of SARS-CoV-2-Specific T-Cell Responses and Unfavorable Disease Courses"***, European Journal of Immunology, 2025; DOI: 10.1002/eji.202451497

Figure 24. Exemplary flow cytometric assessment of T cell reactivity after *in vitro* stimulation of PBMCs with CytoStim™, SARS-CoV-2 PepTivators, and two spike-originating 15-mer peptide pools. (A) Flow plots showing the pre-gating on lymphocytes, singlets, and $CD3^+$ T cells before subdivision into $CD4^+$ and $CD8^+$ T cells. **(B)** Reactive $CD8^+$ T cells were defined as INF-γ^+ TNF-α^+ double-positive, while reactive $CD4^+$ T cells were defined as TNF-α^+CD154^+. Negative, unstimulated controls (w/o antigen) and positive controls stimulated with CytoStim and SARS-CoV-2 PepTivators

were prepared for each donor. Exemplary, flow plots after stimulation with two Spike protein-originating 15-mer peptide pools (Prot_S_121-175 / _165-216) are shown.

In total, 83 core peptide candidates have been identified that showed immunogenic capacity within both *in vitro* stimulation approaches on peptide pool level as well as on single 15-mer peptide level. The complete list of peptide candidates, their HLA-restriction, nucleotide sequence, and the results of the *in vitro* validation of reactivity on PBMC and expanded cells is provided in **Supplementary Table 5**. Some of these epitope candidates could not be verified *in vitro* due to a lack of T-cell reactivity after stimulation or restrictions on rare HLAs that the available donors did not cover. Among the cohort of peptides that have demonstrated multiple reactivity, thereby confirming their status as T-cell epitopes, the core peptide HLA-A01:01_P2 (MSSADSTQA) exhibits distinctive characteristics compared to other epitopes. Notably, despite its initial prediction to bind to the HLA-A01:01 allotype, this novel epitope has demonstrated a notable degree of reactivity at the $CD4^+$ T-cell level, as exemplarily shown for an HLA-A01:01-positive blood donor (**Figure 25**).

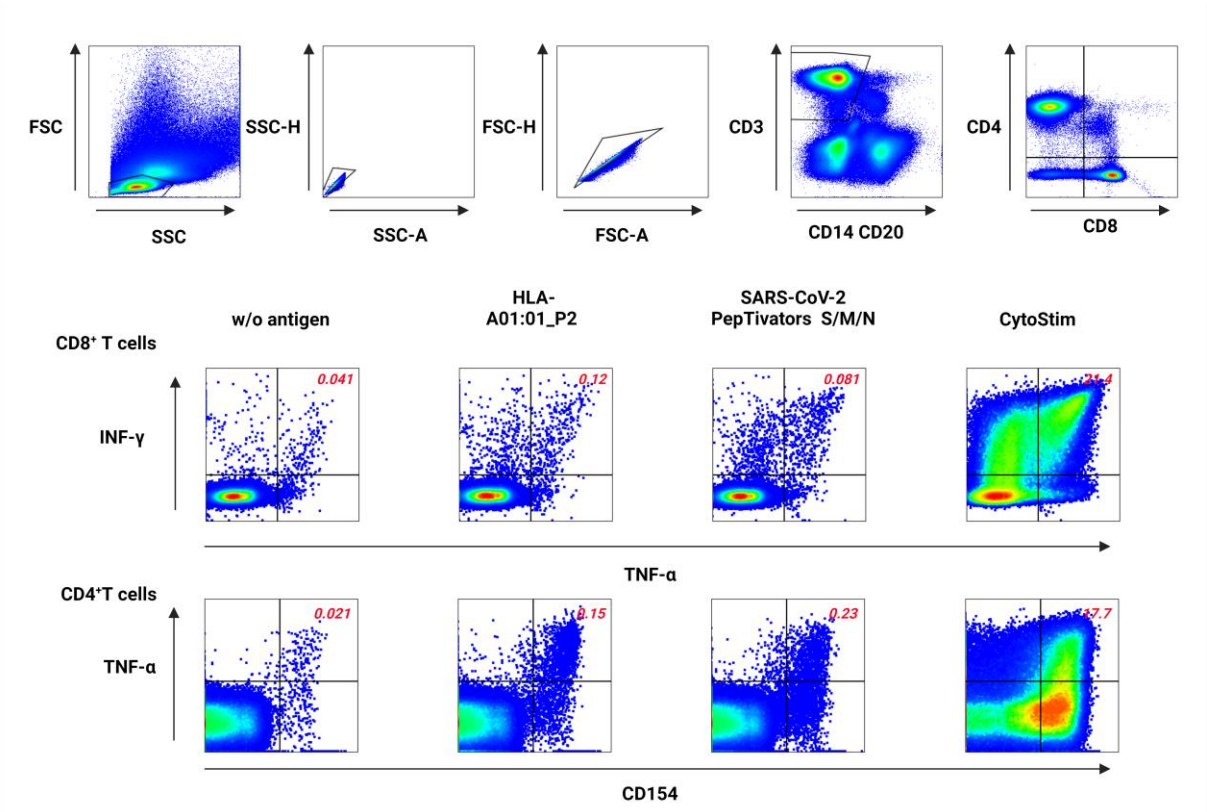

Adapted from " ***Distinct HLA Haplotypes Are Associated With an Altered Strength of SARS-CoV-2-Specific T-Cell Responses and Unfavorable Disease Courses"***, European Journal of Immunology, 2025; DOI: 10.1002/eji.202451497

Figure 25. HLA-A01:01_P2- immunogenicity assessment on an HLA-A01:01-positive donor
Exemplary flow graphs of PBMCs from an HLA-A01:01-positive donor stimulated with peptide HLA-A01:01_P2. The pre-grating is done on lymphocytes, singlets, and $CD3^+$ cells, followed by a subdivision into $CD4^+$ and $CD8^+$ T cells (upper row; going from left to right). Reactivity of T cells was estimated *in*

vitro w/o stimulation and upon stimulation with HLA-A01:01_P2, SARS-CoV-2 PepTivator Prot_S Complete/ Prot_N/ Prot_M or CytoStim (going from left to right). Reactive $CD8^+$ T cells are defined as TNF-α^+INF-γ^+ double positive (middle row). Among the $CD4^+$T cells, reactive cells are gated as $CD154^+$TNF-α^+ double positive (bottom row). Red numbers indicate the frequencies of double-positive cells.

T cell epitope mapping in SARS-CoV-2 structural proteins

Data presented in the following section has been published in the international peer-reviewed journal European Journal of Immunology in April 2025. DOI: 10.1002/eji.202451497

Counting the absolute number of donors from cohorts A to C that showed reactivity among $CD8^+$INF-γ^+TNF-α^+ (upper graph) or $CD4^+CD154^+$INF-γ^+ T cells (lower graph) upon stimulation with SARS-CoV-2 peptide pools covering the indicated 50-amino acid long regions, immunogenic protein regions were mapped (**Figure 26**). While cohort C (red) can be neglected due to low n-numbers, reactivity against all expected protein regions by cohort A (orange) and B (petrol) can be observed. However, the distribution of those reactivities is slightly different for vaccinated and convalescent individuals. While naturally infected individuals show nearly homogenous distribution among all protein subregions, with exceptions for four regions within the S1-RBD region, vaccinated individuals show peaking reactivities for the C-terminal end of the Spike S1-subunit and the S1-receptor binding domain (RBD). The correlation to the absolute number of mutations that were acquired within the currently circulating SARS-CoV-2 Omicron lineages EG.5.1, XBB, BQ.1, BA.2.75, BA.2.12.2, BA.5, BA.5, BA.2 and BA.1 (**Figure 26**, B; pink line), as well as to the mutations affecting the epitopes of nABs (dotted arrows), shows no association with the immunogenic, thus T cell response-inducing regions. Furthermore, the comparison of absolute numbers of responsive donors and the number of NetMHC(II)pan-predicted weak and strong binding peptides (grey line) does not show similar trends for all protein regions.

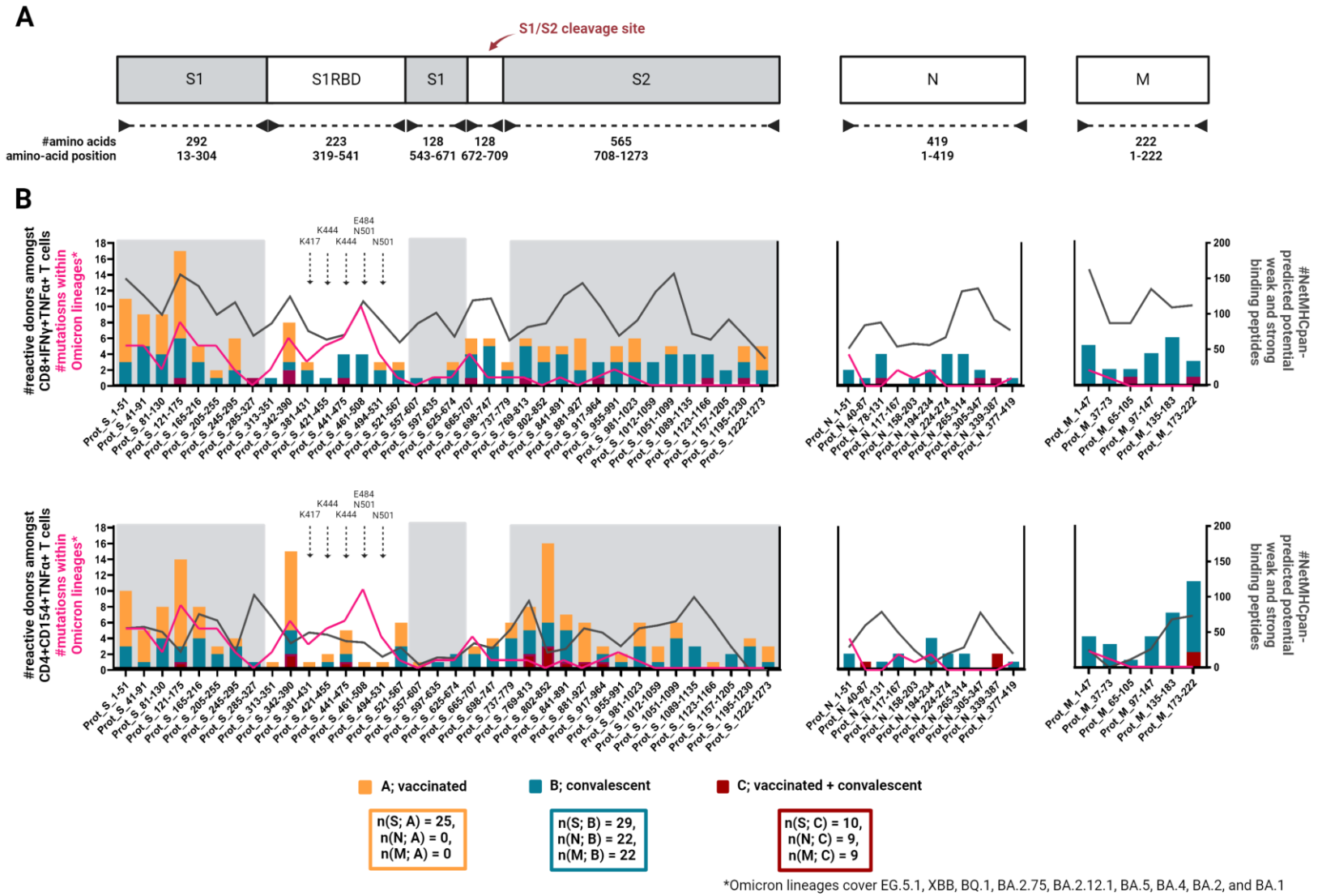

Adapted from " ***Distinct HLA Haplotypes Are Associated With an Altered Strength of SARS-CoV-2-Specific T-Cell Responses and Unfavorable Disease Courses***", European Journal of Immunology, 2025; DOI: 10.1002/eji.202451497

Figure 26. Mapping of T cell response inducing protein regions in cohorts of vaccinated and/or convalescent individuals. (A) Domains of the SARS-CoV-2 Spike (S), Nucleocapsid (N), and Membrane (M) protein, the corresponding number of amino acids, and their respective positions. **(B)** Bar graphs representing the total number of reactive study subjects amongst $CD8^+INF\text{-}\gamma^+TNF\text{-}\alpha^+$ T cells (upper graph) and $CD4^+CD154^+INF\text{-}\gamma^+$ T cells (lower graph) (left y-axes) plotted against 50 amino acid long protein regions, aligned to (A) (x-axes). Cohort A is shown in orange, cohort B is shown in petrol, and cohort C is in red. Pink lines represent the total number of mutations found within Omicron lineages (left y-axes), covering the following strains: EG.5.1, XBB, BQ.1, BA.2.12.1, BA.5, BA.4, BA.2, and BA.1. Grey lines represent the total number of NetMHCpan-predicted potential weak and strong binding peptides for each protein region. Mutations within the S1-RBD regions, affecting the neutralizing capacity of antibodies, are indicated with dashed arrows.

Unfavorable HLA molecules cause prolonged disease and decreased frequencies of virus-specific $CD8^+$ T cells

Data presented in the following section has been published in the international peer-reviewed journal European Journal of Immunology in April 2025. DOI: 10.1002/eji.202451497

The established T cell response-inducing protein pattern was shared with cooperation partners of this PhD project, Dr. Angeliki Datsi and Prof. Dr. Johannes Fischer, working at the Institute for Transplantation Diagnostics and Cell Therapeutics at the University Hospital Düsseldorf (Germany), who recently described the correlation between specific HLA haplotypes and more severe COVID-19 disease courses (**Supplementary Table 6**).[43] In order to determine whether this correlation is caused by the (in)ability of those HLA haplotypes that cause prolonged and more severe disease (from now on referred to as *unfavorable haplotypes*), and those HLA haplotypes that cause short and mild disease (from now on referred to as *favorable haplotypes*), to present peptides to T cells, the immunogenic protein regions for cohorts A to C were re-mapped (**Figure 27**). For this, study subjects of cohort A to C were first categorized according to their expression of favorable and unfavorable allotypes. Based on this categorization, the total numbers of reactive donors among activated $CD4^+$ and $CD8^+$ T cells were plotted. The comparison shows that the pattern of reactive donors with favorable (**Figure 27**, B and C, lower graphs) and unfavorable HLA allotypes (**Figure 27**, B and C, upper graphs) are very similar, indicating that both groups of study subjects have similar capacity to present peptides via their HLA molecules to T cells.

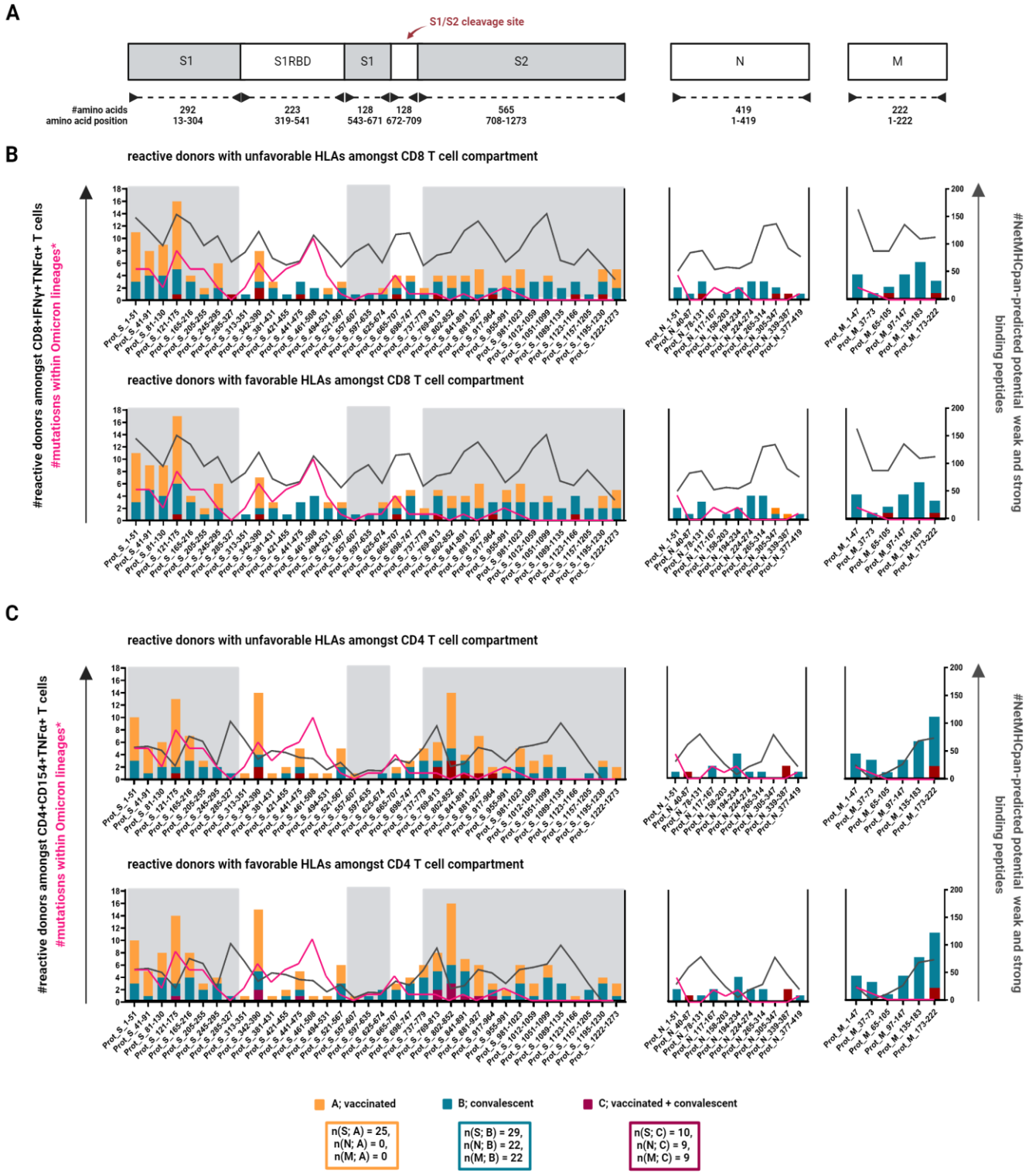

*Omicron lineages cover EG.5.1, XBB, BQ.1, BA.2.75, BA.2.12.1, BA.5, BA.4, BA.2, and BA.1

Adapted from "***Distinct HLA Haplotypes Are Associated With an Altered Strength of SARS-CoV-2-Specific T-Cell Responses and Unfavorable Disease Courses"***, European Journal of Immunology, 2025; DOI: 10.1002/eji.202451497

Figure 27. Comparison of T cell response-inducing protein regions among individuals expressing (un)favorable HLA alleles linked to the disease course. (A) Domains of the SARS-CoV-2 Spike (S), Nucleocapsid (N), and Membrane (M) protein, the corresponding number of amino acids, and their respective positions. **(B, C)** Bar graphs representing the total number of reactive study subjects

expressing unfavorable (upper graphs) or favorable HLA alleles (lower graphs) amongst (B) $CD8^+$ INF-γ^+TNF-α^+ T cells (upper graph) and (C) $CD4^+$ $CD154^+$INF-γ^+ T cells (left y-axes) plotted against 50 amino acid long protein regions, aligned to (A) (x-axes). Cohort A is shown in orange, cohort B is shown in petrol, and cohort C is in red. Pink lines represent the total number of mutations found within Omicron lineages (left y-axes), covering the following strains: EG.5.1, XBB, BQ.1, BA.2.12.1, BA.5, BA.4, BA.2, and BA.1. Grey lines represent the total number of NetMHCpan-predicted potential weak and strong binding peptides for each protein region. Mutations within the S1-RBD regions, affecting the neutralizing capacity of antibodies, are indicated with dashed arrows.

As we did not observe any differences in the presentation of peptides by individuals expressing favorable and unfavorable HLAs, we hypothesized intrinsic factors in the T cell response to be the underlying cause of more severe disease course observed for certain HLAs. To test this hypothesis, a fourth independent cohort D comprising 40 convalescent donors was recruited to examine the SARS-CoV-2-specific T cell response. From those individuals, the clinical phenotype of disease severity and duration was assessed by a questionnaire. Furthermore, the frequency and absolute counts of SARS-CoV-2 Spike-responsive T cells, nAB titers, and subjects' HLA background were determined to identify potential correlations (**Figure 28**).

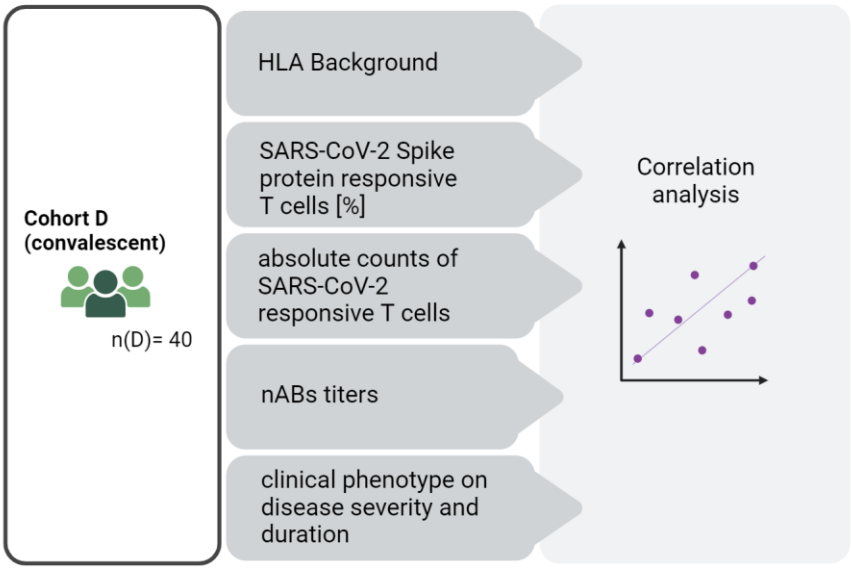

Adapted from " ***Distinct HLA Haplotypes Are Associated With an Altered Strength of SARS-CoV-2-Specific T-Cell Responses and Unfavorable Disease Courses"***, European Journal of Immunology, 2025; DOI: 10.1002/eji.202451497

Figure 28. **Analysis strategy for correlation analysis of SARS-CoV-2 specific T cell responses.** Correlation analyses of cohort D comprised convalescent individuals. HLA background, the frequency of SARS-CoV-2 Spike-responsive T cells, the absolute counts of SARS-CoV-2 responsive T cells, neutralizing antibody (nAB) titers, and the clinical phenotype on disease severity and duration were assessed.

The assessment of the $CD4^+$ and $CD8^+$ T cell responses to SARS-CoV-2 revealed a low frequency of $CD3^+CD8^+$IFN-γ^+ T cells in patients with prolonged diseases, preferably

accumulating for unfavorable HLA-haplotypes (**Figure 29**, A). In contrast, the absolute numbers of activated $CD8^+$ T cells after restimulation with SARS-CoV-2 PepTivator Prot_S, -Prot_N, and -Prot_M were significantly increased in all individuals with prolonged disease, pointing towards a high bystander $CD8^+$ T cell activation (**Figure 29**, B). The same was observed in more severe disease courses. However, it did not reach statistical significance for individuals expressing unfavorable HLAs after re-stimulation with SARS-CoV-2 peptides originating from the S, N, and M proteins (**Figure 29**, C). Virus-specific $CD4^+$ T cells, instead, showed an increased frequency in individuals expressing unfavorable HLAs and suffering from prolonged disease (**Figure 30**, A). This was supported by increased numbers of activated $CD4^+$ T cells in all individuals and individuals exclusively expressing unfavorable HLAs (**Figure 30,** B, and C**)**. As we could only find indications for slightly increased $CD4^+$ T cell responses in individuals with unfavorable haplotypes but no significant changes based on the absolute cell counts in individuals expressing favorable and unfavorable HLA haplotypes, we wanted to investigate whether there is a correlation between $CD4^+$ T cell responses and the corresponding titers of neutralizing antibodies which may contribute to explain differences within the disease course of study subjects. This analysis demonstrated a significant increase of virus-specific $CD4^+$ T cell frequencies accompanied by significantly increased levels of nABs in individuals with prolonged disease (**Figure 31**).

Results - Unfavorable HLA molecules cause prolonged disease and decreased frequencies of virus-specific CD8+ T cells

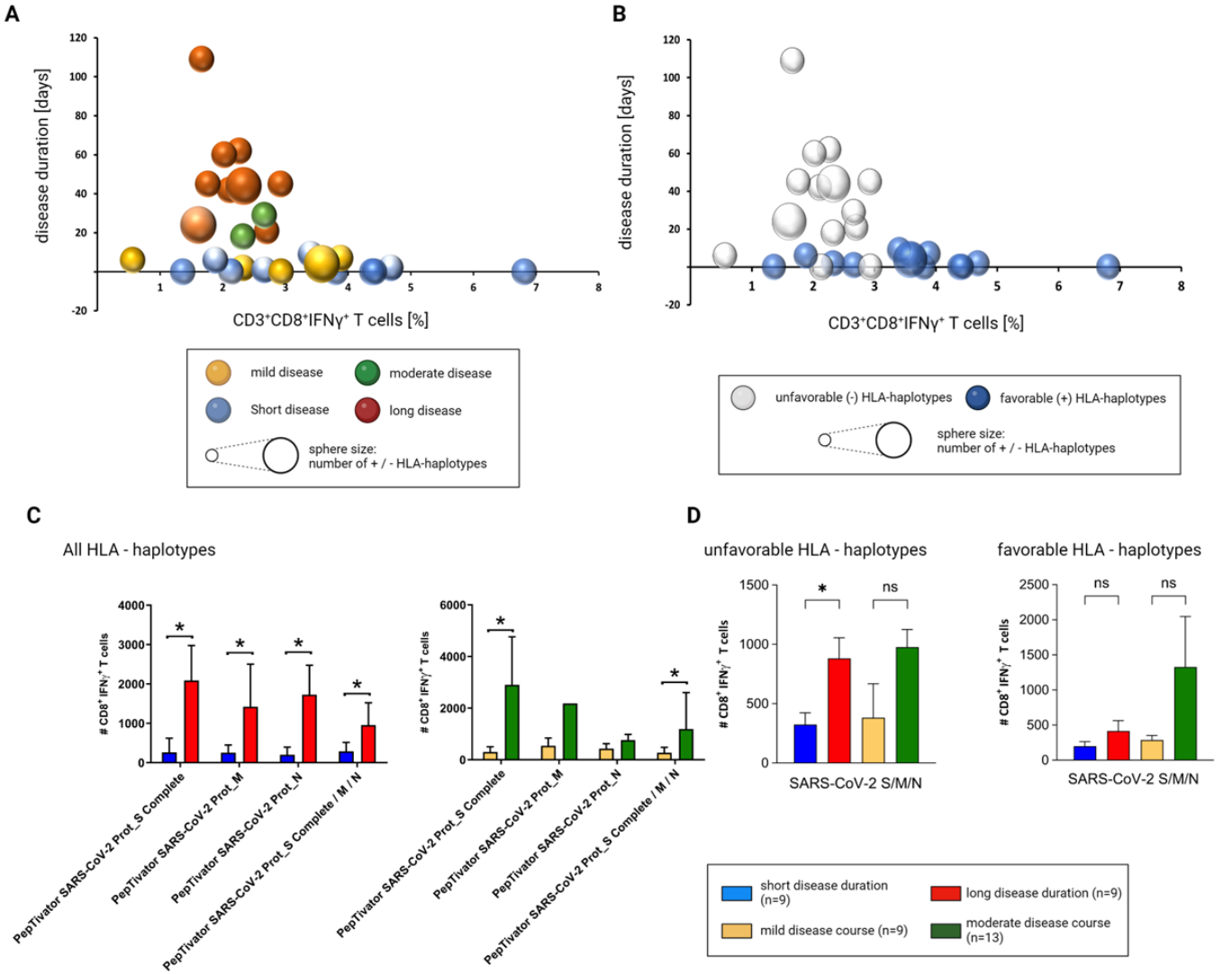

Reprinted from " ***Distinct HLA Haplotypes Are Associated With an Altered Strength of SARS-CoV-2-Specific T-Cell Responses and Unfavorable Disease Courses"***, European Journal of Immunology, 2025; DOI: 10.1002/eji.202451497

Figure 29. Low frequencies of virus-specific $CD8^+$ T cell responses are associated with prolonged disease in convalescent individuals. (A) Disease duration measured in days (y-axis) plotted against the frequency of $CD3^+CD8^+IFN\text{-}\gamma^+$ T cells (x-axis). Unfavorable haplotypes (white spheres) and favorable haplotypes (blue spheres) are shown. The sphere size represents the number of favorable/unfavorable haplotypes. **(B)** Absolute numbers of $CD8^+IFN\text{-}\gamma^+$ T cells after restimulation of PBMCs from convalescent all study subjects with PepTivator® peptide pools, covering the Spike protein sequence (SARS-CoV-2 Prot_S Complete), the Membrane protein sequence (SARS-CoV-2 Prot_M), the Nucleocapsid protein sequence (SARS-CoV-2 Prot_N), or all of the three aforementioned peptide pools (SARS-CoV-2 Prot_S Complete / M / N). **(C)** Absolute number of $CD8^+IFN\text{-}\gamma^+$ T cells after restimulation of PBMCs from convalescent study subject expressing unfavorable HLA haplotypes with mix of PepTivator® SARS-CoV-2 Prot_S Complete / M / N. Study subjects were categorized into groups of short (solid, light-grey bars), long (solid, black bars), mild (striped, light-grey bars) and moderate disease courses (striped, dark-grey bars). n numbers are indicated in the figure legend. Error bars represent the SEM; *; p=<0.05

Results - Unfavorable HLA molecules cause prolonged disease and decreased frequencies of virus-specific CD8+ T cells

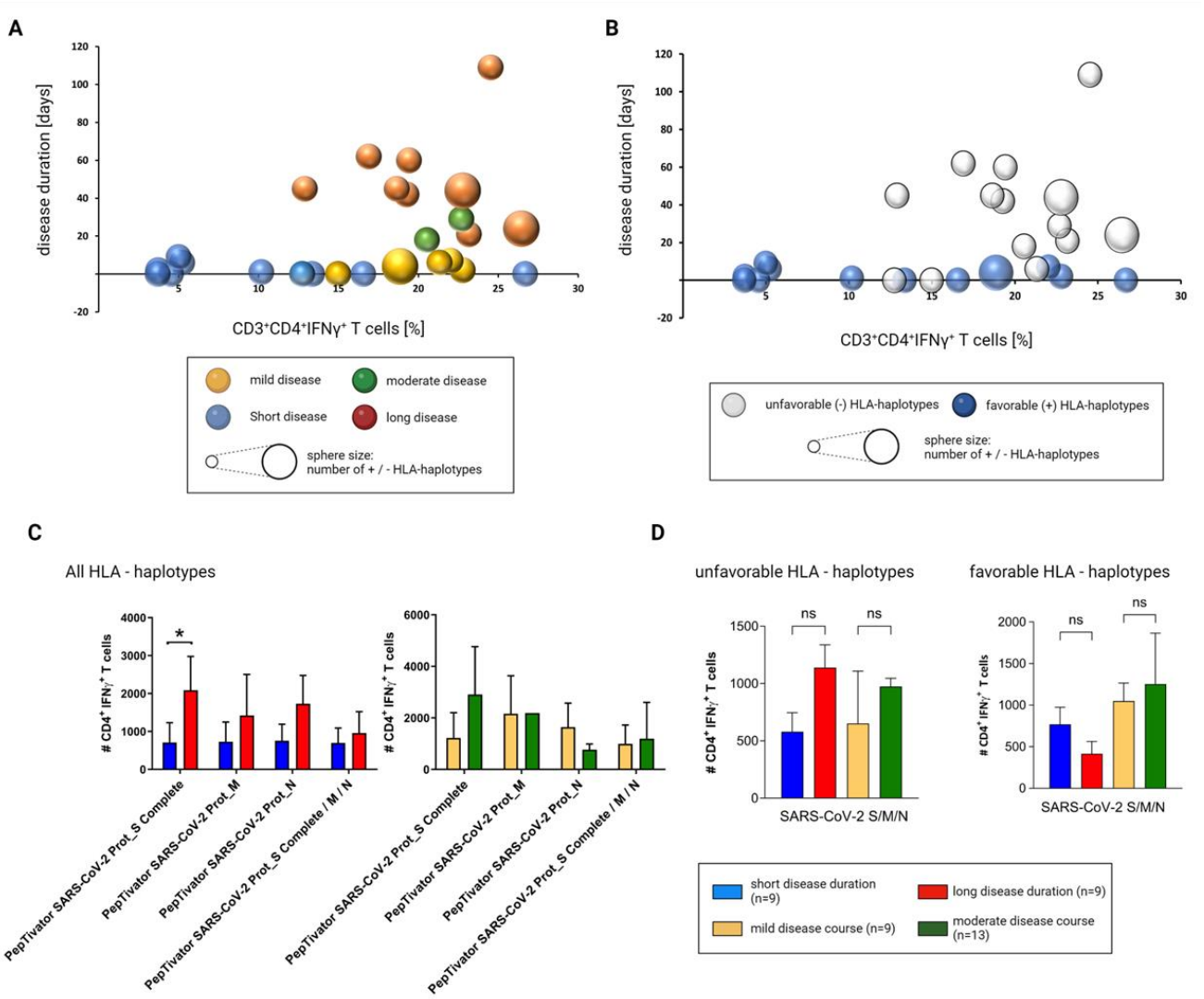

Reprinted from " ***Distinct HLA Haplotypes Are Associated With an Altered Strength of SARS-CoV-2-Specific T-Cell Responses and Unfavorable Disease Courses"***, European Journal of Immunology, 2025; DOI: 10.1002/eji.202451497

Figure 30. High frequencies of virus-specific CD4⁺ T cell responses are associated with prolonged disease in convalescent individuals. (A) Disease duration measured in days (y-axis) plotted against the frequency of $CD3^+CD4^+IFN\text{-}\gamma^+$ T cells (x-axis). Unfavorable haplotypes (white spheres) and favorable haplotypes (blue spheres) are shown. The sphere size represents the number of favorable / unfavorable haplotypes. **(B)** Absolute number of $CD4^+IFN\text{-}\gamma^+$ T cells after restimulation of PBMCs from convalescent all study subjects with PepTivator® peptide pools, covering the Spike protein sequence (SARS-CoV-2 Prot_S Complete), the Membrane protein sequence (SARS-CoV-2 Prot_M), the Nucleocapsid protein sequence (SARS-CoV-2 Prot_N), or all of the three aforementioned peptide pools (SARS-CoV-2 Prot_S Complete / M / N). **(C)** Absolute number of $CD4^+IFN\text{-}\gamma^+$ T cells after restimulation of PBMCs from convalescent study subject expressing unfavorable HLA haplotypes with mix of PepTivator® SARS-CoV-2 Prot_S Complete / M / N. Study subjects were categorized into groups of short (solid, light-grey bars), long (solid, black bars), mild (striped, light-grey bars) and moderate disease courses (striped, dark-grey bars). n numbers are indicated in the figure legend. Error bars represent the SEM; *; p=<0.05

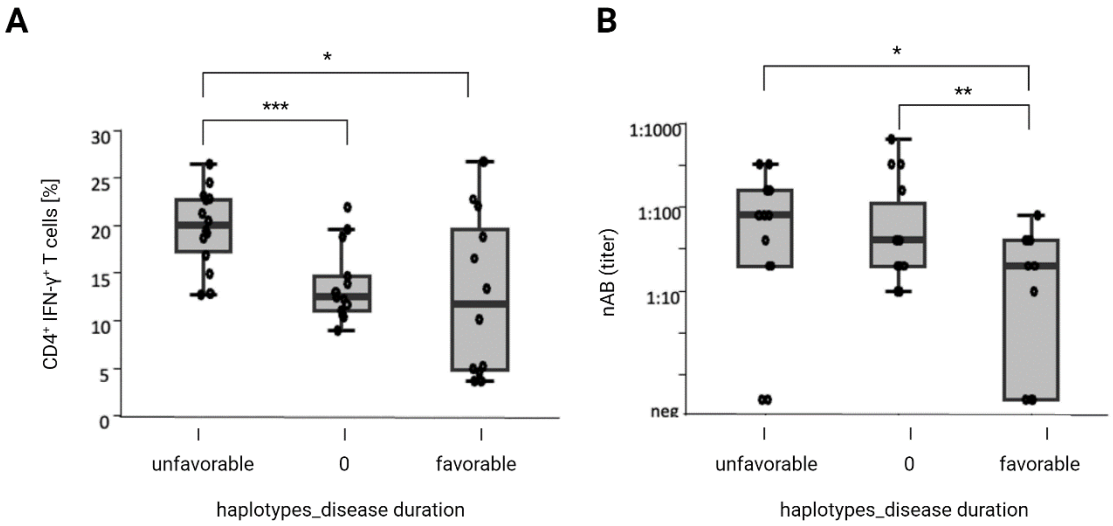

Reprinted from " ***Distinct HLA Haplotypes Are Associated With an Altered Strength of SARS-CoV-2-Specific T-Cell Responses and Unfavorable Disease Courses"***, European Journal of Immunology, 2025; DOI: 10.1002/eji.202451497

Figure 31. **Unfavorable HLAs are associated with increased frequencies of reactive CD4⁺ T cells and elevated frequencies of neutralizing antibodies. (A)** Correlation of unfavorable HLA haplotypes, linked to prolonged disease, with the $CD4^+$ T-cell. **(B)** Correlation of unfavorable HLA haplotypes, linked to prolonged disease, with the titer of neutralizing antibodies (nABs). 0 represents the median response of unfavorable and favorable haplotypes that were linked to disease duration; * = $p < 0.05$, ** = $p < 0.005$, *** = $p < 0.0005$; n = 20; Error bars represent mean values ± SEM

Concept and establishment of a multiplex HLA binding assay

Data presented in the following section are part of a patent application (EP23216590.2) at the European Patent Office, submitted on the 14th of December, 2023.

Depending on the size of the antigen of interest, the identification and validation of T cell epitopes is often inefficient and laborious, especially due to the aforementioned complexity of the human HLA system. One aim of this project is the development of a novel T-cell epitope-identification approach that allows for fast and efficient detection of those epitope candidates through multiplexing. The latter specifically intends to screen the binding capability of one or multiple epitope candidates to multiple HLA allotypes simultaneously. For this, a biotinylated HLA allotype of interest, loaded with a fluorescently (FITC) labeled placeholder peptide (pFITC/MHC), is coupled to a population of streptavidin-APC-PMMA beads (from now on referred to as *beads*) that serve as artificial carrier platform and can be visualized via flow cytometric analysis. To enable the HLA-specific evaluation of peptide binding, each allotype is coupled to its own bead population that can be discriminated by its fluorescent label. In this assay, bead populations emitting different APC-signal mean fluorescent intensities (MFI) are used (**Figure 32**). Subsequently, a peptide exchange on a cognate HLA is catalyzed by incubating the pFITC/MHC-bead complexes with HLA-specific exchange catalysts and epitope candidate peptides. This peptide exchange can be flow cytometrically assessed by the loss of fluorescent signal, priorly emitted by the placeholder peptide. Downstream to this, pMHC/bead complexes could be isolated, e.g., by fluorescent activated cell sorting (FACS), and used for T-cell restimulation. This assay concept was named *multiplex HLA binding assay* (**Figure 33**).

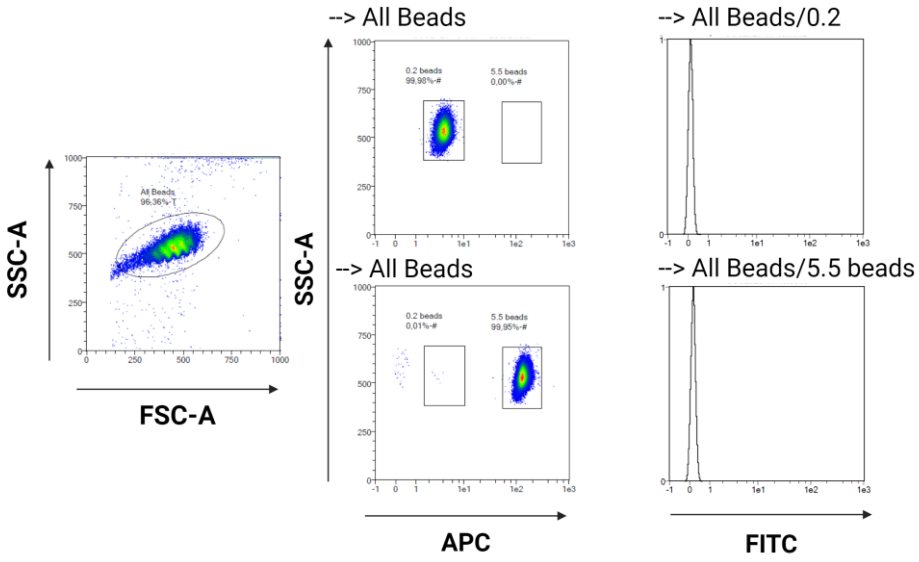

Figure 32. Flow cytometric assessment of fluorescent signal emitted by uncoupled APC-labeled PMMA beads. Flow cytometric characterization of two populations of APC-coupled PMMA beads (0.2 and 5.5 beads) used within the multiplex HLA binding assay. The analysis shows the distinctive APC signals emitted by the bead populations, allowing for their discrimination. A FITC signal is absent for both populations.

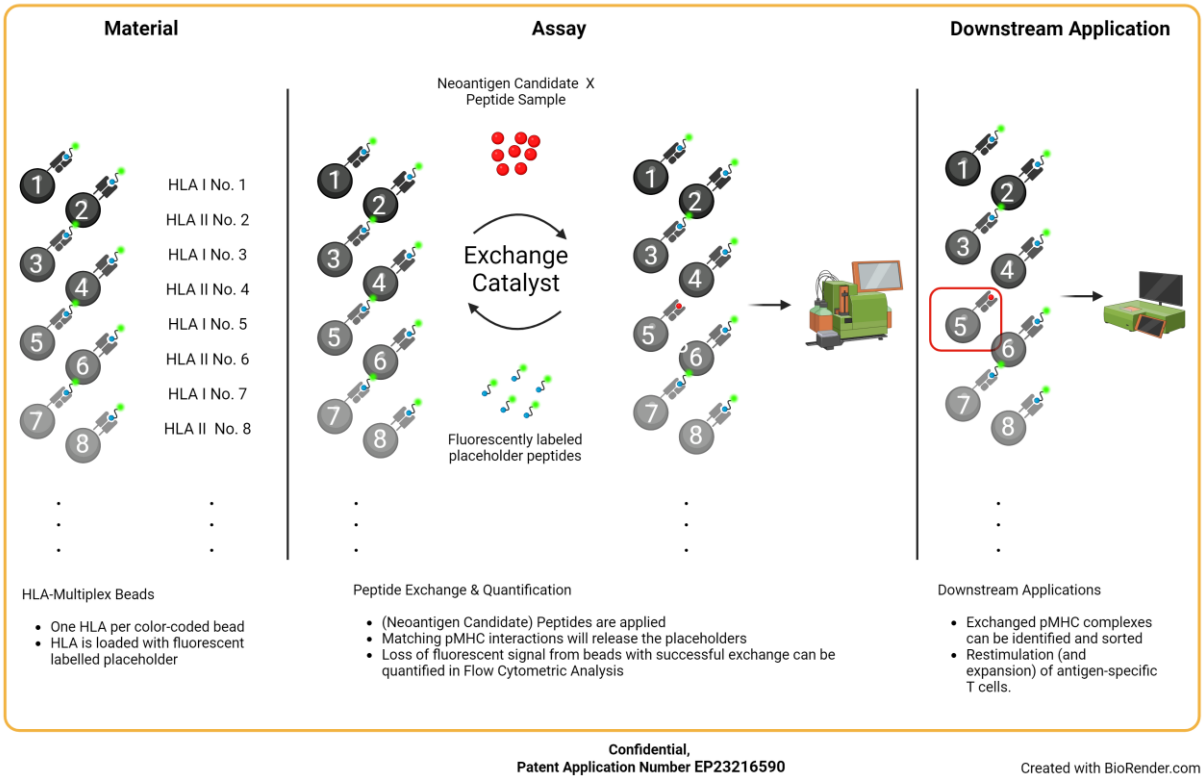

Figure 33. Concept for a multiplex HLA binding assay. Color-coded bead populations attached to an HLA allele of interest with a fluorescently labeled placeholder peptide are used as reaction platforms. Within the assay, those bead-HLA complexes are incubated with potential neoantigen candidate peptides of interest. An HLA-specific exchange catalyst is added to the reaction to support the exchange

of the placeholder peptide by the neoantigen-candidate peptides within the HLA peptide binding groove. This exchange can be assessed by flow cytometric analysis, i.e., the downregulation of the fluorescent signal priorly emitted by the placeholder peptide that is released from the HLA molecules upon peptide exchange. Downstream applications include the isolation of the bead populations that underwent the exchange reaction and the use of those for the restimulation and expansion of antigen-specific T cells.

The successfully established HLA multiplex binding assay must meet several requirements: specificity, robustness, and flexibility. This implies that each step within the assay, the coupling of biotinylated MHC-monomers to beads and the exchange of peptides on corresponding MHC molecules, needs to be optimized. In more detail, this includes (1) the concentration of biotinylated MHC monomers with the FITC-labeled placeholder peptide ([pFITC/MHC]), (2) the number of beads, (3) the concentration of exchange peptide ([ExPep]) and (4) catalyst (C) ([catalyst]) within the exchange reaction, as well as the (5) incubation time. A decreasing FITC signal, induced by the release of the FITC-labeled placeholder peptide from the MHC, serves as a readout (**Figure 34**).

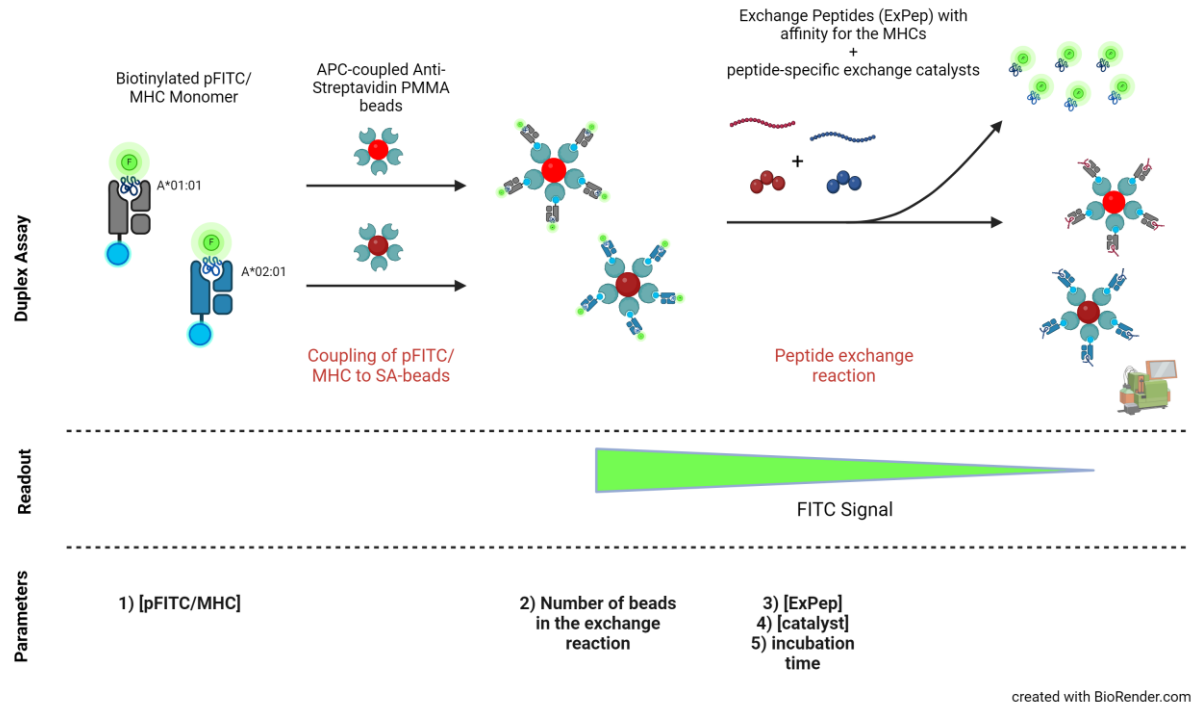

Figure 34. Illustrative experimental procedure of the multiplex HLA binding assay and parameters adapted to improve feasibility. First, biotinylated HLA-monomers with a fluorescently-(FITC-) labeled placeholder peptide attached to the peptide-binding groove are coupled to APC-coupled anti-streptavidin Polymethylmethacrylate (PMMA) beads. Each HLA allele is coupled to a different PMMA-bead population that differs in the intensity of the APC label. Afterward, the exchange of the placeholder by the candidate neoantigen peptide is catalyzed by the addition of an HLA-specific catalyst. It can be evaluated by the flow cytometric assessment of the reduction in fluorescent signal emitted from the reduced number of placeholder peptides attached to the HLA-bead complexes. Parameters that can be adjusted to make this assay feasible are (1) the concentration of placeholder peptide-bound HLA

molecules ([pFITC/MHC]) in the coupling reaction, (2) the number of pFITC/MHC-coupled beads within the exchange reaction, (3) the concentration of exchange peptide ([ExPep]) and (4) catalyst ([catalyst]) in the exchange reaction as well as (5) the incubation time.

To examine optimal settings for HLA multiplex binding assay, several experimental conditions, including the aforementioned parameters, were tested (**Table 3**). The incubation time was 16 h. The FITC-MFI is used as a readout for successful coupling and peptide exchange reactions (**Figure 35**). Conditions (cond.) 1 to 3 and 7 to 9, including 0.001 nM pFITC/MHC within the coupling, show minimal ground states of FITC-MFI. In comparison, high concentrations of 100 nM pFITC/MHC coupled to beads (cond. 4 to 6 and 10 to 12) lead to high FITC-MFI values, indicating successful coupling of pFITC/MHC molecules to beads. For each sample, a negative control without ExPep was prepared to evaluate the effect of the catalyst on the placeholder peptides (catalyst only). Note that conditions 10 and 11 are replicates and serve as controls, simultaneously showing the greatest peptide exchange (w/ ExPep) and the smallest unspecific release of the placeholder peptide induced by the catalyst alone. In contrast, condition 12, with relatively greater catalyst concentrations per bead, shows greater unspecific release of the placeholder peptide induced by the catalyst. However, a minimum catalyst concentration is needed, as too small concentrations do not catalyze the exchange in the presence of ExPep (cond. 4-6).

Table 3 Experimental conditions examined to induce single HLA peptide exchange

Condition	(1) [pFITC/MHC]	(2) number of beads in exchange reaction (no.)	(3) [ExPep] (µM)	(4) [catalyst] (mM)	(5) Incubation time (h)	FITC (%)
1	0.001	20,000	3.86	1	16	?
2	0.001	2,000	0.0386	1	16	?
3	0.001	2,000	3.86	1	16	?
4	100	20,000	0.0386	1	16	?
5	100	20,000	0.0386	1	16	?
6	100	2,000	3.86	1	16	?
7	0.001	20,000	3.86	10	16	?
8	0.001	2,000	0.0386	10	16	?
9	0.001	2,000	3.86	10	16	?
10	100	20,000	0.0386	10	16	?
11	100	20,000	0.0386	10	16	?
12	100	2,000	3.86	10	16	?

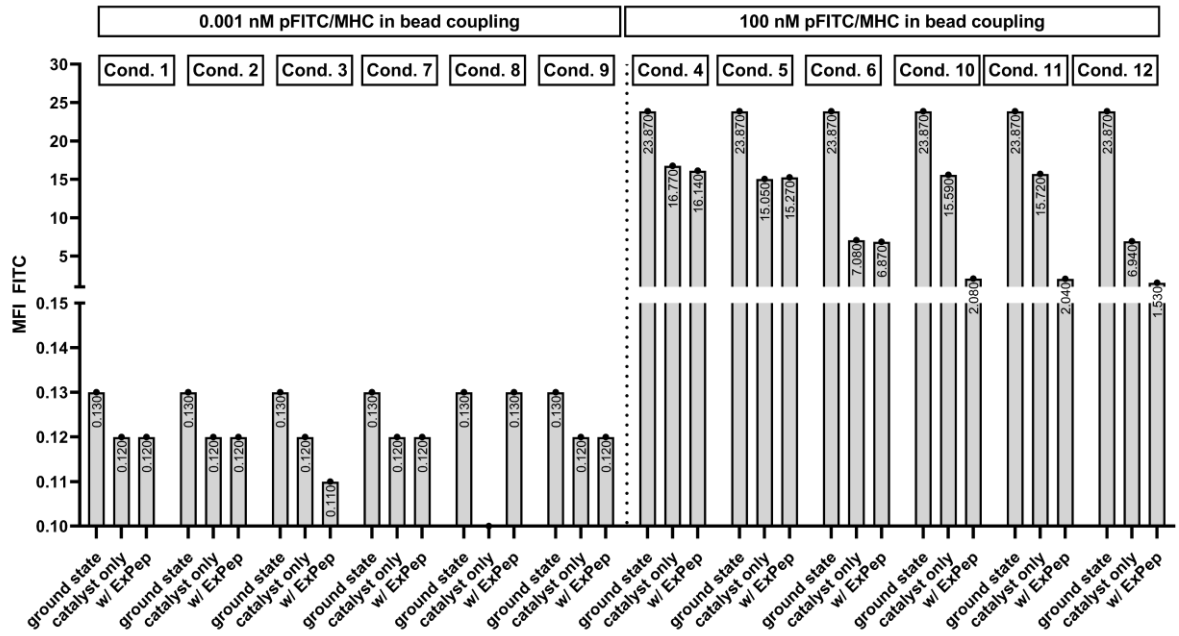

Figure 35. Efficacy of peptide exchange induced by differing parameters of the multiplex HLA binding assay. The mean fluorescent intensity (MFI) of FITC (y-axis), which is associated with the amount of placeholder peptide bound to the HLA, is plotted for different experimental conditions (x-axis). A baseline FITC-MFI (ground state) emitted by pHLA–coupled beads before initiation of a peptide exchange is assessed for the two indicated coupling conditions (0.001 vs. 100 nM pFITC/MHC in bead coupling). For each experimental condition (Cond. 1 – 12), next to the complete peptide exchange reaction mix (w/ ExPep), a control sample to which no exchange peptide (ExPep) was added is measured to evaluate effects of the catalyst on the exchange reaction (catalyst only).

Next, it was investigated whether a duplex exchange, using two different pFITC/MHC constructs, A*0101-His-Cys/ pp50 (245-253)_V3 FITC-bio- (abbreviated with pFITC/MHC I) and A*0201-His-Cys/pp65 (495-503)_V4 FITC-bio (abbreviated with pFITC/MHC II), and two respective exchange peptides pp50_245-253 (abbreviated with ExPep I) and pp65_495-503 (abbreviated with ExPep II), is feasible based on condition 10 / 11 (**Table 3**). Two different concentrations, (A) 10 mM and (B) 5 mM of catalyst (abbreviated with CI and CII), as well as 400 µM ExPep, were tested (**Table 4**). For each bead population, the baseline FITC-MFI was determined after the coupling of beads to FITC-labeled pMHC monomers and subsequent 16 h incubation without peptide exchange reaction mix. Furthermore, several control samples were prepared for each condition, including single peptide exchanges with the accurate catalyst (sample 1 / 10, 4 / 13) and inaccurate catalyst (sample 2 / 11, 3 / 12), single peptide exchanges with both catalysts (sample 8 / 17, 9 / 18), and duplex peptide exchanges including only one catalyst (sample 5 / 14, 6 / 15) within the peptide exchange reaction mix. (**Figure 36**). Thereby, the specificity of the catalyst can be evaluated. As previously shown, lower catalyst concentrations (B) result in lower background dissociation of placeholder-peptide from the

MHCs. The complete reaction mixes (sample 7 / 16) demonstrate a successful peptide exchange on both pFITC/MHC-constructs. However, relatively more exchange is observed for pFITC/MHC I compared to pFITC/MHC II.

Table 4. Experimental conditions examined to induce a duplex HLA peptide exchange. A duplex peptide exchange on A*0101-His-Cys/ pp50 (245-253)_V3 FITC-bio- and A*0201-His-Cys/pp65 (495-503)_V4 FITC-bio – HLA constructs two different experimental conditions were tested varying in the concentration of catalysts added to the reaction mix. As exchange peptide (ExPep), pp50_245-253 and pp65_495-503 were used, respectively. As catalysts, the tri-peptide Met-Ala-Ser and Z-Val-Met were used in two different concentrations, respectively.

Condition	Bead population / HLA construct	(1) [pFITC/MHC] (nM)	(2) beads number	(3) [ExPep] (µM)	(4) [catalyst] (mM)	FITC [%]
A	Red4 0.2 A0101/pp50 / Red 5.5 A0201/pp65	100	20,000	400	10	?
B	Red4 0.2 A0101/pp50 / Red 5.5 A0201/pp65	100	20,000	400	5	?

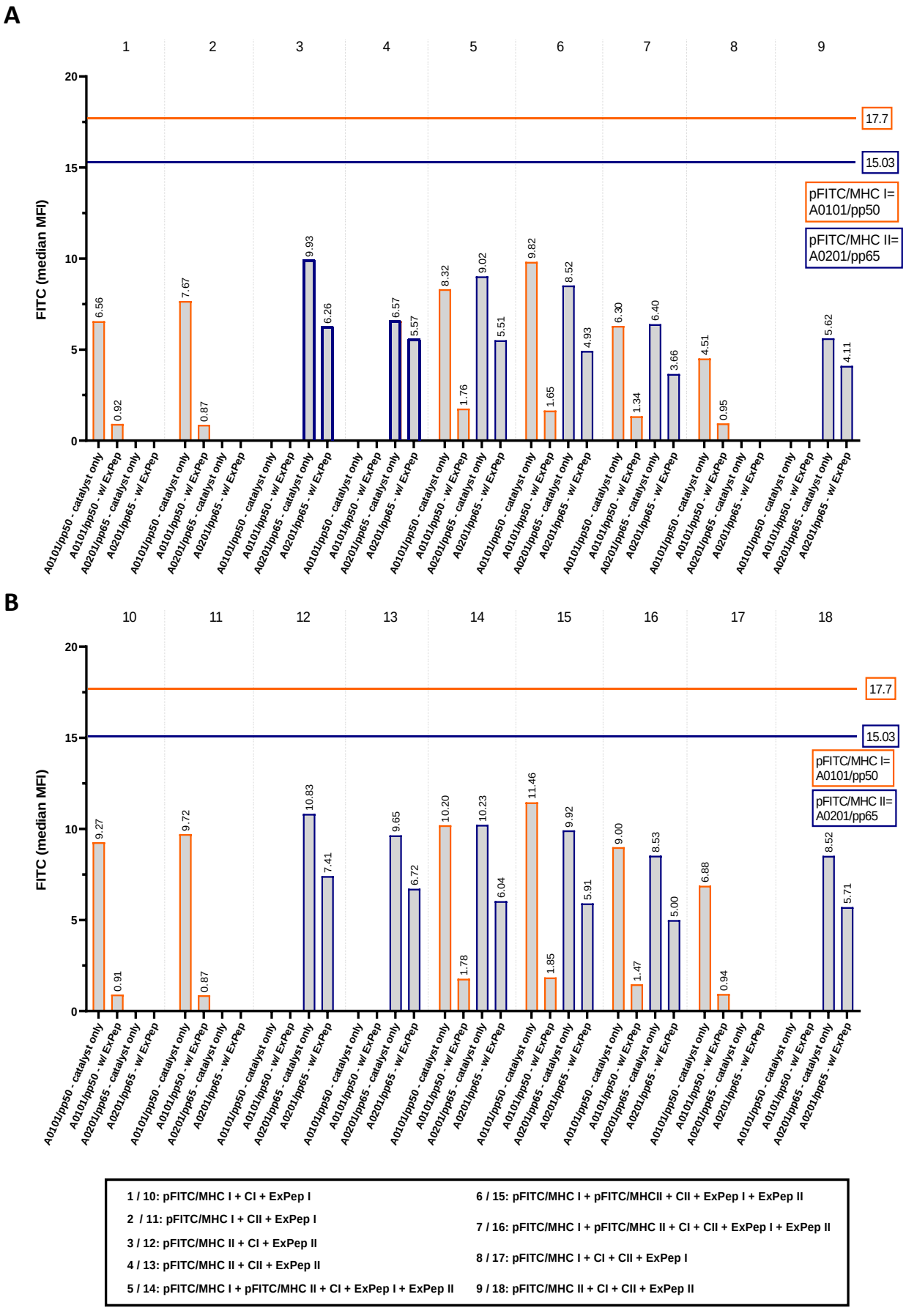
A
B
FITC (median MFI)
17.7
15.03
pFITC/MHC I= A0101/pp50
pFITC/MHC II= A0201/pp65
1 / 10: pFITC/MHC I + CI + ExPep I
2 / 11: pFITC/MHC I + CII + ExPep I
3 / 12: pFITC/MHC II + CI + ExPep II
4 / 13: pFITC/MHC II + CII + ExPep II
5 / 14: pFITC/MHC I + pFITC/MHC II + CI + ExPep I + ExPep II
6 / 15: pFITC/MHC I + pFITC/MHCII + CII + ExPep I + ExPep II
7 / 16: pFITC/MHC I + pFITC/MHC II + CI + CII + ExPep I + ExPep II
8 / 17: pFITC/MHC I + CI + CII + ExPep I
9 / 18: pFITC/MHC II + CI + CII + ExPep II

Figure 36. Duplex HLA exchange assay. Duplex peptide HLA exchange assay using A*0101-His-Cys/ pp50 (245-253)_V3 FITC-bio- (pMHC/FITC I; orange) and A*0201-His-Cys/pp65 (495-503)_V4 FITC-bio – HLA constructs (pMHC/FITC II; blue), pp50_245-253 (ExPep I) and pp65_495-503 (ExPep II) exchange peptides, as well as **(A)** 5 mM vs. **(B)** 10 mM HLA specific catalysts (CI and CII). For each HLA construct, a baseline FITC-MFI, representing a non-exchanged peptide, was assessed (y-axis; solid lines). The sample-specific reaction mix is indicated for each condition. For each sample, a negative control, lacking ExPep, is prepared to evaluate the effects of the catalyst(s). Numbers represent the exact FITC-MFI.

Human bladder carcinomas: a potential model system to identify neoantigens via MHC multiplex analyses

Bladder carcinomas are among the 10th most frequently diagnosed cancers in the world.[44] Conventional therapy includes surgery, i.e., transurethral resection or cystectomy, and adjuvant chemotherapy.[45–47] Unfortunately, this still leads to a poor outcome regarding overall and cancer-free survival.[48] With the third greatest mutational burden,[49] however, bladder carcinoma is an ideal target for neoantigen-directed immunotherapy. Therefore, one aim of this project is the identification of novel neoantigens from bladder carcinoma samples. To reach this aim, a workflow was developed (**Figure 37**). First, tumor biopsies and whole blood were collected from patients. The latter is used for HLA sequencing and the isolation of neutrophil granulocytes, which will be used as a healthy reference for whole exome sequencing. Second, tumor samples were dissociated into single-cell suspensions for downstream DNA isolation and WES. With sequencing results, neoantigen candidates can be identified and subsequently synthesized to verify candidates using the developed multiplex HLA binding assay. Finally, positive hits can be isolated and used for further downstream applications.

Unfortunately, the COVID-19 pandemic and the associated political measures have caused a significant delay in the collection of tumor samples within the period of this PhD project. Therefore, the genomic sequencing of tumor cells could not be accomplished and is, at the time of writing this thesis, pending. Hence, the identification of neoantigens upon use of the multiplex HLA binding assay should be the focus of future investigations.

In immunotherapeutic approaches, the individual's immune cells are directed towards a pathogen-specific target of interest. This approach has made a considerable impact, especially within the treatment of liquid tumors. In contrast, successfully approaching solid tumors within immunotherapeutic approaches is still challenging, as, upon other reasons, immune cell infiltration is often limited.[47] To evaluate the immunological composition of the collected bladder carcinoma samples, a fraction of the tumor single-cell suspension was used to stain

immune cells (**Figure 38**). The frequency of immune cells among leukocytes was assessed for eight study subjects with regard to their individual staging (**Figure 39**). This analysis shows no consistent pattern within samples from stage 0 to stage 3 patients visible. Note that the greatest variety within the frequency of immune cells among stage-3 samples. However, this group also contains the greatest sample number (n (stage 3) = 3). The greatest proportion of immune cells among leukocytes is observed for monocytes, followed by lymphocytes and $CD4^+$ T cells.

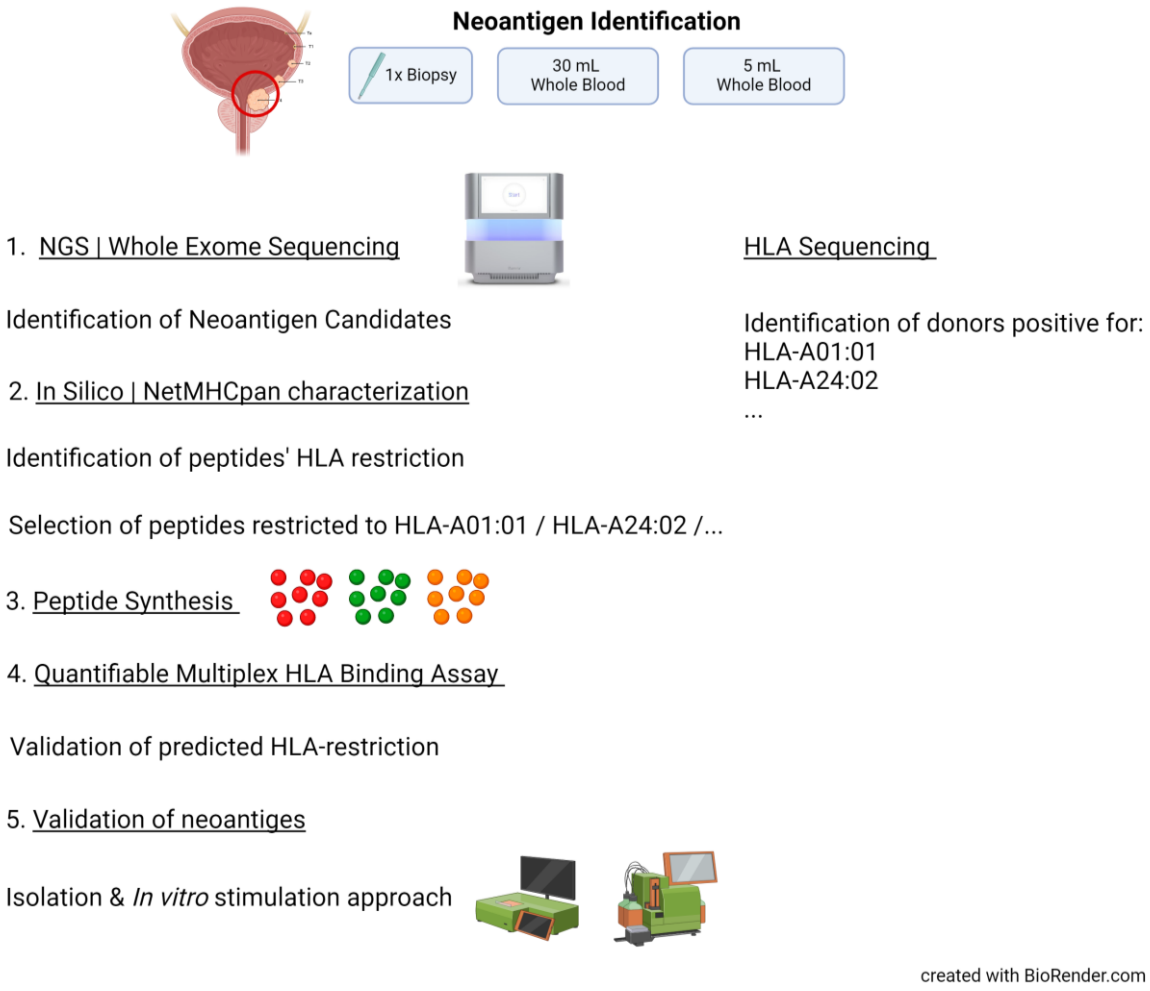

Figure 37. Proposed workflow for a novel identification strategy of bladder carcinoma-derived neoantigens implicating a quantifiable multiplex HLA binding assay. To identify tumor-specific neoantigens, tumor samples and accomplishing whole blood samples are collected. The donor-specific HLA is phenotyped by sequencing whole blood samples. Tumor samples are dissociated to single cell suspensions, e.g., using the tumor cell dissociation kit, human from Miltenyi Biotec. Afterward, the DNA from those cells is isolated and sequenced using whole exome sequencing (WES). In parallel, DNA originating from healthy reference cells, e.g., neutrophil granulocytes or non-cancerous bladder tissue, is isolated and sequenced. Having sequenced tumor cells and healthy reference material, tumor-associated mutations can be identified. These neoantigen candidates are further characterized by in silico analyses, e.g., using NetMHC(II)pan, to determine the theoretical binding affinity to HLA-alleles expressed by the respective donor. Neoantigen peptides with a positive in silico binding potential are synthesized and validated in vitro using the quantifiable multiplex HLA binding assay to bind to a certain

HLA. Lastly, HLA-bound peptides are isolated and used for further downstream applications, e.g., for T cell re-stimulation and cultivation.

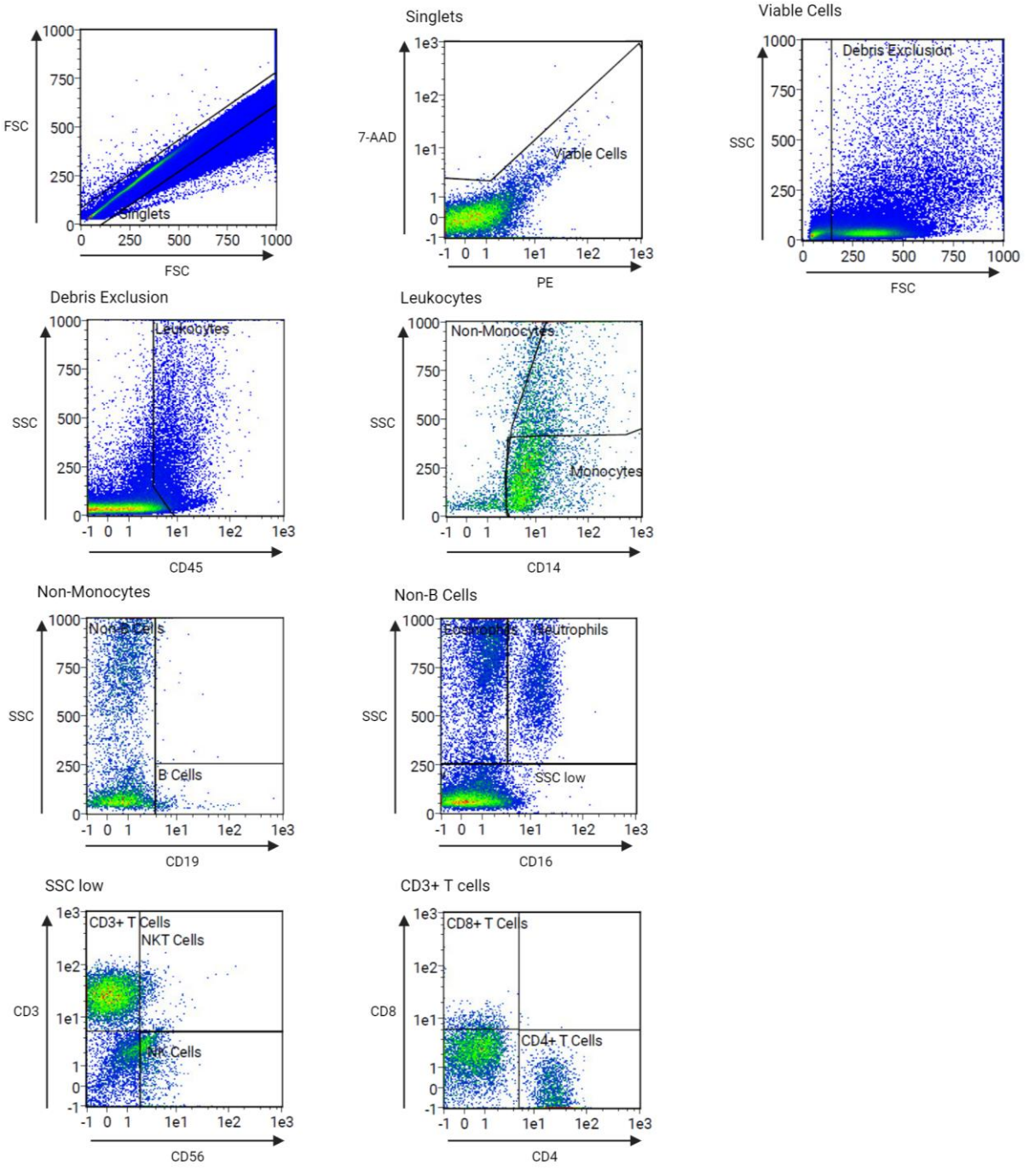

Figure 38. Immunophenotyping of bladder carcinoma sample. Exemplary gating strategy for the analysis of immune composition of a stage 3 bladder carcinoma sample. Pre-gating was done on singlets, viable cells, and a debris exclusion, followed by gating on leukocytes (7-AAD$^-$CD45$^+$) and subdivision into monocytes (7-AAD$^-$ CD45$^+$ CD14$^+$) and non-monocytes. Afterward, B cells (7-AAD$^-$ CD45$^+$ CD14$^+$ CD19$^+$) were identified. Non-B cells, instead, were further differentiated into neutrophils (7-AAD$^-$ CD45$^+$ CD14$^+$ CD19$^-$ SSC^{hi} CD16$^+$) and eosinophils (7-AAD$^-$ CD45$^+$ CD14$^+$ CD19$^-$ SSC^{hi} CD16$^-$). SSC-low cells were further analyzed and subdivided into CD3$^+$ T cells (7-AAD$^-$ CD45$^+$ CD14$^+$ CD19$^-$ SSC^{low}

$CD3^+$), which can be subdivided into $CD4^+$ (7-AAD^- $CD45^+$ $CD14^+$ $CD19^-$ SSC^{low} $CD3^+$ $CD4^+$ $CD8^-$) and $CD8^+$ T cells (7-AAD^- $CD45^+$ $CD14^+$ $CD19^-$ SSC^{low} $CD3^+$ $CD4^-$ $CD8^+$).

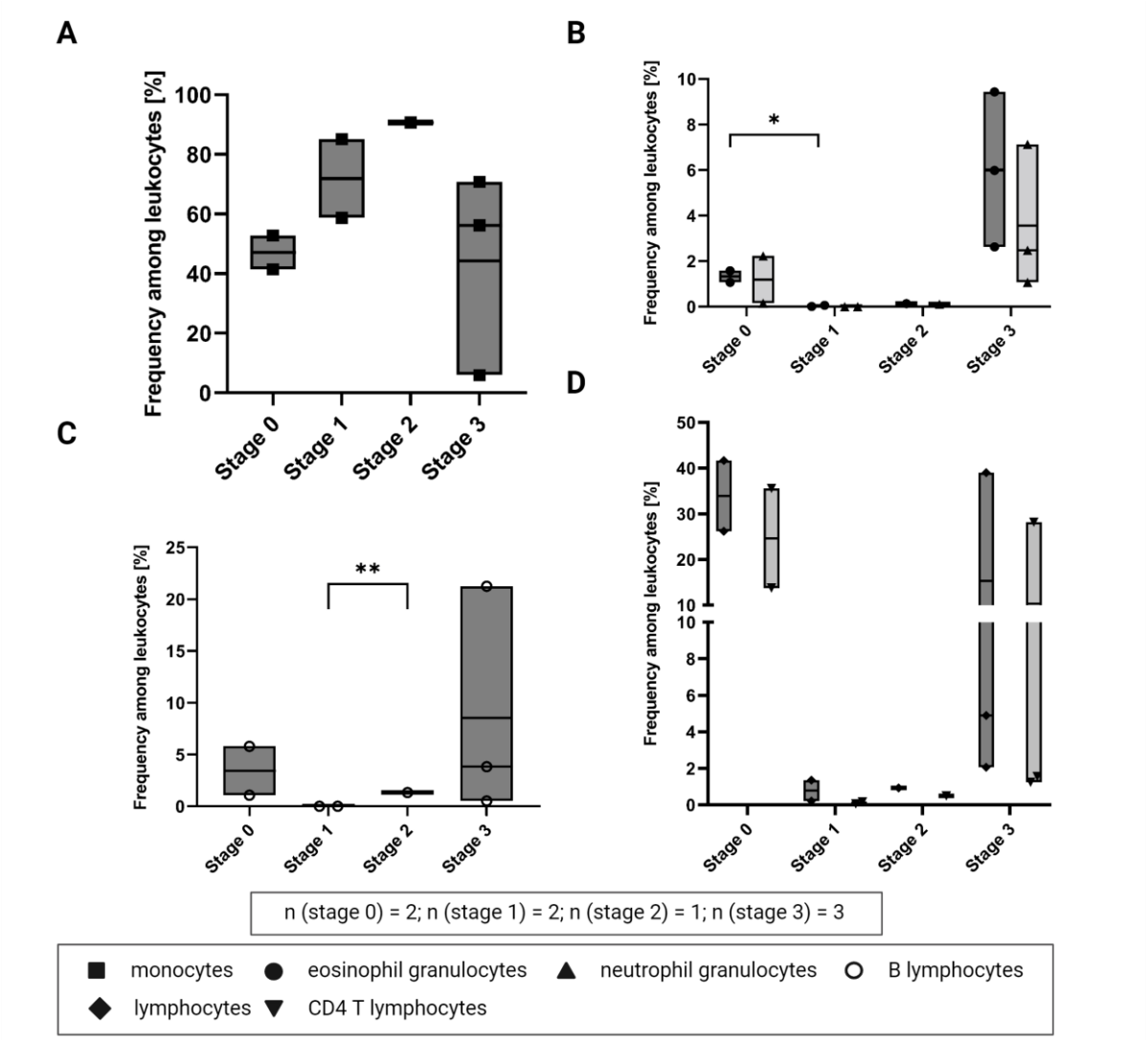

Figure 39. Immunophenotyping of human bladder carcinoma samples. Staining and flow cytometric assessment of the frequency of immune cells from single bladder carcinoma cell suspensions of study subjects with different tumor staging. The frequency of **(A)** monocytes, **(B)** eosinophil- and neutrophil granulocytes, **(C)** B lymphocytes, and **(D)** lymphocytes as well as CD4 T lymphocytes (y-axes) is plotted against the tumor stage 0 (n=2), stage 1 (n=2), stage 2 (n=1) and stage 3 (n=3) (x-axes). Statistical evaluation of inter-stage differences was calculated by unpaired students t-test: * = $p < 0.05$; ** = $p < 0.005$. Lines within box plots represent the mean.

Discussion

The presentation of antigens to T cells marks an essential step within their activation process and, in addition to that, within the initiation of an adaptive immune response. Consequently, upon failure, no adaptive, pathogen-specific immune response can develop, which may result in uncontrolled, severe infections. Likewise, no immunological T cell memory formation can take place, which should provide immune protection upon re-infection with a pathogen. While three different factors determine the activation of T cells: (1) the specificity of the MHC, (2) the specificity of the TCR, and (3) the epitope sequence and therewith binding affinity of the peptide to the MHC, the latter contributes with up to 29% to the whole pMHC-TCR interaction. Hence, identifying T cell antigens, along with their MHC restrictions, is of primary interest and enables identifying immunogenic regions within a pathogen that could be used to estimate the stability of a T cell response and for therapeutic approaches, e.g., within targeted cellular therapies or vaccines.

During this Ph.D. project, the COVID-19 pandemic was a major focus of global scientific efforts, aiming to disentangle the immunopathological mechanisms in SARS-CoV-2 infections to develop therapeutics and vaccines successfully. The global scientific output was remarkably high. After the WHO declared a public health emergency of international concern in January 2020, the first vaccine by BioNTech / Pfizer was approved in December 2020, showing the enormous speed with which progress in the field was made. In SARS-CoV-2 infections, T-cell responses were reported to be essential for an effective viral clearance.[29,50] Specifically, elevated frequencies of circulating memory $CD4^+$ T_{fh} cells were associated with preventing severe disease.[51] Additionally, nABs were shown to be inefficient in viral clearance upon absence of cytotoxic $CD8^+$ T cells in SARS-CoV-2 convalescent macaques[30], further supporting the key role of virus-specific T cells. Moreover, it was shown that the T cell response varies among individuals with mild and severe disease courses, affecting the dominant T cell subset and the epitope landscape recognized by the individuals' T cell repertoire.[31] The stability of the immunological memory on the cellular level, especially for T and B cells is of particular interest as the evolution and accumulation of mutations of SARS-CoV-2 progresses.

SARS-CoV-2 T-cell epitopes and role of low affinity binders

To understand the T cell response, one aim of this project was to identify SARS-CoV-2-specific T-cell epitopes from vaccinated and/or convalescent individuals. The results of these analyzes has been published within the *European Journal of Immunology*.[52] Therefore, an *in vitro*

peptide stimulation approach, accompanied by an *in silico* peptide binding prediction, was performed. From this analysis, we successfully identified numerous 15-mer and 9-mer T cell epitopes.

One novel epitope that has been identified to originate from the Nucleocapsid protein 411-419 (MSSADSTQA) has been shown to elicit dual reactivity on the $CD4^+$ and $CD8^+$ T cell level. Sequence alignment to relatives of the coronavirus family reveals that this epitope is absent within the Middle East respiratory distress syndrome coronavirus (MERS-CoV). In SARS-CoV, the closest relative to SARS-CoV-2, however, there is a high sequence homology, including two insertions at the third and fourth position of the peptide (MS**GA**SADSTQA). This suggests that the MSSADSTQA-epitope is specific for SARS-CoV-2. Looking into dominant circulating SARS-CoV-2 viral strains, a S413R mutation is described for the Omicron-sequences BA.2, BA.4, BA.5, BA.2.12.1, BA.2.75, BQ.1, XBB and EG.5.1. This mutation potentially impacts the peptides' immunogenicity. This is also supported by the peptide's theoretical binding affinity to HLA-A01:01 being nearly halved.

However, compared to epitopes eliciting a extraordinarily high T-cell response (from now on referred to as dominant T-cell epitopes), as Spike protein 269-277 (YLQPRTFLL)[53,54], the T-cell responses upon stimulation with the novel MSSADSTQA-epitope and other non-dominant epitopes that make up the majority of T cell epitopes, are relatively low to moderate. Therefore, the question arises about the role and significance of low-affinity epitopes. As recently described by Straub et al.[55] low avidity TCRs ensure "a tailored but flexible immune response". Straub et al. specifically showed that TCRs presenting with low avidity to non-mutated peptides, leading to minimal to moderate T cell responses, may alter to highly responsive TCRs upon binding to mutated variants of the same peptide. This illustrates the dynamics and high flexibility of the whole pMHC-TCR interaction. Likewise, this observation could be applied to non-dominant epitopes, speculating that such antigens, eliciting a low response in one individual, might lead to higher responses in another individual that expresses a different set of TCRs. Moreover, additional (booster) vaccinations may trigger a broadening and shift of immune response towards the activation of high-affinity TCRs in individuals, even if the identical vaccine is administered multiple times. This is supported by the results describing the analysis of the T cell response against the B.1.1.529 virus strain in twice and triple-vaccinated individuals[56]. This analysis showed that a third vaccination of mainly virus-unexposed individuals led to the development of T cells recognizing non-mutated with additional specificities that might have the potential to bind with higher avidity to formerly low-response

epitopes. Another important aspect in the discussion about the significance of non-dominant epitopes is their vulnerability to mutations within novel virus strains. The loss of a dominant epitope due to a mutation can lead to drastic immune escape due to the loss of recognition by T cells. On average, 30 to 40 SARS-CoV-2 epitopes are recognized by the TCR repertoire of a single individual.[57] Hence, epitopes unaffected by mutations or newly formed epitopes might compensate for the loss of single (dominant) ones. For those reasons, not only the identification of dominant epitopes but also of non-dominant epitopes that can elicit a T-cell response is of fundamental importance.

Another important aspect to discuss is rare cell analyses. These refer to the investigation of cells with a single specificity and are often challenging, as the frequencies of those cells, as well as the responses that they elicit, are low, with less than 1% in abundance.[58] Therefore, defining thresholds for the evaluation of specific responses is challenging. It is important to note that evaluating *in vitro* T-cell responses requires the assessment of negative, unstimulated controls for each single study subject to exclude unspecific responses and background. Depending on the general health of the study subjects, the basic activation of the immune system varies among individuals and between different dates within one individual. Hence, in this project, each individual's peptide stimulation was evaluated separately.

Furthermore, another aspect that needs to be considered for appropriate data interpretation is the potential influence of dominance effects of particular HLA allotypes over others. Thus, it may be that stimulation with particular immunogenic peptides does not result in T-cell activation in the context of a specific HLA allotype, although affinity to one another is given due to the presence of another, dominant HLA expressing greater affinity to bind to a particular peptide. These effects cannot be excluded and may, therefore, lead to false-negative outcomes. To minimize this effect, the validation of core epitope candidates identified within this project was performed using multiple study subjects.

Immunogenic protein regions differ between vaccinated and convalescent individuals

As the immunogenic protein regions emerging from the S, M, and N structural protein aimed to be investigated within individuals that were vaccinated and/or naturally infected, the T cell responses assessed after stimulation with peptide pools covering 50 amino acid-long protein regions were mapped. While cohort C, comprising vaccinated and convalescent study subjects, cannot be included in the comparative analysis due to substantially lower n-numbers, the other

two cohorts, A and B, comprising vaccinated and naturally infected individuals, respectively, demonstrated divergent immune response patterns. While vaccinated individuals showed peaks of reactivity accumulating against specific protein regions of the N-terminal Spike S1 subunit and within the RBD, amongst reactive $CD4^+$ and $CD8^+$ T cells, as well as within the N terminal domain of the S2 subunit amongst reactive $CD4^+$ T cells alone, naturally infected individuals displayed a homogenously distributed responses against the whole protein sequences. This is in line with results described by Grifoni et al., showing $CD4^+$ T cell reactivity against nearly all SARS-CoV-2 proteins in convalescent individuals.[59] SARS-CoV-2 specific $CD4^+$ T cells mainly differentiate into T_{H1} cells and T_{FH} cells.[60–62] The latter substantially supports B cells' affinity maturation in the germinal center. Therefore, those divergent patterns of immunogenic protein regions within the $CD4^+$ T cell compartment may directly affect the specificity of the humoral immune responses formed within the cohorts. As vaccinated individuals may preferably develop antibodies targeting epitopes representing the above-mentioned $CD4^+$ T cell specificity, naturally infected individuals may develop a broad set of antibodies produced by long-lived plasma cells. However, spike-specific B cells internalizing whole virions by, e.g., phagocytosis, are also able to present peptides derived from non-spike proteins and/or non-mutated epitopes on their MHC class II molecules, as it had been shown in a similar model investigating hepatitis B virus-associated adaptive immune responses.[63] A direct association of SARS-CoV-2 specific $CD4^+$ T cell and virus-directed antibody responses is described in other studies.[64,65] As described, T cell responses assessed from cohort A comprised of vaccinated individuals. Most of these individuals were vaccinated with mRNA-based vaccines, primarily manufactured by BioNTech/Pfizer (BNT162b2). Therefore, the question of whether this skew influences the number of study subjects with plotted reactivities for the diverse protein regions and whether the phenomenon of peaking reactivities to certain protein regions in vaccinated individuals is caused by the BNT162b2 vaccine or by vaccination in general cannot be answered with the provided data.

Individuals expressing (un)favorable HLA allotypes show nearly similar peptide-presentation capacities

Next, we wanted to investigate potential links between the T-cellular adaptive immunity against SARS-CoV-2 structural proteins and (un)favorable HLA haplotypes, which were linked to the individuals' disease course, described by Fischer et al.[43] Therefore, study participants from cohort A to C were subcategorized for the expression of (un)favorable HLA allotypes and reactivity against 50-mer amino acid long regions were remapped. This analysis revealed nearly

similar patterns for all three cohorts. Therefore, it is fair to assume that the peptide presentation capacity of study subjects of these cohorts was unaffected by the expression of neither favorable nor unfavorable HLA allotypes. Furthermore, these immunogenic protein regions seem not to be associated with favorable and unfavorable disease courses. However, this study did not include individuals who exclusively expressed HLA allotypes attributed to either a favored or worsened disease course. Hence, with regard to an interpretation for the general public, the cohorts' size would need to be increased to cover as many HLA allotypes as possible in the analysis of these *in vitro* data. Nonetheless, data indicate that the combined expression of favorable and unfavorable HLA allotypes leads to compensation for opposite effects. For this reason, it is likely that for most individuals, the peptide presentation capacity on MHC Class I and II is unaffected. In collaboration with Dr. Angeliki Datsi and Prof. Dr. Johannes Fischer from the University Clinic of Düsseldorf, we therefore looked into intrinsic T cell responses as a potential cause of HLA-associated worsening in COVID-19 disease courses.

Low frequencies of virus-specific $CD8^+$ T cell responses accompanied by high bystander activation is observed in more severe COVID-19

Correlation analysis of the frequency of virus-specific reactive $CD8^+$ and $CD4^+$ T cells to the disease duration revealed that low frequencies of reactive $CD8^+$ T cells were linked to prolonged disease in study subjects expressing unfavorable HLA haplotypes. Controversially, the absolute number of reactive $CD8^+$ T cells after restimulation with SARS-CoV-2 derived peptide pool covering the complete sequences of the S-, M-, and N-protein was increased in both all study subjects and study subjects expressing HLA haplotypes that are being categorized as unfavorable. This points towards a high bystander, virus-unspecific T cell activation in individuals with a worsened disease course and, therefore, a lack of mounting of proper MHC I responses. However, the opposite applies to $CD4^+$ T cell responses. Here, prolonged disease shows tendencies toward mounting higher frequencies of virus-specific $CD4^+$ T cells in study subjects expressing unfavorable haplotypes. Looking into T cell response strengths elicited by individuals exclusively expressing unfavorable or favorable haplotypes, however, no significant differences were found that could explain the associated disease courses. To further disentangle the $CD4^+$ T cell responses, neutralizing activated $CD4^+$ T cell frequencies and antibody titers were assessed for individuals with prolonged disease. Here, significantly increased cell frequencies and titers of nABs were found compared to individuals expressing favorable haplotypes associated with short disease. This suggests a link between virus-directed

$CD4^+$ T cell responses directly leading to the production of virus-reactive antibody titers in SARS-CoV-2.

T-cell immunity is preserved against SARS-CoV-2 B.1.1.529 in individuals vaccinated with 1st generation COVID-19 vaccines

Mutations in the viral genome lead to the development of novel virus strains. Each SARS-CoV-2 variant showed increased transmissibility compared to the previous strains due to novel mutations. This includes mutations resulting in immune escape, e.g., at nAB-binding sites, mutations enhancing ACE2 binding, but also mutations at the furin cleavage site that optimize the enzymatic cleavage of the S1 and S1 subunits, which enables the fusion of the virus with the host cell membrane.[66] SARS-CoV-2 B1.1.529 (also called Omicron), which was first detected in November 2021[67], is a unique variant in two ways: (1) it significantly increased its fitness through mutations associated with high immune escape, more specifically through antibody escape.[68] (2) Unlike previous VOCs, which developed from pre-VOC forms, novel variants now evolve from Omicron and are still globally dominant. Evaluating VOCs' mutation rate and immune escape is of fundamental importance because with every new variant, altered transmissibility, sensitivity to therapeutics, disease courses, and protection by former immunization through vaccination or natural infection have been observed. The alignment of T-cell immunogenic protein regions, which originate from the SARS-CoV-2 Wuhan strain, to mutation rates found within SARS-CoV-2 B.1.1.529 showed limited correlation, suggesting that for a complete loss of the T-cell response, a major reorganization of the viral genome encoding for the structural proteins, would be necessary. To confirm this evidence-driven hypothesis in more detail, one aim of this Ph.D. project was the evaluation of virus-specific T cell responses in twice and triple-vaccinated individuals to date that the novel SARS-CoV-2 B.1.1.529 variant started spreading globally and simultaneously, the administration booster vaccine doses were advised to a broader public by federal authorities. The results have been published in the peer-reviewed journal *Communications Medicine* in November 2022.[56] We observed that although study participants received twice and triple vaccination with first-generation vaccines, i.e., vaccines that were based on the wildtype, Wuhan-strain of SARS-CoV-2, T cell reactivity was observed after stimulation with B.1.1.529-derived peptides. For both T cell subsets, $CD4^+$ and $CD8^+$ T cells, we observed a general increase in the response magnitude in triple-vaccinated study subjects, even without stimulation. This observation is likely caused by the vaccines being administered only a few days before performing these in vitro peptide stimulation analyses, causing the generally higher basic activation of the immune

system. Comparative analysis of T cell activity as a response to stimulation with B.1.1.529 mutation- and wildtype reference peptides, the reactivity against mutated peptides was significantly decreased in $CD4^+$ T cells of twice vaccinated study subjects. This activity decrease was diminished in triple-vaccinated study subjects, indicating the priming of T cells with improved recognition of mutated viral peptides. For $CD8^+$ T cells, we observed the opposite. Here, $CD8^+$ T cell responses towards mutated and reference peptides were nearly identical, only showing slightly insignificantly increased frequencies of activated $CD8^+$ T cells as a response to stimulation with mutated peptides. These observations for $CD4^+$ and $CD8^+$ T cells were supported by the ratio of T cell responses directed against mutated vs. non-mutated viral regions. These calculations showed that roughly 20% more $CD4^+$ T cells with specificity against non-mutated regions are primed with the third vaccination. In contrast, an increase of around 13% of $CD8^+$ T cells, specifically recognizing non-mutated regions, was observed. Note that these ratios might vary for individuals not analyzed in these *in vitro* studies, in dependence on the HLA molecules being expressed. Overall, by selecting a random cohort of vaccinated individuals, those *in vitro* analyses suggest that T cell responses against SARS-CoV-2 B.1.1.529 can be effectively supported by vaccination with first-generation vaccines. However, this analysis was performed on non-matched study subjects, which does not allow for tracking the individual T-cell response development after twice and triple vaccination. Furthermore, due to the limited number of study participants ($n_{\text{2 times vaccinated}} = 8$; $n_{\text{3 times vaccinated}} = 10$), the results only represent a limited number of HLA allotypes that are being expressed by the individuals. Hence, an additional *in silico* analysis was performed to predict the T cell responses towards wildtype vs. mutated peptides, including 95% of all HLAs being expressed in the European-Caucasian population. The resulting conversions between categories of non-, weak-, and strong-binding peptides to HLA Class I and HLA Class II molecules revealed a general tendency towards T-cell immune escape by SARS-CoV-2 B.1.1.529. However, this analysis only allows for conclusions about the absolute quantity, not the binding quality of the pMHC interactions. As previously noted, the activation of T cells is contingent not only upon the peptide-MHC interaction but also on the specificity of the TCR and its HLA restriction. The peptide loaded onto the MHC contributes to on average 29% to the whole interaction. Thus, although most peptides bind with worsened affinity to the HLA molecules of interest, the corresponding *in vitro* analysis revealed that this prediction does not seem to affect the strength of the elicited T-cell responses. Therefore, it is likely that only a few individuals expressing a specific set of disadvantageous HLA allotypes present with major T cell immune escape to SARS-CoV-2 B.1.1529. This has also been described in other studies by Naranbhai et al.,

exemplifying a >50% reduced T cell response to the highly mutated Omicron strain only for some individuals.[69] Thus, from our analyses, it can be concluded that a major reorganization of the SARS-CoV-2 genome would be needed to induce a T cell escape that affects a general public.

Introducing a new tool for the efficient identification of MHC-binding peptides and recognition by cognate T cells

The investigation of peptide-MHC:TCR interactions by conventional *in vitro* peptide stimulation and accompanying *in silico* peptide-binding predictions, as described within this Ph.D. project, bears three major disadvantages: (1) the *in vitro* testing of T cell reactivity upon stimulation with respective peptides requires a large cohort of study participants to cover a maximum number of different HLA alleles; (2) although a direct readout of T cell activation is available *in vitro*, e.g., via flow cytometry, the MHC restriction can only be narrowed down to the respective HLA background of the reactive donor; (3) the reliability of available *in silico* peptide binding prediction tools is limited, as the algorithms' training data focus in the most common MHC allotypes and peptide interactions. Although these algorithms are constantly evaluated and improved, a final *in vitro* verification is necessary.

To improve the T cell epitope identification strategy as part of this Ph.D. project, we aimed to develop a novel assay that allows for multiplexing. The introduced multiplex HLA binding assay, currently under evaluation at the European Patent Office (Application number EP23216590), bears several advantages. Each HLA allele of interest can be analyzed simultaneously, as they are coupled to different populations of beads that can be discriminated in flow cytometric analysis. The subsequent addition of one or multiple fluorescently-labeled epitope candidates, i.e., synthesized peptides and MHC-specific exchange catalysts, enables direct identification of peptide-MHC interactions by the evaluation of the release of a fluorescently-labeled placeholder peptide that is formerly incorporated into the MHC peptide binding cleft. This can be performed without the need for human samples, whose number and availability are often limited. So far, the feasibility of this assay using two different MHC alleles with two respective binders with known affinity for the MHC was demonstrated. Ultimately, I could verify the release of placeholder peptides from both HLA alleles. However, such approaches, including the testing of multiple epitope candidates, require additional verification of peptides bound to respective MHC alleles, e.g., by mass spectrometry analysis. For this and other downstream applications, exchanged pMHC molecules need to be isolated, e.g., using the

MACS Quant Tyto cell sorter. Another downstream application could include the restimulation of antigen-specific T cells, which would also serve as a final validation of peptides as T cell epitopes.

This novel approach has the potential to transform the standard techniques used for studying pMHC- and downstream TCR interactions. However, some improvements are still needed to increase the feasibility of the assay. This requires investigation of (1) the dependence of the assay on the concentration of the single reactants and (2) the sensitivity of the assay for varying binding affinities of epitope candidates to the HLA molecules. With regard to (1) the dependency of the assay outcome on the concentrations of single reactants, especially the relative concentration of the catalyst, showed to play an important role, as background signals are majorly influenced by increasing concentration of catalyst. As the catalysts' binding affinity to the HLA is slightly higher compared to the placeholder peptide, the release of the placeholder is induced. For this reason, the addition of the catalysts alone resulted in a decrease in fluorescent signal. However, to enable an efficient binding of epitope candidates to the HLA, the latter, in turn, needs to have a greater affinity to bind to the HLA molecule compared to the catalyst. Therefore, the question arises whether the catalysts' affinity to the HLA defines the lower limit of detection within this assay. Furthermore, regarding (2) the sensitivity of the assay to naturally accruing variances in the binding affinities of candidate epitopes to an HLA molecule of interest, the question arises whether the assay can reflect those differences with its readout. As observed within the performed duplex exchange using HLA-A0101/pp50 and HLA-A0201/pp65, exchange on HLA0101/pp50 resulted in greater exchange than exchange on the second HLA. This observation correlates with the binding affinities of HLA-A0201 to pp65 being relatively lower compared to the binding affinity of HLA-A0101 to pp50. Further experiments are required to verify this potential correlation, pointing towards the binding affinity as a determinant of the degree of exchange that takes place.

Bladder carcinoma presents with a potential high mutational burden and varying numbers of immune cell infiltrates

Bladder carcinoma is amongst the tenth most frequently diagnosed cancer diseases worldwide[70] with incidences of 17.6 diagnoses and 5.2 diagnoses among 100,000 male and female individuals in Germany, respectively, as reported by the Robert Koch Institute in 2020.[71] Bladder carcinoma is especially attractive for immunotherapy targeting neoantigens, i.e. antigens that are gained via mutations within cancerous cells and are therefore exclusively

expressed by the tumor tissue[72–74], as it presents with the froth highest mutational burden compared to other tumor entities.[49] However, conventional therapy currently comprises surgery and adjuvant chemotherapy.[45–47] In this project, bladder carcinoma was chosen as a model system for the identification of neoantigens through WES and the application of the aforementioned novel multiplex HLA binding assay. Therefore, samples of 12 patients diagnosed with differentially staged bladder carcinoma were recruited, and biopsies were taken. Those samples were processed into single-cell suspensions as described. The majority of cells are stored for pending WES analysis. However, from eight samples bearing high numbers of available tumor-associated cells, a cell staining assessing the immunological composition of the samples was performed. This analysis revealed varying immune cell composition for every patient and staging. With regard to lymphocytes, especially $CD4^+$ T cells displayed increased frequencies among leukocytes in two stage 0 and one stage 3 bladder carcinoma patients. $CD8^+$ T cell, however, didn't show elevated frequencies for any of the analyzed patients (data not shown). For successful immunotherapy, classification of the tumor as a "hot" tumor is thought to be favorable. Those tumors are characterized by a high degree of immune cell infiltration, PD-L1 overexpression, genomic instability, and reported antitumor immune responses.[75] Having assessed the frequencies of infiltrated immune cells from single tumor cell suspensions of one biopsy does not enable a definite categorization of the tumor samples from recruited study subjects into "cold" or "hot" tumor entities. Nevertheless, the data contributes a minor yet integral component to the overall understanding, indicating that bladder carcinoma is generally infiltrated with immune cells irrespective of the individual tumor staging. However, to get a complete and reliable picture, the assessment of multiple tumor biopsies and additional data associated with "hot" tumors is required.

Conclusions

One aim of this Ph.D. project was to determine the stability of T-cell responses toward SARS-CoV-2. Therefore, several aims targeting the investigation of SARS-CoV-2 specific T cell responses were defined. In this project, an experimental strategy for the identification of SARS-CoV-2 specific T cell epitopes was introduced, including the sequential testing of virus-derived peptides on SARS-CoV-2 – experienced individuals, accompanied by the computational determination of peptides' immunogenicity in terms of HLA binding specificities. Thereby, numerous T cell epitopes were identified. Furthermore, the HLA-independent mapping of immunogenic protein regions within SARS-CoV-2 structural protein allowed for the direct comparison of T cell immunity mounted via vaccination and natural infection. This analysis

revealed that although mRNA vaccines primarily included complete Spike proteins, T-cell responses were mainly developed against specific, more isolated protein regions. At the same time, T-cell reactivity within naturally infected individuals was distributed more homogeneously.

Severe SARS-CoV-2 infections were linked to inappropriate T-cell responses. There was no effect of unfavorable HLA haplotypes, which were associated with more severe disease courses, on the number of T cell epitopes, suggesting that those HLAs can unalterably present peptides to T cells. Therefore, focusing on finding potential causes for such severe SARS-CoV-2 infections, the strength of virus-specific $CD4^+$ and $CD8^+$ T cell responses was assessed, finding low frequencies and bystander $CD8^+$ T cell responses being associated with more severe disease. Simultaneously, we could confirm an association between unfavorable HLA haplotypes and increased frequencies of $CD4^+$ T cells accompanied by increased titers of virus-neutralizing antibodies. Despite these findings, this study is limited by the lack of investigations of T-cell responses elicited by severely infected individuals. Furthermore, currently dominant circulating viral strains show to cause less severe disease. Nevertheless, individuals with severe primary infections may suffer from long-Covid, which is attributed to persistent COVID-19-associated symptoms.[76] Therefore, future investigations should contribute to understanding the immunopathological processes involved in such cases.

The evolution of a virus and, therewith, the accumulation of mutations represents the highest chance of escape from gained (T cell) immunity. Therefore, by applying the established peptide stimulation approaches, we investigated the T-cell responses of twice and triple-vaccinated individuals against infections with the novel, highly mutated Omicron / B.1.1.529 SARS-CoV-2 strain. *In silico* peptide-binding prediction analysis suggest a general tendency towards immune escape, caused by mutation with the viral genome. However, we could conclude that there is a general profit from booster vaccinations resulting in increased frequencies of $CD4^+$ and $CD8^+$ virus-specific T cell responses and activation of T cells specifically recognizing non-mutated protein regions, thereby ensuring stable T cell responses against Omicron. Additionally, the alignment of the SARS-CoV-2 ancestral T-cell epitope landscape to the mutational landscape gained within novel B1.1.529 virus strains only showed in minimal overlap. Together, these data indicate that viral evolution does not directly target an escape from T-cell immunity.

An HLA binding assay was successfully developed and verified using a binary approach to improve the T cell epitope identification strategy. This assay, using artificial MHC-binding platforms and peptide exchange reactions, ensures fast and efficient identification of HLA-

binding peptides with the possibility for downstream applications, including cognate-T cell stimulation, sorting, and analysis. Bladder carcinoma samples, as a model system for the identification of neoantigens, were collected and immunophenotyped. This analysis showcases a non-homogenous infiltration with immune cells. However, this analysis fails to present a complete picture of the tumors' immune composition as we only had one biopsy per patient. However, it shows that the application of neoantigen-targeting immunotherapy for bladder carcinoma is of potential interest. However, the analysis of the collected tumor samples via WES and subsequent identification and testing of neoantigen candidates is pending and should be the focus of future research.

References

1. ADAPTIVE | English meaning - Cambridge Dictionary. https://dictionary.cambridge.org/dictionary/english/adaptive.

2. Hanahan, D. & Weinberg, R. A. *The Hallmarks of Cancer*. *Cell* vol. 100 (2000).

3. Hanahan, D. & Weinberg, R. A. Hallmarks of cancer: The next generation. *Cell* vol. 144 646–674 Preprint at https://doi.org/10.1016/j.cell.2011.02.013 (2011).

4. Rehwinkel, J. & Gack, M. U. RIG-I-like receptors: their regulation and roles in RNA sensing. *Nat Rev Immunol* doi:10.1038/s41577-020-0288-3.

5. Sievers, B. L., Cheng, M. T. K., Csiba, K., Meng, B. & Gupta, R. K. SARS-CoV-2 and innate immunity: the good, the bad, and the "goldilocks". *Cellular and Molecular Immunology* vol. 21 171–183 Preprint at https://doi.org/10.1038/s41423-023-01104-y (2024).

6. Cui, S. *et al.* The C-terminal regulatory domain is the RNA 5'-triphosphate sensor of RIG-I. *Mol Cell* **29**, 169–179 (2008).

7. Designed Research; S, J. M. C. D. & Performed Research; S, A. G. K. C. D. Structural basis for m7G recognition and 2′-O-methyl discrimination in capped RNAs by the innate immune receptor RIG-I . **113**, (2016).

8. Li, D. & Wu, M. Pattern recognition receptors in health and diseases. *Signal Transduction and Targeted Therapy* vol. 6 Preprint at https://doi.org/10.1038/s41392-021-00687-0 (2021).

9. Murphy, K. (Kenneth M.), Weaver, C. & Janeway, C. *Janeway's Immunobiology*.

10. Volpe, J. M. & Kepler, T. B. Large-scale analysis of human heavy chain V(D)J recombination patterns. *Immunome Res* **4**, 3 (2008).

11. Malissen, M. *et al.* Regulation of TCR α and β gene allelic exclusion during T-cell development. *Immunol Today* **13**, 315–322 (1992).

12. Gebert, C. *et al.* Chromosome choice for initiation of V-(D)-J recombination is not governed by genomic imprinting. *Immunol Cell Biol* **95**, 473–477 (2017).

13. Mionnet, C. *et al.* High endothelial venules as traffic control points maintaining lymphocyte population homeostasis in lymph nodes. *Blood* **118**, 6115–6122 (2011).

14. Girard, J. P., Moussion, C. & Förster, R. HEVs, lymphatics and homeostatic immune cell trafficking in lymph nodes. *Nature Reviews Immunology 2012 12:11* **12**, 762–773 (2012).

15. Boyman, O. & Sprent, J. The role of interleukin-2 during homeostasis and activation of the immune system. *Nature Reviews Immunology* vol. 12 180–190 Preprint at https://doi.org/10.1038/nri3156 (2012).

16. Haring, J. S., Badovinac, V. P. & Harty, J. T. Inflaming the CD8+ T Cell Response. *Immunity* vol. 25 19–29 Preprint at https://doi.org/10.1016/j.immuni.2006.07.001 (2006).

17. Curtsinger, J. M. & Mescher, M. F. Inflammatory Cytokines as a Third Signal for T Cell Activation. (2010) doi:10.1016/j.coi.2010.02.013.

18. Heller, K. N., Gurer, C. & Münz, C. Virus-specific CD4+ T cells: Ready for direct attack. *Journal of Experimental Medicine* vol. 203 805–808 Preprint at https://doi.org/10.1084/jem.20060215 (2006).

19. Hewitt, E. W. *The MHC Class I Antigen Presentation Pathway: Strategies for Viral Immune Evasion*.

20. Watts, C. The endosome-lysosome pathway and information generation in the immune system ☆. (2011) doi:10.1016/j.bbapap.2011.07.006.

21. Lin, M. L., Zhan, Y., Villadangos, J. A. & Lew, A. M. The cell biology of cross-presentation and the role of dendritic cell subsets. *Immunology and Cell Biology* vol. 86 353–362 Preprint at https://doi.org/10.1038/icb.2008.3 (2008).

22. Rodriguez, A., Regnault, A., Kleijmeer, M., Ricciardi-Castagnoli, P. & Amigorena, S. *Selective Transport of Internalized Antigens to the Cytosol for MHC Class I Presentation in Dendritic Cells*. *NATURE CELL BIOLOGY* vol. 1 (1999).

23. Szeto, C., Lobos, C. A., Nguyen, A. T. & Gras, S. TCR Recognition of Peptide–MHC-I Rule Makers and Breakers. *Int J Mol Sci* (2021).

24. Brown, J. H. *et al. Three-Dimensional Structure of the Humanclass II Histocompatibility Antigen HLA-DR1*. *98. Sugiura, N. &Hashizume, K. Earth planet. Sci. Lett* vol. 55 (1993).

25. Choo, S. Y. The HLA System: Genetics, Immunology, Clinical Testing, and Clinical Implications. *Yonsei Med J* (2007).

26. WHO declares Public Health Emergency on novel coronavirus - PAHO/WHO | Pan American Health Organization. https://www.paho.org/en/news/30-1-2020-who-declares-public-health-emergency-novel-coronavirus.

27. Le, K. *et al.* Structural understanding of SARS-CoV-2 virus entry to host cells. *Frontiers in Molecular Biosciences* vol. 10 Preprint at https://doi.org/10.3389/fmolb.2023.1288686 (2023).

28. Sette, A. & Crotty, S. Adaptive immunity to SARS-CoV-2 and COVID-19. *Cell* vol. 184 861–880 Preprint at https://doi.org/10.1016/j.cell.2021.01.007 (2021).

29. Tan, A. T. *et al.* Early induction of functional SARS-CoV-2-specific T cells associates with rapid viral clearance and mild disease in COVID-19 patients. *Cell Rep* **34**, (2021).

30. McMahan, K. *et al.* Correlates of protection against SARS-CoV-2 in rhesus macaques. *Nature* **590**, 630–634 (2021).

31. Swadling, L. & Maini, M. K. T cells in COVID-19 — united in diversity. *Nat Immunol* **21**, 1307–1308 (2020).

32. Zeng, B., Gao, L., Zhou, Q., Yu, K. & Sun, F. Effectiveness of COVID-19 vaccines against SARS-CoV-2 variants of concern: a systematic review and meta-analysis. *medRxiv* 2021.09.23.21264048 (2021) doi:10.1101/2021.09.23.21264048.

33. Agapiou, D. *et al.* COVID-19 convalescents exhibit deficient humoral and T cell responses to variant of concern Spike antigens at 12 month post-infection. 1–45 (2021).

34. Association, W. M. World Medical Association Declaration of Helsinki: Ethical Principles for Medical Research Involving Human Subjects. *JAMA* **310**, 2191–2194 (2013).

35. WHO. *Interim Recommendations for an Extended Primary Series with an Additional Vaccine Dose for COVID-19 Vaccination in Immunocompromised Persons Interim Guidance*. https://www.who.int/groups/strategic-advisory-group- (2021).

36. Rki. *Epidemiologisches Bulletin 48/2021*. www.rki.de/epidbull (2021).

37. Ramasamy, M. N. *et al.* Safety and immunogenicity of ChAdOx1 nCoV-19 vaccine administered in a prime-boost regimen in young and old adults (COV002): a single-blind, randomised, controlled, phase 2/3 trial. *The Lancet* **396**, 1979–1993 (2020).

38. Poland, G. A., Ovsyannikova, I. G. & Kennedy, R. B. SARS-CoV-2 immunity: review and applications to phase 3 vaccine candidates. *The Lancet* vol. 396 1595–1606 Preprint at https://doi.org/10.1016/S0140-6736(20)32137-1 (2020).

39. Polack, F. P. *et al.* Safety and Efficacy of the BNT162b2 mRNA Covid-19 Vaccine. *New England Journal of Medicine* **383**, 2603–2615 (2020).

40. Sadoff, J. *et al.* Interim Results of a Phase 1–2a Trial of Ad26.COV2.S Covid-19 Vaccine. *New England Journal of Medicine* **384**, 1824–1835 (2021).

41. Mazzoni, A. *et al.* First dose mRNA vaccination is sufficient to reactivate immunological memory to SARS-CoV-2 in ex COVID-19 subjects. doi:10.1101/2021.03.05.21252590.

42. Madhi, S. A. *et al.* Efficacy of the ChAdOx1 nCoV-19 Covid-19 Vaccine against the B.1.351 Variant. *New England Journal of Medicine* **384**, 1885–1898 (2021).

43. Fischer, J. C. *et al.* Prognostic markers for the clinical course in the blood of patients with SARS-CoV-2 infection. *Eur J Med Res* **27**, 255 (2022).

44. Sung, H. *et al.* Global Cancer Statistics 2020: GLOBOCAN Estimates of Incidence and Mortality Worldwide for 36 Cancers in 185 Countries. *CA Cancer J Clin* **71**, 209–249 (2021).

45. Stein, J. P. & Skinner, D. G. Radical cystectomy for invasive bladder cancer: Long-term results of a standard procedure. *World J Urol* **24**, 296–304 (2006).

46. Dalbagni, G. *et al.* CYSTECTOMY FOR BLADDER CANCER: A CONTEMPORARY SERIES. *J Urol* **165**, 1111–1116 (2001).

47. Stein, J. P. *et al.* Radical Cystectomy in the Treatment of Invasive Bladder Cancer: Long-Term Results in 1,054 Patients. *https://doi.org/10.1200/JCO.2001.19.3.666* **19**, 666–675 (2016).

48. Bruins, H. M. *et al.* Clinical Outcomes and Recurrence Predictors of Lymph Node Positive Urothelial Cancer After Cystectomy. *J Urol* **182**, 2182–2187 (2009).

49. Lawrence, M. S. *et al.* Mutational heterogeneity in cancer and the search for new cancer-associated genes. *Nature* (2013) doi:10.1038/nature12213.

50. Tan, L. *et al.* Lymphopenia predicts disease severity of COVID-19: a descriptive and predictive study. *Signal Transduct Target Ther* **5**, 16–18 (2020).

51. Meckiff, B. J. *et al.* Imbalance of Regulatory and Cytotoxic SARS-CoV-2-Reactive CD4+ T Cells in COVID-19. *Cell* **183**, 1340-1353.e16 (2020).

52. Dörnte, C. *et al.* Distinct HLA Haplotypes Are Associated With an Altered Strength of SARS-CoV-2-Specific T-Cell Responses and Unfavorable Disease Courses. *Eur J Immunol* **55**, (2025).

53. Dolton, G. *et al.* Emergence of immune escape at dominant SARS-CoV-2 killer T cell epitope. *Cell* **185**, 2936-2951.e19 (2022).

54. Shomuradova, A. S. *et al.* SARS-CoV-2 Epitopes Are Recognized by a Public and Diverse Repertoire of Human T Cell Receptors. *Immunity* **53**, 1245-1257.e5 (2020).

55. Straub, A. *et al.* Recruitment of epitope-specific T cell clones with a low-avidity threshold supports efficacy against mutational escape upon re-infection. *Immunity* **56**, 1269-1284.e6 (2023).

56. Dörnte, C. *et al.* Vaccines against the original strain of SARS-CoV-2 provide T cell memory to the B.1.1.529 variant. *Communications Medicine* **2**, 1–6 (2022).

57. Tarke, A. *et al.* Comprehensive analysis of T cell immunodominance and immunoprevalence of SARS-CoV-2 epitopes in COVID-19 cases. *Cell Rep Med* **2**, (2021).

58. Chen, Y. *et al.* Rare cell isolation and analysis in microfluidics. *Lab on a Chip* vol. 14 626–645 Preprint at https://doi.org/10.1039/c3lc90136j (2014).

59. Grifoni, A. *et al.* Targets of T Cell Responses to SARS-CoV-2 Coronavirus in Humans with COVID-19 Disease and Unexposed Individuals. *Cell* **181**, 1489-1501.e15 (2020).

60. Weiskopf, D. *et al. Phenotype and Kinetics of SARS-CoV-2-Specific T Cells in COVID-19 Patients with Acute Respiratory Distress Syndrome*. *Sci. Immunol* vol. 5 https://www.science.org (2020).

61. Thevarajan, I. *et al.* Breadth of concomitant immune responses prior to patient recovery: a case report of non-severe COVID-19. *Nature Medicine* vol. 26 453–455 Preprint at https://doi.org/10.1038/s41591-020-0819-2 (2020).

62. Braun, J. *et al.* SARS-CoV-2-reactive T cells in healthy donors and patients with COVID-19. *Nature* **587**, 270–274 (2020).

63. Milicht, D. R., McLachlan, A., Thornton, G. B. & Hughes, J. L. *Antibody Production to the Nucleocapsid and Envelope of the Hepatitis B Virus Primed by a Single Synthetic T Cell Site*. (1987).

64. Wang, Z. *et al.* SARS-CoV-2-specific CD4+ T cells are associated with long-term persistence of neutralizing antibodies. *Signal Transduct Target Ther* **7**, (2022).

65. Painter, M. M. *et al.* Rapid induction of antigen-specific CD4+ T cells is associated with coordinated humoral and cellular immunity to SARS-CoV-2 mRNA vaccination. *Immunity* **54**, 2133-2142.e3 (2021).

66. Carabelli, A. M. *et al.* SARS-CoV-2 variant biology: immune escape, transmission and fitness. *Nature Reviews Microbiology* vol. 21 162–177 Preprint at https://doi.org/10.1038/s41579-022-00841-7 (2023).

67. WHO. *Classification of Omicron (B.1.1.529): SARS-CoV-2 Variant of Concern*. https://www.who.int/news/item/26-11-2021-classification-of-omicron-(b.1.1.529)-sars-cov-2-variant-of-concern (2021).

68. Cao, Y. *et al.* Omicron escapes the majority of existing SARS-CoV-2 neutralizing antibodies. *Nature* | **602**, 657 (2022).

69. Naranbhai, V. *et al.* T cell reactivity to the SARS-CoV-2 Omicron variant is preserved in most but not all individuals. *Cell* **185**, 1041-1051.e6 (2022).

70. Bladder cancer statistics | World Cancer Research Fund International. https://www.wcrf.org/cancer-trends/bladder-cancer-statistics/.

71. Krebs - Harnblasenkrebs. https://www.krebsdaten.de/Krebs/DE/Content/Krebsarten/Harnblasenkrebs/harnblasenkrebs_node.html.

72. Gubin, M. M., Artyomov, M. N., Mardis, E. R. & Schreiber, R. D. Tumor neoantigens: building a framework for personalized cancer immunotherapy. *J Clin Invest* **125**, 3413–3421 (2015).

73. Zhang, Z. *et al.* Neoantigen: A New Breakthrough in Tumor Immunotherapy. *Front Immunol* **12**, 672356 (2021).

74. Apavaloaei, A., Hardy, M.-P., Thibault, P. & Perreault, C. The Origin and Immune Recognition of Tumor-Specific Antigens. doi:10.3390/cancers12092607.

75. Galon, J. & Bruni, D. Approaches to treat immune hot, altered and cold tumours with combination immunotherapies. *Nature Reviews Drug Discovery* vol. 18 197–218 Preprint at https://doi.org/10.1038/s41573-018-0007-y (2019).

76. Evans, R. A. *et al*. Physical, cognitive, and mental health impacts of COVID-19 after hospitalisation (PHOSP-COVID): a UK multicentre, prospective cohort study. *Lancet Respir Med* **9**, 1275–1287 (2021).

Appendix

Supplementary Information

Supplementary Figure 1. HLA allotype distribution among cohort A – C. 88

Supplementary Table 1. Detailed background information on study subjects of cohort A, B, C and D. 86

Supplementary Table 2. Number of reactive donors among activated T cells against 50 amino-acid long regions of SARS-CoV-2 structural proteins. 93

Supplementary Table 3. T cell response-inducing 15-mer peptides identified from in vitro stimulation assays.. 97

Supplementary Table 4. **15-mer peptides with predicted immunogenic capacity.**. 109

Supplementary Table 5. Validation of core peptides' immunogenicity. 128

Supplementary Table 6. Unfavorable and favorable HLA Class I and Class II haplotypes.. 144

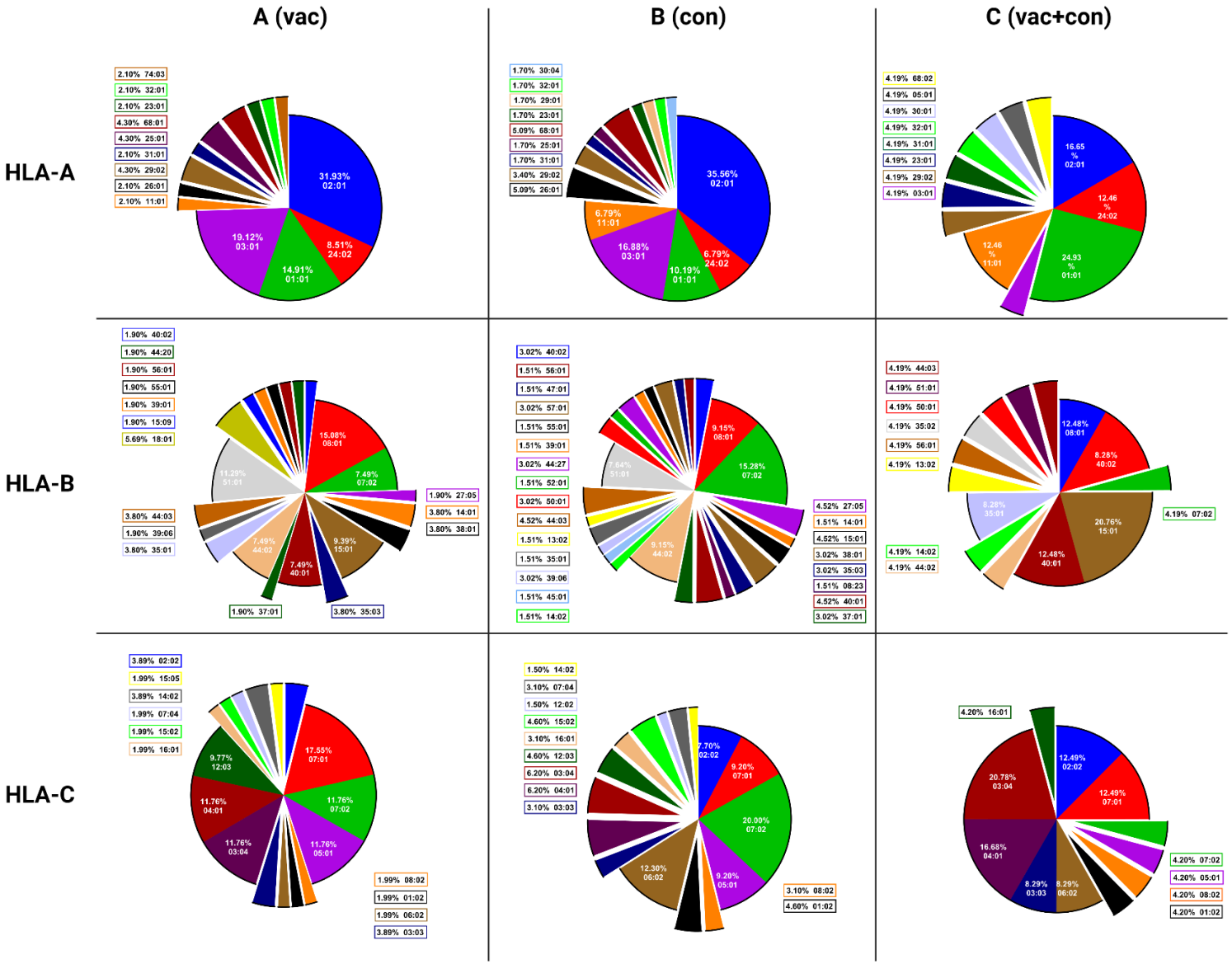
A (vac)
B (con)
C (vac+con)
HLA-A
HLA-B
HLA-C
2.10% 74:03
2.10% 32:01
2.10% 23:01
4.30% 68:01
4.30% 25:01
2.10% 31:01
4.30% 29:02
2.10% 26:01
2.10% 11:01
31.93% 02:01
8.51% 24:02
14.91% 01:01
19.12% 03:01
1.70% 30:04
1.70% 32:01
1.70% 29:01
1.70% 23:01
5.09% 68:01
1.70% 25:01
1.70% 31:01
3.40% 29:02
5.09% 26:01
35.56% 02:01
6.79% 24:02
10.19% 01:01
16.88% 03:01
6.79% 11:01
4.19% 68:02
4.19% 05:01
4.19% 30:01
4.19% 32:01
4.19% 31:01
4.19% 23:01
4.19% 29:02
4.19% 03:01
16.65 % 02:01
12.46 % 24:02
24.93 % 01:01
12.46 % 11:01
1.90% 40:02
1.90% 44:20
1.90% 56:01
1.90% 55:01
1.90% 39:01
1.90% 15:09
5.69% 18:01
3.80% 44:03
1.90% 39:06
3.80% 35:01
15.08% 08:01
7.49% 07:02
11.29% 51:01
1.90% 27:05
3.80% 14:01
3.80% 38:01
9.39% 15:01
7.49% 44:02
7.49% 40:01
1.90% 37:01
3.80% 35:03
3.02% 40:02
1.51% 56:01
1.51% 47:01
3.02% 57:01
1.51% 55:01
1.51% 39:01
3.02% 44:27
1.51% 52:01
3.02% 50:01
4.52% 44:03
1.51% 13:02
1.51% 35:01
3.02% 39:06
1.51% 45:01
1.51% 14:02
9.15% 08:01
15.28% 07:02
7.84% 51:01
9.15% 44:02
4.52% 27:05
1.51% 14:01
4.52% 15:01
3.02% 38:01
3.02% 35:03
1.51% 08:23
4.52% 40:01
3.02% 37:01
4.19% 44:03
4.19% 51:01
4.19% 50:01
4.19% 35:02
4.19% 56:01
4.19% 13:02
12.48% 08:01
8.28% 40:02
8.28% 35:01
20.76% 15:01
4.19% 07:02
4.19% 14:02
4.19% 44:02
12.48% 40:01
3.89% 02:02
1.99% 15:05
3.89% 14:02
1.99% 07:04
1.99% 15:02
1.99% 16:01
17.55% 07:01
11.76% 07:02
11.76% 05:01
11.76% 03:04
11.76% 04:01
9.77% 12:03
1.99% 08:02
1.99% 01:02
1.99% 06:02
3.89% 03:03
1.50% 14:02
3.10% 07:04
1.50% 12:02
4.60% 15:02
3.10% 16:01
4.60% 12:03
6.20% 03:04
6.20% 04:01
3.10% 03:03
7.70% 02:02
9.20% 07:01
20.00% 07:02
9.20% 05:01
12.30% 06:02
3.10% 08:02
4.60% 01:02
4.20% 16:01
12.49% 02:02
12.49% 07:01
20.78% 03:04
16.68% 04:01
8.29% 03:03
8.29% 06:02
4.20% 07:02
4.20% 05:01
4.20% 08:02
4.20% 01:02

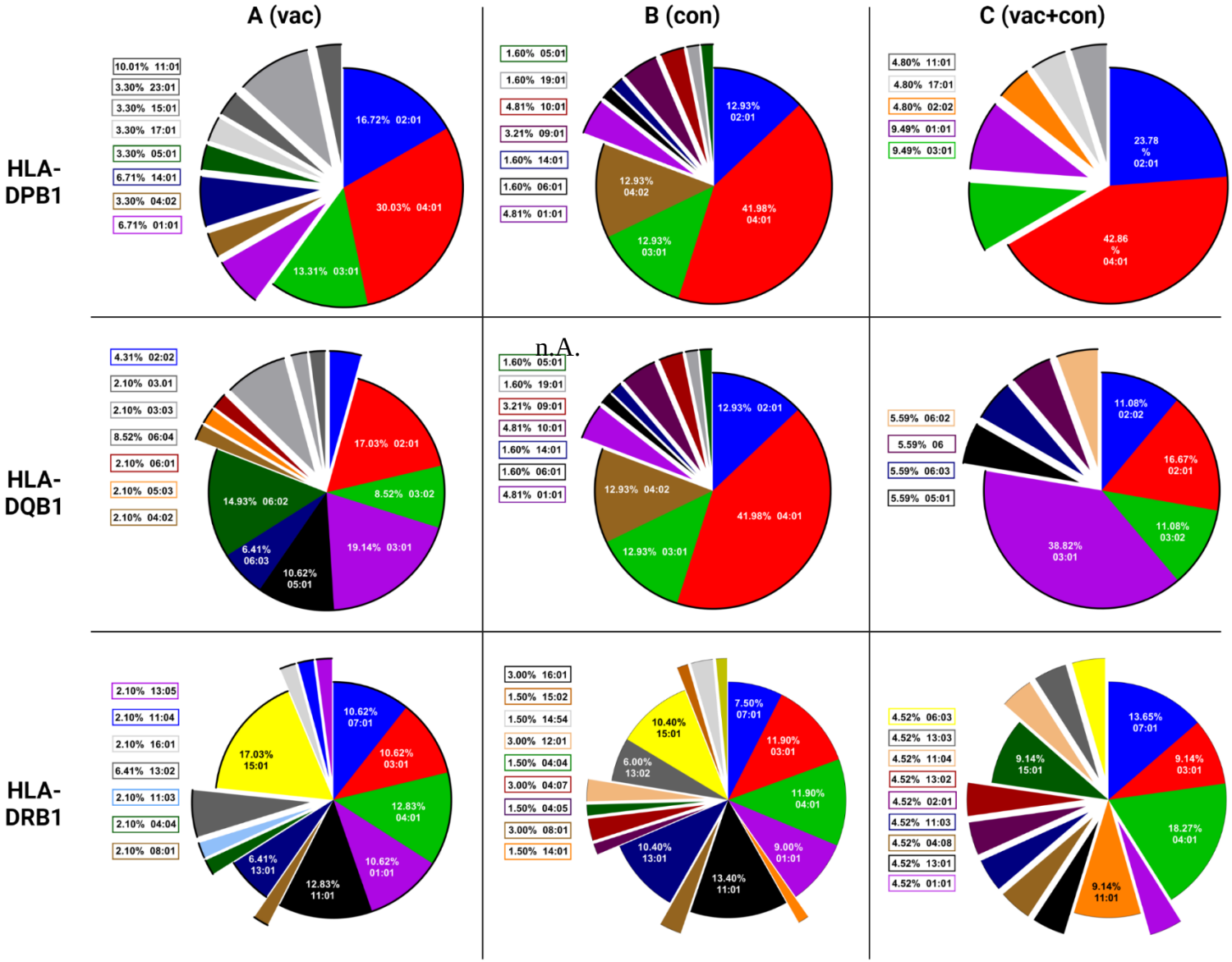
A (vac)
B (con)
C (vac+con)
HLA-DPB1
HLA-DQB1
HLA-DRB1
10.01% 11:01
3.30% 23:01
3.30% 15:01
3.30% 17:01
3.30% 05:01
6.71% 14:01
3.30% 04:02
6.71% 01:01
16.72% 02:01
30.03% 04:01
13.31% 03:01
1.60% 05:01
1.60% 19:01
4.81% 10:01
3.21% 09:01
1.60% 14:01
1.60% 06:01
4.81% 01:01
12.93% 02:01
41.98% 04:01
12.93% 03:01
12.93% 04:02
4.80% 11:01
4.80% 17:01
4.80% 02:02
9.49% 01:01
9.49% 03:01
23.78 % 02:01
42.86 % 04:01
4.31% 02:02
2.10% 03.01
2.10% 03:03
8.52% 06:04
2.10% 06:01
2.10% 05:03
2.10% 04:02
17.03% 02:01
8.52% 03:02
19.14% 03:01
10.62% 05:01
6.41% 06:03
14.93% 06:02
n.A.
1.60% 05:01
1.60% 19:01
3.21% 09:01
4.81% 10:01
1.60% 14:01
1.60% 06:01
4.81% 01:01
12.93% 02:01
41.98% 04:01
12.93% 03:01
12.93% 04:02
5.59% 06:02
5.59% 06
5.59% 06:03
5.59% 05:01
11.08% 02:02
16.67% 02:01
11.08% 03:02
38.82% 03:01
2.10% 13:05
2.10% 11:04
2.10% 16:01
6.41% 13:02
2.10% 11:03
2.10% 04:04
2.10% 08:01
10.62% 07:01
10.62% 03:01
12.83% 04:01
10.62% 01:01
12.83% 11:01
6.41% 13:01
17.03% 15:01
3.00% 16:01
1.50% 15:02
1.50% 14:54
3.00% 12:01
1.50% 04:04
3.00% 04:07
1.50% 04:05
3.00% 08:01
1.50% 14:01
7.50% 07:01
11.90% 03:01
11.90% 04:01
9.00% 01:01
13.40% 11:01
10.40% 13:01
6.00% 13:02
10.40% 15:01
4.52% 06:03
4.52% 13:03
4.52% 11:04
4.52% 13:02
4.52% 02:01
4.52% 11:03
4.52% 04:08
4.52% 13:01
4.52% 01:01
13.65% 07:01
9.14% 03:01
18.27% 04:01
9.14% 11:01
9.14% 15:01

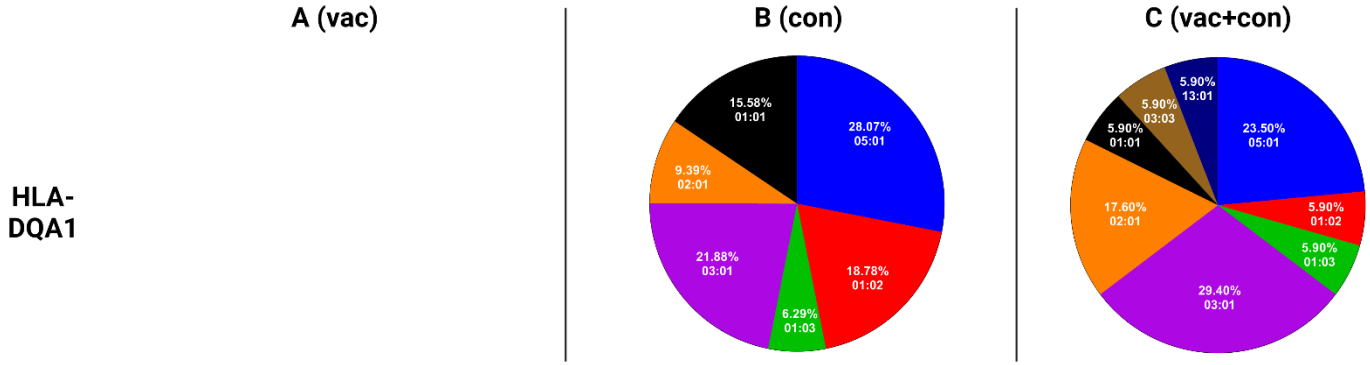

Supplementary Figure 1. HLA allotype distribution among cohort A – C. Pie charts representing the distribution of HLA class I and class II allotypes within cohort A (vaccinated study subject; left column), cohort B (convalescent study subjects; middle column) and cohort C (vaccinated and convalescent study subjects; right column). For each allotype the percentage of presenting donors within the particular cohort is given.

Supplementary Table 1. Detailed background information on study subjects of cohort A, B, C and D. Study subjects demographic information on cohort, sex, age, administered SARS-CoV-2 vaccine, sub-cohort (cohort D only), day of analysis and HLA-background. Cohort A = vaccinated study subjects, cohort B = convalescent study subjects, cohort C = vaccinated and convalescent study subjects, D ; m = male, f = female; n.A. = not applicable, NI = no information; sd= short disease, ld = long disease, mid = mild disease, mod = moderate disease

ID	Co-hort	sex	age	vaccine	sub-cohort	interim (days)	HLA-A		HLA-B		HLA-C		HLA-DPB1		HLA-DQB1		HLA-DRB1		HLA-DQA1	
1	B	m	42	n.A.	n.A.	NI	*02:01	*29:02	*40:02	*44:03	*02:02	*16:01	*02:01	*04:01	*02:02	*03:01	*07:01	*11:01	NI	NI
2	B	f	36	n.A.	n.A.	21	*24:02	*31:01	*08:01	*35:03	*07:01	*12:03	*04:01	*04:02	*02:01	*03:01	*03:01	*11:01	*05:01	*05:01
3	B	f	35	n.A.	n.A.	191	*01:01	*03:01	*07:02	*51:01	*07:02	*15:02	*03:01	*04:01	*03:02	*06:02	*04:01	*15:01	NI	NI
4	B	f	19	n.A.	n.A.	14	*03:01	*24:02	*07:02	*07:02	*07:02	*07:02	*02:01	*04:01	*03:02	*06:02	*04:01	*15:01	NI	NI
5	B	f	52	n.A.	n.A.	21	*02:01	*02:01	*27:05	*44:02	*02:02	*05:01	*04:01	*04:01	*03:01	*05:01	*01:01	*04:01	NI	NI
6	B	m	25	n.A.	n.A.	21	*02:01	*03:01	*07:02	*44:02	*05:01	*07:02	*02:01	*04:02	*05:03	*06:02	*14:01	*15:01	NI	NI
7	B	f	54	n.A.	n.A.	28	*02:01	*26:01	*14:01	*51:01	*08:02	*15:02	*04:01	*10:01	*03:02	*06:03	*04:01	*13:01	NI	NI
8	B	m	22	n.A.	n.A.	28	*02:01	*26:01	*27:05	*51:01	*01:02	*15:02	*04:01	*10:01	*05:01	*06:03	*01:01	*13:01	NI	NI
9	B	m	33	n.A.	n.A.	28	*03:01	*25:01	*38:01	*50:01	*06:02	*12:03	*02:01	*09:01	*02:01	*06:03	*03:01	*13:01	NI	NI
10	B	m	50	n.A.	n.A.	28	*01:01	*68:01	*08:01	*40:02	*02:02	*07:01	*04:01	*04:02	*02:01	*03:01	*03:01	*11:01	NI	NI
11	B	m	26	n.A.	n.A.	28	*02:01	*23:01	*15:01	*38:01	*03:03	*04:01	*04:01	*19:01	*03:01	*06:03	*11:01	*13:01	NI	NI
12	B	m	52	n.A.	n.A.	28	*11:01	*29:01	*35:03	*52:01	*04:01	*12:02	*03:01	*04:01	*04:02	*06:01	*08:01	*15:02	NI	NI
13	B	m	33	n.A.	n.A.	28	*26:01	*68:01	*08:23	*13:02	*06:02	*07:02	*04:01	*04:02	*02:01	*02:01	*03:01	*07:01	NI	NI
14	B	f	26	n.A.	n.A.	28	*01:01	*24:02	*07:02	*44:27	*07:02	*07:04	*03:01	*04:01	*04:02	*05:02	*08:01	*16:01	NI	NI
15	B	m	37	n.A.	n.A.	56	*02:01	*02:01	*08:01	*39:01	*07:01	*12:03	*03:01	*04:01	*02:01	*03:01	*03:01	*11:01	*05:01	*05:01
16	B	f	35	n.A.	n.A.	49	*02:01	*02:01	*40:01	*44:02	*03:04	*05:01	*02:01	*04:01	*03:01	*06:04	*04:01	*13:02	*01:02	*03:01
17	B	f	57	n.A.	n.A.	56	*02:01	*32:01	*37:01	*44:02	*05:01	*06:02	*01:01	*04:02	*03:01	*03:01	*11:01	*12:01	*05:01	*05:01
18	B	f	60	n.A.	n.A.	56	*02:01	*11:01	*44:02	*55:01	*03:03	*05:01	*04:01	*04:02	*05:03	*06:03	*13:01	*14:54	*01:03	*01:01
19	B	f	29	n.A.	n.A.	n.A.	*02:01	*03:01	*14:02	*39:06	*07:02	*08:02	*04:01	*05:01	*03:02	*06:09	*04:01	*13:02	NI	NI
20	B	m	48	n.A.	n.A.	56	*02:01	*02:01	*07:02	*08:01	*07:01	*07:02	*02:01	*03:01	*02:01	*03:01	*03:01	*04:01	*03:01	*05:01
21	B	m	47	n.A.	n.A.	56	*02:01	*02:01	*45:01	*57:01	*06:02	*06:02	*02:01	*04:01	*03:02	*03:03	*04:05	*07:01	*02:01	*03:01
22	B	f	54	n.A.	n.A.	56	*02:01	*03:01	*44:02	*47:01	*05:01	*06:02	*04:01	*04:01	*05:01	*06:02	*01:01	*15:01	*01:01	*01:02
23	B	m	54	n.A.	n.A.	56	*02:01	*02:01	*07:02	*51:01	*07:02	*14:02	*04:01	*04:01	*03:01	*06:03	*04:07	*13:01	*01:03	*03:01
24	B	f	39	n.A.	n.A.	56	*02:01	*02:01	*37:01	*44:03	*06:02	*06:02	*03:01	*10:01	*03:01	*05:01	*01:01	*04:07	*01:01	*03:01
25	B	m	24	n.A.	n.A.	56	*02:01	*11:01	*27:05	*35:01	*02:02	*04:01	*04:01	*04:01	*02:01	*03:02	*04:04	*07:01	*02:01	*03:01
26	B	m	46	n.A.	n.A.	28	*02:01	*24:02	*39:06	*40:01	*03:04	*07:02	*03:01	*04:02	*03:01	*06:04	*11:01	*13:02	NI	NI
27	B	f	49	n.A.	n.A.	56	*01:01	*03:01	*07:02	*08:01	*07:01	*07:02	*01:01	*04:01	*02:01	*06:02	*03:01	*15:01	*01:02	*05:01

ID	Co-hort	sex	age	vaccine	sub-cohort	interim (days)	HLA-A		HLA-B		HLA-C		HLA-DPB1		HLA-DQB1		HLA-DRB1		HLA-DQA1	
28	B	m	63	n.A.	n.A.	56	*02:01	*02:01	*07:02	*57:01	*06:02	*07:02	*04:01	*04:02	*03:01	*06:02	*11:01	*15:01	*01:02	*05:01
29	B	f	53	n.A.	n.A.	56	*02:01	*03:01	*15:01	*44:27	*04:01	*07:04	*01:01	*04:01	*03:01	*05:02	*12:01	*16:01	*01:02	*05:01
30	B	f	55	n.A.	n.A.	56	*01:01	*30:04	*08:01	*50:01	*06:02	*07:01	*04:01	*09:01	*02:01	*02:01	*03:01	*07:01	*02:01	*05:01
31	B	m	26	n.A.	n.A.	56	*03:01	*68:01	*07:02	*15:01	*03:04	*07:02	*02:01	*04:01	*03:02	*06:02	*04:01	*15:01	*01:02	*03:01
32	B	f	54	n.A.	n.A.	28	*03:01	*03:01	*51:01	*51:01	*01:02	*02:02	*03:01	*04:01	*03:01	*05:01	*01:01	*11:01	*01:01	*05:01
33	B	m	39	n.A.	n.A.	21	*11:01	*29:02	*44:03	*56:01	*01:02	*16:01	*06:01	*14:01	*05:01	*05:01	*01:01	*01:01	*01:01	*01:01
34	B	f	30	BNT162b2	n.A.	499	*01:01	*02:01	*07:02	*40:01	*03:04	*07:02	NI	NI	*06:03	*06:04	*13:01	*13:02	NI	NI
35	C	f	56	AZD1222	n.A.	90	*11:01	*24:02	*35:01	*40:02	*02:02	*04:01	*02:01	*04:01	*02:02	*03:01	*07:01	*11:01	*02:01	*05:01
36	C	m	51	NI	n.A.	56	*01:01	*02:01	*15:01	*35:02	*03:04	*04:01	*02:01	*04:01	*03:01	*03:02	*04:01	*11:04	NI	NI
37	C	f	64	NI	n.A.	63	*02:01	*30:01	*13:02	*15:01	*03:03	*06:02	*02:01	*17:01	*02:02	*03:01	*04:08	*07:01	*02:01	*03:03
38	C	m	68	NI	n.A.	63	*01:01	*02:01	*08:01	*15:01	*03:04	*07:01	*02:02	*04:01	*02:01	*03:02	*03:01	*04:01	*03:01	*05:01
39	C	f	46	BNT162b2	n.A.	4	*29:02	*31:01	*44:03	*50:01	*06:02	*16:01	*04:01	*11:01	*02:01	*02:01	*07:01	*07:01	*02:01	*02:01
40	C	m	48	BNT162b2	n.A.	4	*11:01	*05:01	*40:01	*56:01	*01:02	*03:04	*04:01	*04:01	*03:01	*06:03	*04:01	*13:01	*01:03	*03:01
41	C	f	50	AZD1222	n.A.	56	*01:01	*23:01	*35:01	*40:01	*03:04	*04:01	*04:01	*04:01	*05:01	*06:02	*01:01	*15:01	*01:01	*01:02
42	C	m	50	AD26.COV 2.S	n.A.	34	*02:01	*24:02	*44:02	*51:01	*02:02	*05:01	*04:01	*04:01	*03:01	*03:01	*04:01	*04:01	*03:01	*03:01
43	C	m	34	mRNA-1273	n.A.	30	*01:01	*68:02	*08:01	*14:02	*07:01	*08:02	*01:01	*02:01	*02:01	*03:01	*03:01	*13:03	*05:01	*05:01
44	C	f	27	mRNA-1273	n.A.	30	*11:01	*24:02	*15:01	*40:02	*02:02	*03:03	*02:01	*04:01	*03:01	*03:01	*11:01	*11:03	*05:01	*05:01
45	C	f	23	mRNA-1273	n.A.	49	*01:01	*32:01	*08:01	*15:01	*04:01	*07:01	*01:01	*03:01	NI	NI	*02:01	*06:03	*03:01	*13:01
46	C	f	55	BNT162b2	n.A.	8	*01:01	*03:01	*07:02	*40:01	*03:04	*07:02	*03:01	*04:01	*06	*06	*13:02	*15:01	NI	NI
47	A	f	42	BNT162b2	n.A.	18	*02:01	*24:02	*40:01	*51:01	*03:04	*05:01	*15:01	*15:01	*03:01	*06:03	*11:03	*13:01	NI	NI
48	A	f	37	NI	n.A.	12	*02:01	*31:01	*38:01	*51:01	*04:01	*12:03	NI	NI	NI	NI	NI	NI	NI	NI
49	A	f	49	BNT162b2	n.A.	18	*03:01	*68:01	*07:02	*35:03	*04:01	*07:02	*03:01	*04:01	*03:01	*03.01	*04:01	*11:01	NI	NI
50	A	f	41	BNT162b2	n.A.	26	*02:01	*02:01	*15:01	*39:01	*03:04	*07:02	*02:01	*03:01	*04:02	*05:01	*01:01	*08:01	NI	NI
51	A	m	26	BNT162b2	n.A.	5	*03:01	*03:01	*08:01	*15:01	*06:02	*07:01	NI	NI	*02:01	*03:02	*03:01	*04:01	NI	NI
52	A	m	44	NI	n.A.	28	*03:01	*29:02	*07:02	*44:03	*07:02	*16:01	*02:01	*11:01	*02:02	*06:02	*07:01	*15:01	NI	NI
53	A	f	54	BNT162b2	n.A.	19	*01:01	*03:01	*08:01	*35:01	*04:01	*07:01	*04:02	*17:01	*05:01	*06:02	*01:01	*15:01	NI	NI
54	A	f	26	BNT162b2	n.A.	46	*01:01	*25:01	*08:01	*18:01	*07:01	*12:03	*04:01	*04:01	*02:01	*05:01	*01:01	*15:01	NI	NI
55	A	f	37	BNT162b2	n.A.	20	*02:01	*25:01	*44:02	*56:01	*01:02	*05:01	NI	NI	*05:01	*05:01	*01:01	*01:01	NI	NI
56	A	f	30	BNT162b2	n.A.	55	*03:01	*11:01	*07:02	*51:01	*07:02	*14:02	*01:01	*04:01	*03:01	*03:01	*11:01	*13:05	NI	NI
57	A	f	34	BNT162b2	n.A.	55	*02:01	*02:01	*18:01	*44:20	*05:01	*12:03	*23:01	*23:01	*03:02	*06:02	*04:01	*15:01	NI	NI
58	A	m	30	BNT162b2	n.A.	56	*01:01	*01:01	*08:01	*08:01	*07:01	*07:01	*02:01	*03:01	*02:01	*03:01	*03:01	*11:01	NI	NI

ID	Co-hort	sex	age	vaccine	sub-cohort	interim (days)	HLA-A		HLA-B		HLA-C		HLA-DPB1		HLA-DQB1		HLA-DRB1		HLA-DQA1	
59	A	f	34	BNT162b2	n.A.	50	*01:01	*02:01	*08:01	*15:01	*03:03	*07:01	*04:01	*04:01	*03:01	*06:03	*04:01	*13:01	NI	NI
60	A	f	32	AZD1222	n.A.	83	*02:01	*03:01	*27:05	*44:02	*02:02	*05:01	*04:01	*04:01	*05:03	*06:02	NI	*15:01	NI	NI
61	A	f	31	BNT162b2	n.A.	57	*02:01	*68:01	*15:01	*51:01	*03:04	*14:02	NI	NI	*06:01	*06:03	*13:01	*13:01	NI	NI
62	A	f	55	mRNA-1273	n.A.	63	*02:01	*24:02	*35:03	*40:01	*03:04	*04:01	NI	NI	*03:01	*06:04	*11:01	*13:02	NI	NI
63	A	m	50	BNT162b2	n.A.	91	*02:01	*23:01	*18:01	*39:06	*07:01	*07:02	*02:01	*04:01	*03:01	*03:01	*11:01	*11:04	NI	NI
64	A	m	40	NI	n.A.	54	*24:02	*29:02	*15:09	*40:01	*03:04	*07:04	*14:01	*14:01	*06:04	*06:04	*13:02	*13:02	NI	NI
65	A	f	28	BNT162b2	n.A.	55	*01:01	*02:01	*08:01	*44:02	*05:01	*07:01	*04:01	*04:01	*02:01	*03:01	*03:01	*04:01	NI	NI
66	A	f	28	mRNA Vaccine	n.A.	50	*02:01	*02:01	*15:01	*37:01	*04:01	*12:03	*02:01	*02:01	*03:01	*03:03	*07:01	*11:01	NI	NI
67	A	f	27	mRNA Vaccine	n.A.	86	*01:01	*02:01	*08:01	*51:01	*07:01	*15:02	*04:01	*04:01	*02:01	*03:02	*03:01	*04:04	NI	NI
68	A	m	32	mRNA-1273	n.A.	65	*02:01	*26:01	*38:01	*51:01	*12:03	*12:03	NI	NI	NI	NI	*16:01	*16:01	NI	NI
69	A	f	32	BNT162b2	n.A.	128	*01:01	*24:02	*08:01	*55:01	*03:03	*07:01	*01:01	*05:01	*02:01	*06:04	*03:01	*13:02	NI	NI
70	A	f	26	BNT162b2	n.A.	110	*02:01	*02:01	*14:01	*44:02	*05:01	*08:02	*04:01	*14:01	*02:01	*06:02	*07:01	*15:01	NI	NI
71	A	f	28	BNT162b2	n.A.	94	*03:01	*32:01	*07:02	*40:02	*02:02	*07:02	*11:01	*11:01	*02:01	*06:02	*07:01	*15:01	NI	NI
72	A	f	62	AZD1222	n.A.	113	*03:01	*74:03	*35:01	*44:03	*04:01	*04:01	NI	NI	*05:01	*06:02	*01:01	*15:01	NI	NI
73	A	f	42	AZD1222/BNT162b2	n.A.	82	*03:01	*03:01	*14:01	*40:01	*03:04	*15:05	*03:01	*11:01	*02:02	*03:02	*04:01	*07:01	NI	NI
74	D	f	NI	NI	sd	NI	*02:01	*02:01	*27:05	*50:01	*02:02	*06:02	NI	NI	*02:01	*03:02	*03:01	*04:04	05MZ	*03:01
75	D	f	NI	NI	sd	NI	*01:01	*02:01	*07:02	*37:01	*07:02	*06:02	NI	NI	*03:02	*06:02	*04:01	*13:01	03*01	*01:03
76	D	m	NI	NI	sd	NI	*01:01	*32:01	*08:01	*44:01	*07:01	*16:04	NI	NI	*02:01	*06:03	*03:01	*13:01	05MZ	*01:03
77	D	f	NI	NI	sd	NI	*02:01	*11:01	*15:01	*51:01	*03:03	*15:02	NI	NI	*03:01	*06:03	*11:01	*13:01	05MZ	*01:03
78	D	f	NI	NI	sd	NI	*02:01	*24:02	*44:02	*07:02	*05:01	*07:02	NI	NI	*04:02	*06:03	*08:01	*13:01	*04:01	*01:03
79	D	f	NI	NI	sd	NI	*02:01	*24:02	*27:05	*39:06	*02:02	*07:02	NI	NI	*03:03	*03:01	*09:01	*11:01	03BC	05MZ
80	D	f	NI	NI	sd	NI	*02:01	*02:01	*15:01	*49:01	*03:03	*07:01	NI	NI	*03:01	*06:03	*11:01	*13:01	05MZ	*01:03
81	D	f	NI	NI	sd	NI	*11:01	*01:01	*35:01	*27:05	*04:01	*02:02	NI	NI	*02:01	*03:01	*03:01	*13:05	NI	NI
82	D	m	NI	NI	sd	NI	*02:01	*24:02	*07:02	*14:02	*07:02	*08:02	NI	NI	*05:01	*02:02	*02:0	*07:01	*01:01	*01:02
83	D	m	NI	NI	ld	NI	*01:01	*26:01	*08:01	*45:01	*07:01	*06:02	NI	NI	*04:02	*03:01	*08:01	*13:03	*04:01	NI
84	D	m	NI	NI	ld	NI	*24:02	*66:01	*41:02	*07:04	*17:01	*07:02	NI	NI	*03:01	*06:02	*13:03	*15:01	*01:02	NI
85	D	f	NI	NI	ld	NI	*03:01	*01:01	*07:02	*57:01	*07:02	*06:02	NI	NI	*03:03	*06:02	*07:01	*15:01	*02:01	*01:02
86	D	f	NI	NI	ld	NI	*03:01	*02:17	*07:02	*18:01	*07:02	*07:01	NI	NI	*02:02	*06:02	*07:01	*15:01	*02:01	*01:02
87	D	f	NI	NI	ld	NI	*03:01	*02:01	*07:02	*35:01	*07:02	*04:01	NI	NI	*05:01	*06:02	*01:01	*15:01	*01:01	*01:02

ID	Co-hort	sex	age	vaccine	sub-cohort	interim (days)	HLA-A		HLA-B		HLA-C		HLA-DPB1		HLA-DQB1		HLA-DRB1		HLA-DQA1	
88	D	f	NI	NI	ld	NI	*02:01	*02:01	*44:27	*40:01	*07:04	*03:04	NI	NI	*06:02	*06:02	*15:01	*16:01	*01:02	*01:02
89	D	f	NI	NI	ld	NI	*03:01	*02:01	*07:02	*41:02	*07:02	*17:01	NI	NI	*03:01	*06:02	*13:03	*15:01	*01:02	NI
90	D	m	NI	NI	ld	NI	*11:01	*68:02	*35:01	*14:02	*04:01	*08:02	NI	NI	*05:01	*06:02	*01:01	*15:01	*01:01	*01:02
91	D	f	NI	NI	ld	NI	*02:01	*11:01	*07:02	*44:27	*07:02	*07:04	NI	NI	*06:02	*05:02	*15:01	*16:01	*01:02	*01:02
92	D	m	NI	NI	mid	NI	*03:01	*24:02	*35:01	*18:01	*04:01	*07:01	NI	NI	*05:01	*03:01	*01:01	*12:01	*01:01	05MZ
93	D	m	NI	NI	mid	NI	*68:01	*03:01	*07:05	*38:01	*15:05	*12:03	NI	NI	*03:05	*06:03	*04:03	*13:01	*03	*01:03
94	D	m	NI	NI	mid	NI	*11:01	*26:01	*35:01	*38:01	*04:01	*12:03	NI	NI	*03:01	*06:03	*11:04	*13:01	05MZ	*01:03
95	D	f	NI	NI	mid	NI	*30:01	*32:01	*38:01	*15:01	*12:03	*03:03	NI	NI	*03:01	*06:03	*11:01	*13:01	05MZ	*01:03
96	D	f	NI	NI	mid	NI	*24:02	*24:02	*07:02	*35:03	*07:02	*04:01	NI	NI	*03:01	*06:02	*12:01	*15:01	*01:02	NI
97	D	m	NI	NI	mid	NI	*01:01	*32:01	*08:01	*04:02	*07:01	*02:02	NI	NI	*02:01	*03:01	*03:01	*12:01	05MZ	05MZ
98	D	m	NI	NI	mid	NI	*01:01	*02:01	*08:01	*07:02	*07:01	*07:02	NI	NI	*02:01	*06:02	*03:01	*15:01	*01:02	NI
99	D	f	NI	NI	mid	NI	*02:01	*24:02	*07:02	*49:01	*07:02	*07:01	NI	NI	*03:01	*06:02	*11:04	*15:01	05MZ	*01:02
100	D	f	NI	NI	mid	NI	*24:02	*66:01	*38:01	*27:05	*12:03	*02:02	NI	NI	*06:03	*06:04	*13:01	*13:02	*01:03	*01:02
101	D	f	NI	NI	mid	NI	*26:01	*32:01	*38:01	*38:01	*12:03	*12:03	NI	NI	*03:02	*06:03	*04:02	*13:01	*03:01	*01:03
102	D	m	NI	NI	mid	NI	*02:01	*11:01	*07:02	*18:01	*07:02	*07:01	NI	NI	*06:04	*03:01	*13:02	*11:04	*01:02	05MZ
103	D	f	NI	NI	mid	NI	*02:01	*02:01	*07:02	*51:01	*07:02	*14:02	NI	NI	*03:01	*03:01	*11:01	*11:04	05MZ	05MZ
104	D	m	NI	NI	mid	NI	*02:01	*30:02	*44:02	*18:01	*05:01	*05:01	NI	NI	*02:01	*03:01	*03:01	*12:01	05MZ	05MZ
105	D	f	NI	NI	mod	NI	*32:01	*68:01	*57:01	*44:02	*06:02	*05:01	NI	NI	*03:03	*03:01	*07:01	*11:01	*02:01	05MZ
106	D	m	NI	NI	mod	NI	*01:01	*02:01	*57:01	*07:02	*06:02	*07:02	NI	NI	*02:01	*06:02	*03:01	*15:01	*01:02	NI
107	D	f	NI	NI	mod	NI	*01:01	*02:01	*15:01	*57:01	*03:04	*06:02	NI	NI	*03:02	*06:02	*04:01	*15:01	*03:01	*01:02
108	D	m	NI	NI	mod	NI	*24:02	*29:01	*35:02	*57:01	*04:01	*06:02	NI	NI	*03:01	*06:04	*11:01	*13:02	05MZ	*01:02
109	D	f	NI	NI	mod	NI	*11:01	*02:01	*35:01	*40:01	*04:01	*03:02	NI	NI	*05:01	*03:03	*01:01	*07:01	*01:01	*02:01
110	D	m	NI	NI	mod	NI	*02:01	*03:01	*57:01	*35:01	*06:02	*04:01	NI	NI	*05:01	*03:01	*01:01	*04:08	*01:01	03BC
111	D	f	NI	NI	mod	NI	NI	NI	NI	NI	NI	NI	NI	NI	*03:03	*03:01	*07:01	*11:01	*02:01	05MZ
112	D	m	NI	NI	mod	NI	*30:01	*32:01	*08:01	*57:01	*07:01	*06:02	NI	NI	*02:01	*04:02	*03:01	*08:01	05MZ	*04:01
113	D	f	NI	NI	mod	NI	*02:05	*24:02	*50:01	*40:01	*06:02	*03:04	NI	NI	*02:02	*03:03	*07:01	*07:01	*02:01	*02:01

Supplementary Table 2. Number of reactive donors among activated T cells against 50 amino-acid long regions of SARS-CoV-2 structural proteins. Rows refer to an individual 50 amino acid long region derived from the Spike, Nucleocapsid or Membrane protein (1st column). Each region is covered by ten consecutive 15-mer single peptides. The individual name of the peptide pool (2nd column), as well as the specific sequence (3rd column) are indicated, followed by the number (and frequency of total) of reactive donors from cohort A, B and C among $CD8^+TNF\alpha^+IFN\gamma^+$ - and $CD4^+CD154^+TNF\alpha^+$ T cells

Protein	Peptide Pool	Sequence covered by 15-mer peptide pools	Number of reactive donors among $CD8^+TNF\alpha^+IFN\gamma^+$ T cells (frequency of total)			Number of reactive donors among $CD4^+CD154^+TNF\alpha^+$ T cells (frequency of total)		
			Cohort A	Cohort B	Cohort C	Cohort A	Cohort B	Cohort C
Spike	Prot_S_1-51	MFVFLVLLPLVSSQCVNLTTRTQLPPAYTNSFTRGVYYPDKVFRSSVLHST	8 (72.7)	3 (27.3)	0	3 (30)	7 (70)	0
	Prot_S_41-91	KVFRSSVLHSTQDLFLPFFSNVTWFHAIHVSGTNGTKRFDNPVLPFNDGVY	4 (44.4)	5 (55.6)	0	1 (20)	4 (80)	0
	Prot_S_81-130	NPVLPFNDGVYFASTEKSNIIRGWIFGTTLDSKTQSLLIVNNATNVVIKV	5 (55.6)	4 (44.4)	0	4 (50)	4 (50)	0
	Prot_S_121-175	NNATNVVIKVCEFQFCNDPFLGVYYHKNNKSWMESEFRVYSSANNCTFEY VSQPF	11 (64.7)	5 (29.4)	1 (5.9)	2 (15.4)	10 (76.9)	1 (7.7)
	Prot_S_165-216	NCTFEYVSQPFLMDLEGKQGNFKNLREFVFKNIDGYFKIYSKHTPINLVRDL	1 (25)	3 (75)	0	4 (50)	4 (50)	0
	Prot_S_205-255	SKHTPINLVRDLPQGFSALEPLVDLPIGINITRFQTLLALHRSYLTPGDSS	1 (50)	1 (50)	0	2 (66.7)	1 (33.3)	0
	Prot_S_245-295	HRSYLTPGDSSSGWTAGAAAYYVGYLQPRTFLLKYNENGTITDAVDCALD P	4 (66.7)	2 (33.3)	0	3 (75)	1 (25)	0
	Prot_S_285-327	ITDAVDCALDPLSETKCTLKSFTVEKGIYQTSNFRVQPTESIV	0	0	1 (100)	1 (100)	0	0
	Prot_S_313-351	YQTSNFRVQPTESIVRFPNITNLCPFGEVFNATRFASVY	0	1 (100)	0	0	1 (100)	0
	Prot_S_342-390	FNATRFASVYAWNRKRISNCVADYSVLYNSASFSTFKCYGVSPTKLNDL	5 (62.5)	1 (12.5)	2 (25)	3 (20)	10 (66.7)	2 (13.3)
	Prot_S_381-431	GVSPTKLNDLCFTNVYADSFVIRGDEVRQIAPGQTGKIADYNYKLPDDFTG	1 (33.3)	2 (66.7)	0	0	1 (100)	0
	Prot_S_421-455	YNYKLPDDFTGCVIAWNSNNLDSKVGGNYNYLYRL	0	1 (100)	0	1 (50)	1 (50)	0
	Prot_S_441-475	LDSKVGGNYNYLYRLFRKSNLKPFERDISTEIYQA	0	3 (75)	1 (25)	1 (20)	3 (60)	1 (20)
	Prot_S_461-508	LKPFERDISTEIYQAGSTPCNGVEGFNCYFPLQSYGFQPTNGVGYQPY	0	4 (100)	0	0	1 (100)	0
	Prot_S_494-531	SYGFQPTNGVGYQPYRVVVLSFELLHAPATVCGPKKST	1 (33.3)	2 (66.7)	0	0	1 (100)	0

Protein	Peptide Pool	Sequence covered by 15-mer peptide pools	Number of reactive donors among $CD8^+TNF\alpha^+IFN\gamma^+$ T cells (frequency of total)			Number of reactive donors among $CD4^+CD154^+TNF\alpha^+$ T cells (frequency of total)		
			Cohort A	Cohort B	Cohort C	Cohort A	Cohort B	Cohort C
	Prot_S_521-567	PATVCGPKKSTNLVKNKCVNFNFNGLTGTGVLTESNKKFLPFQQFGR	1 (33.3)	2 (66.7)	0	3 (50)	3 (50)	0
	Prot_S_557-607	KKFLPFQQFGRDIADTTDAVRDPQTLEILDITPCSFGGVSVITPGTNTSNQ	0	1 (100)	0	0	1 (100)	0
	Prot_S_597-635	VITPGTNTSNQVAVLYQDVNCTEVPVAIHADQLTPTWRV	0	1 (100)	0	1 (100)	0	0
	Prot_S_625-674	HADQLTPTWRVYSTGSNVFQTRAGCLIGAEHVNNSYECDIPIGAGICASY	1 (33.3)	2 (66.7)	0	2 (100)	0	0
	Prot_S_665-707	PIGAGICASYQTQTNSPRRARSVASQSIIAYTMSLGAENSVAY	2 (33.3)	3 (50)	1 (16.7)	2 (66.7)	1 (33.3)	0
	Prot_S_698-747	SLGAENSVAYSNNSIAIPTNFTISVTTEILPVSMTKTSVDCTMYICGDST	1 (16.7)	5 (83.3)	0	3 (100)	0	0
	Prot_S_737-779	DCTMYICGDSTECSNLLLQYGSFCTQLNRALTGIAVEQDKNTQ	1 (33.3)	2 (66.7)	0	4 (66.7)	2 (33.3)	0
	Prot_S_769-813	GIAVEQDKNTQEVFAQVKQIYKTPPIKDFGGFNFSQILPDPSKPS	1 (16.7)	4 (66.7)	1 (16.7)	3 (37.5)	3 (37.5)	2 (25)
	Prot_S_802-852	FSQILPDPSKPSKRSFIEDLLFNKVTLADAGFIKQYGDCLGDIAARDLICA	2 (40)	3 (60)	0	3 (18.8)	10 (62.5)	3 (18.8)
	Prot_S_841-891	LGDIAARDLICAQKFNGLTVLPPLLTDEMIAQYTSALLAGTITSGWTFGAG	1 (20)	4 (80)	0	4 (66.7)	1 (16.7)	1 (16.7)
	Prot_S_881-927	TITSGWTFGAGAALQIPFAMQMAYRFNGIGVTQNVLYENQKLIANQF	4 (66.7)	2 (33.3)	0	0	6 (85.7)	1 (14.3)
	Prot_S_917-964	YENQKLIANQFNSAIGKIQDSLSSTASALGKLQDVVNQNAQALNTLVK	0	2 (66.7)	1 (33.3)	1 (33.3)	1 (33.3)	1 (33.3)
	Prot_S_955-991	NAQALNTLVKQLSSNFGAISSVLNDILSRLDKVEAEV	2 (40)	3 (60)	0	1 (50)	1 (50)	0
	Prot_S_981-1023	LSRLDKVEAEVQIDRLITGRLQSLQTYVTQQLIRAAEIRASAN	3 (50)	3 (50)	0	3 (50)	3 (50)	0
	Prot_S_1012-1059	LIRAAEIRASANLAATKMSECVLGQSKRVDFCGKGYHLMSFPQSAPHG	0	3 (100)	0	1 (33.3)	2 (66.7)	0

Protein	Peptide Pool	Sequence covered by 15-mer peptide pools	Number of reactive donors among $CD8^+TNF\alpha^+IFN\gamma^+$ T cells (frequency of total)			Number of reactive donors among $CD4^+CD154^+TNF\alpha^+$ T cells (frequency of total)		
			Cohort A	Cohort B	Cohort C	Cohort A	Cohort B	Cohort C
	Prot_S_1051-1099	SFPQSAPHGVVFLHVTYVPAQEKNFTTAPAICHDGKAHFPREGVFVSNG	1 (20)	4 (80)	0	4 (66.7)	2 (33.3)	0
	Prot_S_1089-1135	FPREGVFVSNGTHWFVTQRNFYEPQIITTDNTFVSGNCDVVIGIVNN	0	4 (100)	0	3 (100)	0	0
	Prot_S_1123-1166	SGNCDVVIGIVNNTVYDPLQPELDSFKEELDKYFKNHTSPDVDL	0	3 (75)	1 (25)	0	1 (100)	0
	Prot_S_1157-1205	KNHTSPDVDLGDISGINASVVNIQKEIDRLNEVAKNLNESLIDLQELGK	0	2 (100)	0	2 (100)	0	0
	Prot_S_1195-1230	ESLIDLQELGKYEQYIKWPWYIWLGFIAGLIAIVMV	2 (40)	2 (40)	1 (20)	3 (75)	1 (25)	0
	Prot_S_1222-1273	AGLIAIVMVTIMLCCMTSCCSCLKGCCSCGSCCKFDEDDSEPVLKGVKLHYT	3 (60)	2 (40)	0	1 (33.3)	2 (66.7)	0
Nucleocapsid	Prot_N_1-51	MSDNGPQNQRNAPRITFGGPSDSTGSNQNGERSGARSKQRRPQGLPNNTAS	0	2 (100)	0	2 (100)	0	0
	Prot_N_40-87	RRPQGLPNNTASWFTALTQHGKEDLKFPRGQGVPINTNSSPDDQIGYY	0	1 (100)	0	0	0	1 (100)
	Prot_N_78-131	SSPDDQIGYYRRATRRIRGGDGKMKDLSPRWYFYYLGTGPEAGLPYGANK	0	3 (75)	1 (25)	1 (100)	0	0
	Prot_N_117-167	PEAGLPYGANKDGIIWVATEGALNTPKDHIGTRNPANNAAIVLQLPQGTTL	0	0	0	2 (100)	0	0
	Prot_N_158-203	VLQLPQGTTLPKGFYAEGSRGGSQASSRSSSRSRNSSRNSTPGSSR	0	1 (100)	0	0	0	0
	Prot_N_194-234	SRNSTPGSSRGTSPARMAGNGGDAALALLLLDRLNQLESKM	0	2 (100)	0	4 (100)	0	0
	Prot_N_224-274	LDRLNQLESKMSGKGQQQQGQTVTKKSAAEASKKPRQKRTATKAYNVTQAF	0	4 (100)	0	2 (100)	0	0
	Prot_N_265-314	TKAYNVTQAFGRRGPEQTQGNFGDQELIRQGTDYKHWPQIAQFAPSASAF	0	4 (100)	0	2 (100)	0	0
	Prot_N_305-347	AQFAPSASAFFGMSRIGMEVTPSGTWLTYTGAIKLDDKDPNFK	0	1 (50)	1 (50)	0	0	0

Protein	Peptide Pool	Sequence covered by 15-mer peptide pools	Number of reactive donors among $CD8^+TNF\alpha^+IFN\gamma^+$ T cells (frequency of total)			Number of reactive donors among $CD4^+CD154^+TNF\alpha^+$ T cells (frequency of total)		
			Cohort A	Cohort B	Cohort C	Cohort A	Cohort B	Cohort C
	Prot_N_339-387	LDDKDPNFKDQVILLNKHIDAYKTFPPTEPKKDKKKKADETQALPQRQK	0	0	1 (100)	0	0	2 (100)
	Prot_N_377-419	DETQALPQRQKKQQTVTLLPAADLDDFSKQLQQSMSSADSTQA	0	1 (100)	0	1 (100)	0	0
Membrane	Prot_M_1-47	MADSNGTITVEELKKLLEQWNLVIGFLFLTWICLLQFAYANRNRFLY	0	5 (100)	0	4 (100)	0	0
	Prot_M_37-73	FAYANRNRFLYIIKLIFLWLLWPVTLACFVLAAVYRI	0	2 (100)	0	3 (100)	0	0
	Prot_M_65-105	FVLAAVYRINWITGGIAIAMACLVGLMWLSYFIASFRLFAR	0	1 (50)	1 (50)	1 (100)	0	0
	Prot_M_97-147	IASFRLFARTRSMWSFNPETNILLNVPLHGTILTRPLLESELVIGAVILRG	0	4 (100)	0	4 (100)	0	0
	Prot_M_135-183	ESELVIGAVILRGHLRIAGHHLGRCDIKDLPKEITVATSRTLSYYKLGA	0	6 (100)	0	7 (100)	0	0
	Prot_M_173-222	SRTLSYYKLGASQRVAGDSGFAAYSRYRIGNYKLNTDHSSSSDNIALLVQ	0	2 (66.7)	1 (33.3)	9 (81.8)	0	2 (18.2)

Supplementary Table 3. T cell response-inducing 15-mer peptides identified from in vitro stimulation assays. Rows refer to individual 15-mer peptides derived from the SARS-CoV-2 Spike (S), Nucleocapsid (N) or Membrane (M) protein (1st column), as well as their ancestor peptide pools (2nd column). The specific peptide sequence (3rd column) and the number of reactive donors found four each of the peptides after in vitro stimulation (4th column) are indicated. Likewise, the likely HLA restriction of the peptides, that were predicted by NetMHCpan given the HLA allotypes by reactive donors, are listed (5th column).

15-mer peptide	ancestor peptide pool	peptide sequence	# reactive donors	predicted HLA restriction						
CoV_Prot_S_1-14	CoV_Prot_S_1-51	MFVFLVLLPLVSSQ	3	HLA-C03:04	HLA-C02:02					
CoV_Prot_S_1-14	CoV_Prot_S_1-51	MFVFLVLLPLVSSQ	1	DRB1_1501						
CoV_Prot_S_5-19	CoV_Prot_S_1-51	LVLLPLVSSQCVNLT	2	HLA-B51:01	HLA-C03:04					
CoV_Prot_S_10-24	CoV_Prot_S_1-51	LVSSQCVNLTTRTQL	1	HLA-C07:04						
CoV_Prot_S_13-27	CoV_Prot_S_1-51	SQCVNLTTRTQLPPA	1	HLA-B37:01						
CoV_Prot_S_13-27	CoV_Prot_S_1-51	SQCVNLTTRTQLPPA	1	DRB1_1301						
CoV_Prot_S_18-32	CoV_Prot_S_1-51	LTTRTQLPPAYTNSF	1	DRB1_0101						
CoV_Prot_S_24-38	CoV_Prot_S_1-51	LPPAYTNSFTRGVYY	2	HLA-C15:02						
CoV_Prot_S_29-43	CoV_Prot_S_1-51	TNSFTRGVYYPDKVF	2	HLA-C02:02	HLA-C07:01					
CoV_Prot_S_29-43	CoV_Prot_S_1-51	TNSFTRGVYYPDKVF	1	DRB1_0401						
CoV_Prot_S_33-47	CoV_Prot_S_1-51	TRGVYYPDKVFRSSV	1	HLA-B15:01						
CoV_Prot_S_33-47	CoV_Prot_S_1-51	TRGVYYPDKVFRSSV	2	DRB1_0401						
CoV_Prot_S_37-51	CoV_Prot_S_1-51	YYPDKVFRSSVLHST	1	DRB1_0401						

15-mer peptide	ancestor peptide pool	peptide sequence	# reactive donors	predicted HLA restriction						
CoV_Prot_S_41-55	CoV_Prot_S_1-51	KVFRSSVLHSTQDLF	1	HLA-B14:01						
CoV_Prot_S_44-58	CoV_Prot_S_1-51	RSSVLHSTQDLFLPF	2	HLA-A26:01						
CoV_Prot_S_44-58	CoV_Prot_S_41-91	RSSVLHSTQDLFLPF	1	DRB1_0101						
CoV_Prot_S_49-63	CoV_Prot_S_41-91	HSTQDLFLPFFSNVT	1	HLA-A26:01						
CoV_Prot_S_57-71	CoV_Prot_S_41-91	PFFSNVTWFHAIHVS	1	HLA-C15:02						
CoV_Prot_S_57-71	CoV_Prot_S_41-91	PFFSNVTWFHAIHVS	1	DRB1_0101						
CoV_Prot_S_62-76	CoV_Prot_S_41-91	VTWFHAIHVSGTNGT	2	HLA-C15:02						
CoV_Prot_S_62-76	CoV_Prot_S_41-91	VTWFHAIHVSGTNGT	1	DRB1_0101						
CoV_Prot_S_72-86	CoV_Prot_S_41-91	GTNGTKRFDNPVLPF	1	HLA-B27:05						
CoV_Prot_S_72-86	CoV_Prot_S_41-91	GTNGTKRFDNPVLPF	1	DRB1_1501						
CoV_Prot_S_77-91	CoV_Prot_S_41-91	KRFDNPVLPFNDGVY	1	HLA-B27:05						
CoV_Prot_S_81-95	CoV_Prot_S_81-130	NPVLPFNDGVYFAST	1	HLA-B35:01						
CoV_Prot_S_117-130	CoV_Prot_S_81-130	LLIVNNATNVVIKV	1	HLA-B51:01						
CoV_Prot_S_117-130	CoV_Prot_S_81-130	LLIVNNATNVVIKV	1	DRB1_0401						
CoV_Prot_S_121-135	CoV_Prot_S_121-175	NNATNVVIKVCEFQF	1	HLA-B51:01						
CoV_Prot_S_129-143	CoV_Prot_S_121-175	KVCEFQFCNDPFLGV	1	HLA-C07:02						

15-mer peptide	ancestor peptide pool	peptide sequence	# reactive donors	predicted HLA restriction						
CoV_Prot_S_129-143	CoV_Prot_S_121-175	KVCEFQFCNDPFLGV	1	DRB1_1101						
CoV_Prot_S_133-147	CoV_Prot_S_121-175	FQFCNDPFLGVYYHK	3	DRB1_1501	DRB1_1501					
CoV_Prot_S_138-152	CoV_Prot_S_121-175	DPFLGVYYHKNNKSW	1	DRB1_1501						
CoV_Prot_S_150-164	CoV_Prot_S_121-175	KSWMESEFRVYSSAN	2	HLA-A29:02	HLA-A01:01					
CoV_Prot_S_150-164	CoV_Prot_S_121-175	KSWMESEFRVYSSAN	1	DRB1_1101						
CoV_Prot_S_154-168	CoV_Prot_S_121-175	ESEFRVYSSANNCTF	1	HLA-C16:01						
CoV_Prot_S_157-171	CoV_Prot_S_121-175	FRVYSSANNCTFEYV	1	HLA-B35:01						
CoV_Prot_S_157-171	CoV_Prot_S_121-175	FRVYSSANNCTFEYV	1	DRB1_1501						
CoV_Prot_S_161-175	CoV_Prot_S_121-175	SSANNCTFEYVSQPF	1	HLA-C04:01						
CoV_Prot_S_165-179	CoV_Prot_S_165-216	NCTFEYVSQPFLMDL	3	HLA-B40:01	HLA-C04:01	HLA-B40:02				
CoV_Prot_S_165-179	CoV_Prot_S_165-216	NCTFEYVSQPFLMDL	2	DRB1_1601	DRB1_1501					
CoV_Prot_S_170-184	CoV_Prot_S_165-216	YVSQPFLMDLEGKQG	1	HLA-C02:02						
CoV_Prot_S_178-192	CoV_Prot_S_165-216	DLEGKQGNFKNLREF	1	HLA-B15:01						
CoV_Prot_S_178-192	CoV_Prot_S_165-216	DLEGKQGNFKNLREF	1	DQA10102-DQB10502						
CoV_Prot_S_189-203	CoV_Prot_S_165-216	LREFVFKNIDGYFKI	2	DRB1_1501						
CoV_Prot_S_194-208	CoV_Prot_S_165-216	FKNIDGYFKIYSKHT	2	DRB1_1501						

15-mer peptide	ancestor peptide pool	peptide sequence	# reactive donors	predicted HLA restriction						
CoV_Prot_S_198-212	CoV_Prot_S_165-216	DGYFKIYSKHTPINL	2	DRB1_1501						
CoV_Prot_S_202-216	CoV_Prot_S_165-216	KIYSKHTPINLVRDL	2	DRB1_1501						
CoV_Prot_S_229-243	CoV_Prot_S_205-255	LPIGINITRFQTLLA	1	HLA-B08:01						
CoV_Prot_S_233-247	CoV_Prot_S_205-255	INITRFQTLLALHRS	1	DQA10501-DQB10501						
CoV_Prot_S_236-250	CoV_Prot_S_205-255	TRFQTLLALHRSYLT	1	DRB1_0101						
CoV_Prot_S_241-255	CoV_Prot_S_205-255	LLALHRSYLTPGDSS	1	DRB1_1501						
CoV_Prot_S_245-259	CoV_Prot_S_245-295	HRSYLTPGDSSSGWT	1	DQA10501-DQB10301						
CoV_Prot_S_249-263	CoV_Prot_S_245-295	LTPGDSSSGWTAGAA	1	HLA-A01:01						
CoV_Prot_S_253-267	CoV_Prot_S_245-295	DSSSGWTAGAAAYYV	1	HLA-A01:01						
CoV_Prot_S_257-271	CoV_Prot_S_245-295	GWTAGAAAYYVGYLQ	1	HLA-A01:01						
CoV_Prot_S_261-275	CoV_Prot_S_245-295	GAAAYYVGYLQPRTF	1	HLA-C03:03						
CoV_Prot_S_265-279	CoV_Prot_S_245-295	YYVGYLQPRTFLLKY	3	HLA-A02:01						
CoV_Prot_S_265-279	CoV_Prot_S_245-295	YYVGYLQPRTFLLKY	1	DRB1_1101						
CoV_Prot_S_269-283	CoV_Prot_S_245-295	YLQPRTFLLKYNENG	3	HLA-A02:01						
CoV_Prot_S_269-283	CoV_Prot_S_245-295	YLQPRTFLLKYNENG	1	DRB1_1101						
CoV_Prot_S_285-299	CoV_Prot_S_285-327	ITDAVDCALDPLSET	1	HLA-C05:01						

15-mer peptide	ancestor peptide pool	peptide sequence	# reactive donors	predicted HLA restriction						
CoV_Prot_S_289-303	CoV_Prot_S_285-327	VDCALDPLSETKCTL	1	HLA-C05:01						
CoV_Prot_S_304-319	CoV_Prot_S_285-327	KSFTVEKGIYQTSNFR	1	HLA-C02:02						
CoV_Prot_S_342-356	CoV_Prot_S_342-390	FNATRFASVYAWNRK	3	DQA10501-DQB10301	DRB1_1501					
CoV_Prot_S_345-359	CoV_Prot_S_342-390	TRFASVYAWNRKRIS	2	HLA-A03:01	HLA-B27:05					
CoV_Prot_S_345-359	CoV_Prot_S_342-390	TRFASVYAWNRKRIS	7	DRB1_1103	DRB1_1302	DRB1_1101	DRB1_1301	DRB1_1501	DRB1_1501	DRB1_1302
CoV_Prot_S_349-363	CoV_Prot_S_342-390	SVYAWNRKRISNCVA	5	DRB1_1101	DRB1_1301	DRB1_0401	DRB1_1302			
CoV_Prot_S_353-367	CoV_Prot_S_342-390	WNRKRISNCVADYSV	4	DRB1_0401	DRB1_1501	DRB1_1302				
CoV_Prot_S_369-383	CoV_Prot_S_342-390	YNSASFSTFKCYGVS	1	HLA-C02:02						
CoV_Prot_S_369-383	CoV_Prot_S_342-390	YNSASFSTFKCYGVS	3	DRB1_1501	DRB1_0701					
CoV_Prot_S_373-387	CoV_Prot_S_342-390	SFSTFKCYGVSPTKL	5	HLA-A24:02	HLA-A03:01					
CoV_Prot_S_373-387	CoV_Prot_S_342-390	SFSTFKCYGVSPTKL	2	DRB1_1501						
CoV_Prot_S_376-390	CoV_Prot_S_342-390	TFKCYGVSPTKLNDL	4	HLA-A24:02	HLA-A03:01					
CoV_Prot_S_376-390	CoV_Prot_S_342-390	TFKCYGVSPTKLNDL	2	DRB1_1501						
CoV_Prot_S_385-399	CoV_Prot_S_381-431	TKLNDLCFTNVYADS	1	DRB1_0701						
CoV_Prot_S_445-459	CoV_Prot_S_441-475	VGGNYNYLYRLFRKS	1	HLA-A23:01						
CoV_Prot_S_445-459	CoV_Prot_S_441-475	VGGNYNYLYRLFRKS	1	DRB1_0301						

15-mer peptide	ancestor peptide pool	peptide sequence	# reactive donors	predicted HLA restriction						
CoV_Prot_S_457-471	CoV_Prot_S_441-475	RKSNLKPFERDISTE	1	DRB1_0301						
CoV_Prot_S_457-471	CoV_Prot_S_441-475	RKSNLKPFERDISTE	1	DRB1_0301						
CoV_Prot_S_461-475	CoV_Prot_S_441-475	LKPFERDISTEIYQA	1	DRB1_0401						
CoV_Prot_S_509-523	CoV_Prot_S_494-531	RVVVLSFELLHAPAT	1	DRB1_0101						
CoV_Prot_S_553-567	CoV_Prot_S_521-567	TESNKKFLPFQQFGR	1	HLA-C07:01						
CoV_Prot_S_553-567	CoV_Prot_S_521-567	TESNKKFLPFQQFGR	1	DRB1_1302						
CoV_Prot_S_669-683	CoV_Prot_S_665-707	GICASYQTQTNSPRR	2	HLA-A11:01						
CoV_Prot_S_685-699	CoV_Prot_S_665-707	RSVASQSIIAYTMSL	1	HLA-A02:01						
CoV_Prot_S_698-712	CoV_Prot_S_698-747	SLGAENSVAYSNNSI	1	HLA-C14:02						
CoV_Prot_S_702-716	CoV_Prot_S_698-747	ENSVAYSNNSIAIPT	1	HLA-B55:01						
CoV_Prot_S_713-727	CoV_Prot_S_698-747	AIPTNFTISVTTEIL	1	HLA-B51:01						
CoV_Prot_S_719-733	CoV_Prot_S_698-747	TISVTTEILPVSMTK	1	HLA-A11:01						
CoV_Prot_S_722-736	CoV_Prot_S_698-747	VTTEILPVSMTKTSV	1	HLA-A11:01						
CoV_Prot_S_725-739	CoV_Prot_S_698-747	EILPVSMTKTSVDCT	1	HLA-A11:01						
CoV_Prot_S_753-765	CoV_Prot_S_737-779	LLQYGSFCTQLNR	1	DRB1_1501						
CoV_Prot_S_765-779	CoV_Prot_S_737-779	RALTGIAVEQDKNTQ	1	DRB1_1301						

15-mer peptide	ancestor peptide pool	peptide sequence	# reactive donors	predicted HLA restriction						
CoV_Prot_S_777-791	CoV_Prot_S_769-813	NTQEVFAQVKQIYKT	2	DRB1_1301	DRB1_1501					
CoV_Prot_S_781-795	CoV_Prot_S_769-813	VFAQVKQIYKTPPIK	1	DRB1_1501						
CoV_Prot_S_788-802	CoV_Prot_S_769-813	IYKTPPIKDFGGFNF	1	DRB1_1301						
CoV_Prot_S_799-813	CoV_Prot_S_769-813	GFNFSQILPDPSKPS	1	HLA-B15:01						
CoV_Prot_S_799-813	CoV_Prot_S_769-813	GFNFSQILPDPSKPS	1	DRB1_1301						
CoV_Prot_S_802-816	CoV_Prot_S_802-852	FSQILPDPSKPSKRS	8	DRB1_1501	DRB1_0401	DRB1_1501	DRB1_0301			
CoV_Prot_S_809-823	CoV_Prot_S_802-852	PSKPSKRSFIEDLLF	2	DRB1_1501						
CoV_Prot_S_813-827	CoV_Prot_S_802-852	SKRSFIEDLLFNKVT	1	HLA-C07:01						
CoV_Prot_S_813-827	CoV_Prot_S_802-852	SKRSFIEDLLFNKVT	8	DQA10102-DQB10501	DRB1_0401	DRB1_0101	DRB1_0301			
CoV_Prot_S_817-831	CoV_Prot_S_802-852	FIEDLLFNKVTLADA	2	DRB1_0801	DRB1_0401					
CoV_Prot_S_821-835	CoV_Prot_S_802-852	LLFNKVTLADAGFIK	1	HLA-B08:01						
CoV_Prot_S_821-835	CoV_Prot_S_802-852	LLFNKVTLADAGFIK	2	DRB1_0101	DRB1_0301					
CoV_Prot_S_825-839	CoV_Prot_S_802-852	KVTLADAGFIKQYGD	1	HLA-B18:01						
CoV_Prot_S_825-839	CoV_Prot_S_802-852	KVTLADAGFIKQYGD	1	DRB1_0801						
CoV_Prot_S_829-843	CoV_Prot_S_802-852	ADAGFIKQYGDCLGD	1	DRB1_0101						
CoV_Prot_S_838-852	CoV_Prot_S_802-852	GDCLGDIAARDLICA	1	HLA-C12:03						

15-mer peptide	ancestor peptide pool	peptide sequence	# reactive donors	predicted HLA restriction						
CoV_Prot_S_838-852	CoV_Prot_S_802-852	GDCLGDIAARDLICA	1	DRB1_0301						
CoV_Prot_S_844-858	CoV_Prot_S_841-891	IAARDLICAQKFNGL	1	HLA-C08:02						
CoV_Prot_S_865-879	CoV_Prot_S_841-891	LTDEMIAQYTSALLA	2	HLA-C08:02	HLA-A01:01					
CoV_Prot_S_865-879	CoV_Prot_S_841-891	LTDEMIAQYTSALLA	1	DRB1_1501						
CoV_Prot_S_869-883	CoV_Prot_S_841-891	MIAQYTSALLAGTIT	1	DRB1_1501						
CoV_Prot_S_873-887	CoV_Prot_S_841-891	YTSALLAGTITSGWT	1	DRB1_1302						
CoV_Prot_S_885-899	CoV_Prot_S_881-927	GWTFGAGAALQIPFA	1	HLA-C03:03						
CoV_Prot_S_885-899	CoV_Prot_S_881-927	GWTFGAGAALQIPFA	1	DRB1_0401						
CoV_Prot_S_889-902	CoV_Prot_S_881-927	GAGAALQIPFAMQM	1	HLA-B15:01						
CoV_Prot_S_892-906	CoV_Prot_S_881-927	AALQIPFAMQMAYRF	3	HLA-B56:01	HLA-B15:01	HLA-C03:03				
CoV_Prot_S_892-906	CoV_Prot_S_881-927	AALQIPFAMQMAYRF	1	DRB1_0101						
CoV_Prot_S_896-910	CoV_Prot_S_881-927	IPFAMQMAYRFNGIG	2	HLA-B56:01	HLA-C03:03					
CoV_Prot_S_896-910	CoV_Prot_S_881-927	IPFAMQMAYRFNGIG	1	DRB1_0101						
CoV_Prot_S_917-931	CoV_Prot_S_917-964	YENQKLIANQFNSAI	1	DRB1_1302						
CoV_Prot_S_921-935	CoV_Prot_S_917-964	KLIANQFNSAIGKIQ	1	DRB1_1302						
CoV_Prot_S_977-991	CoV_Prot_S_955-991	LNDILSRLDKVEAEV	1	HLA-B51:01						

15-mer peptide	ancestor peptide pool	peptide sequence	# reactive donors	predicted HLA restriction						
CoV_Prot_S_986-1000	CoV_Prot_S_981-1023	KVEAEVQIDRLITGR	1	HLA-B40:01						
CoV_Prot_S_990-1004	CoV_Prot_S_981-1023	EVQIDRLITGRLQSL	1	HLA-C03:04						
CoV_Prot_S_990-1004	CoV_Prot_S_981-1023	EVQIDRLITGRLQSL	1	DRB1_1501						
CoV_Prot_S_994-1008	CoV_Prot_S_981-1023	DRLITGRLQSLQTYV	2	HLA-C03:04	HLA-B27:05					
CoV_Prot_S_997-1011	CoV_Prot_S_981-1023	ITGRLQSLQTYVTQQ	2	HLA-C15:05	HLA-B27:05					
CoV_Prot_S_997-1011	CoV_Prot_S_981-1023	ITGRLQSLQTYVTQQ	1	DRB1_1501						
CoV_Prot_S_1000-1014	CoV_Prot_S_981-1023	RLQSLQTYVTQQLIR	1	DRB1_1501						
CoV_Prot_S_1055-1068	CoV_Prot_S_1051-1099	SAPHGVVFLHVTYV	1	DRB1_1201						
CoV_Prot_S_1056-1070	CoV_Prot_S_1051-1099	APHGVVFLHVTYVPA	2	DRB1_1201	DRB1_1501					
CoV_Prot_S_1097-1111	CoV_Prot_S_1089-1135	SNGTHWFVTQRNFYE	1	DRB1_0405						
CoV_Prot_S_1101-1115	CoV_Prot_S_1089-1135	HWFVTQRNFYEPQII	1	DRB1_0405						
CoV_Prot_S_1117-1131	CoV_Prot_S_1089-1135	TDNTFVSGNCDVVIG	1	HLA-C05:01						
CoV_Prot_S_1141-1155	CoV_Prot_S_1123-1166	LQPELDSFKEELDKY	1	DRB1_1601						
CoV_Prot_S_1149-1163	CoV_Prot_S_1123-1166	KEELDKYFKNHTSPD	1	HLA-B40:01						
CoV_Prot_S_1203-1215	CoV_Prot_S_1195-1230	LGKYEQYIKWPWY	1	HLA-B44:02						
CoV_Prot_S_1205-1219	CoV_Prot_S_1195-1230	KYEQYIKWPWYIWLG	2	HLA-B44:02	HLA-A23:01					

15-mer peptide	ancestor peptide pool	peptide sequence	# reactive donors	predicted HLA restriction						
CoV_Prot_S_1209-1223	CoV_Prot_S_1195-1230	YIKWPWYIWLGFIAG	2	HLA-A02:01	HLA-B35:01					
CoV_Prot_S_1214-1228	CoV_Prot_S_1195-1230	WYIWLGFIAGLIAIV	1	HLA-A02:01						
CoV_Prot_S_1215-1225	CoV_Prot_S_1195-1230	YIWLGFIAGLI	1	HLA-A02:01						
CoV_Prot_S_1217-1231	CoV_Prot_S_1195-1230	WLGFIAGLIAIVMVT	1	HLA-A02:01						
CoV_Prot_S_1218-1228	CoV_Prot_S_1195-1230	LGFIAGLIAIV	1	HLA-A02:01						
CoV_Prot_S_1220-1230	CoV_Prot_S_1195-1230	FIAGLIAIVMV	1	HLA-A02:01						
CoV_Prot_Nuc_37-51	CoV_Prot_Nuc_1-51	SKQRRPQGLPNNTAS	1	DRB1_1501						
CoV_Prot_Nuc_49-61	CoV_Prot_Nuc_40-87	TASWFTALTQHGK	1	DQA10301-DQB10201						
CoV_Prot_Nuc_73-87	CoV_Prot_Nuc_40-87	PINTNSSPDDQIGYY	1	DQA10501-DQB10201						
CoV_Prot_N_102-116	CoV_Prot_Nuc_78-127	KDLSPRWYFYYLGTG	1	HLA-B07:02						
CoV_Prot_N_105-119	CoV_Prot_Nuc_78-127	SPRWYFYYLGTGPEA	1	HLA-B07:02						
CoV_Prot_Nuc_339-353	CoV_Prot_Nuc_339-387	LDDKDPNFKDQVILL	1	DQA10201-DQB10201						
CoV_Prot_Nuc_341-355	CoV_Prot_Nuc_339-387	DKDPNFKDQVILLNK	2	DRB1_0408	DQA10201-DQB10201					
CoV_Prot_N_360-374	CoV_Prot_Nuc_339-387	IDAYKTFPPTEPKKD	1	HLA-A30:01						
CoV_Prot_N_405-419	CoV_Prot_Nuc_377-419	KQLQQSMSSADSTQA	1	HLA-A01:01						
CoV_Prot_M_9-23	CoV_Prot_M_1-47	TVEELKKLLEQWNLV	1	HLA-C01:02						

15-mer peptide	ancestor peptide pool	peptide sequence	# reactive donors	predicted HLA restriction						
CoV_Prot_M_9-23	CoV_Prot_M_1-47	TVEELKKLLEQWNLV	1	DRB1_1101						
CoV_Prot_M_12-26	CoV_Prot_M_1-47	ELKKLLEQWNLVIGF	2	HLA-A02:01	HLA-A25:01					
CoV_Prot_M_21-31	CoV_Prot_M_1-47	NLVIGFLFLTW	1	HLA-C01:02						
CoV_Prot_M_21-31	CoV_Prot_M_1-47	NLVIGFLFLTW	1	DQA10101-DQB10501						
CoV_Prot_M_27-37	CoV_Prot_M_1-47	LFLTWICLLQF	1	HLA-C02:02						
CoV_Prot_M_27-37	CoV_Prot_M_1-47	LFLTWICLLQF	1	DQA10101-DQB10501						
CoV_Prot_M_42-56	CoV_Prot_M_37-73	RNRFLYIIKLIFLWL	1	HLA-A23:01						
CoV_Prot_M_47-57	CoV_Prot_M_37-73	YIIKLIFLWLL	1	DRB1_1101						
CoV_Prot_M_60-70	CoV_Prot_M_37-73	VTLACFVLAAV	1	HLA-A02:01						
CoV_Prot_M_137-151	CoV_Prot_M_135-183	ELVIGAVILRGHLRI	2	HLA-A68:01	HLA-A03:01					
CoV_Prot_M_144-158	CoV_Prot_M_135-183	ILRGHLRIAGHHLGR	1	HLA-B08:01						
CoV_Prot_M_149-163	CoV_Prot_M_135-183	LRIAGHHLGRCDIKD	1	HLA-A03:01						
CoV_Prot_M_149-163	CoV_Prot_M_135-183	LRIAGHHLGRCDIKD	3	DRB1_1301	DQA10201-DQB10303					
CoV_Prot_M_157-171	CoV_Prot_M_135-183	GRCDIKDLPKEITVA	2	DRB1_0405						
CoV_Prot_M_165-179	CoV_Prot_M_135-183	PKEITVATSRTLSYY	1	HLA-C02:02						
CoV_Prot_M_169-183	CoV_Prot_M_173-222	TVATSRTLSYYKLGA	1	DQA10201-DQB10302						

15-mer peptide	ancestor peptide pool	peptide sequence	# reactive donors	predicted HLA restriction						
CoV_Prot_M_173-187	CoV_Prot_M_173-222	SRTLSYYKLGASQRV	5	DRB1_1501	DRB1_0701	DQA10301-DQB10301				
CoV_Prot_M_177-191	CoV_Prot_M_173-222	SYYKLGASQRVAGDS	4	DRB1_0701	DQA10301-DQB10301					
CoV_Prot_M_193-207	CoV_Prot_M_173-222	FAAYSRYRIGNYKLN	3	HLA-C02:02	HLA-C14:02	HLA-A30:01				
CoV_Prot_M_197-211	CoV_Prot_M_173-222	SRYRIGNYKLNTDHS	1	HLA-A30:01						
CoV_Prot_M_197-211	CoV_Prot_M_173-222	SRYRIGNYKLNTDHS	1	DRB1_1501						
CoV_Prot_M_201-215	CoV_Prot_M_173-222	IGNYKLNTDHSSSSD	3	DRB1_0405	DRB1_0408	DRB1_0401				
CoV_Prot_M_208-222	CoV_Prot_M_173-222	TDHSSSSDNIALLVQ	1	HLA-A01:01						
CoV_Prot_M_208-222	CoV_Prot_M_173-222	TDHSSSSDNIALLVQ	1	DRB1_0401						

Supplementary Table 4. **15-mer peptides with predicted immunogenic capacity.** Rows refer to individual 15-mer peptides derived from the SARS-CoV-2 Spike (S), Nucleocapsid (N) or Membrane (M) protein (1st column), as well as their ancestor peptide pools (2nd column) and the specific peptide sequence (3rd column). Likewise, the likely HLA restriction of the peptides, that were predicted by NetMHCpan given the HLA allotypes by reactive donors, are listed (4th column).

15-mer peptide	ancestor peptide pool	peptide sequence	predicted HLA restriction							
CoV_Prot_S_13-27	CoV_Prot_S_1-51	SQCVNLTTRTQLPPA	DRB1_1401							
CoV_Prot_S_18-32	CoV_Prot_S_1-51	LTTRTQLPPAYTNSF	HLA-C07:02	HLA-B35:03	HLA-C07:01					
CoV_Prot_S_21-35	CoV_Prot_S_1-51	RTQLPPAYTNSFTRG	HLA-B35:03							
CoV_Prot_S_24-38	CoV_Prot_S_1-51	LPPAYTNSFTRGVYY	HLA-B35:03	HLA-C12:03	HLA-A29:02	HLA-C15:02				
CoV_Prot_S_29-43	CoV_Prot_S_1-51	TNSFTRGVYYPDKVF	HLA-C12:03	HLA-A29:02						
CoV_Prot_S_33-47	CoV_Prot_S_1-51	TRGVYYPDKVFRSSV	HLA-A31:01	DRB1_0101	DRB1_1302	DRB1_1101	DRB1_0301			
CoV_Prot_S_37-51	CoV_Prot_S_1-51	YYPDKVFRSSVLHST	HLA-B14:01	DRB1_1501						
CoV_Prot_S_41-55	CoV_Prot_S_41-91	KVFRSSVLHSTQDLF	HLA-A03:01							
CoV_Prot_S_44-58	CoV_Prot_S_41-91	PFFSNVTWFHAIHVS	DRB1_1501							
CoV_Prot_S_65-79	CoV_Prot_S_41-91	FHAIHVSGTNGTKRF	DRB1_1302							
CoV_Prot_S_72-86	CoV_Prot_S_41-91	GTNGTKRFDNPVLPF	HLA-C04:01	HLA-C07:02						

15-mer peptide	ancestor peptide pool	peptide sequence	predicted HLA restriction							
CoV_Prot_S_77-91	CoV_Prot_S_41-91	KRFDNPVLPFNDGVY	HLA-C04:01	HLA-C07:02						
CoV_Prot_S_81-95	CoV_Prot_S_81-130	NPVLPFNDGVYFAST	HLA-B35:03	DRB1_1501						
CoV_Prot_S_85-99	CoV_Prot_S_81-130	PFNDGVYFASTEKSN	HLA-A03:01	HLA-DQA10401-DQB10601	HLA-DQA10401-DQB10402	HLA-DQA10103-DQB10603	DRB1_0404			
CoV_Prot_S_89-103	CoV_Prot_S_81-130	GVYFASTEKSNIIRG	HLA-A03:01							
CoV_Prot_S_93-107	CoV_Prot_S_81-130	ASTEKSNIIRGWIFG	HLA-C15:02							
CoV_Prot_S_105-119	CoV_Prot_S_81-130	IFGTTLDSKTQSLLI	HLA-A02:01	HLA-C07:04	HLA-C04:01	HLA-B08:01	DRB1_0301			
CoV_Prot_S_109-123	CoV_Prot_S_81-130	TLDSKTQSLLIVNNA	HLA-A02:01	HLA-C07:04	HLA-C04:01	HLA-B08:01				
CoV_Prot_S_121-135	CoV_Prot_S_121-175	NNATNVVIKVCEFQF	HLA-C12:03	HLA-C12:03	HLA-B51:01					
CoV_Prot_S_138-152	CoV_Prot_S_121-175	DPFLGVYYHKNNKSW	HLA-A03:01	HLA-A24:02	HLA-DQA10103-DQB10402	DRB1_1301				
CoV_Prot_S_150-164	CoV_Prot_S_121-175	KSWMESEFRVYSSAN	HLA-B50:01	DRB1_0301	DRB1_1101					
CoV_Prot_S_154-168	CoV_Prot_S_121-175	ESEFRVYSSANNCTF	HLA-B50:01	DRB1_1501	DRB1_0404					
CoV_Prot_S_157-171	CoV_Prot_S_121-175	FRVYSSANNCTFEYV	HLA-C16:01	HLA-A01:01						

15-mer peptide	ancestor peptide pool	peptide sequence	predicted HLA restriction							
CoV_Prot_S_161-175	CoV_Prot_S_121-175	SSANNCTFEYVSQPF	HLA-A01:01							
CoV_Prot_S_165-179	CoV_Prot_S_165-216	NCTFEYVSQPFLMDL	HLA-C07:02							
CoV_Prot_S_181-195	CoV_Prot_S_165-216	GKQGNFKNLREFVFK	DRB1_1201							
CoV_Prot_S_198-212	CoV_Prot_S_165-216	DGYFKIYSKHTPINL	HLA-C03:03	HLA-C07:04	DRB1_0801	HLA-DQA10301-DQB10503	DRB1_1101			
CoV_Prot_S_202-216	CoV_Prot_S_165-216	KIYSKHTPINLVRDL	HLA-B07:02	HLA-C03:03	HLA-C07:04					
CoV_Prot_S_205-219	CoV_Prot_S_205-255	SKHTPINLVRDLPQG	HLA-DQA10103-DQB10603	HLA-DQA10101-DQB10603	HLA-DQA10101-DQB10301	HLA-DQA10101-DQB10501				
CoV_Prot_S_217-231	CoV_Prot_S_205-255	PQGFSALEPLVDLPI	HLA-C03:03							
CoV_Prot_S_221-235	CoV_Prot_S_205-255	SALEPLVDLPIGINI	HLA-C03:03							
CoV_Prot_S_233-247	CoV_Prot_S_205-255	INITRFQTLLALHRS	HLA-C07:01							
CoV_Prot_S_236-250	CoV_Prot_S_205-255	TRFQTLLALHRSYLT	HLA-C07:01							
CoV_Prot_S_245-259	CoV_Prot_S_245-295	HRSYLTPGDSSSGWT	HLA-A02:01							
CoV_Prot_S_249-263	CoV_Prot_S_245-295	LTPGDSSSGWTAGAA	HLA-C12:03							

15-mer peptide	ancestor peptide pool	peptide sequence	predicted HLA restriction							
CoV_Prot_S_253-267	CoV_Prot_S_245-295	DSSSGWTAGAAAYYV	HLA-DQA10501-DQB10301							
CoV_Prot_S_257-271	CoV_Prot_S_245-295	GWTAGAAAYYVGYLQ	HLA-DQA10501-DQB10301							
CoV_Prot_S_265-279	CoV_Prot_S_245-295	YYVGYLQPRTFLLKY	HLA-A02:01							
CoV_Prot_S_269-283	CoV_Prot_S_245-295	YLQPRTFLLKYNENG	HLA-A02:01							
CoV_Prot_S_273-287	CoV_Prot_S_245-295	RTFLLKYNENGTITD	DRB1_0301							
CoV_Prot_S_302-316	CoV_Prot_S_285-327	TLKSFTVEKGIYQTS	DRB1_1101							
CoV_Prot_S_322-335	CoV_Prot_S_313-351	PTESIVRFPNITNL	HLA-C07:02							
CoV_Prot_S_323-335	CoV_Prot_S_313-351	TESIVRFPNITNL	HLA-C07:02							
CoV_Prot_S_324-338	CoV_Prot_S_313-351	ESIVRFPNITNLCPF	HLA-C07:02							
CoV_Prot_S_326-338	CoV_Prot_S_313-351	IVRFPNITNLCPF	HLA-C07:02							
CoV_Prot_S_342-356	CoV_Prot_S_342-390	FNATRFASVYAWNRK	HLA-C07:01	HLA-B27:05	HLA-DQA10401-DQB10402	HLA-DQA10103-DQB10402				
CoV_Prot_S_345-359	CoV_Prot_S_342-390	TRFASVYAWNRKRIS	HLA-A03:01	HLA-A74:03	DRB1_1301					

15-mer peptide	ancestor peptide pool	peptide sequence	predicted HLA restriction							
CoV_Prot_S_349-363	CoV_Prot_S_342-390	SVYAWNRKRISNCVA	HLA-A03:01	HLA-A74:03						
CoV_Prot_S_357-371	CoV_Prot_S_342-390	RISNCVADYSVLYNS	HLA-A01:01							
CoV_Prot_S_362-376	CoV_Prot_S_313-351	VADYSVLYNSASFST	DRB1_0401	DRB1_0101	DRB1_1101					
CoV_Prot_S_364-378	CoV_Prot_S_342-390	DYSVLYNSASFSTFK	HLA-A11:01	DRB1_1302						
CoV_Prot_S_369-383	CoV_Prot_S_342-390	YNSASFSTFKCYGVS	HLA-A11:01	DRB1_1501						
CoV_Prot_S_373-387	CoV_Prot_S_342-390	SFSTFKCYGVSPTKL	HLA-A03:01							
CoV_Prot_S_376-390	CoV_Prot_S_342-390	TFKCYGVSPTKLNDL	HLA-A03:01							
CoV_Prot_S_397-411	CoV_Prot_S_381-431	ADSFVIRGDEVRQIA	HLA-C06:02							
CoV_Prot_S_401-415	CoV_Prot_S_381-431	VIRGDEVRQIAPGQT	HLA-C06:02							
CoV_Prot_S_405-419	CoV_Prot_S_381-431	DEVRQIAPGQTGKIA	HLA-A03:01							
CoV_Prot_S_413-427	CoV_Prot_S_381-431	GQTGKIADYNYKLPD	HLA-A02:01							
CoV_Prot_S_417-431	CoV_Prot_S_381-431	KIADYNYKLPDDFTG	HLA-A02:01							
CoV_Prot_S_430-444	CoV_Prot_S_421-455	TGCVIAWNSNNLDSK	HLA-DQA10103-DQB10501	HLA-DQA10101-DQB10501	DRB1_1501					
CoV_Prot_S_438-452	CoV_Prot_S_421-455	SNNLDSKVGGNYNYL	HLA-C07:02							

15-mer peptide	ancestor peptide pool	peptide sequence	predicted HLA restriction							
CoV_Prot_S_441-455	CoV_Prot_S_421-455	LDSKVGGNYNYLYRL	HLA-C07:02							
CoV_Prot_S_445-459	CoV_Prot_S_441-475	VGGNYNYLYRLFRKS	DRB1_1101							
CoV_Prot_S_453-467	CoV_Prot_S_441-475	YRLFRKSNLKPFERD	HLA-A31:01							
CoV_Prot_S_461-475	CoV_Prot_S_441-475	LKPFERDISTEIYQA	HLA-B52:01	HLA-B50:01	DRB1_0101	HLA-B52:01	HLA-B56:01			
CoV_Prot_S_464-478	CoV_Prot_S_461-508	FERDISTEIYQAGST	HLA-B52:01							
CoV_Prot_S_486-500	CoV_Prot_S_461-508	FNCYFPLQSYGFQPT	HLA-C07:02							
CoV_Prot_S_489-503	CoV_Prot_S_461-508	YFPLQSYGFQPTNGV	HLA-C07:02							
CoV_Prot_S_494-508	CoV_Prot_S_461-508	SYGFQPTNGVGYQPY	HLA-B15:01	DRB1_1302						
CoV_Prot_S_500-513	CoV_Prot_S_494-531	TNGVGYQPYRVVVL	HLA-C01:02							
CoV_Prot_S_501-515	CoV_Prot_S_494-531	NGVGYQPYRVVVLSF	HLA-C01:02							
CoV_Prot_S_502-515	CoV_Prot_S_494-531	GVGYQPYRVVVLSF	HLA-C01:02							
CoV_Prot_S_505-519	CoV_Prot_S_494-531	YQPYRVVVLSFELLH	HLA-B52:01	HLA-C01:02	HLA-C01:02	HLA-B08:01				
CoV_Prot_S_521-535	CoV_Prot_S_521-567	PATVCGPKKSTNLVK	HLA-C01:02							
CoV_Prot_S_526-539	CoV_Prot_S_521-567	GPKKSTNLVKNKCV	HLA-A03:01							

15-mer peptide	ancestor peptide pool	peptide sequence	predicted HLA restriction							
CoV_Prot_S_529-543	CoV_Prot_S_521-567	KSTNLVKNKCVNFNF	HLA-A03:01	DRB1_1302						
CoV_Prot_S_541-555	CoV_Prot_S_521-567	FNFNGLTGTGVLTES	DRB1_0101							
CoV_Prot_S_543-557	CoV_Prot_S_521-567	FNGLTGTGVLTESNK	HLA-DQA10103-DQB10601							
CoV_Prot_S_553-567	CoV_Prot_S_521-567	TESNKKFLPFQQFGR	DRB1_1501							
CoV_Prot_S_557-571	CoV_Prot_S_557-607	KKFLPFQQFGRDIAD	DRB1_1501							
CoV_Prot_S_573-587	CoV_Prot_S_557-607	TDAVRDPQTLEILDI	HLA-C07:02							
CoV_Prot_S_581-595	CoV_Prot_S_557-607	TLEILDITPCSFGGV	HLA-C05:01							
CoV_Prot_S_621-635	CoV_Prot_S_597-635	PVAIHADQLTPTWRV	DRB1_0301							
CoV_Prot_S_656-670	CoV_Prot_S_597-635	VNNSYECDIPIGAGI	HLA-B50:01	DRB1_0301	DRB1_0401					
CoV_Prot_S_660-674	CoV_Prot_S_597-635	YECDIPIGAGICASY	HLA-B50:01	HLA-B56:01						
CoV_Prot_S_673-687	CoV_Prot_S_665-707	SYQTQTNSPRRARSV	HLA-A68:01							
CoV_Prot_S_678-692	CoV_Prot_S_625-674	TNSPRRARSVASQSI	HLA-B07:02	HLA-B07:02	HLA-B56:01					
CoV_Prot_S_683-696	CoV_Prot_S_625-674	RARSVASQSIIAYT	HLA-C12:02	HLA-C12:03	DRB1_0301					
CoV_Prot_S_685-699	CoV_Prot_S_625-674	RSVASQSIIAYTMSL	HLA-C12:02	HLA-C12:03						

15-mer peptide	ancestor peptide pool	peptide sequence	predicted HLA restriction							
CoV_Prot_S_689-703	CoV_Prot_S_665-707	SQSIIAYTMSLGAEN	HLA-DQA10102-DQB10503							
CoV_Prot_S_702-716	CoV_Prot_S_698-747	ENSVAYSNNSIAIPT	HLA-DQA10103-DQB10402	HLA-DQA10103-DQB10601	HLA-DQA10102-DQB10503	DRB1_1501				
CoV_Prot_S_706-720	CoV_Prot_S_698-747	AYSNNSIAIPTNFTI	HLA-B52:01							
CoV_Prot_S_709-723	CoV_Prot_S_698-747	NNSIAIPTNFTISVT	HLA-B52:01	HLA-B55:01	HLA-B51:01					
CoV_Prot_S_713-727	CoV_Prot_S_698-747	AIPTNFTISVTTEIL	HLA-C05:01	HLA-B51:01						
CoV_Prot_S_719-733	CoV_Prot_S_698-747	TISVTTEILPVSMTK	HLA-A03:01	HLA-DQA10501-DQB10201						
CoV_Prot_S_722-736	CoV_Prot_S_698-747	VTTEILPVSMTKTSV	HLA-A03:01							
CoV_Prot_S_725-739	CoV_Prot_S_698-747	EILPVSMTKTSVDCT	HLA-A03:01							
CoV_Prot_S_745-759	CoV_Prot_S_737-779	DSTECSNLLLQYGSF	HLA-C05:01							
CoV_Prot_S_749-763	CoV_Prot_S_737-779	CSNLLLQYGSFCTQL	HLA-C14:02	DRB1_1501						
CoV_Prot_S_753-765	CoV_Prot_S_737-779	LLQYGSFCTQLNR	HLA-A11:01	HLA-C14:02						
CoV_Prot_S_756-767	CoV_Prot_S_737-779	YGSFCTQLNRAL	HLA-A11:01							

15-mer peptide	ancestor peptide pool	peptide sequence	predicted HLA restriction							
CoV_Prot_S_757-770	CoV_Prot_S_737-779	GSFCTQLNRALTGI	HLA-A11:01							
CoV_Prot_S_765-779	CoV_Prot_S_737-779	RALTGIAVEQDKNTQ	HLA-DQA10401-DQB10402	HLA-DQA10501-DQB10201	HLA-DQA10102-DQB10602	HLA-DQA10501-DQB10602				
CoV_Prot_S_769-783	CoV_Prot_S_769-813	GIAVEQDKNTQEVFA	HLA-B38:01	DRB1_0301						
CoV_Prot_S_773-787	CoV_Prot_S_769-813	EQDKNTQEVFAQVKQ	HLA-B38:01							
CoV_Prot_S_777-791	CoV_Prot_S_769-813	NTQEVFAQVKQIYKT	HLA-A29:01	HLA-C14:02	DRB1_1401					
CoV_Prot_S_781-795	CoV_Prot_S_769-813	VFAQVKQIYKTPPIK	HLA-A11:01	HLA-A03:01	HLA-C14:02					
CoV_Prot_S_785-799	CoV_Prot_S_769-813	VKQIYKTPPIKDFGG	HLA-A11:01	HLA-A03:01	HLA-C07:01					
CoV_Prot_S_788-802	CoV_Prot_S_769-813	IYKTPPIKDFGGFNF	HLA-C07:01							
CoV_Prot_S_792-806	CoV_Prot_S_769-813	PPIKDFGGFNFSQIL	DRB1_1501							
CoV_Prot_S_796-810	CoV_Prot_S_769-813	DFGGFNFSQILPDPS	HLA-DQA10401-DQB10402							
CoV_Prot_S_802-816	CoV_Prot_S_802-852	FSQILPDPSKPSKRS	HLA-DQA10301-DQB10503	DRB1_1302	DRB1_0401	DRB1_1301	DRB1_1601			
CoV_Prot_S_817-831	CoV_Prot_S_802-852	FIEDLLFNKVTLADA	HLA-A02:01	HLA-B08:01						

15-mer peptide	ancestor peptide pool	peptide sequence	predicted HLA restriction							
CoV_Prot_S_821-835	CoV_Prot_S_802-852	LLFNKVTLADAGFIK	HLA-A02:01							
CoV_Prot_S_825-839	CoV_Prot_S_802-852	KVTLADAGFIKQYGD	HLA-B44:02							
CoV_Prot_S_829-843	CoV_Prot_S_802-852	ADAGFIKQYGDCLGD	HLA-B44:02	HLA-DQA10103-DQB10501	DRB1_1501					
CoV_Prot_S_841-855	CoV_Prot_S_841-891	LGDIAARDLICAQKF	HLA-C05:01							
CoV_Prot_S_847-861	CoV_Prot_S_841-891	RDLICAQKFNGLTVL	HLA-B14:02							
CoV_Prot_S_852-866	CoV_Prot_S_841-891	AQKFNGLTVLPPLLT	HLA-B14:02							
CoV_Prot_S_860-874	CoV_Prot_S_841-891	VLPPLLTDEMIAQYT	DRB1_0301							
CoV_Prot_S_865-879	CoV_Prot_S_841-891	LTDEMIAQYTSALLA	HLA-B50:01	HLA-C03:04	HLA-DQA10101-DQB10501	DRB1_1501				
CoV_Prot_S_869-883	CoV_Prot_S_841-891	MIAQYTSALLAGTIT	HLA-B08:01	HLA-B50:01	HLA-C03:04	HLA-DQA10401-DQB10601	HLA-DQA10102-DQB10602			
CoV_Prot_S_881-895	CoV_Prot_S_881-927	TITSGWTFGAGAALQ	HLA-C03:04	HLA-C03:03						
CoV_Prot_S_885-899	CoV_Prot_S_881-927	GWTFGAGAALQIPFA	HLA-C03:04	HLA-C03:03	HLA-DQA10501-DQB10301	DRB1_0101				
CoV_Prot_S_889-902	CoV_Prot_S_881-927	GAGAALQIPFAMQM	HLA-B52:01							

15-mer peptide	ancestor peptide pool	peptide sequence	predicted HLA restriction							
CoV_Prot_S_892-906	CoV_Prot_S_881-927	AALQIPFAMQMAYRF	HLA-B52:01							
CoV_Prot_S_896-910	CoV_Prot_S_881-927	IPFAMQMAYRFNGIG	DRB1_1101							
CoV_Prot_S_902-915	CoV_Prot_S_881-927	MAYRFNGIGVTQNV	HLA-B39:06							
CoV_Prot_S_904-918	CoV_Prot_S_881-927	YRFNGIGVTQNVLYE	HLA-B39:06							
CoV_Prot_S_912-923	CoV_Prot_S_881-927	TQNVLYENQKLI	HLA-A02:01	DRB1_1501						
CoV_Prot_S_915-927	CoV_Prot_S_881-927	VLYENQKLIANQF	HLA-A02:01	HLA-B15:01						
CoV_Prot_S_933-947	CoV_Prot_S_917-964	KIQDSLSSTASALGK	HLA-A11:01							
CoV_Prot_S_937-951	CoV_Prot_S_917-964	SLSSTASALGKLQDV	HLA-A11:01							
CoV_Prot_S_945-959	CoV_Prot_S_917-964	LGKLQDVVNQNAQAL	HLA-C08:02	HLA-C03:04						
CoV_Prot_S_948-962	CoV_Prot_S_917-964	LQDVVNQNAQALNTL	HLA-C08:02	HLA-C03:04	DRB1_0301	DRB1_1302				
CoV_Prot_S_959-973	CoV_Prot_S_955-991	LNTLVKQLSSNFGAI	DRB1_1501							
CoV_Prot_S_963-976	CoV_Prot_S_955-991	VKQLSSNFGAISSV	HLA-C15:02							
CoV_Prot_S_967-981	CoV_Prot_S_955-991	SSNFGAISSVLNDIL	HLA-DQA10501-DQB10201							
CoV_Prot_S_972-984	CoV_Prot_S_955-991	AISSVLNDILSRL	HLA-A11:01	HLA-A02:01						

15-mer peptide	ancestor peptide pool	peptide sequence	predicted HLA restriction							
CoV_Prot_S_975-987	CoV_Prot_S_955-991	SVLNDILSRLDKV	HLA-A11:01	HLA-A02:01						
CoV_Prot_S_981-995	CoV_Prot_S_981-1023	LSRLDKVEAEVQIDR	HLA-A02:01							
CoV_Prot_S_986-1000	CoV_Prot_S_981-1023	KVEAEVQIDRLITGR	DRB1_0301							
CoV_Prot_S_994-1008	CoV_Prot_S_981-1023	DRLITGRLQSLQTYV	HLA-C07:02							
CoV_Prot_S_997-1011	CoV_Prot_S_981-1023	ITGRLQSLQTYVTQQ	HLA-C07:02							
CoV_Prot_S_1000-1014	CoV_Prot_S_981-1023	RLQSLQTYVTQQLIR	HLA-B52:01							
CoV_Prot_S_1004-1018	CoV_Prot_S_981-1023	LQTYVTQQLIRAAEI	HLA-B52:01							
CoV_Prot_S_1009-1023	CoV_Prot_S_981-1023	TQQLIRAAEIRASAN	HLA-DQA10103-DQB10603	HLA-DQA10101-DQB10603	HLA-DQA10102-DQB10602	HLA-DQA10301-DQB10602	HLA-DQA10102-DQB10503	HLA-DQA10301-DQB10503		
CoV_Prot_S_1012-1026	CoV_Prot_S_1012-1059	LIRAAEIRASANLAA	HLA-B39:06	HLA-DQA10102-DQB10602						
CoV_Prot_S_1014-1028	CoV_Prot_S_1012-1059	RAAEIRASANLAATK	HLA-B39:06	HLA-DQA10301-DQB10602	HLA-DQA10102-DQB10503	HLA-DQA10301-DQB10503	DRB1_1501	IRASANLAA	DRB1_0404	
CoV_Prot_S_1045-1059	CoV_Prot_S_1012-1059	KGYHLMSFPQSAPHG	HLA-A02:01							
CoV_Prot_S_1061-1075	CoV_Prot_S_1051-1099	VFLHVTYVPAQEKNF	HLA-A11:01	HLA-A03:01						

15-mer peptide	ancestor peptide pool	peptide sequence	predicted HLA restriction							
CoV_Prot_S_1066-1080	CoV_Prot_S_1051-1099	TYVPAQEKNFTTAPA	HLA-B45:01							
CoV_Prot_S_1069-1083	CoV_Prot_S_1051-1099	PAQEKNFTTAPAICH	HLA-B45:01							
CoV_Prot_S_1073-1087	CoV_Prot_S_1051-1099	KNFTTAPAICHDGKA	HLA-DQA10103-DQB10601							
CoV_Prot_S_1077-1091	CoV_Prot_S_1051-1099	TAPAICHDGKAHFPR	DRB1_0301	DRB1_1401						
CoV_Prot_S_1093-1107	CoV_Prot_S_1089-1135	GVFVSNGTHWFVTQR	HLA-A11:01	HLA-A03:01						
CoV_Prot_S_1097-1111	CoV_Prot_S_1089-1135	SNGTHWFVTQRNFYE	HLA-A11:01	HLA-A03:01	DRB1_0301	HLA-DQA10102-DQB10503				
CoV_Prot_S_1131-1145	CoV_Prot_S_1123-1166	GIVNNTVYDPLQPEL	HLA-C04:01	HLA-C05:01	HLA-C06:02	HLA-C01:02				
CoV_Prot_S_1136-1149	CoV_Prot_S_1123-1166	TVYDPLQPELDSFK	HLA-C04:01	HLA-C05:01	HLA-C06:02	HLA-C01:02				
CoV_Prot_S_1167-1181	CoV_Prot_S_1157-1205	GDISGINASVVNIQK	HLA-DQA10401-DQB10601	HLA-DQA10103-DQB10601	HLA-DQA10501-DQB10301					
CoV_Prot_S_1171-1185	CoV_Prot_S_1157-1205	GINASVVNIQKEIDR	DRB1_0801							
CoV_Prot_S_1175-1189	CoV_Prot_S_1157-1205	SVVNIQKEIDRLNEV	HLA-B40:01							
CoV_Prot_S_1179-1193	CoV_Prot_S_1157-1205	IQKEIDRLNEVAKNL	HLA-B40:01							

15-mer peptide	ancestor peptide pool	peptide sequence	predicted HLA restriction							
CoV_Prot_S_1181-1195	CoV_Prot_S_1157-1205	KEIDRLNEVAKNLNE	HLA-B40:01							
CoV_Prot_S_1186-1200	CoV_Prot_S_1157-1205	LNEVAKNLNESLIDL	HLA-C12:02							
CoV_Prot_S_1189-1203	CoV_Prot_S_1157-1205	VAKNLNESLIDLQEL	HLA-C12:02							
CoV_Prot_S_1197-1211	CoV_Prot_S_1195-1230	LIDLQELGKYEQYIK	HLA-B44:02	HLA-B18:01	DRB1_0801	DRB1_0401				
CoV_Prot_S_1217-1231	CoV_Prot_S_1195-1230	WLGFIAGLIAIVMVT	HLA-DQA10501-DQB10301							
CoV_Prot_S_1255-1268	CoV_Prot_S_1222-1273	KFDEDDSEPVLKGV	HLA-B38:01	DRB1_0401						
CoV_Prot_S_1257-1271	CoV_Prot_S_1222-1273	DEDDSEPVLKGVKLH	HLA-B35:03							
CoV_Prot_S_1259-1273	CoV_Prot_S_1222-1273	DDSEPVLKGVKLHYT	HLA-C02:02	HLA-B15:01	HLA-B35:03	HLA-DQA10103-DQB10601				
CoV_Prot_Nuc_5-19	CoV_Prot_N_1-51	GPQNQRNAPRITFGG	HLA-DQA10102-DQB10602	HLA-B38:01						
CoV_Prot_Nuc_10-24	CoV_Prot_N_1-51	RNAPRITFGGPSDST	HLA-DQA10401-DQB10601							
CoV_Prot_Nuc_13-27	CoV_Prot_N_1-51	PRITFGGPSDSTGSN	HLA-DQA10401-DQB10601							

15-mer peptide	ancestor peptide pool	peptide sequence	predicted HLA restriction							
CoV_Prot_Nuc_37-51	CoV_Prot_N_1-51	SKQRRPQGLPNNTAS	HLA-B07:02							
CoV_Prot_Nuc_54-68	CoV_Prot_N_40-87	TALTQHGKEDLKFPR	HLA-B38:01							
CoV_Prot_Nuc_57-71	CoV_Prot_N_40-87	TQHGKEDLKFPRGQG	HLA-B38:01							
CoV_Prot_Nuc_78-92	CoV_Prot_N_78-127	SSPDDQIGYYRRATR	HLA-C04:01							
CoV_Prot_Nuc_81-95	CoV_Prot_N_78-127	DDQIGYYRRATRRIR	HLA-A24:02							
CoV_Prot_Nuc_85-99	CoV_Prot_N_78-127	GYYRRATRRIRGGDG	HLA-A24:02							
CoV_Prot_Nuc_113-127	CoV_Prot_N_78-127	LGTGPEAGLPYGANK	HLA-DQA10401-DQB10601							
CoV_Prot_Nuc_149-163	CoV_Prot_N_117-167	RNPANNAAIVLQLPQ	HLA-DQA10103-DQB10603							
CoV_Prot_Nuc_158-172	CoV_Prot_N_158-203	VLQLPQGTTLPKGFY	HLA-C07:02							
CoV_Prot_Nuc_197-211	CoV_Prot_N_194-234	STPGSSRGTSPARMA	HLA-DQA10101-DQB10603	HLA-DQA10101-DQB10301						
CoV_Prot_Nuc_217-230	CoV_Prot_N_194-234	AALALLLLDRLNQL	HLA-A02:01	DRB1_1101						

15-mer peptide	ancestor peptide pool	peptide sequence	predicted HLA restriction							
CoV_Prot_Nuc_220-234	CoV_Prot_N_194-234	ALLLLDRLNQLESKM	HLA-A02:01							
CoV_Prot_Nuc_243-256	CoV_Prot_N_224-274	GQTVTKKSAAEASK	HLA-DQA10103-DQB10402	HLA-DQA10501-DQB10301						
CoV_Prot_Nuc_253-267	CoV_Prot_N_224-274	EASKKPRQKRTATKA	HLA-B07:02							
CoV_Prot_Nuc_257-271	CoV_Prot_N_224-274	KPRQKRTATKAYNVT	HLA-B07:02							
CoV_Prot_Nuc_261-274	CoV_Prot_N_224-274	KRTATKAYNVTQAF	HLA-C03:03	HLA-C06:02						
CoV_Prot_Nuc_265-278	CoV_Prot_N_265-314	TKAYNVTQAFGRRG	HLA-C12:02							
CoV_Prot_Nuc_293-307	CoV_Prot_N_265-314	RQGTDYKHWPQIAQF	HLA-B38:01	HLA-C07:02						
CoV_Prot_Nuc_297-311	CoV_Prot_N_265-314	DYKHWPQIAQFAPSA	HLA-B38:01	HLA-C07:02						
CoV_Prot_Nuc_300-314	CoV_Prot_N_265-314	HWPQIAQFAPSASAF	HLA-DQA10103-DQB10402							

15-mer peptide	ancestor peptide pool	peptide sequence	predicted HLA restriction							
CoV_Prot_Nuc_318-331	CoV_Prot_N_305-347	SRIGMEVTPSGTWL	HLA-B44:03							
CoV_Prot_Nuc_321-335	CoV_Prot_N_305-347	GMEVTPSGTWLTYTG	HLA-B44:03							
CoV_Prot_Nuc_333-347	CoV_Prot_N_305-347	YTGAIKLDDKDPNFK	HLA-C04:01							
CoV_Prot_Nuc_357-371	CoV_Prot_N_339-387	YKTFPPTEPKKDKKK	HLA-A30:01							
CoV_Prot_Nuc_357-371	CoV_Prot_N_339-387	IDAYKTFPPTEPKKD	DRB1_0408	DRB1_0701						
CoV_Prot_M_1-15	CoV_Prot_M_1-47	MADSNGTITVEELKK	HLA-DQA10103-DQB10603							
CoV_Prot_M_9-23	CoV_Prot_M_1-47	TVEELKKLLEQWNLV	HLA-A02:01							
CoV_Prot_M_12-26	CoV_Prot_M_1-47	ELKKLLEQWNLVIGF	HLA-B52:01	HLA-A02:01						
CoV_Prot_M_14-29	CoV_Prot_M_1-47	KKLLEQWNLVIGFLFL	HLA-B52:01	HLA-A02:01						
CoV_Prot_M_34-47	CoV_Prot_M_1-47	LLQFAYANRNRFLY	HLA-C03:03	HLA-C12:03	HLA-C02:02	DRB1_1101				
CoV_Prot_M_37-51	CoV_Prot_M_37-73	FAYANRNRFLYIIKL	HLA-C12:02	HLA-C03:03						

15-mer peptide	ancestor peptide pool	peptide sequence	predicted HLA restriction							
CoV_Prot_M_39-53	CoV_Prot_M_37-73	YANRNRFLYIIKLIF	HLA-A29:01	HLA-DQA10101-DQB10501						
CoV_Prot_M_42-56	CoV_Prot_M_37-73	RNRFLYIIKLIFLWL	DRB1_1101	DRB1_0301						
CoV_Prot_M_65-76	CoV_Prot_M_65-105	FVLAAVYRINWI	HLA-A02:01							
CoV_Prot_M_72-85	CoV_Prot_M_65-105	RINWITGGIAIAMA	HLA-DQA10501-DQB10301	HLA-DQA10501-DQB10201						
CoV_Prot_M_89-103	CoV_Prot_M_65-105	GLMWLSYFIASFRLF	HLA-A23:01							
CoV_Prot_M_93-105	CoV_Prot_M_65-105	LSYFIASFRLFAR	HLA-A23:01							
CoV_Prot_M_97-111	CoV_Prot_M_97-147	IASFRLFARTRSMWS	DRB1_0801							
CoV_Prot_M_102-116	CoV_Prot_M_97-147	LFARTRSMWSFNPET	HLA-C07:01							
CoV_Prot_M_105-119	CoV_Prot_M_97-147	RTRSMWSFNPETNIL	HLA-C04:01							
CoV_Prot_M_110-124	CoV_Prot_M_97-147	WSFNPETNILLNVPL	HLA-C04:01	DRB1_0101						
CoV_Prot_M_117-131	CoV_Prot_M_97-147	NILLNVPLHGTILTR	HLA-C01:02							
CoV_Prot_M_120-134	CoV_Prot_M_97-147	LNVPLHGTILTRPLL	HLA-C01:02							
CoV_Prot_M_129-143	CoV_Prot_M_97-147	LTRPLLESELVIGAV	HLA-B45:01							

15-mer peptide	ancestor peptide pool	peptide sequence	predicted HLA restriction							
CoV_Prot_M_133-147	CoV_Prot_M_97-147	LLESELVIGAVILRG	HLA-B45:01	DRB1_0301						
CoV_Prot_M_135-148	CoV_Prot_M_135-183	ESELVIGAVILRGH	HLA-DQA10401-DQB10601	HLA-DQA10102-DQB10602						
CoV_Prot_M_165-179	CoV_Prot_M_135-183	PKEITVATSRTLSYY	HLA-C03:03	HLA-A01:01	HLA-DQA10103-DQB10402	DRB1_0101	DRB1_0701			
CoV_Prot_M_169-183	CoV_Prot_M_135-183	TVATSRTLSYYKLGA	HLA-C07:02	HLA-A01:01	HLA-C02:02					
CoV_Prot_M_173-187	CoV_Prot_M_173-222	SRTLSYYKLGASQRV	HLA-C07:02	HLA-C06:02						
CoV_Prot_M_177-191	CoV_Prot_M_173-222	SYYKLGASQRVAGDS	HLA-DQA10501-DQB10301	DRB1_0101						
CoV_Prot_M_201-215	CoV_Prot_M_173-222	IGNYKLNTDHSSSSD	HLA-DQA10103-DQB10402	HLA-DQA10101-DQB10603	HLA-DQA10103-DQB10603	HLA-DQA10102-DQB10201				
CoV_Prot_M_205-219	CoV_Prot_M_173-222	KLNTDHSSSSDNIAL	HLA-DQA10101-DQB10603							

Supplementary Table 5. Validation of core peptides' immunogenicity. Rows refer to individual 9-mer core peptides derived from *in vitro* and *in silico* derived analyzes of (potential) immunogenic 15-mer SARS-CoV-2 Spike, Nucleocapsid and Membrane specific proteins. Form left to right columns refer to the individual core peptide ID, the respective ancestor 15-mer peptide and pool, the predicted HLA restriction towards which the tests were performed, as well as the results of tests on PBMCs (6^{th} to 11^{th} column) and expanded cells (12^{th} to 17^{th} column).

core peptide ID	ancestor 15mer peptide	ancestor peptide pool	HLA-restric-tion	core peptide sequence	PBMC						expanded cells					
					#Tests total	#CD4$^+$/CD8$^+$ res-ponse	#CD4$^+$ res-ponse	#CD8$^+$ res-ponse	#total postive hits	total postive hits [%]	#Tests total	#CD4$^+$/CD8$^+$ res-ponse	#CD4$^+$ res-ponse	#CD8$^+$ res-ponse	#total postive hits	total postive hits [%]
DRB1_0101_P1	CoV_Prot_S_821-835	CoV_Prot_S_802-852	DRB1_0101	VTLADAGFI	1	0	0	1	1	1 / 1 (100)	1	0	0	0	0	0 / 1
DRB1_0101_P2	CoV_Prot_S_829-843	CoV_Prot_S_802-852	DRB1_0101	FIKQYGDCL	1	0	0	1	1	1 / 1 (100)	1	0	0	0	0	0 / 1
DRB1_0101_P3	CoV_Prot_S_896-910	CoV_Prot_S_881-927	DRB1_0101	FAMQMAYRF	1	0	0	1	1	1 / 1 (100)	1	0	0	0	0	0 / 1
DRB1_0101_P4	CoV_Prot_S_813-827	CoV_Prot_S_802-852	DRB1_0101	IEDLLFNKV	1	0	0	1	1	1 / 1 (100)	1	0	1	0	1	1 / 1 (100)
DRB1_0301_0401_P1	CoV_Prot_S_445-459	CoV_Prot_S_441-475	DRB1_0301	YNYLYRLFR	1	0	1	0	1	1 / 1 (100)	2	0	0	0	0	0 / 2
DRB1_0301_0401_P1	CoV_Prot_S_445-459	CoV_Prot_S_441-475	DRB1_0401	YNYLYRLFR	1	0	0	0	0	0 / 1	4	0	0	0	0	0 / 4
DRB1_0301_P1	CoV_Prot_S_457-471	CoV_Prot_S_441-475	DRB1_0301	LKPFERDIS	1	0	0	0	0	0 / 1	2	0	0	0	0	0 / 2
DRB1_0301_P2	CoV_Prot_S_765-779	CoV_Prot_S_737-779	DRB1_0301	LTGIAVEQD	2	0	0	0	0	0 / 2	3	0	1	0	1	1 / 3 (33,33)
DRB1_0401_0701_P1	CoV_Prot_M_201-215	CoV_Prot_M_173-222	DRB1_0401	YKLNTDHSS	1	0	0	0	0	0 / 1	3	0	0	1	1	1 / 3 (33)

core peptide ID	ancestor 15mer peptide	ancestor peptide pool	HLA-restric-tion	core peptide sequence	PBMC						expanded cells					
					#Tests total	#CD4$^+$/CD8$^+$ res-ponse	#CD4$^+$ res-ponse	#CD8$^+$ res-ponse	#total postive hits	total postive hits [%]	#Tests total	#CD4$^+$/CD8$^+$ res-ponse	#CD4$^+$ res-ponse	#CD8$^+$ res-ponse	#total postive hits	total postive hits [%]
DRB1_0401_0701_P1	CoV_Prot_M_201-215	CoV_Prot_M_173-222	DRB1_0701	YKLNTDHSS	1	0	0	0	0	0 / 1	3	0	0	1	1	1 / 3 (33)
DRB1_0401_1501_P1	CoV_Prot_S_799-813	CoV_Prot_S_769-813	DRB1_0401	ILPDPSKPS	1	0	0	0	0	0 / 1	3	0	0	2	2	2 / 3 (66,67)
DRB1_0401_1501_P1	CoV_Prot_S_799-813	CoV_Prot_S_769-813	DRB1_1501	ILPDPSKPS	5	0	0	1	1	1 / 5 (20)	6	0	0	0	0	0 / 6
DRB1_0401_HLA-A02:01_P1	CoV_Prot_S_817-831	CoV_Prot_S_802-852	DRB1_0401	LLFNKVTLA	1	0	0	0	0	0 / 1	3	0	0	1	1	1 / 3 (33)
DRB1_0401_HLA-A02:01_P1	CoV_Prot_S_817-831	CoV_Prot_S_802-852	HLA-A02:01	LLFNKVTLA	9	0	0	0	0	0 / 9	8	0	1	1	2	2 / 8 (25)
DRB1_0401_P1	CoV_Prot_S_813-827	CoV_Prot_S_802-852	DRB1_0401	FIEDLLFNK	1	0	0	0	0	0 / 1	3	0	0	1	1	1 / 3 (33)
DRB1_0701_P2	CoV_Prot_M_173-187	CoV_Prot_M_173-222	DRB1_0701	YKLGASQRV	1	0	0	0	0	0 / 1	2	0	0	1	1	1 / 2 (50)
DRB1_1101_HLA-A02:01_P1	CoV_Prot_S_265-279	CoV_Prot_S_245-295	DRB1_1101	YLQPRTFLL	3	0	0	0	0	0 / 3	3	0	0	2	2	2 / 3 (67)
DRB1_1101_HLA-A02:01_P1	CoV_Prot_S_265-279	CoV_Prot_S_245-295	HLA-A02:01	YLQPRTFLL	10	0	0	1	1	1 / 10 (10)	10	0	0	8	8	8 / 10 (80)
DRB1_1101_P1	CoV_Prot_M_009-023	CoV_Prot_M_1-47	DRB1_1101	VEELKKLLE	2	0	1	0	1	1 / 2 (50)	2	0	0	0	0	0 / 2

core peptide ID	ancestor 15mer peptide	ancestor peptide pool	HLA-restric-tion	core peptide sequence	PBMC						expanded cells					
					#Tests total	#CD4$^+$/CD8$^+$ res-ponse	#CD4$^+$ res-ponse	#CD8$^+$ res-ponse	#total postive hits	total postive hits [%]	#Tests total	#CD4$^+$/CD8$^+$ res-ponse	#CD4$^+$ res-ponse	#CD8$^+$ res-ponse	#total postive hits	total postive hits [%]
DRB1_1101_P2	CoV_Prot_S_269-283	CoV_Prot_S_245-295	DRB1_1101	FLLKYNENG	3	0	0	0	0	0 / 3	3	0	0	0	0	0 / 3
DRB1_1101_P3	CoV_Prot_S_150-164	CoV_Prot_S_121-175	DRB1_1101	MESEFRVYS	2	0	0	0	0	0 / 2	2	0	0	1	1	1 / 2 (50)
DRB1_1101_P4	CoV_Prot_S_349-363	CoV_Prot_S_342-390	DRB1_1101	YAWNRKRIS	2	0	0	0	0	0 / 2	1	1	0	0	1	1 / 1 (100)
DRB1_1101_P6	CoV_Prot_S_253-267	CoV_Prot_S_245-295	DRB1_1101	WTAGAAAYY	3	0	0	0	0	0 / 3	3	0	0	0	0	0 / 3
DRB1_1301_HLA-C14:02_P1	CoV_Prot_S_781-795	CoV_Prot_S_769-813	DRB1_1301	VFAQVKQIY	1	1	0	0	1	1 / 1 (100)	1	0	0	0	0	0 / 1
DRB1_1301_HLA-C14:02_P1	CoV_Prot_S_781-795	CoV_Prot_S_769-813	HLA-C14:02	VFAQVKQIY	2	1	0	0	1	1 / 2 (50)	2	0	0	0	0	0 / 2
DRB1_1501_HLA-C03:03_P1	CoV_Prot_S_202-216	CoV_Prot_S_165-216	DRB1_1501	YSKHTPINL	1	0	0	1	1	1 / 1 (100)	1	0	0	0	0	0 / 1
DRB1_1501_HLA-C03:03_P1	CoV_Prot_S_198-212	CoV_Prot_S_165-216	HLA-C03:03	YSKHTPINL	2	0	0	0	0	0 / 2	1	0	0	0	0	0 / 1
DRB1_1501_P1	CoV_Prot_M_173-187	CoV_Prot_M_173-222	DRB1_1501	LSYYKLGAS	5	2	0	0	2	2 / 5 (40)	6	1	1	0	2	2 / 6 (33)
DRB1_1501_P10	CoV_Prot_S_194-208	CoV_Prot_S_165-216	DRB1_1501	IDGYFKIYS	5	0	0	1	1	1 / 5 (20)	6	0	0	0	0	0 / 6

core peptide ID	ancestor 15mer peptide	ancestor peptide pool	HLA-restric-tion	core peptide sequence	PBMC						expanded cells					
					#Tests total	#CD4$^+$/CD8$^+$ res-ponse	#CD4$^+$ res-ponse	#CD8$^+$ res-ponse	#total postive hits	total postive hits [%]	#Tests total	#CD4$^+$/CD8$^+$ res-ponse	#CD4$^+$ res-ponse	#CD8$^+$ res-ponse	#total postive hits	total postive hits [%]
DRB1_1501_P11	CoV_Prot_S_353-367	CoV_Prot_S_342-390	DRB1_1501	ISNCVADYS	5	0	1	1	2	2 / 5 (40)	5	0	0	0	0	0 / 5
DRB1_1501_P12	CoV_Prot_S_198-212	CoV_Prot_S_165-216	DRB1_1501	FKIYSKHTP	5	0	0	1	1	1 / 5 (20)	6	0	0	0	0	0 / 6
DRB1_1501_P13	CoV_Prot_S_345-359	CoV_Prot_S_342-390	DRB1_1501	VYAWNRKRI	5	0	1	1	2	2 / 5 (40)	6	0	1	0	1	1 / 6 (17)
DRB1_1501_P14	CoV_Prot_S_753-765	CoV_Prot_S_737-779	DRB1_1501	YGSFCTQLN	5	0	0	1	1	1 / 5 (20)	6	1	0	0	1	1 / 6 (17)
DRB1_1501_P15	CoV_Prot_S_990-1004	CoV_Prot_S_981-1023	DRB1_1501	IDRLITGRL	5	0	0	0	0	0 / 5	6	1	0	0	1	1 / 6 (17)
DRB1_1501_P16	CoV_Prot_S_997-1011	CoV_Prot_S_981-1023	DRB1_1501	LQSLQTYVT	5	1	0	1	2	2 / 5 (40)	6	0	0	1	1	1 / 6 (17)
DRB1_1501_P17	CoV_Prot_S_1056-1070	CoV_Prot_S_1051-1099	DRB1_1501	VVFLHVTYV	5	0	0	0	0	0 / 5	6	0	0	1	1	1 / 6 (17)
DRB1_1501_P18	CoV_Prot_S_342-356	CoV_Prot_S_342-390	DRB1_1501	FASVYAWNR	5	0	0	0	0	0 / 5	5	0	1	0	1	2 / 6 (33)
DRB1_1501_P19	CoV_Prot_N_49-61	CoV_Prot_N_40-87	DRB1_1501	WFTALTQHG	5	0	0	0	0	0 / 5	6	0	1	0	1	1 / 6 (16,67)
DRB1_1501_P2	CoV_Prot_M_197-211	CoV_Prot_M_173-222	DRB1_1501	IGNYKLNTD	5	1	3	0	4	4 / 5 (80)	5	1	0	1	2	2 / 5 (40)
DRB1_1501_P3	CoV_Prot_N_037-051	CoV_Prot_N_1-51	DRB1_1501	PQGLPNNTA	5	0	0	0	0	0 / 5	6	0	1	1	2	2 / 6 (33)

core peptide ID	ancestor 15mer peptide	ancestor peptide pool	HLA-restric-tion	core peptide sequence	PBMC						expanded cells					
					#Tests total	#CD4$^+$/CD8$^+$ res-ponse	#CD4$^+$ res-ponse	#CD8$^+$ res-ponse	#total postive hits	total postive hits [%]	#Tests total	#CD4$^+$/CD8$^+$ res-ponse	#CD4$^+$ res-ponse	#CD8$^+$ res-ponse	#total postive hits	total postive hits [%]
DRB1_1501_P4	CoV_Prot_S_001-014	CoV_Prot_S_1-51	DRB1_1501	LVLLPLVSS	5	0	1	1	2	2 / 5 (40)	6	0	0	0	0	0 / 6
DRB1_1501_P5	CoV_Prot_S_369-383	CoV_Prot_S_342-390	DRB1_1501	FSTFKCYGV	5	0	0	0	0	0 / 5	6	0	0	0	0	0 / 6
DRB1_1501_P6	CoV_Prot_S_376-390	CoV_Prot_S_342-390	DRB1_1501	FKCYGVSPT	5	0	0	0	0	0 / 5	5	0	0	0	0	0 / 5
DRB1_1501_P7	CoV_Prot_S_072-086	CoV_Prot_S_41-91	DRB1_1501	TKRFDNPVL	5	0	0	0	0	0 / 5	6	0	0	0	0	0 / 6
DRB1_1501_P8	CoV_Prot_S_138-152	CoV_Prot_S_121-175	DRB1_1501	VYYHKNNKS	5	0	0	0	0	0 / 5	6	0	0	0	0	0 / 6
DRB1_1501_P9	CoV_Prot_S_189-203	CoV_Prot_S_165-216	DRB1_1501	FVFKNIDGY	5	0	0	0	0	0 / 5	6	0	0	0	0	0 / 6
HLA-A01:01_P1	CoV_Prot_M_208-222	CoV_Prot_M_173-222	HLA-A01:01	SSDNIALLV	7	0	0	0	0	0 / 7	7	0	1	1	2	2 / 7 (29)
HLA-A01:01_P2	CoV_Prot_N_405-419	CoV_Prot_N_377-419	HLA-A01:01	MSSADSTQA	12	7	2	0	9	9 / 12 (75)	7	0	1	2	3	3 / 7 (43)
HLA-A01:01_P3	CoV_Prot_S_157-171	CoV_Prot_S_121-175	HLA-A01:01	SANNCTFEY	4	1	0	1	2	2 / 4 (50)	5	0	0	1	1	1 / 5 (20)
HLA-A01:01_P4	CoV_Prot_M_165-179	CoV_Prot_M_135-183	HLA-A01:01	ATSRTLSYY	6	0	1	0	1	1 / 6 (16,67)	6	0	2	0	2	2 / 6 (33,33)
HLA-A02:01_HLAC04:01_P1	CoV_Prot_S_105-119	CoV_Prot_S_81-130	HLA-A02:01	TLDSKTQSL	10	0	0	0	0	0 / 10	10	1	0	3	4	4 / 10 (40)

core peptide ID	ancestor 15mer peptide	ancestor peptide pool	HLA-restric-tion	core peptide sequence	PBMC						expanded cells					
					#Tests total	#CD4$^+$/CD8$^+$ res-ponse	#CD4$^+$ res-ponse	#CD8$^+$ res-ponse	#total postive hits	total postive hits [%]	#Tests total	#CD4$^+$/CD8$^+$ res-ponse	#CD4$^+$ res-ponse	#CD8$^+$ res-ponse	#total postive hits	total postive hits [%]
HLA-A02:01_HLAC04:01_P1	CoV_Prot_S_105-119	CoV_Prot_S_81-130	HLA-C04:01	TLDSKTQSL	1	0	0	1	1	1 / 1 (100)	1	0	0	0	0	0 / 1
HLA-A02:01_P1	CoV_Prot_M_012-026	CoV_Prot_M_1-47	HLA-A02:01	KLLEQWNLV	6	0	0	0	0	0 / 6	6	0	0	1	1	1 / 6 (17)
HLA-A02:01_P10	CoV_Prot_S_972-984	CoV_Prot_S_955-991	HLA-A02:01	VLNDILSRL	10	0	0	0	0	0 / 10	10	0	0	3	3	3 / 10 (30)
HLA-A02:01_P11	CoV_Prot_S_981-995	CoV_Prot_S_981-1023	HLA-A02:01	RLDKVEAEV	5	0	0	0	0	0 / 5	4	1	0	1	2	2 / 4 (50)
HLA-A02:01_P12	CoV_Prot_S_1045-1059	CoV_Prot_S_1012-1059	HLA-A02:01	HLMSFPQSA	10	0	0	1	1	1 / 10 (10)	10	0	0	1	1	1 / 10 (10)
HLA-A02:01_P13	CoV_Prot_S_1209-1223	CoV_Prot_S_1195-1230	HLA-A02:01	IKWPWYIWL	9	0	0	0	0	0 / 9	9	0	0	1	1	1 / 9 (11,11)
HLA-A02:01_P14	CoV_Prot_S_245-259	CoV_Prot_S_245-295	HLA-A02:01	YLTPGDSSS	9	0	0	0	0	0 / 9	9	0	1	1	2	2 / 9 (22,22)
HLA-A02:01_P2	CoV_Prot_M_060-070	CoV_Prot_M_37-73	HLA-A02:01	TLACFVLAA	5	0	1	0	1	1 / 5 (20)	6	0	0	2	2	2 / 6 (33)
HLA-A02:01_P3	CoV_Prot_S_685-699	CoV_Prot_S_665-707	HLA-A02:01	SIIAYTMSL	5	0	1	0	1	1 / 5 (20)	5	0	0	2	2	2 / 5 (40)
HLA-A02:01_P6	CoV_Prot_M_65-76	CoV_Prot_M_65-105	HLA-A02:01	FVLAAVYRI	6	0	0	0	0	0 / 6	6	0	0	0	0	0 / 6
HLA-A02:01_P7	CoV_Prot_N_217-230	CoV_Prot_N_194-234	HLA-A02:01	LLLDRLNQL	6	0	0	0	0	0 / 6	7	0	1	0	1	1 / 7 (14,29)

core peptide ID	ancestor 15mer peptide	ancestor peptide pool	HLA-restric-tion	core peptide sequence	PBMC						expanded cells					
					#Tests total	#CD4$^+$/CD8$^+$ res-ponse	#CD4$^+$ res-ponse	#CD8$^+$ res-ponse	#total postive hits	total postive hits [%]	#Tests total	#CD4$^+$/CD8$^+$ res-ponse	#CD4$^+$ res-ponse	#CD8$^+$ res-ponse	#total postive hits	total postive hits [%]
HLA-A02:01_P8	CoV_Prot_S_417-431	CoV_Prot_S_381-431	HLA-A02:01	KIADYNYKL	10	0	0	0	0	0 / 10	9	0	0	0	0	0 / 9
HLA-A02:01_P9	CoV_Prot_S_915-927	CoV_Prot_S_881-927	HLA-A02:01	VLYENQKLI	5	1	1	0	2	2 / 5 (40)	5	0	0	2	2	2 / 5 (40)
HLA-A03:01_HLA-A11:01_P1	CoV_Prot_S_1061-1075	CoV_Prot_S_1051-1099	HLA-A03:01	VTYVPAQEK	6	0	0	0	0	0 / 6	8	0	0	5	5	5 / 8 (62,5)
HLA-A03:01_HLA-A11:01_P1	CoV_Prot_S_1061-1075	CoV_Prot_S_1051-1099	HLA-A11:01	VTYVPAQEK	1	0	0	0	0	0 / 1	1	0	0	1	1	1 / 1 (100)
HLA-A03:01_P1	CoV_Prot_M_149-163	CoV_Prot_M_135-183	HLA-A03:01	RIAGHHLGR	6	1	0	0	1	1 / 6 (17)	7	1	0	1	2	2 / 7 (29)
HLA-A03:01_P2	CoV_Prot_S_345-359	CoV_Prot_S_342-390	HLA-A03:01	SVYAWNRKR	8	0	0	1	1	1 / 8 (13)	11	2	0	2	4	4 / 11 (36)
HLA-A03:01_P3	CoV_Prot_S_376-390	CoV_Prot_S_342-390	HLA-A03:01	KCYGVSPTK	6	0	0	4	4	4 / 6 (66,67)	8	1	0	7	8	8 / 8 (100)
HLA-A03:01_P4	CoV_Prot_S_526-539	CoV_Prot_S_521-567	HLA-A03:01	KSTNLVKNK	7	0	0	1	1	1 / 7 (14,29)	10	0	0	2	2	2 / 10 (20)
HLA-A03:01_P5	CoV_Prot_S_41-55	CoV_Prot_S_41-91	HLA-A03:01	KVFRSSVLH	6	0	0	0	0	0 / 6	7	0	0	2	2	2 / 7 (28,57)
HLA-A03:01_P6	CoV_Prot_S_138-152	CoV_Prot_S_121-175	HLA-A03:01	GVYYHKNNK	8	1	0	0	1	1 / 8 (12,5)	10	1	0	0	1	1 / 10 (10)
HLA-A11:01_P1	CoV_Prot_S_669-683	CoV_Prot_S_665-707	HLA-A11:01	QTQTNSPRR	1	0	1	0	1	1 / 1 (100)	1	0	0	0	0	0 / 1

core peptide ID	ancestor 15mer peptide	ancestor peptide pool	HLA-restric-tion	core peptide sequence	PBMC						expanded cells					
					#Tests total	#CD4$^+$/CD8$^+$ res-ponse	#CD4$^+$ res-ponse	#CD8$^+$ res-ponse	#total postive hits	total postive hits [%]	#Tests total	#CD4$^+$/CD8$^+$ res-ponse	#CD4$^+$ res-ponse	#CD8$^+$ res-ponse	#total postive hits	total postive hits [%]
HLA-A11:01_P2	CoV_Prot_S_719-733	CoV_Prot_S_698-747	HLA-A11:01	EILPVSMTK	1	0	0	0	0	0 / 1	1	0	0	1	1	1 / 1 (100)
HLA-A11:01_P3	CoV_Prot_S_753-765	CoV_Prot_S_737-779	HLA-A11:01	GSFCTQLNR	1	0	0	0	0	0 / 1	1	0	0	1	1	1 / 1 (100)
HLA-A11:01_P4	CoV_Prot_S_546-560	CoV_Prot_S_521-567	HLA-A11:01	GVLTESNKK	2	0	0	0	0	0 / 2	1	0	0	0	0	0 / 1
HLA-A11:01_P5	CoV_Prot_S_781-795	CoV_Prot_S_769-813	HLA-A11:01	QIYKTPPIK	1	0	0	0	0	0 / 1	1	0	0	1	1	1 / 1 (100)
HLA-A11:01_P6	CoV_Prot_S_1093-1107	CoV_Prot_S_1089-1135	HLA-A11:01	GTHWFVTQR	1	0	0	0	0	0 / 1	1	0	0	0	0	0 / 1
HLA-A11:01_P7	CoV_Prot_S_364-378	CoV_Prot_S_342-390	HLA-A11:01	NSASFSTFK	1	0	0	0	0	0 / 1	1	0	0	0	0	0 / 1
HLA-A23:01_P1	CoV_Prot_M_042-056	CoV_Prot_M_37-73	HLA-A23:01	LYIIKLIFL	1	0	0	0	0	0 / 1	1	0	0	0	0	0 / 1
HLA-A23:01_P2	CoV_Prot_M_89-103	CoV_Prot_M_65-105	HLA-A23:01	YFIASFRLF	1	0	0	0	0	0 / 1	1	0	0	0	0	0 / 1
HLA-A25:01_P1	CoV_Prot_M_12-26	CoV_Prot_M_1-47	HLA-A25:01	ELKKLLEQW	1	0	0	0	0	0 / 1	2	0	0	0	0	0 / 2
HLA-A26:01_P1	CoV_Prot_S_044-058	CoV_Prot_S_41-91	HLA-A26:01	STQDLFLPF	1	0	0	0	0	0 / 1	1	0	0	0	0	0 / 1
HLA-A29:02_HLA-C02:02_P1	CoV_Prot_S_024-038	CoV_Prot_S_1-51	HLA-A29:02	NSFTRGVYY	1	0	0	0	0	0 / 1	1	0	0	0	0	0 / 1

core peptide ID	ancestor 15mer peptide	ancestor peptide pool	HLA-restric-tion	core peptide sequence	PBMC						expanded cells					
					#Tests total	#CD4$^+$/CD8$^+$ res-ponse	#CD4$^+$ res-ponse	#CD8$^+$ res-ponse	#total postive hits	total postive hits [%]	#Tests total	#CD4$^+$/CD8$^+$ res-ponse	#CD4$^+$ res-ponse	#CD8$^+$ res-ponse	#total postive hits	total postive hits [%]
HLA-A29:02_HLA-C02:02_P1	CoV_Prot_S_024-038	CoV_Prot_S_1-51	HLA-C02:02	NSFTRGVYY	1	0	0	0	0	0 / 1	2	0	0	0	0	0 / 2
HLA-A68:01_P1	CoV_Prot_M_137-151	CoV_Prot_M_135-183	HLA-A68:01	LVIGAVILR	2	0	0	0	0	0 / 2	1	0	0	0	0	0 / 1
HLA-A68:01_P2	CoV_Prot_S_673-687	CoV_Prot_S_665-707	HLA-A68:01	QTNSPRRAR	2	0	0	0	0	0 / 2	2	0	0	0	0	0 / 2
HLA-B07:02_P1	CoV_Prot_N_102-116	CoV_Prot_N_78-127	HLA-B07:02	SPRWYFYYL	5	0	0	0	0	0 / 5	6	1	1	2	4	4 / 6 (67)
HLA-B07:02_P2	CoV_Prot_N_37-51	CoV_Prot_N_1-51	HLA-B07:02	RPQGLPNNT	6	0	0	0	0	0 / 6	6	0	0	0	0	0 / 6
HLA-B07:02_P3	CoV_Prot_N_253-267	CoV_Prot_N_224-274	HLA-B07:02	KPRQKRTAT	6	0	0	0	0	0 / 6	7	0	1	1	2	2 / 7 (28,57)
HLA-B07:02_P4	CoV_Prot_S_678-692	CoV_Prot_S_665-707	HLA-B07:02	SPRRARSVA	8	0	0	1	1	1 / 8 (12,5)	7	0	0	4	4	4 / 7 (57,14)
HLA-B07:02_P5	CoV_Prot_S_202-216	CoV_Prot_S_165-216	HLA-B07:02	TPINLVRDL	7	0	0	0	0	0 / 7	8	0	0	0	0	0 / 8
HLA-B08:01_P1	CoV_Prot_M_144-158	CoV_Prot_M_135-183	HLA-B08:01	HLRIAGHHL	4	0	0	0	0	0 / 4	5	0	1	0	1	1 / 5 (20)
HLA-B08:01_P2	CoV_Prot_S_869-883	CoV_Prot_S_841-891	HLA-B08:01	MIAQYTSAL	4	0	0	0	0	0 / 4	6	0	1	1	2	2 / 6 (33,33)
HLA-B14:01_P1	CoV_Prot_S_37-51	CoV_Prot_S_1-51	HLA-B14:01	DKVFRSSVL	1	0	0	0	0	0 / 1	1	0	0	0	0	0 / 1
HLA-B14:01_P2	CoV_Prot_S_41-55	CoV_Prot_S_41-91	HLA-B14:01	FRSSVLHST	1	0	0	0	0	0 / 1	1	0	0	0	0	0 / 1

core peptide ID	ancestor 15mer peptide	ancestor peptide pool	HLA-restric-tion	core peptide sequence	PBMC						expanded cells					
					#Tests total	#CD4$^+$/CD8$^+$ res-ponse	#CD4$^+$ res-ponse	#CD8$^+$ res-ponse	#total postive hits	total postive hits [%]	#Tests total	#CD4$^+$/CD8$^+$ res-ponse	#CD4$^+$ res-ponse	#CD8$^+$ res-ponse	#total postive hits	total postive hits [%]
HLA-B15:01_P1	CoV_Prot_S_494-508	CoV_Prot_S_461-508	HLA-B15:01	FQPTNGVGY	2	0	0	0	0	0 / 2	2	0	0	2	2	2 / 2 (100)
HLA-B15:01_P2	CoV_Prot_S_799-813	CoV_Prot_S_769-813	HLA-B15:01	SQILPDPSK	1	0	1	0	1	1 / 1 (100)	1	0	0	1	1	1 / 1 (100)
HLA-B15:01_P3	CoV_Prot_S_178-192	CoV_Prot_S_165-216	HLA-B15:01	GNFKNLREF	2	0	0	0	0	0 / 2	2	0	0	0	0	0 / 2
HLA-B27:05_HLA-C07:02_P1	CoV_Prot_S_994-1008	CoV_Prot_S_981-1023	HLA-B27:05	GRLQSLQTY	1	0	0	0	0	0 / 1	1	0	0	1	1	1 / 1 (100)
HLA-B27:05_HLA-C07:02_P1	CoV_Prot_S_994-1008	CoV_Prot_S_981-1023	HLA-C07:02	GRLQSLQTY	7	0	0	1	1	1 / 7 (14)	9	0	0	2	2	2 / 9 (22)
HLA-B27:05_P1	CoV_Prot_S_077-091	CoV_Prot_S_41-91	HLA-B27:05	KRFDNPVLP	1	1	0	0	1	1 / 1 (100)	1	0	0	0	0	0 / 1
HLA-B27:05_P2	CoV_Prot_S_342-356	CoV_Prot_S_342-390	HLA-B27:05	TRFASVYAW	1	0	0	0	0	0 / 1	1	0	0	0	0	0 / 1
HLA-B35:03_P1	CoV_Prot_S_081-095	CoV_Prot_S_81-130	HLA-B35:03	LPFNDGVYF	1	0	0	1	1	1 / 1 (100)	1	0	0	0	0	0 / 1
HLA-B35:03_P2	CoV_Prot_S_1257-1271	CoV_Prot_S_1222-1273	HLA-B35:03	EPVLKGVKL	1	0	0	0	0	0 / 1	1	0	0	1	1	1 / 1 (100)
HLA-B35:03_P3	CoV_Prot_S_18-32	CoV_Prot_S_1-51	HLA-B35:03	LPPAYTNSF	1	0	0	0	0	0 / 1	1	0	0	0	0	0 / 1
HLA-B38:01_P1	CoV_Prot_S_769-783	CoV_Prot_S_769-813	HLA-B38:01	EQDKNTQEV	1	0	0	0	0	0 / 1	1	0	1	0	1	1 / 1 (100)

core peptide ID	ancestor 15mer peptide	ancestor peptide pool	HLA-restric-tion	core peptide sequence	PBMC						expanded cells					
					#Tests total	#CD4$^+$/CD8$^+$ res-ponse	#CD4$^+$ res-ponse	#CD8$^+$ res-ponse	#total postive hits	total postive hits [%]	#Tests total	#CD4$^+$/CD8$^+$ res-ponse	#CD4$^+$ res-ponse	#CD8$^+$ res-ponse	#total postive hits	total postive hits [%]
HLA-B40:01_P1	CoV_Prot_S_1149-1163	CoV_Prot_S_1123-1166	HLA-B40:01	KYFKNHTSP	1	0	0	0	0	0 / 1	2	0	0	0	0	0 / 2
HLA-B40:01_P2	CoV_Prot_S_1175-1189	CoV_Prot_S_1157-1205	HLA-B40:01	KEIDRLNEV	4	0	0	0	0	0 / 4	3	0	0	0	0	0 / 3
HLA-B44:02_P1	CoV_Prot_S_1203-1215	CoV_Prot_S_1195-1230	HLA-B44:02	YEQYIKWPW	2	0	0	0	0	0 / 2	2	0	0	0	0	0 / 2
HLA-B44:02_P2	CoV_Prot_S_825-839	CoV_Prot_S_802-852	HLA-B44:02	ADAGFIKQY	2	0	0	0	0	0 / 2	2	0	0	1	1	1 / 2 (50)
HLA-B44:02_P3	CoV_Prot_S_1197-1211	CoV_Prot_S_1195-1230	HLA-B44:02	QELGKYEQY	2	0	0	0	0	0 / 2	2	0	0	0	0	0 / 2
HLA-B44:03_P1	CoV_Prot_N_321-335	CoV_Prot_N_305-347	HLA-B44:03	MEVTPSGTW	1	0	0	0	0	0 / 1	1	0	0	0	0	0 / 1
HLA-B51:01_P1	CoV_Prot_S_005-019	CoV_Prot_S_1-51	HLA-B51:01	LPLVSSQCV	4	0	1	0	1	1 / 4 (25)	5	0	0	0	0	0 / 5
HLA-B51:01_P2	CoV_Prot_S_709-723	CoV_Prot_S_698-747	HLA-B51:01	IPTNFTISV	5	0	0	0	0	0 / 5	5	0	0	1	1	1 / 5 (20)
HLA-C02:02_DRB1_0701_P1	CoV_Prot_M_165-179	CoV_Prot_M_135-183	HLA-C02:02	VATSRTLSY	1	0	0	0	0	0 / 1	2	1	0	0	1	1 / 2 (50)
HLA-C02:02_DRB1_0701_P1	CoV_Prot_M_177-191	CoV_Prot_M_173-222	DRB1_0701	VATSRTLSY	1	0	0	0	0	0 / 1	3	0	0	0	0	0 / 3
HLA-C02:02_HLA-C12:02_P1	CoV_Prot_S_683-696	CoV_Prot_S_665-707	HLA-C02:02	VASQSIIAY	1	0	0	0	0	0 / 1	2	0	0	0	0	0 / 2

core peptide ID	ancestor 15mer peptide	ancestor peptide pool	HLA-restric-tion	core peptide sequence	PBMC						expanded cells					
					#Tests total	#CD4$^+$/CD8$^+$ res-ponse	#CD4$^+$ res-ponse	#CD8$^+$ res-ponse	#total postive hits	total postive hits [%]	#Tests total	#CD4$^+$/CD8$^+$ res-ponse	#CD4$^+$ res-ponse	#CD8$^+$ res-ponse	#total postive hits	total postive hits [%]
HLA-C02:02_HLA-C12:02_P1	CoV_Prot_S_683-696	CoV_Prot_S_665-707	HLA-C12:02	VASQSIIAY	1	0	0	0	0	0 / 1	2	0	0	0	0	0 / 2
HLA-C02:02_P1	CoV_Prot_M_193-207	CoV_Prot_M_173-222	HLA-C02:02	YSRYRIGNY	1	0	0	0	0	0 / 1	2	0	0	0	0	0 / 2
HLA-C02:02_P3	CoV_Prot_S_170-184	CoV_Prot_S_165-216	HLA-C02:02	VSQPFLMDL	1	0	0	0	0	0 / 1	2	0	0	0	0	0 / 2
HLA-C02:02_P4	CoV_Prot_S_304-319	CoV_Prot_S_285-327	HLA-C02:02	KGIYQTSNF	1	0	0	0	0	0 / 1	2	0	0	0	0	0 / 2
HLA-C02:02_P5	CoV_Prot_S_369-383	CoV_Prot_S_342-390	HLA-C02:02	ASFSTFKCY	1	0	0	0	0	0 / 1	2	0	0	1	1	1 / 2 (50)
HLA-C02:02_P7	CoV_Prot_M_34-47	CoV_Prot_M_1-47	HLA-C02:02	FAYANRNRF	1	0	0	0	0	0 / 1	2	1	0	1	2	2 / 2 (100)
HLA-C02:02_P8	CoV_Prot_M_27-37	CoV_Prot_M_1-47	HLA-C02:02	LTWICLLQF	1	0	0	0	0	0 / 1	2	0	1	1	2	2 / 2 (100)
HLA-C02:02_P9	CoV_Prot_S_1259-1273	CoV_Prot_S_1222-1273	HLA-C02:02	VLKGVKLHY	1	0	0	0	0	0 / 1	2	0	0	0	0	0 / 2
HLA-C03:04_P1	CoV_Prot_S_881-895	CoV_Prot_S_881-927	HLA-C03:04	WTFGAGAAL	2	0	1	0	1	1 / 2 (50)	3	0	0	1	1	1 / 3 (33)
HLA-C03:04_P2	CoV_Prot_S_865-879	CoV_Prot_S_841-891	HLA-C03:04	IAQYTSALL	5	0	0	0	0	0 / 5	5	0	1	0	1	1 / 5 (20)
HLA-C04:01_DRB1_1501_P1	CoV_Prot_S_165-179	CoV_Prot_S_165-216	HLA-C04:01	TFEYVSQPF	4	0	0	0	0	0 / 4	4	0	0	0	0	0 / 4

core peptide ID	ancestor 15mer peptide	ancestor peptide pool	HLA-restric-tion	core peptide sequence	PBMC						expanded cells					
					#Tests total	#CD4$^+$/CD8$^+$ res-ponse	#CD4$^+$ res-ponse	#CD8$^+$ res-ponse	#total postive hits	total postive hits [%]	#Tests total	#CD4$^+$/CD8$^+$ res-ponse	#CD4$^+$ res-ponse	#CD8$^+$ res-ponse	#total postive hits	total postive hits [%]
HLA-C04:01_DRB1_1501_P1	CoV_Prot_S_161-175	CoV_Prot_S_121-175	DRB1_1501	TFEYVSQPF	5	0	0	1	1	1 / 5 (20)	6	0	0	0	0	0 / 6
HLA-C04:01_DRB1_1501_P1	CoV_Prot_S_161-175	CoV_Prot_S_121-175	HLA-C04:01	TFEYVSQPF	1	0	0	1	1	1 / 1 (100)	1	0	0	1	1	1 / 1 (100)
HLA-C04:01_HLA-C07:02_P1	CoV_Prot_S_72-86	CoV_Prot_S_41-91	HLA-C04:01	RFDNPVLPF	4	0	0	1	1	1 / 4 (25)	3	0	1	0	1	1 / 3 (33,33)
HLA-C04:01_HLA-C07:02_P1	CoV_Prot_S_72-86	CoV_Prot_S_41-91	HLA-C07:02	RFDNPVLPF	6	2	0	0	2	2 / 6 (33,33)	6	0	0	1	1	1 / 6 (16,67)
HLA-C04:01_P1	CoV_Prot_M_105-119	CoV_Prot_M_97-147	HLA-C04:01	SFNPETNIL	2	0	0	0	0	0 / 2	2	0	0	1	1	1 / 2 (50)
HLA-C04:01_P2	CoV_Prot_N_78-92	CoV_Prot_N_78-127	HLA-C04:01	SPDDQIGYY	2	0	0	1	1	1 / 2 (50)	2	0	0	0	0	0 / 2
HLA-C04:01_P3	CoV_Prot_N_333-347	CoV_Prot_N_305-347	HLA-C04:01	KLDDKDPNF	2	0	0	0	0	0 / 2	2	1	0	0	1	1 / 2 (50)
HLA-C04:01_P6	CoV_Prot_S_1136-1149	CoV_Prot_S_1123-1166	HLA-C04:01	VYDPLQPEL	4	0	0	0	0	0 / 4	4	0	0	1	1	1 / 4 (25)
HLA-C05:01_P1	CoV_Prot_S_285-299	CoV_Prot_S_285-327	HLA-C05:01	ITDAVDCAL	2	0	0	0	0	0 / 2	2	0	0	0	0	0 / 2
HLA-C05:01_P2	CoV_Prot_S_581-595	CoV_Prot_S_557-607	HLA-C05:01	ILDITPCSF	2	0	0	0	0	0 / 2	2	0	0	0	0	0 / 2

core peptide ID	ancestor 15mer peptide	ancestor peptide pool	HLA-restric-tion	core peptide sequence	PBMC						expanded cells					
					#Tests total	#CD4$^+$/CD8$^+$ res-ponse	#CD4$^+$ res-ponse	#CD8$^+$ res-ponse	#total postive hits	total postive hits [%]	#Tests total	#CD4$^+$/CD8$^+$ res-ponse	#CD4$^+$ res-ponse	#CD8$^+$ res-ponse	#total postive hits	total postive hits [%]
HLA-C05:01_P3	CoV_Prot_S_713-727	CoV_Prot_S_698-747	HLA-C05:01	FTISVTTEI	2	0	0	0	0	0 / 2	2	0	0	0	0	0 / 2
HLA-C05:01_P4	CoV_Prot_S_745-759	CoV_Prot_S_737-779	HLA-C05:01	STECSNLLL	2	0	0	0	0	0 / 2	2	0	0	0	0	0 / 2
HLA-C05:01_P5	CoV_Prot_S_841-855	CoV_Prot_S_841-891	HLA-C05:01	LGDIAARDL	2	0	0	0	0	0 / 2	2	0	0	1	1	1 / 2 (50)
HLA-C05:01_P6	CoV_Prot_S_1117-1131	CoV_Prot_S_1089-1135	HLA-C05:01	FVSGNCDVV	2	0	0	0	0	0 / 2	2	0	0	0	0	0 / 2
HLA-C05:01_P7	CoV_Prot_S_289-303	CoV_Prot_S_285-327	HLA-C05:01	ALDPLSETK	2	0	0	0	0	0 / 2	2	0	1	1	2	2 / 2 (100)
HLA-C07:01_P1	CoV_Prot_S_553-567	CoV_Prot_S_521-567	HLA-C07:01	KKFLPFQQF	4	0	0	1	1	1 / 4 (25)	4	0	0	1	1	1 / 4 (25)
HLA-C07:01_P2	CoV_Prot_M_102-116	CoV_Prot_M_97-147	HLA-C07:01	ARTRSMWSF	4	0	0	0	0	0 / 4	6	0	0	0	0	0 / 6
HLA-C07:01_P3	CoV_Prot_S_785-799	CoV_Prot_S_769-813	HLA-C07:01	YKTPPIKDF	5	0	0	1	1	1 / 5 (20)	6	0	0	0	0	0 / 6
HLA-C07:02_P11	CoV_Prot_S_322-335	CoV_Prot_S_313-351	HLA-C07:02	VRFPNITNL	8	1	1	0	2	2 / 8 (25)	9	0	1	0	1	1 / 9 (11,11)
HLA-C07:02_P2	CoV_Prot_M_169-183	CoV_Prot_M_135-183	HLA-C07:02	SRTLSYYKL	7	1	0	0	1	1 / 7 (14,29)	7	0	1	1	2	2 / 7 (28,57)
HLA-C07:02_P3	CoV_Prot_N_158-172	CoV_Prot_N_158-203	HLA-C07:02	LQLPQGTTL	7	0	1	1	2	2 / 7 (28,57)	7	0	1	0	1	1 / 7 (14,29)
HLA-C07:02_P4	CoV_Prot_S_438-452	CoV_Prot_S_421-455	HLA-C07:02	SKVGGNYNY	8	0	0	2	2	2 / 8 (25)	9	0	0	1	1	1 / 9 (11,11)

core peptide ID	ancestor 15mer peptide	ancestor peptide pool	HLA-restric-tion	core peptide sequence	PBMC						expanded cells					
					#Tests total	#CD4$^+$/CD8$^+$ res-ponse	#CD4$^+$ res-ponse	#CD8$^+$ res-ponse	#total postive hits	total postive hits [%]	#Tests total	#CD4$^+$/CD8$^+$ res-ponse	#CD4$^+$ res-ponse	#CD8$^+$ res-ponse	#total postive hits	total postive hits [%]
HLA-C07:02_P5	CoV_Prot_S_486-500	CoV_Prot_S_461-508	HLA-C07:02	YFPLQSYGF	8	0	0	1	1	1 / 8 (12,5)	7	0	1	2	3	3 / 7 (42,86)
HLA-C07:02_P6	CoV_Prot_S_573-587	CoV_Prot_S_557-607	HLA-C07:02	VRDPQTLEI	8	0	0	2	2	2 / 8 (25)	9	0	1	0	1	1 / 9 (11,11)
HLA-C07:02_P7	CoV_Prot_S_165-179	CoV_Prot_S_165-216	HLA-C07:02	EYVSQPFLM	8	1	0	0	1	1 / 8 (12,5)	9	0	0	2	2	2 / 9 (22,22)
HLA-C07:02_P8	CoV_Prot_S_18-32	CoV_Prot_S_1-51	HLA-C07:02	TRTQLPPAY	7	0	0	1	1	1 / 7 (14,29)	9	0	1	0	1	1 / 9 (11,11)
HLA-C08:02_P1	CoV_Prot_S_865-879	CoV_Prot_S_841-891	HLA-C08:02	LTDEMIAQY	1	0	0	0	0	0 / 1	1	0	0	1	1	1 / 1 (100)
HLA-C12:02_P1	CoV_Prot_S_1189-1203	CoV_Prot_S_1157-1205	HLA-C12:02	VAKNLNESL	1	0	0	0	0	0 / 1	2	0	0	0	0	0 / 2
HLA-C12:03_HLA-B51:01_P1	CoV_Prot_S_117-130	CoV_Prot_S_81-130	HLA-B51:01	NATNVVIKV	5	0	0	0	0	0 / 5	5	0	0	3	3	3 / 5 (60)
HLA-C12:03_HLA-B51:01_P1	CoV_Prot_S_121-135	CoV_Prot_S_121-175	HLA-C12:03	NATNVVIKV	1	0	0	0	0	0 / 1	2	0	0	0	0	0 / 2
HLA-C12:03_HLA-B51:01_P1	CoV_Prot_S_121-135	CoV_Prot_S_121-175	HLA-B51:01	NATNVVIKV	4	0	1	0	1	1 / 4 (25)	5	0	0	3	3	3 / 5 (60)
HLA-C12:03_P2	CoV_Prot_S_249-263	CoV_Prot_S_245-295	HLA-C12:03	SSSGWTAGA	2	0	0	0	0	0 / 2	4	1	0	0	1	1 / 4 (25)
HLA-C14:02_P1	CoV_Prot_M_193-207	CoV_Prot_M_173-222	HLA-C14:02	RYRIGNYKL	2	0	0	0	0	0 / 2	2	0	0	0	0	0 / 2

core peptide ID	ancestor 15mer peptide	ancestor peptide pool	HLA-restric-tion	core peptide sequence	PBMC						expanded cells					
					#Tests total	#CD4$^+$/ CD8$^+$ res-ponse	#CD4$^+$ res-ponse	#CD8$^+$ res-ponse	#total postive hits	total postive hits [%]	#Tests total	#CD4$^+$/ CD8$^+$ res-ponse	#CD4$^+$ res-ponse	#CD8$^+$ res-ponse	#total postive hits	total postive hits [%]
HLA-C14:02_P2	CoV_Prot_S_698-712	CoV_Prot_S_698-747	HLA-C14:02	LGAENSVAY	2	0	0	0	0	0 / 2	2	0	0	1	1	1 / 2 (50)
HLA-C15:02_P1	CoV_Prot_S_024-038	CoV_Prot_S_1-51	HLA-C15:02	YTNSFTRGV	1	0	0	0	0	0 / 1	1	0	0	0	0	0 / 1
HLA-C15:02_P2	CoV_Prot_S_057-071	CoV_Prot_S_41-91	HLA-C15:02	VTWFHAIHV	2	0	0	0	0	0 / 2	2	0	0	2	2	2 / 2 (100)
HLA-C15:02_P3	CoV_Prot_S_93-107	CoV_Prot_S_81-130	HLA-C15:02	ASTEKSNII	3	0	0	0	0	0 / 3	3	1	0	1	2	2 / 3 (66,67)
HLA-C16:01_DRB1_1501_P1	CoV_Prot_S_154-168	CoV_Prot_S_121-175	HLA-C16:01	YSSANNCTF	1	0	0	0	0	0 / 1	1	0	0	0	0	0 / 1
HLA-C16:01_DRB1_1501_P1	CoV_Prot_S_154-168	CoV_Prot_S_121-175	DRB1_1501	YSSANNCTF	5	0	0	1	1	1 / 5 (20)	6	0	0	0	0	0 / 6

Supplementary Table 6. Unfavorable and favorable HLA Class I and Class II haplotypes. HLA-haplotypes associated to more severe (unfavorable) and mild (favorable) COVID-19 disease courses.

	Haplotypes		**Haplotypes**
Unfavorable HLA-Class I		**Unfavorable HLA-Class II**	
HLA_ABC_04	**#02:01_07:02_07:02**	HLA_DRB_DQA_DQB_02	**#15:01_01:02_06:02**
HLA_ABC_05	**#02:01_40:01_03:04**	HLA_DRB_DQA_DQB_05	**#11:01_05:01_03:01**
HLA_ABC_11	**#03:01_35:01_04:01**	HLA_DRB_DQA_DQB_06	**#07:01_02:01_03:03**
HLA_ABC_17	**#01:01_07:02_07:02**	HLA_DRB_DQA_DQB_07	**#13:01_01:03_06:03**
HLA_ABC_22	**#29:02_44:03_16:01**	HLA_DRB_DQA_DQB_10	**#04:01_03:01_03:01**
Favorable HLA-Class I		HLA_DRB_DQA_DQB_12	**#13:02_01:02_06:04**
HLA_ABC_01	**01:01_08:01_07:01**	HLA_DRB_DQA_DQB_15	**#12:01_05:01_03:01**
HLA_ABC_02	**03:01_07:02_07:02**	HLA_DRB_DQA_DQB_16	**#13:03_05:01_03:01**
HLA_ABC_03	**02:01_44:02_05:01**	HLA_DRB_DQA_DQB_17	**#16:01_01:02_05:02**
HLA_ABC_06	**02:01_13:02_06:02**	HLA_DRB_DQA_DQB_18	**#09:01_03:01_03:03**
HLA_ABC_07	**24:02_07:02_07:02**	**Favorable HLA-Class II**	
HLA_ABC_08	**02:01_35:01_04:01**	HLA_DRB_DQA_DQB_01	**07:01_02:01_02:01**
HLA_ABC_09	**01:01_35:01_04:01**	HLA_DRB_DQA_DQB_03	**01:01_01:01_05:01**
HLA_ABC_10	**02:01_15:01_03:03**	HLA_DRB_DQA_DQB_04	**03:01_05:01_02:01**
HLA_ABC_12	**01:01_57:01_06:02**	HLA_DRB_DQA_DQB_08	**04:01_03:01_03:02**
HLA_ABC_13	**02:01_15:01_03:04**	HLA_DRB_DQA_DQB_09	**11:04_05:01_03:01**
HLA_ABC_14	**11:01_35:01_04:01**	HLA_DRB_DQA_DQB_11	**08:01_04:01_04:02**
HLA_ABC_15	**02:01_08:01_07:01**	HLA_DRB_DQA_DQB_13	**14:54_01:04_05:03**
HLA_ABC_16	**02:01_51:01_15:02**	HLA_DRB_DQA_DQB_14	**04:04_03:01_03:02**
HLA_ABC_18	**02:01_18:01_07:01**	HLA_DRB_DQA_DQB_19	**04:07_03:01_03:01**
HLA_ABC_19	**02:01_27:05_02:02**	HLA_DRB_DQA_DQB_20	**01:02_01:01_05:01**
HLA_ABC_20	**02:01_57:01_06:02**	HLA_DRB_DQA_DQB_21	**11:03_05:01_03:01**
HLA_ABC_21	**03:01_40:01_03:04**	HLA_DRB_DQA_DQB_22	**10:01_01:04_05:01**

List of Abbreviations

Abbreviation	**Translation**
ACE2	Angiotensin converting enzyme 2
APC	antigen-presenting cell
BCR	B cell receptor
C	catalyst
CARD	caspase activation and recruitment domain
CCR	chemokine receptor
CD	cluster of differentiation
CLIP	class II associated invariant chain peptide
cond.	condition
COVID-19	Coronavirus disease 2019
CPE	cytopathic effect
CTD	carboxy- terminal domain
CTL	Cytotoxic T lymphocyte
DAMP	damage-associated molecular pattern
DC	dendritic cell
DMSO	Dimethylsulfoxide
DN	double negative
DP	double positive
ER	Endoplasmatic reticulum
ETDA	Ethylenediaminetetraacetic acid
ExPep	exchange peptide
FACS	fluorescent activated cell sorting
fc	final concentration
HEV	high endothelial venule
HLA	human leukocyte antigen
ICS	intracellular cytokine staining
IFN	interferon
Ii	Invariant chain

Abbreviation	Translation
IKKε	IκB kinase- ε
IL	Interleukin
IL-2	Interleukin-2
INF-ɣ	Interferon-ɣ
IRF	interferon regulatory factor
LGP2	laboratory of genetics and physiology 2
M	Membrane protein
MAM	mitochondrial-associated membranes
MAVS	mitochondrial antiviral-signaling protein
MDA5	melanoma differentiation-associated protein 5
MHC	major histocompatibility complex
N	Nucleocapsid protein
nAB	neutralizing antibody
NB	non-binding peptide
NF-κB	nuclear-factor-κB
NK cell	Natural killer cell
NLR	NOD-like receptors
ORF	open-reading frame
PAMP	pathogen-associated molecular pattern
pMHC	peptide-MHC complex
PMMA	Polymethylmethacrylate
PRR	pattern-recognition receptor
RAG	recombination activation gene
RBD	receptor binding domain
RIG-I	retinoic acid-inducable gene I
RLR	RIG-I like receptors
ROS	reactive oxygen species
RT	room temperature
S	Spike protein
SARS-CoV-2	Severe acute respiratory syndrome coronavirus 2

Abbreviation	**Translation**
SB	strong-binding peptide
ssRNA	single-stranded RNA
TAP	Transporter associated with antigen processing
TBK1	TANK- binding kinase 1
TCR	T cell receptor
TIL	tumor-infiltrating lymphocyte
TLR	Toll-like receptor
WB	weak-binding peptide
WES	Whole Exome Sequencing
WHO	World Health Association
WT	wildtype

List of Reagents

Reagent	Clone	Lot	Manufacturer	Cat.No.	Final Concentration (fc)
CD3 APC	REA613	5181206204	Miltenyi Biotec	130-113-135	1:50
CD14 VioBlue	REA599	5180910628	Miltenyi Biotec	130-110-524	1:50
CD20 VioBlue	REA780	5171211151	Miltenyi Biotec	130-111-531	1:50
CD4 VioBright515	REA623	5200709700	Miltenyi Biotec	130-114-535	1:50
CD8 VioGreen	REA734	520070671	Miltenyi Biotec	130-110-684	1:50
IFN-ɣ PE	45-15	5200311108	Miltenyi Biotec	130-113-493	1:50
TNF-α PEVio770	cA2	5180821363	Miltenyi Biotec	130-120-492	1:50
CD154 APCVio770	5C8	5180525019	Miltenyi Biotec	130-114-130	1:50
IL-2 PEVio615	REA689	5160630212	Miltenyi Biotec	130-111-307	1:50
CD3-PE-Dazzle	UCHT1	-	Biolegend	300449	1:100
CD4 BV650	OKT4	-	Biolegend	317436	1:100
CD45RO_BV570	UCHL1	-	Biolegend	304226	1:100
CD154_PE-Cy7	24-31	-	Biolegend	310832	1:100
IFN-γ-BV421	4S.B3	-	Biolegend	502532	1:100
Inside Stain Kit	n.A.	Inside Perm: 5180709913 Inside Fix: 5190930001	Miltenyi Biotec	130-090-477	n.A.
7-AAD	n.A.	n.A.	Miltenyi Biotec	130-111-568	1:110
Human IL-2 IS	n.A.	-	Miltenyi Biotec	130-097-745	250 iU / mL
PepTivator SARS-CoV-2 S Complete	n.A.	PP20061602	Miltenyi Biotec	130-129-712	1µg/mL

Reagent	Clone	Lot	Manufacturer	Cat.No.	Final Concentration (fc)
PepTivator SARS-CoV-2 N	n.A.	PP20052002	Miltenyi Biotec	130-126-699	1 µg/mL
PepTivator SARS-CoV-2 M	n.A.	PP20052002	Miltenyi Biotec	130-126-703	1 µg/mL
PepTivator SARS-CoV-2 Prot_S B.1.1.529	n.A.	n.A.	Miltenyi Biotec	130-129-928	1 µg/mL
PepTivator SARS-CoV-2 Prot_S B.1.1.529 WT Refence Pool	n.A.	n.A.	Miltenyi Biotec	130-129-927	1 µg/mL
Viobility 405/452 Fixable Dye	n.A.	n.A.	Miltenyi Biotec	130-110-205	1:100
Anti-Rea MACS Comp Bead Kits	n.A.	5160412101	Miltenyi Biotec	130-104-693	2:50
MACSxpress whole blood neutrophil isolation kit	n.A.	n.A.	Miltenyi Biotec	130-104-434	n.A.
DNeasy® Blood & Tissue Kit	n.A.	-	Qiagen	69504	n.A.
Brefeldin A	n.A.	n.A.	Sigma-Aldrich	B7651	2 µg/mL
CytoStim, human	n.A.	51712201	Miltenyi Biotec	130-092-173	1:100
PMMA Red4 Beads	n.A:	MG220113SAV3/ MG220113SAV5	PolyAn	10652005	n.A.
Catalyst I	n.A.	n.A.	Miltenyi Biotec (Internal use)	n.A.	n.A.
Catalyst II	n.A.	n.A.	Miltenyi Biotec (Internal use)	n.A.	n.A.
ExPep I	n.A.	n.A.	Miltenyi Biotec (Internal use)	n.A.	n.A.
ExPep II	n.A.	n.A.	Miltenyi Biotec (Internal use)	n.A.	n.A.
pFITC/MHC I	n.A.	n.A.	Miltenyi Biotec (Internal use)	n.A.	n.A.
pFITC/MHC II	n.A.	n.A.	Miltenyi Biotec (Internal use)	n.A.	n.A.

List of Devices

Device	**Manufacturer**	**Catalog No.**
Heraeus Multifuge X3 FR Centrifuge	Thermo Scientific	42395452
100 µL Eppendorf pipette	Eppendorf	K48928F
1000 µL Eppendorf pipette	Eppendorf	L25423F
10 µL Eppendorf pipette	Eppendorf	L18736F
S1 Pipette Filler	Thermo Scientific	200573
Heracell 240i Incubator	Thermo Fisher Scientific	51026331
MACSQuant16-flow cytometer	Miltenyi Biotec	130-109-803
CytoFelx S Flow-cytometer	Beckmann Coulter	B75408
Sysmex XP-300 Hematological Analysis System	Sysmex	XP-300
ThermoMixer C	Eppendorf	5382000015
Titramax 100	heidolph	544-11200-00
gentleMACS™ Octo Dissociator with Heaters	Miltenyi Biotec	130-096-427
MACSmix™ Tube rotator	Miltenyi Biotec	130-090-753

List of Consumables

Consumable	Lot	Manufacturer	Catalog No.
96 well V-bottom microplate	E19113KV	Greiner Bio-One	651201
96 well flat bottom plate	-	Falcon	10141161
250 mL Storage Bottle	4720008	Corning	430281
10 µL Graduated Tips	I125842N	Starlab	S1111-3700
200 µL Graduated Tips	J127166H	Starlab	S1111-0706
300 µL Graduated Tips	I126073O	Starlab	S1110-9700
1000 µL Graduated Tips	I126945R	Starlab	S1111-6701
5 mL serological pipette	9255	Sarstedt	86.1253.025
10 mL serological pipette	9266	Sarstedt	86.1254.025
25 mL serological pipette	7327	Sarstedt	86.1685.020
50 mL serological pipette	6376	Sarstedt	86.1256.001
15 mL Conical Tube	34519024	Falcon	352096
50 mL Conical Tube	30419045	Falcon	352070
5 mL Round Bottom Tube	05820033	Falcon	352058
1.5 mL Natural Flat Cap Microcentrifuge Tubes	J188159H-1703	StarLab	S1615-5500
MACS Running Buffer	7200108392	Miltenyi Biotec	130-091-221
CliniMACS Buffer	D0729	Miltenyi Biotec	700-25
PBS (pH 7.4)	n.A.	Miltenyi Biotec	*internal use only*
PBS / EDTA buffer	n.A.	Miltenyi Biotec	*internal use only*
Pancoll	165919	PAN Biotec	P04-60500
AutoMACS Running Buffer	7200600071	Miltenyi Biotec	130-091-221
RPMI Medium	MS00H3	BioWest	L0501-500
AB Serum	B10217	LSP	S-102B-US
Anti/Anti		Thermo Fischer Scientific	111580486
L-Glutamine	OMB024	Lonza	BE17-605E
DSMO	059M4011V	Sigma Aldrich	D2650-100ML
X-Vivo 15	-	Lonza	11695120
FiltrEX™ 96-well plates	E23083GS	Greiner	651261
6-well plates	-	Falcon	353046

List of Software

Software	**Manufacturer**
FlowJo10	BD
MACSQuantify	Miltenyi Biotec
Prism	GraphPad
NetMHCpan	DTU Bioinformatics
Jmp 15	jmp
BioRender	Biorender.com

Acknowledgements

„Die Wissenschaft besteht aus Fakten, so wie ein Haus aus Steinen; aber eine Ansammlung von Fakten ist noch keine Wissenschaft, ebenso wie ein Haufen Steine noch kein Haus ist." – Henri Poincaré

Von der Entscheidung zur Promotion bis zum Schreiben der Dissertation durchläuft ein PhD Student viele Höhen und Tiefen. Es ist eine Zeit, die eine gute Portion Ausdauer erfordert. Rückblickend kann ich sagen, dass meine Doktorarbeit von einigen Herausforderungen aber vor allem von viel persönlichen Wachstum geprägt war. Wachstum als Wissenschaftlerin und als Mensch, welcher jedoch ohne die Unterstützung vieler Menschen aus meinem Umfeld nicht möglich gewesen wäre.

Mein besonderer Dank gilt deshalb nicht nur meinen Finanzier Miltenyi Biotec, der gesamten Gruppe von Dr. Christian Dose, sowie der Universität zu Köln mit der IPMM-Graduiertenschule, Prof. Holger Winkels, und meine Tutoren; Prof. Kay Hofmann und Prof. Florian Klein sondern vielen Einzelnen die mich besonders und zu jeder Zeit unterstützt haben.

Marc, als mein Betreuer und Mentor hast du mich stets unterstützt und warst mein erster Ansprechpartner für alle inhaltlichen Themen. Danke für Dein stets offenes Ohr, die vielen Diskussionen und großartige Zusammenarbeit!

Ohne zahlreiche Kaffee- und Mittagspausen, Feierabendbierchen und Freudentränen wäre diese Zeit nicht dieselbe gewesen. Danke an meine wundervollen Kollegen und Leidensgenossen: Dave, Lilli, Jens, Diana, Nicole, Verena, Manuel, Sebastian, Laura, Cris, Anja, Xueting und Vielen mehr. Ich bin sehr dankbar, dass ihr Teil dieser Reise wart und stolz einige von euch als Freunde gewonnen zu haben.

Immense Unterstützung habe ich auch durch meine Familie, meine Freunde fernab des Labors, und ganz besonders durch meinen Mann Jan erhalten. Gemeinsam haben wir Erfolge gefeiert. Ihr wart für mich da, wenn es mal nicht so gut lief. Jeder braucht Menschen wie Euch, um erfolgreich zu sein. Danke für Alles!

List of Publications

Published

04/2025	European Journal of Immunology "**Distinct HLA Haplotypes Are Associated With an Altered Strength of SARS-CoV-2-Specific T-Cell Responses and Unfavorable Disease Courses**", DOI: 10.1002/eji.202451497, **1st author**
05/2023	Frontiers Immunology **„Machine learning analysis of humoral and cellular responses to SARS-CoV-2 infection in young adults"**; DOI: 10.3389/fimmu.2023.1158905, **2nd author**
11/2022	Nature Communications Medicine „**Vaccines against the original strain of SARS-CoV-2 provide T cell memory to the B.1.1.529 variant**"; DOI: https://doi.org/10.1038/s43856-022-00203-7, **1st author**
06/2020	BMC Cancer **„Defective migration and dysmorphology of neutrophil granulocytes in atypical chronic myeloid leukemia treated with ruxolitinib";** DOI: https://doi.org/10.1186/s12885-020-07130-7, Co-author
10/2018	Journal of Immunology „**Surveillance of Myelodysplastic Syndrome via Migration Analyses of Blood Neutrophils: A Potential Prognostic Tool**"; DOI: https://doi.org/10.4049/jimmunol.1801071, Co-author

Erklärung:

Ich versichere, dass ich alle Angaben wahrheitsgemäß nach bestem Wissen und Gewissen gemacht habe und verpflichte mich, jedmögliche, die obigen Angaben betreffenden Veränderungen, dem Promotionsausschuss unverzüglich mitzuteilen.

Bottrop, _____ _____

(Place / Date) (Charlyn Dörnte)

Declaration / eidesstattliche Erklärung

Ich versichere, dass ich die von mir vorgelegte Dissertation selbstständig angefertigt, die benutzten Quellen und Hilfsmittel vollständig angegeben und die Stellen der Arbeit - einschließlich Tabellen, Karten und Abbildungen -, die anderen Werken im Wortlaut oder dem Sinn nach entnommen sind, in jedem Einzelfall als Entlehnung kenntlich gemacht habe; dass diese Dissertation noch keiner anderen Fakultät oder Universität zur Prüfung vorgelegen hat; dass sie - abgesehen von unten angegebenen Teilpublikationen -noch nicht veröffentlicht worden ist sowie, dass ich eine solche Veröffentlichung vor Abschluss des Promotionsverfahrens nicht vornehmen werde. Die Bestimmungen dieser Promotionsordnung sind mir bekannt. Die von mir vorgelegte Dissertation ist von Prof. Dr. Holger Winkels betreut worden.

Bottrop, 25.04.2025 _____

(Place / Date) (Charlyn Dörnte)